INFORMATION TO USERS

This manuscript has been reproduced from the microfilm master. UMI films the text directly from the original or copy submitted. Thus, some thesis and dissertation copies are in typewriter face, while others may be from any type of computer printer.

The quality of this reproduction is dependent upon the quality of the copy submitted. Broken or indistinct print, colored or poor quality illustrations and photographs, print bleedthrough, substandard margins, and improper alignment can adversely affect reproduction.

In the unlikely event that the author did not send UMI a complete manuscript and there are missing pages, these will be noted. Also, if unauthorized copyright material had to be removed, a note will indicate the deletion.

Oversize materials (e.g., maps, drawings, charts) are reproduced by sectioning the original, beginning at the upper left-hand corner and continuing from left to right in equal sections with small overlaps.

Photographs included in the original manuscript have been reproduced xerographically in this copy. Higher quality 6" x 9" black and white photographic prints are available for any photographs or illustrations appearing in this copy for an additional charge. Contact UMI directly to order.

Bell & Howell Information and Learning
300 North Zeeb Road, Ann Arbor, MI 48106-1346 USA
800-521-0600

UMI®

The Petrography and Mineralogy of the Lac de Gras Kimberlite Field, Slave Province, Northwest Territories: A Comparative Study

by
Katharine Melanie Masun ©

Submitted in partial fulfillment of
the requirements for the degree of

Master of Science

Supervisor: Dr. Roger H. Mitchell

Department of Geology
Lakehead University
Thunder Bay, Ontario
Canada
November, 1999

ABSTRACT

The kimberlites studied from the Lac de Gras area are composed of two broad textural types: hypabyssal kimberlite and volcaniclastic kimberlite. Hypabyssal kimberlite is present within small isolated dyke segments and in direct contact with volcaniclastic kimberlite within vent infill. The latter likely represents small, sub-horizontal sills emplaced subsequent to vent excavation and infill. Volcaniclastic kimberlite occurs as well-to-poorly sorted, often poorly consolidated vent infill. Abundant xenoliths of wall rock and xenocrysts of mica, feldspar, and quartz characterize the volcaniclastic rock, suggesting that most of the volcaniclastic kimberlite has been subjected to resedimentation processes. Juvenile lapilli (both vesiculated and non-vesiculated) are very common, but are often poorly-developed. A conspicuous feature of these kimberlite vents is the presence of wood fragments, discrete xenoliths of non-kimberlitic sediment and well-laminated beds of non-kimberlitic mudstone and siltstone. Pyroclastic kimberlite appears to be present within the kimberlites at Lac de Gras, but only accounts for a minor part of the vent infill. The pyroclastic kimberlite contains abundant juvenile lapilli and may show textures indicative of welding and molding. The Lac de Gras kimberlites are mainly small, steep-sided vents infilled with resedimented volcaniclastic kimberlite ± pyroclastic kimberlite ± non-kimberlitic sediment ± small hypabyssal sills. No tuffisitic breccias, the hallmark of diatreme-facies kimberlite, were recognized within the kimberlite vents and appear to be absent from the Lac de Gras kimberlites.

All features observed within the Lac de Gras kimberlites are characteristic of, but not exclusive to, kimberlites. The composition of spinel, phlogopite and monticellite are typical of archetypal kimberlites, although spinels are conspicuously aluminous and phlogopites Ba-rich. The nature of the primary texture, mineralogy and mantle-derived xenocrysts indicates that these rocks are archetypal kimberlites.

Comparing the character of kimberlite vents from the Fort à la Corne area (maar-like phreatomagmatic model) and the Orapa A/K1 kimberlite (southern African "classic" diatreme model) shows that there are two contrasting end-member emplacement mechanisms which are repeated in time and space. The former is driven by meteoric water in phreatomagmatic processes, while much debate exists whether the later is driven by juvenile gases (fluidization model) or hydrovolcanic processes. Near-surface geological setting at the time of emplacement appears to have played a critical role in determining the emplacement process of the kimberlite magma. Kimberlites discovered in the Lac de Gras area do not conform to either end-member

emplacement models and serve to highlight that a third, intermediate model will need to be developed to account for the features observed.

Clearly, two distinct processes were responsible for the emplacement of the Lac de Gras kimberlites: vent excavation and vent infill. Phreatomagmatic processes likely contributed significantly to the excavation of the kimberlite vents and a flaring explosion crater or maar was excavated into the soft, overlying sediments. The resultant ejecta was deposited as extra-crater material as a tuff ring or cone. This material was subsequently reworked and redeposited within the evacuated vent by debris flow and mass wasting processes incorporating a large amount of xenolithic material. The thin pyroclastic kimberlite beds within the vents are the result of either minor pyroclastic activity that continued through a central conduit during vent infill, or primary pyroclastic kimberlite initially deposited within the tuff cone/ring, which subsequently fell back into the vent with little reworking, as a coherent mass preserving the primary textures of the tuff. In the later scenario the "pyroclastic kimberlite" units are in fact resedimented "pseudo-pyroclastic" volcaniclastic kimberlite.

Clearly, more detailed studies need to be undertaken on these enigmatic kimberlites to constrain further the nature of their infill and emplacement. This can only occur with the creation of better exposures during mining and advanced exploration activities.

ACKNOWLEDGEMENTS

First, and foremost, I would like to thank Dr. Roger Mitchell for supervising this study and for allowing me to pursue my interest in kimberlites.

Many people have assisted me with various aspects of this study, and I wish to acknowledge Anne Hammond for preparing many sections of these horrible rocks, Alan MacKenzie for technical assistance with electron microscopy, and Sam Spivak for drafting advice and assistance.

I am indebted to Kennecott Canada Exploration Inc. for allowing me the opportunity to examine their kimberlites and for their financial support of this study.

Lastly, I would like to thank my co-pilot, Craig Geddes, for his countless hours of assistance with drill core logging and his delicious cooking.

TABLE OF CONTENTS

LIST OF FIGURES

LIST OF TABLES

CHAPTER 1. INTRODUCTION AND REGIONAL GEOLOGICAL SETTING

1.1. INTRODUCTION

The understanding of the complex geology of kimberlites has increased substantially over the last two decades as a result of detailed studies undertaken on good exposures created during mining and exploration activities. Kimberlites differ from many volcanic rocks, for example, in that no extrusive magmatic or effusive rocks or plutonic equivalents have yet been discovered. As a result, unique styles of emplacement have been postulated for kimberlites, which differ from most standard volcanic processes described within the literature. Despite this, proposed kimberlite emplacement models are generally not well understood.

Comparing the nature of many kimberlite vents shows that there are two contrasting end member emplacement mechanisms repeated in space and time: 1. Southern African "classic" diatreme model; 2. Saskatchewan maar-like phreatomagmatic model. The kimberlites of the Lac de Gras area (Northwest Territories) do not conform to either two end member emplacement models and a third, intermediate model must be developed to properly explain the nature of these intrusions. It is proposed that the near-surface geological setting at the time of kimberlite emplacement has a major impact on determining the emplacement process of each kimberlite magma.

The principal objective of this study is to detail and illustrate the petrography and mineralogy of the Lac de Gras kimberlites. These features are compared and contrasted with kimberlites of the Fort à la Corne field (Saskatchewan) and the Orapa A/K1 kimberlite of Botswana to demonstrate conclusively that the Lac de Gras kimberlites do not conform the end-member kimberlite models.

1.2. REGIONAL GEOLOGICAL SETTING

The Lac de Gras area is located in the central Slave Structural Province of the Northwest Territories. The Slave Structural Province is a fragment of amalgamated

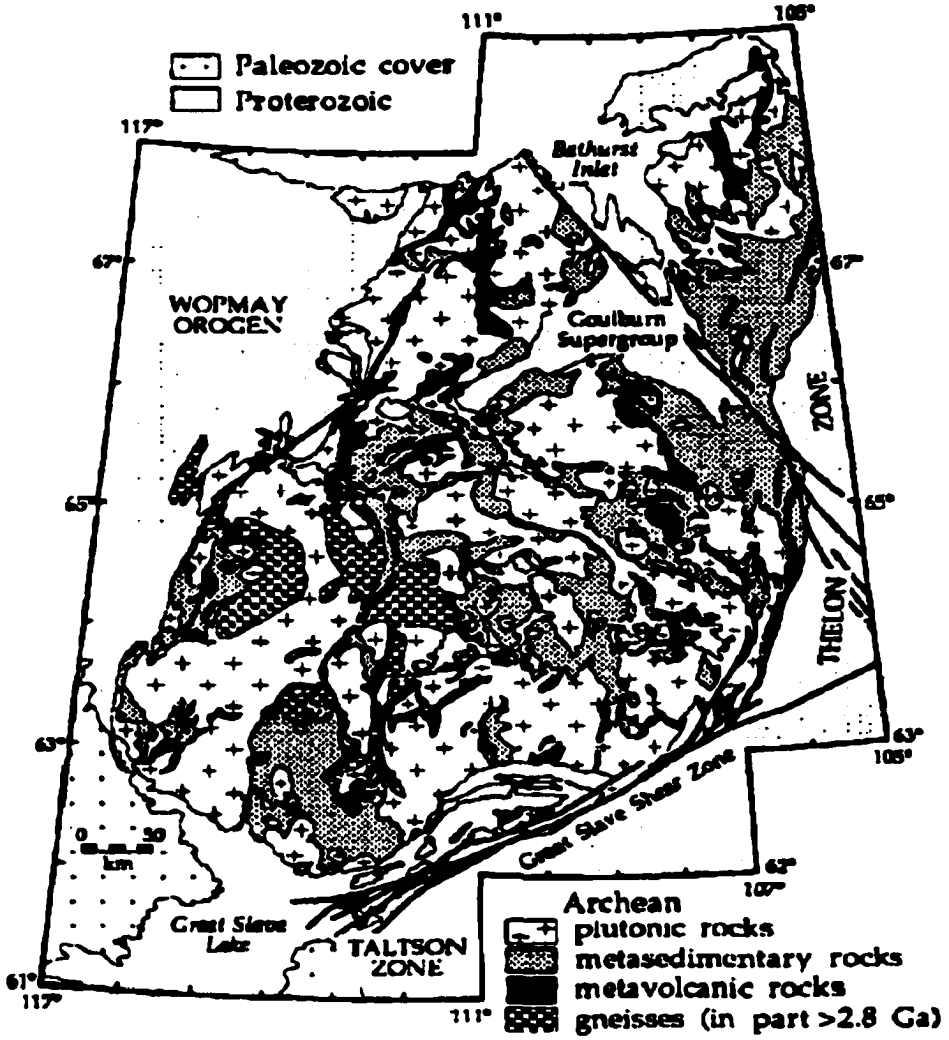

Figure 1.1. General geology of the Slave Structural Province (modified from Hoffman 1989; in Card and King 1992).

early-to-late Archean rocks assembled over a period of more than a billion years (Figure 1.1). The Slave Province is a relatively small Archean craton, with a surface area of approximately 213 000 km^2 (Padgham and Fyson 1992). The general character is that of a granite-greenstone terrane comprising numerous belts of metavolcanic and metasedimentary rocks (supracrustal belts) that were extensively intruded by syn- to post-volcanic granitoid plutons. The Slave Province contains abundant gneiss, tonalite, migmatite and volcanogenic base-metal deposits (Padgham and Fyson 1992). The supracrustal rocks structurally overlie older (>2.8 Ga) continental crust (sialic basement remnants or prevolcanic granitoid basement rocks) preserved in the western part of the

province and include the oldest known terrestrial rocks; the Acasta gneiss which has an age of 3.96 Ga (Bowring *et al.* 1989). Quartz arenites are closely associated with some sialic basement remnants, characterizing a shelf environment (Roscoe *et al.* 1989)

Supracrustal rocks of the Slave Province, formed essentially between 2.71 and 2.65 Ga, are dominated by a volcanic and greywacke-mudstone sequence, inferred to be deposited in a tectonically active environment. These rocks, which cover approximately 33% of the province, consist of 73% greywacke-mudstone and 27% volcanic rocks (Padgham and Fyson 1992). The supracrustal rocks have generally been equated with the Yellowknife Supergroup on the basis of gross lithological affinities, although distinct sedimentary units have been excluded from it (Padgham 1991).

Yellowknife Supergroup sedimentary rocks are mainly turbidites of intermediate-to-felsic plutonic and volcanic provenance with minor conglomerate, iron formation and carbonate. Quartzite-rhyolite-iron formation assemblages underlying the supergroup were recognized by Padgham (1991) and are thought to predate it. Also excluded from the Yellowknife Supergroup are several polymictic conglomerate units that contain boulders of post-Yellowknife Supergroup granites.

The Yellowknife Supergroup volcanic rocks comprise nearly 45% felsic-intermediate and include both tholeiitic bimodal mafic-felsic series and calc-alkaline intermediate series. Komatiitic and alkaline lavas are rare (Padgham and Fyson 1992). Stratigraphic and temporal relationships between the volcanic and sedimentary rocks are not yet well understood.

The original stratigraphic relationship between the younger supracrustal rocks and the older, pre-2.8 Ga sialic basement terrane, especially the volcanic units, is not well-determined. However, a local unconformity at Keskarrah Bay and >2.8 Ga clasts and detrital zircons in sedimentary units indicates at least some parts of the basement terrane were uplifted and eroded during deposition of the sedimentary units (Card and King 1992).

Granitoid rocks, cutting basement rocks and the volcanic-turbidite assemblages, predominate over large areas (over 65%) of the Slave Structural Province, as in other Archean cratons. Syn- to post-volcanic plutons ("volcanic" referring to the combined

volcanic-turbidite assemblage), ranging in composition from anorthosite-to-granite were emplaced from 2.7 to 2.58 Ga. Two suites are recognized: syn-deformation, predominantly metaluminous diorite-to-granodiorite and late- to post-deformation, peraluminous tonalite-to-syenogranite. Available radio-metric data imply that a magmatic hiatus occurred at ca. 2645-2625 Ma (Card and King 1992).

Diabase dykes, ranging in width from 15 to 100 m, are common throughout the Slave Province and postdate older Archean rocks. The dykes are distinguished on the basis of orientation and are correlated with known dyke swarms in the Slave Province. Four, possibly five, swarms of Proterozoic diabase dykes are represented in the province: the east-trending (080°) MacKay dykes (2.4 Ga K/Ar whole-rock age), the northeast-trending (045°) Contwoyto dykes (2.23 Ga U-Pb age), the southerly (190°) trending Lac de Gras dykes (2.02 Ga U-Pb age), the northwest-trending (335°) Mackenzie dykes (2.02 Ga U-Pb age) and the northwest-trending (300-310°) "305" dyke, whose age and relationship to other swarms is unknown (LeCheminant and van Breeman 1994).

Regional polyphase deformation, including multiple folding, cleavage formation and thrusting, and normal and transcurrent faulting, occurred after ca. 2.66 Ga and continued through to <2.6 Ga. Broadly syntectonic, high-temperature-low pressure metamorphism characterized the entirety of the Slave Province (Thompson 1978). Prethermal-peak metamorphic mineral growth (locally including kyanite) is also recognized throughout much of the province, although the associated pressure-temperature conditions and timing of the episode(s) have not yet been well confined (Card and King 1992).

The tectonic environments and formation of volcanic belts in the Slave Province are poorly constrained. Proposed tectonic models for the Slave Province are of two schools: intracratonic and collisional-accretionary. Adherents of an intracratonic model interpret the volcanic-turbidite belts as collapsed ensialic rifts and the interceding granitoid domains as reactivated basement that has been extensively intruded by younger granitoid plutons. Collisional-accretionary models include either variations of island arc-continent collisions or an Andean-type margin (King *et al.* 1992).

CHAPTER 2. CHARACTERISTICS OF KIMBERLITES WITHIN THE SLAVE STRUCTURAL PROVINCE: A LITERATURE REVIEW

2.1. INTRODUCTION

Since the discovery of the Point Lake kimberlite pipe in 1991, nearly 200 kimberlites have been found in the Slave Province of the Northwest Territories.

Within the Slave Structural Province, kimberlites appear to be concentrated in the central accretionary domain, in the vicinity of Lac de Gras. The Diavik and BHP-Dia Met properties host the majority of the kimberlite intrusions within this region, each with several clusters numbering several tens of intrusions (Carlson *et al.* 1998). Central Slave craton intrusion ages range from 47 Ma to 74 Ma (Davis and Kjarsgaard 1997).

The study of kimberlites in the Slave Structural Province is in its infancy. Much information on the mineralogy, petrology, age and location of individual kimberlite intrusions is still proprietary and held by exploration companies. Recent reviews of kimberlites in the Slave province by Pell (1996, 1997), Carlson *et al.* (1998) and Field and Scott Smith (1998) attempt to summarize and interpret what little information is available.

Kimberlites in the Slave Province intrude granitoid, gneiss, migmatite, metasedimentary-metavolcanic sequences and rarely diabase. Few kimberlite intrusions are known to outcrop, hence discoveries have been achieved using a combination of heavy mineral sampling, geophysical techniques (both ground and airborne methods) and drilling (Fipke *et al.* 1995).

Many intrusions are characterized by resistivity lows, magnetic anomalies (either highs or lows) and by well-developed indicator mineral trains (*i.e.* garnet, chromite, ilmenite, Cr-diopside, and olivine). The majority of the discoveries have been in the Lac de Gras/MacKay/Aylmer Lake area of the Mackenzie District, Northwest Territories. Figure 2.1 shows the distribution of kimberlites within the Slave Province.

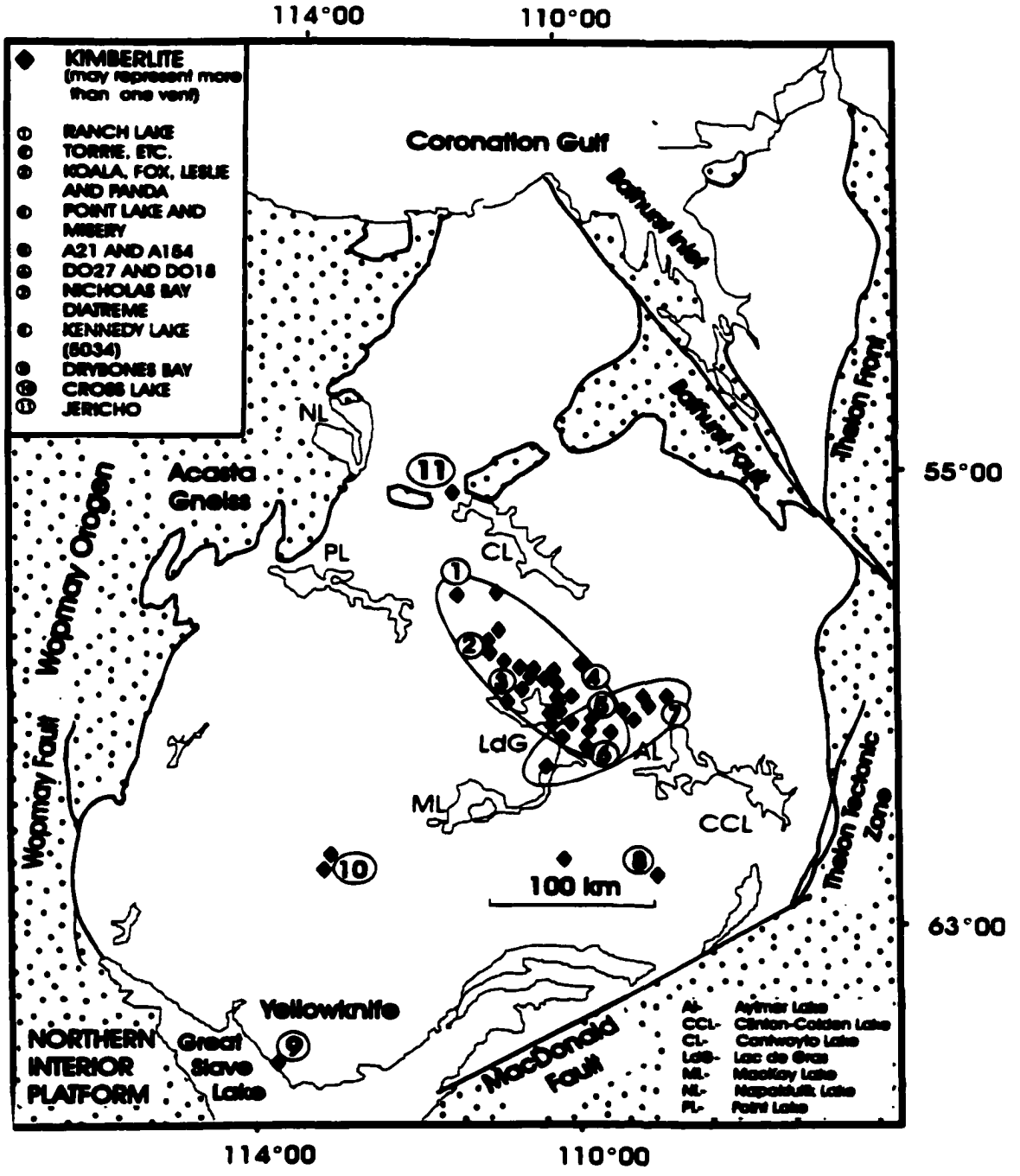

Figure 2.1. Distribution of kimberlites within the Slave Province (after Pell 1997).

2.2. UPPER CRETACEOUS-TERTIARY KIMBERLITES OF THE LAC DE GRAS AREA

2.2.1. Introduction

Pell (1996, 1997) has subdivided the intrusions within the Lac de Gras area on the basis of their general petrography and location, into two groups: Lac de Gras field and the MacKay/Aylmer Lake field (see Figure 2.1):

1. The majority of known kimberlite intrusions within the Slave Province are located within a 135 km long, northwest-trending zone, centred north of Lac de Gras. Some kimberlites within this field are aligned in northeast-trending, conjugate clusters. The Lac de Gras field roughly parallels the Bathurst Fault, a Proterozoic structure related to the docking of the Slave with the Churchill Province.

2. A second group of intrusions, outlining an east-northeasterly-trending zone, approximately 100 km in length, overlapping the southern edge of the Lac de Gras field, defines the MacKay/Aylmer Lake region. This field roughly parallels the MacDonald Fault, another Proterozoic structure related to the docking of the Slave Province.

In this review, as in Field and Scott Smith (1998), it seems more prudent to include both of Pell's kimberlite fields into one broad category. Until further detailed information is available, all these kimberlites will be considered together and referred to as the Lac de Gras kimberlite field. This region will include all the kimberlites occurring on the Lac de Gras properties and the more northerly claims, including Lytton's Ranch Lake kimberlite (Figure 2.2). These intrusions show broad geological similarities and have Upper Cretaceous and Early Tertiary ages. However, the broad age range (≈47-86 Ma) observed in preliminary data suggests that treating these kimberlites as one province may not be valid (Field and Scott Smith 1998).

Surface areas of kimberlite intrusions within the Lac de Gras region range from less than 2 to 15 hectares. Many intrusions are less than 5 ha. Kimberlite bodies which have been extensively investigated by drilling and for which public information is available, appear to be steep-sided, pipe-shaped intrusions that reach depths of 400-500m

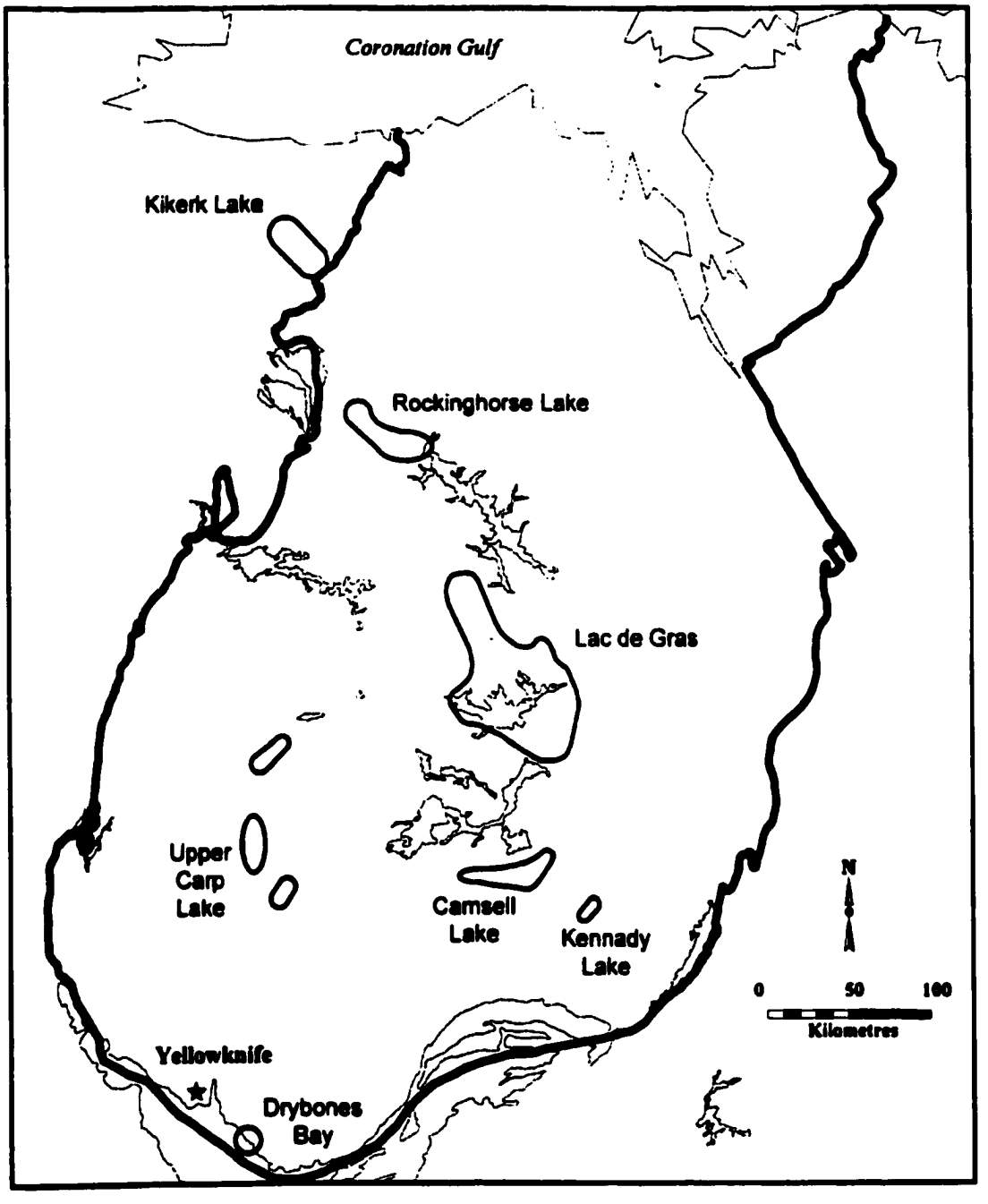

Figure 2.2. Location of kimberlite fields within the Slave Province (Field and Scott Smith 1998).

below the present surface. Country rock-kimberlite contacts do vary and most intrusions taper with depth. Significant amounts of the kimberlite intrusions probably do not exist below a depth of 500-600 m (Field and Scott Smith 1998). Crater, diatreme and hypabyssal facies rocks have all been postulated to be present (Pell 1997).

Many of the kimberlites in the Lac de Gras field are infilled with volcaniclastic kimberlite. A conspicuous feature of these intrusions is the presence of very common discrete xenoliths of mudstone and shale. Shale clasts commonly display features suggesting poor consolidation prior to kimberlite emplacement (Field and Scott Smith 1998). In most cases, the youngest fossils retrieved within the xenoliths are of late Paleocene age implying post-Paleocene kimberlite emplacement. Cretaceous and Tertiary fossils, pollen and spores, in addition to wood fragments and teleost fish parts have been recovered (Pell 1997). Palynological studies on mudstone fragments from 13 kimberlite intrusions in the Lac de Gras field contain fossils that range in age from Early Cretaceous (≈97 Ma) to Tertiary (55 Ma) (Stasiak and Nassichuk 1995). Similar results have been reported for kimberlites on the Diavik property (100-55 Ma mudstones, Graham *et al.* 1998). These data reveal that, prior to the emplacement of the Lac de Gras kimberlites, Archean rocks in the area were overlain by a veneer of mainly marine Cretaceous strata and lacustrine Paleocene deposits (Nassichuk and Dyck 1998). It has been concluded that the Western Interior Seaway, for perhaps the first time in geological history, extended over the Slave Province during the Upper Cretaceous (Field and Scott Smith 1998).

Although all the Cretaceous and Paleocene strata have been lost, the erosion of the Archean basement of the Slave Province is presumed to be minimal (Pell 1997; Field and Scott Smith 1998). Field and Scott Smith (1998), Pell (1997) and Carlson *et al.* (1996) all suggest that the sediment cover merely formed a veneer of less than 300 m in thickness (presumably 100-150 m). However, Field and Scott Smith (1998) further propose that the thickness of the sediment cover varied, both temporally and laterally throughout the Slave, perhaps locally within the Lac de Gras area, and therefore during kimberlite emplacement.

Upper Cretaceous shale was shown by McKinlay *et al.* (1998) to be deposited largely under marine conditions, indicating that older kimberlites were potentially emplaced in a submarine environment. However, the youngest sediments studied were determined to have a terrestrial origin indicating that the younger kimberlites at Lac de Gras were emplaced under subaerial conditions. This presence of wood fragments within numerous kimberlitic bodies further supports this theory (Field and Scott Smith 1998).

The intrusions of the Lac de Gras field appear to be comprised of two broad textural types of kimberlite. The first type is typical hypabyssal kimberlite, which is not common within the Lac de Gras field (Pell 1997). Intrusions studied to date have been described as macrocrystal hypabyssal kimberlites with olivine macrocrysts comprising up to 50% of the rock, set in a uniform groundmass (Pell 1997). Hypabyssal phases may crosscut crater-facies material, occur as dykes or sills (ex. DO27, Doyle *et al.* 1998) and, in some instances, appear to have completely replaced the volcaniclastic material within the intrusion (ex. Leslie intrusion, Kirkley *et al.* 1998). Kimberlites infilled with hypabyssal rock are not common and appear to represent a low proportion of the kimberlites in the Lac de Gras field.

Kimberlites of the Lac de Gras field appear to be predominantly filled with extrusively-formed, commonly bedded volcaniclastic material which may persist to depths greater than 400-500 m below surface (Field and Scott Smith 1998). Field and Scott Smith (1998) stress that the presence of volcaniclastic material within these steep-sided, pipe-shaped intrusions requires prudent use of the term diatreme. Field and Scott Smith (1998) suggest that the term diatreme has very specific genetic implications, *i.e.* material which can be shown to be formed by the process of fluidization which results in the formation of diatremes which are typically infilled by tuffisitic kimberlite breccia or diatreme-facies kimberlite. However, it has yet to be unequivocally proven that fluidization of kimberlite magma occurs. Field and Scott Smith (1998) further propose that the term pipe (which has no genetic implications and refers to a body that is not sheet-like in shape), *not* diatreme, be adopted when referring to these kimberlites. However, the term *vent*, defined as "the opening at the earth's surface through which volcanic materials are extruded; also, the channel or conduit through which they pass"

(Bates *et al.* 1984) is more specific in reference to process than *pipe*, which has a broad range of meanings and usages. Therefore, in this work, the colloquial term *pipe* shall be henceforth replaced with the term *vent*.

Volcaniclastic infill generally consists of breccia that commonly displays well-developed layering. Laminated, re-worked sediments may overlie primary crater facies deposits. Pelletal lapilli may be present and groundmass textures may vary from uniform to segregationary. Pyroclastic ash tuffs, lapilli tuffs and olivine crystal-rich tuffs and lesser amounts of epiclastic kimberlite mudstones, siltstones, sandstone and rarely conglomerates have been recognized (Carlson *et al.* 1998).

Whether or not diatreme-facies kimberlite is present within the Lac de Gras field is a subject of current debate. Field and Scott Smith (1998) believe that many of the reported diatreme-facies kimberlite have been incorrectly interpreted and have seen no evidence or samples to suggest that classic tuffisitic kimberlite breccias, typical of the infill of southern African kimberlite diatremes, are present within the Lac de Gras kimberlite field.

Lac de Gras kimberlites are characterized by copious olivine macrocrysts (up to 1 cm in maximum dimension) and a xenocryst suite of Cr-diopside (>2cm), garnet (up to 0.5 cm), chromite and ilmenite. Serpentine, calcite, Ba-phlogopite-kinoshitalite (Mitchell pers. comm.), monticellite, perovskite and magnetite comprise the main groundmass mineral assemblage. Lithic clasts of surrounding country rock (metasediments, granites) are commonly incorporated within the kimberlite. Autolithic fragments and peridotite xenoliths are known to occur in some pipes (Pell 1996, 1997).

2.2.2. Tli Kwi Cho (Do 27 and Do 18) Kimberlite Complex

Located 360 km north of Yellowknife, the Tli Kwi Cho kimberlite complex is considered a member of the Lac de Gras kimberlite field and is held under mineral claims belonging to the DHK joint venture. The joint ventures ownership consists of 40% Kennecott Canada Exploration Inc., 10% SouthernEra Resources Inc., 15% Aber

Resources Ltd. and 35% DHK (Dentonia Resources Ltd., Horseshoe Gold Mining Inc. and Kettle River Resources Ltd.).

The kimberlite complex consists of two distinct electromagnetic and magnetic anomalies and was initially drill tested in 1993. The Tli Kwi Cho complex intrudes medium-grained, two-mica granite of the Archean Contwoyto terrain and is overlain by 20-55 m of glacial till and up to 10 m of water. Based on drill testing and underground excavation, four main textural rock types have been identified within the complex. These include a precursor hypabyssal sill and dyke intrusion followed by up to four pyroclastic/volcaniclastic kimberlite (PK/VK) events (Doyle *et al.* 1998).

The four main textural kimberlite types comprise:

1. HK – DO 27 hypabyssal macrocrystal monticellite kimberlite +/- minor kimberlite breccia, central dyke/sill complex. HK is characterized by the presence of fresh olivine macrocrysts (<2-3 mm), rare garnet, diopside and ilmenite macrocrysts (existing garnets have a thick kelphytic corona and diopside is ovoid in nature), and a paucity of shale fragments.

2. PK – main southern DO 27 green crater facies kimberlite or lapilli-bearing olivine tuff. This xenolith-poor unit is characterized by fresh-to-partially altered olivine macrocrysts (<5mm), abundant garnet, diopside and ilmenite macrocrysts, set in a mesostasis of serpentine +/- carbonate. Juvenile lapilli are common. PK is interpreted as being primary sub-aerial pyroclastic kimberlite.

3. VK – northern DO 27 black crater facies kimberlite or shale-rich olivine lapilli tuff. Altered olivine macrocrysts (<2-3mm) and numerous juvenile lapilli containing pseudomorphed olivine crystals characterize this unit. Garnet, diopside and ilmenite macrocrysts are not common, however, existing garnet macrocrysts often display thick kelphytic coronas and diopside crystals are ovoid in habit. The matrix contains prevalent shale xenoliths. This unit is probably re-sedimented crater facies material.

4. XPK - DO 18 xenolith- and xenocryst-rich lapilli-bearing olivine tuff +/- breccia/microbreccia. Pseudomorphed olivine macrocrysts (<2-3 mm) and abundant garnet, diopside and ilmenite macrocrysts characterized this unit. Thorough mixing of granite xenoliths is noted. Doyle *et al.* (1998) do not discuss the nature of the matrix within this unit.

Due to the lack of suitable minerals, an age of intrusion for the Tli Kwi Cho complex has been difficult to obtain. However, palynology has given a maximum age of

74 Ma and the similarity of wood fragments in volcaniclastic units with other kimberlites in which ages have been determined suggests an Eocene age is likely.

The distinctive nature of the above-described units suggests that they resulted from different phases and styles of kimberlite emplacement. The HK event preceded PK and VK and likely XPK. The xenolith-poor PK, the shale-rich VK and the xenolith-rich XPK are distinctly different types of volcaniclastic kimberlite that formed by at least three separate eruptions at different volcanic centres forming separate craters. Following the intrusion of HK, PK and VK, craters were excavated into the granite. PK forms a bowl-shaped crater with a surficial area of 9 ha and a present depth of at least 250 m. XPK forms a pipe-shaped body 6 ha in area and at least 250 metres in depth. The shape of VK crater has not been defined. No evidence has been found to suggest a possible eruptive sequence of the three separate craters (Doyle *et al.* 1998).

No evidence to suggest the formation of diatreme-facies rocks or the derivation or association of diatreme facies material, as described in the classic kimberlite emplacement model (*sensu* Hawthorne 1975; Clement and Skinner 1985; Mitchell 1986; Mitchell 1995) has been observed in the rocks of the Tli Kwi Cho complex.

2.2.3. The Diavik Kimberlites

The Diavik Diamond Project is located approximately 300 km northeast of Yellowknife and some 30 km southeast of the Ekati Diamond Mine. The project comprises planned development of four high-grade diamondiferous kimberlite intrusions of Eocene age (≈53 Ma, Carlson *et al.* 1998) located beneath the waters of Lac de Gras. The Diavik claim block was staked by Aber Resources Ltd. and joint venture partners. In 1992, a joint venture was formed between Aber Resources and partners, and Kennecott Canada Inc. (now Kennecott Canada Exploration Inc.), to explore the Diavik claims. Diavik Diamond Mines Inc. (DDMI) was established in 1996 to develop the joint venture prospects. The property is held 60% by DDMI and 40% by Aber Resources (Graham *et al.* 1998). Exploration on the Diavik claims has resulted in the discovery of more than 50 kimberlite occurrences. The four diamond-bearing kimberlite intrusions, on which final

feasibility studies are currently being undertaken, are designated as A-154 North, A-154 South, A-418 and A-21.

The Diavik kimberlites form small (<2 ha), steep-sided, cone-shaped bodies, hosted within a complex of Archean granitoids and micaceous metasediments. All four intrusions are located in the near-shore environment of Lac de Gras, overlain by up to 20 m of Quaternary glacial till, a veneer of lacustrine sediments and up to 25 m of water (Carlson *et al.* 1998).

The Diavik intrusions are dominated, volumetrically, by volcaniclastic crater facies assemblages, including pyroclastic and debris flow sequences which fill the cone-shaped chasms excavated into the Archean host rock. Pyroclastic rocks include tuffs, breccias and minor welded tuffs, while debris flows range from tephra dominated kimberlite to xenolithic mudflows and breccias. Units range in scale (cm to >15 m) and occur as massive, graded and bedded/laminated lithologies. Progressive enlargement and deepening of the kimberlite vent with successive eruptions has resulted in a downward stoping of the volcaniclastic units and superposition of younger units upon earlier deposits. Local zones of chaotic texture and intense alteration attest to fluidization/gas streaming effects of multiple events. Volumetrically insignificant hypabyssal kimberlite occurs as deep magmatic feeders to the intrusions and as contact intrusions along vent margins. Flow differentiation is commonly observed (Graham *et al.* 1998). No evidence for the derivation of, or association with diatreme facies rocks (*sensu* Hawthorne 1975; Clement and Skinner 1985; Mitchell 1986 and Mitchell 1995) has been recognized in the Diavik kimberlite occurrences.

Within the volcaniclastic units of the Diavik kimberlites primary magmatic kimberlite minerals and their relics, both mantle and crustal xenoliths and xenocrysts have been recognized. Replacement of primary magmatic minerals by serpentine, calcite and Mg-smectite is profound, however perovskite and phlogopite typically remain fresh. Macrocrystal olivines are ubiquitous and are the primary indicator of sorting and grading within the successions of units of the volcaniclastic piles. Mantle xenoliths include fragments of peridotitic and eclogitic parentage; xenocrysts include ilmenite, garnet and phlogopite. The crustal assemblage found in the Diavik kimberlites is characterized by a

suite of xenoliths derived from Phanerozoic platform sediments extant in the region during kimberlite emplacement. Dominated by mudrock types, with rare siltsones, these xenoliths are angular (lithified), soft sediment, plastically deformed mudclast fragments. These mudrocks frequently comprise a disaggregated matrix to the debris flow-derived kimberlite units and contain the same palynological assemblages as the mudrock xenoliths. Other common crustal xenoliths include variably altered granite, schist and diabase of surrounding host rock. Less prevalent xenolithic fragments found include deep crustal granulitic/eclogitic facies xenoliths.

2.2.4. Ekati Kimberlites

The first kimberlites to be discovered in the Slave Province occurred on the BHP-Diamet Exeter Lake Property in the Lac de Gras area in the Northwest Territories. Over 100 kimberlite bodies have been discovered to date (Kirkley *et al.* 1998), five of which comprise the new Ekati Mine. In the Exeter Lake property, kimberlite bodies are generally less than 5ha, or less than 250m in diameter (ex. Misery at 180x160m, or 1.5 ha, Panda at 200m, or 3.1 ha, Koala at 300x20m, or 4.5 ha; Field and Scott Smith 1998). Larger bodies are also present, for example Fox at 540x380m, or 14.7ha and Point Lake and Grizzly at approximately 14 ha (Field and Scott Smith 1998). Most bodies appear to be steep-sided pipe-shaped intrusions that may reach a depth of 500m from the present surface. Some of the intrusions have variable kimberlite to country rock dips and most taper with depth (Field and Scott Smith 1998).

The Panda intrusion is nearly circular in plan, occupying a small lake and is overlain by 15-25m of glacial sediment. The intrusion is comprised of crater facies material to a depth of at least 300m and is composed of predominantly volcaniclastic kimberlite with minor blocks or lenses of kimberlitic mudstone, siltstone and sandstone. A Rb/Sr isochron obtained from a phlogopite macrocrysts yields an age of 53.2±3.8 Ma (Carson *et al.* 1998). The main volcaniclastic units comprise olivine crystal tuff, lapilli tuff and tuff breccia. Volcaniclastic kimberlite has a distinctive pelletal lapilli texture and

contains abundant olivine macrocrysts, garnet, chrome diopside and chromite xenocrysts set in a fine-grained, intensely altered matrix (Carlson *et al.* 1998).

In addition to the Ekati kimberlites, the 7ha Leslie intrusion is located within the Exeter Lake property. The Leslie body is filled with hypabyssal kimberlite to the present surface except for a narrow remnant of tuffisitic kimberlite breccia intersected at the vent contact at a depth of approximately 400m (Berg and Carlson 1998).

The Leslie body is infilled predominantly with fresh hypabyssal macrocrystal monticellite kimberlite. Inequigranular olivine characterizes this material and may be as large as 15mm in dimension. Minor serpentinization of olivine is sparse and intensely altered orthopyroxene macrocrysts are rare. The groundmass in characterized by the presence of microphenocrystal olivine, monticellite, calcite, perovskite and opaques together with minor phlogopite and apatite. Lithic fragments are sparse to extensive. Tuffisitic kimberlite breccia encountered along the margins of the intrusion is strongly altered but discernible by the presence of rare pelletal lapilli. An altered microphenocrystal kimberlite ash mantles these lapilli (Berg and Carlson 1998).

Leslie is unlike many intrusions found in the Slave province in that the pipe-shaped body is apparently infilled with hypabyssal kimberlite. Berg and Carlson (1998) have proposed several method of emplacement to explain this phenomenon. They suggested that Leslie initially conformed to the vent-forming mechanisms typical of diatreme-bearing kimberlites. Leslie subsequently blew an open vent and was filled by magmatic kimberlite or magma displaced an earlier TKB-infill. A Rb/Sr isochron of 53.9±2.0 Ma from phlogopite macrocrysts has been obtained for the Leslie intrusion (Berg and Carlson 1998). The Leslie intrusion can be contrasted with the Panda intrusion, of similar age, located 6km northeast of Leslie. As noted above, it is infilled with crater facies kimberlite material and is also emplaced into porphyritic biotite granite. Carlson and Berg (1998) suggest that sufficient volatile pressure was maintained by mechanical over-pressure of the overlying material to allow intrusion of the large volumes of magmatic kimberlite to shallow levels, as observed at Leslie.

2.2.5. Summary of the Lac de Gras Kimberlites

Although single samples may display relatively homogeneous olivine sizes, suites of samples from the same intrusions typically show a broad range of olivine dimensions (<0.2mm to >10mm; Field and Scott Smith 1998). This suggests that sorting is a common process in volcaniclastic kimberlites at Lac de Gras, which is consistent with common reports of bedding within many kimberlite vents. Many reported volcaniclastic kimberlites (Graham *et al.* 1998; McKinlay *et al.* 1998; Doyle *et al.* 1998) have interclast matrices that are composed of thoroughly mixed disseminated shale. Volcaniclastic kimberlites with such shale matrices were most likely deposited by resedimentation processes and can thus be termed resedimented volcaniclastic kimberlites (Field and Scott Smith 1998). Graham *et al.* (1998) reported such features and interpreted these units as debris flows.

Kimberlitic mudstones, siltstones and sandstones are also reportedly present (Field and Scott Smith 1998). Thinly laminated, non-kimberlitic mud, silt and sandstones have been observed at depths greater than 100m and may represent water-lain crater infill (Field and Scott Smith 1998). Other more juvenile-rich material is also interpreted as being resedimented (Graham *et al.* 1998). Olivine-rich pyroclastic rocks appear to be common at Lac de Gras and can account for a small or major part of many kimberlite vents (Doyle *et al.* 1998; Graham *et al.* 1998; Carlson *et al.* 1998; Kirkley *et al.* 1998). Each volcaniclastic kimberlite vent, however, has a unique internal geology, ranging from internally uniform volcaniclastic kimberlite of A154S to the well-layered infill of A154N (Field and Scott Smith 1998). Nearby A418 reportedly contains pyroclastic kimberlite while A21 is infilled by mud-rich resedimented horizons, which give way to pyroclastic kimberlite with depth (Field and Scott Smith 1998). Kimberlites within the BHP-Diamet property, just north of the Diavik claims, appear to be composed of mainly volcaniclastic kimberlite ranging from chaotic but uniform to well-layered, subhorizontal units (Field and Scott Smith 1998). In most cases, Field and Scott Smith (1998) have noted that hypabyssal kimberlite is absent in the volcaniclastic vents. Graham *et al.* (1998) suggest that at Diavik hypabyssal kimberlite occurs only as feeders to the vents.

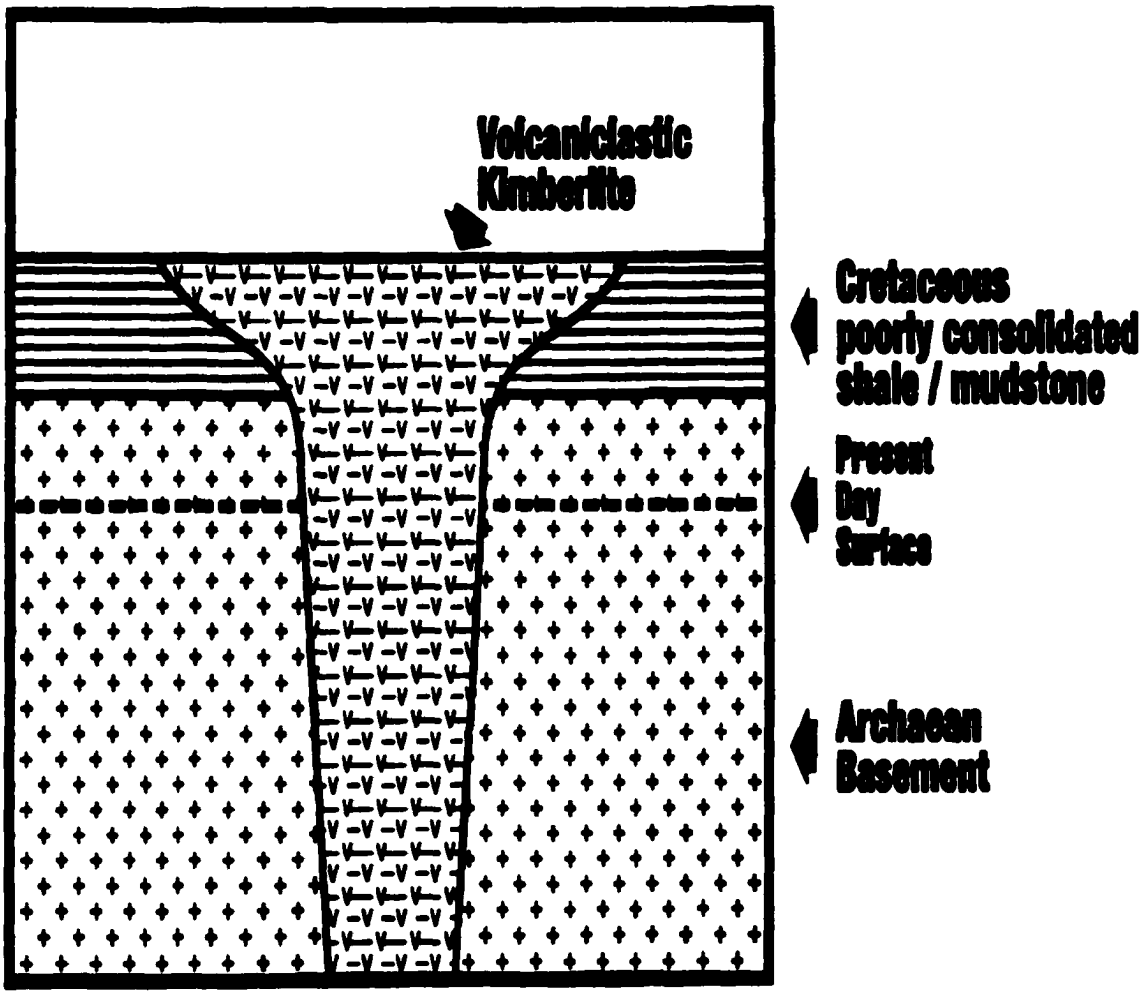

Figure 2.3. Schematic model of a Lac de Gras kimberlite vent in Cretaceous times. Note the vent is infilled with volcaniclastic kimberlite and not diatreme-facies tuffisitic kimberlite breccia (Field and Scott Smith 1998)

Doyle *et al.* (1998) note that at Tli Kwi Cho hypabyssal rocks were emplaced as a sub surface sill complex prior to the excavation of kimberlite vents containing volcaniclastic infill. Although the hypabyssal kimberlite underlies the vents, it has no direct relationship to it.

In summary, the Lac de Gras kimberlites appear to be steep-sided bodies. Their shape is superficially similar to the southern African diatremes, however, relative to these vents, those at Lac de Gras appear to be quite small. Kimberlites of the Lac de Gras fields are infilled mainly with either primary pyroclastic kimberlite or resedimented volcaniclastic kimberlite (Figure 2.3). Less commonly the vents are infilled with hypabyssal kimberlite. It is not clear whether the hypabyssal kimberlite infilled a void vent, which had been previously evacuated, or displaced earlier volcaniclastic infill (Field and Scott Smith 1998).

Field and Scott Smith (1998) suggest that two processes formed the Lac de Gras kimberlites: vent excavation and vent infilling. The presence of resedimented volcaniclastic kimberlite, minor primary pyroclastic kimberlite and non-kimberlitic sediments within the vents suggests that infilling was a relatively long-lived process. Furthermore, excavation and subsequent infilling of vents by hypabyssal kimberlite has occurred in rare examples. However, whether hypabyssal rocks infilled a void vent or displaced previous infill is not known.

2.3. PRE-CRETACEOUS KIMBERLITES OF THE SLAVE PROVINCE

2.3.1. Introduction

Outside of the Lac de Gras area, kimberlites appear to be pre-Cretaceous in age and quite different in style to their Lac de Gras counterparts in that diatreme-formation may be a part of their emplacement style. It must be stressed, however, that a pre-Cretaceous age in certain instances has only be inferred due to the absence of Cretaceous xenolithic material.

2.3.2. Drybones Bay Kimberlite

The Drybones Bay kimberlite is located at the southwestern edge of the Slave Craton, some 300km from the Lac de Gras kimberlite field and 120km from the Cross Lake kimberlite. The intrusion is oval in plan, with an estimated surface area of 22ha. The kimberlite is intruded into an Archean age plutonic suite consisting of biotite tonalite, white granodiorite and minor inclusions of Yellowknife Supergroup metasediment. Three ages have been obtained from the intrusion. Ages were determined from mantle zircons. A concordant age of 441±2 Ma was obtained form the easternmost part of the intrusion, a discordant age of 485 Ma was obtained near the centre of the intrusion and one further Permian age of 270 Ma was also obtained (Kretschmar 1997).

Geological relationships within the Drybones Bay kimberlite are complex and are the subject of ongoing investigation. Both crater and diatreme faces kimberlite have been identified. The most abundant macrocrystal mineral within the intrusion is olivine, which may be fresh or serpentinized. Olivine may have pelletal rims and occur as aggregates in kimberlite autoliths. Ilmenite and phlogopite macrocrysts, eclogitic and pyrope garnet, chromite, minor calcite, pyrite, pyrrhotite, chalcopyrite and nickel sulphides exsolved from olivine are also common. Serpentine, chlorite, calcite and clay characterize secondary mineralogy. The fine-grained matrix is composed of predominantly serpentine, clays, calcite and chlorite (Kretschmar 1997).

2.3.3. Rockinghorse Lake

The Jericho kimberlite, located in the Rockinghorse Lake region and held under mineral claims belonging to Lytton Minerals Ltd. and New Indigo Resources, is a diamondiferous kimberlite intrusion located 400km northeast of Yellowknife. The Jericho kimberlite intrudes Archean granitic country rock and is overlain by 10 to 35m of glacial till. Mineralogically, Jericho is a typical non-micaceous kimberlite lacking groundmass phlogopite. Chemically, Jericho is classified as Group 1a, based on TiO_2, K_2O, Pb and SiO_2 abundances (Kopylova *et al.* 1998). Rb/Sr ages obtained from

phlogopite indicate Mid Jurassic (172 Ma) kimberlite emplacement (Heaman *et al.* 1997). This age is considerably older than the Late Cretaceous and Early Tertiary ages published for kimberlite intrusions in the Lac de Gras kimberlites, 100km to the south.

Based on logging of drill core (86 drill holes) and underground excavation, the Jericho kimberlite intrusion has been subdivided into three distinct phases. The earliest phase (Phase 1) is a hypabyssal kimberlite that forms a precursor dyke and occurs as autolithic fragments within the later phases of the kimberlite. Phases 2 and 3 kimberlites are pipe-shaped bodies whose textural characteristics suggest a diatreme facies-affinity (Kopylova *et al.* 1998).

Phase 1 kimberlite is a hypabyssal, macrocrystal, calcite serpentine kimberlite characterized by the presence of olivine, phlogopite, ilmenite, pyroxene and garnet macrocrysts. The groundmass is a mesostasis of anhedral calcite and serpentine enclosing euhedral microphenocrystal olivine and spinel, euhedral and skeletal apatite, phlogopite and euhedral perovskite and ilmenite. Phlogopite laths typically show marginal Ba-enrichment. The groundmass often displays a segregationary texture, hosting calcite segregations, globular and irregular in shape. Autoliths within the Phase 1 kimberlite are rare although aphanitic phlogopite kimberlite and macrocrystal serpentine calcite kimberlite fragments have been recognized (Kopylova *et al.* 1998).

Phase 2 and 3 kimberlites comprise macrocrystal, serpentine kimberlite. Phase 2 was the first kimberlite-forming event. It fills the carrot-shaped northern and southern lobes with steeply inward dipping (approximately 85°) contacts, typical of a diatreme, and hosts numerous autoliths of hypabyssal kimberlite (Cookenboo 1998). Phase 2 kimberlite is characterized by partially-to-completely serpentinized olivine macrocrysts set in an intensely serpentinized groundmass. In addition to olivine, macrocrysts of Cr-pyrope (lherzolitic) garnet, Cr-diopside, ilmenite, enstatite, eclogitic garnet, minor chromite and rare phlogopite. Well-preserved mantle xenoliths (ecolgite and lherzolite) and crustal fragments including fossiliferous (Middle Devonian) limestone are prevalent. Texturally, Phase 2 kimberlite is fragmental and characterized by the presence of minor pelletal lapilli (Cookenboo 1998).

Phase 3 kimberlite, a central volcanic vent between the northern and southern lobes, comprise macrocrystal, serpentine kimberlite characterized by the presence of fresh macrocrysts of olivine set in a matrix of serpentine, opaques and euhedral, primary carbonate. Phlogopite and ilmenite megacrysts are common. Numerous autoliths of hypabyssal kimberlite, essentially identical to Phase 1 kimberlite are present. Ten to fifteen percent crustal xenoliths, including limestone fragments characterize this phase. Pelletal lapilli are abundant, giving Phase 3 a more fragmental appearance than Phase 2 (Kopylova *et al.* 1998; Cookenboo 1998).

Cookenboo (1998) suggested that the northern lobe (Phase 2) formed after magma moving along the precursor dyke (Phase 1) vented to the surface through a now-eroded Paleozoic limestone cover. Rapid magma devolatization excavated a diatreme-shaped body down into the Archean basement. The southern lobe (Phase 2) is interpreted to have formed as a magmatic blow on the pre-existing dyke during the same emplacement event. The southern lobe may or may not have vented to the surface. The central volcanic vent (Phase 3) is thought to have coalesced into a single vent with the northern lobe at the time of emplacement before subsequent erosion to the current level.

Monopros Ltd. has discovered additional kimberlite bodies in the Rockinghorse Lake area. These include the Muskox intrusion that measures approximately 225x350 m. The Muskox intrusion is infilled by two texturally distinct kimberlites: fresh, dark-gray macrocrystal hypabyssal carbonate-bearing monticellite kimberlite, and paler coloured carbonate-poor tuffisitic kimberlite. The latter contains serpentinized olivine pseudomorphs and microlitic clinopyroxene in the inter-clast matrices. These textures are indicative of diatreme-facies kimberlite (Field and Scott Smith 1998). Transitional textures are also observed within the Muskox intrusion.

2.3.4. Kennedy Lake Kimberlites

At Kennedy Lake, located in the southeastern Slave Province on the Mountain Province-Camphor property, are four small kimberlite intrusions, including three new intrusions, discovered by Monopros Ltd. The four intrusions include both hypabyssal

kimberlite and diatreme facies, tuffisitic kimberlite breccias containing common pelletal lapilli and microlitic clinopyroxene (Field and Scott Smith 1998). The textures can be seen to be gradational from tuffisitic kimberlite breccia to hypabyssal kimberlite with depth, suggesting these intrusions represent the lower part of the diatreme-to-root-zone transition of the kimberlite. Lithic fragments found within these kimberlites appear to be granites and no evidence exists to suggest the presence of other capping rocks; a conclusion consistent with the regional geology (Field and Scott Smith 1998).

The 5034 intrusion is an irregular kidney-shaped kimberlite in plan view, consistent with the suggestion that these intrusions represent lower diatreme-root-zone material. The 5034 kimberlite is characterized by olivine and minor orthopyroxene macrocrysts set in a groundmass of serpentine, calcite, apatite, perovskite and chrome spinel (Pell 1997; Carlson *et al.* 1998). Whole rock geochemistry suggests that 5034 is similar to Group 2 kimberlite (orangeite) and micaceous olivine lamproites (Cookenboo 1996; Carlson *et al.* 1998). However, Field and Scott Smith (1998) proposed that this is in fact an artifact of modification of the magma composition by xenolith digestion and 5034 (and the three recently discovered kimberlites) are typical of Group 1 kimberlite. Isotopic studies on groundmass phlogopite have yielded a reportedly precise Rb/Sr isochron of 538.6 ± 2.5 Ma (Carlson *et al.* 1998).

2.3.5. Camsell Lake Kimberlites

The Camsell Lake kimberlites occur south of Lac de Gras, on the Winspear Resources Ltd.-Aber Resources Ltd. The CL25 intrusion at Camsell Lake is a small vent of some 100-150 m x 50 m in dimension, intruding granitic basement rock. The intrusion is infilled primarily by homogeneous tuffisitic kimberlite breccias, characteristic of diatreme facies rock. Pelletal lapilli and microlitic textures are noted, indicating diatreme formation processes did occur (Field and Scott Smith 1998). Rare, non-granitic xenoliths of unknown parentage have been observed. Some kimberlite has textures transitional between typical hypabyssal and tuffisitic diatreme rock. Again, these features suggest that this intrusion represents the lower part of the diatreme-root zone, as seen in the

deeper parts of the southern African-style diatreme-bearing kimberlite vents (Field and Scott Smith 1998). Age determinations for CL25 have yet to be satisfactorily completed, therefore, it is not possible to comment on the nature of the country rock setting at the time of emplacement.

2.3.6. Cross Lake and Upper Carp Lake

The Cross Lake kimberlite is located on Ashton-Pure Gold property in the southwestern portion of the Slave Structural Province. It is small, <2 ha in size, and is comprised of heterolithic kimberlite breccia. A radiometric age of 450 Ma has been obtained for the Cross Lake kimberlite (Pell 1997). The olivine population is generally serpentinized and the xenocrystal suite is dominated by ilmenite together with common tetraferriphlogopite and spinel (Pell 1997). Lithic fragments characterizing these breccias include predominantly granitoid and Mid-Paleozoic carbonate rock fragments. Therefore, the country rock geology at the time of emplacement comprised carbonate overlying the Archean basement terrain, and kimberlite diatremes developed (Field and Scott Smith 1998). This kimberlite has been referred to as crater- and diatreme-facies, however no further details are available.

Upper Carp Lake, located southwest of Lac de Gras and slightly northwest of the Cross Lake kimberlite, is the location of the Monopros kimberlites, Jean and Rich. The Jean and Rich kimberlites are comprised of tuffisitic kimberlite breccia containing juvenile pelletal lapilli. Hypabyssal kimberlite is also present. Lithic fragments include both limestone and other fine-grained sediments (Field and Scott Smith 1998). The ages of these kimberlites are not known. Again, according to Field and Scott Smith (1998), the presence of limestone xenoliths suggests that at the time of emplacement, Paleozoic carbonates capped the Archean basement and kimberlite diatremes may have formed.

2.3.7. Summary of the Pre-Cretaceous kimberlites of the Slave Province

In contrast to the Lac de Gras field, kimberlites outside the Lac de Gras area appear to be pre-Cretaceous in age (many known, some inferred) and hence pre-date the Cretaceous sediments that formed in the Lac de Gras area. These areas were comprised of Archean basement with or without a Paleozoic limestone cap rock at the time of kimberlite emplacement. Although both volcaniclastic and hypabyssal kimberlite are also present, the situation was such that small diatremes were developed. These diatremes seem to be analogous, but smaller, then their southern African counterparts and are infilled with the diagnostic tuffisitic kimberlite breccias (Field and Scott Smith 1998). Figure 2.4 shows idealized sections of the Cretaceous Lac de Gras kimberlites and the Pre-Cretaceous kimberlites of the Slave Province. At Drybones Bay, both xenoliths and therefore cover rocks at the time of emplacement differ from both Cretaceous and pre-Cretaceous kimberlites of the Slave Province and the above described situation may to apply to this intrusion (Field and Scott Smith 1998).

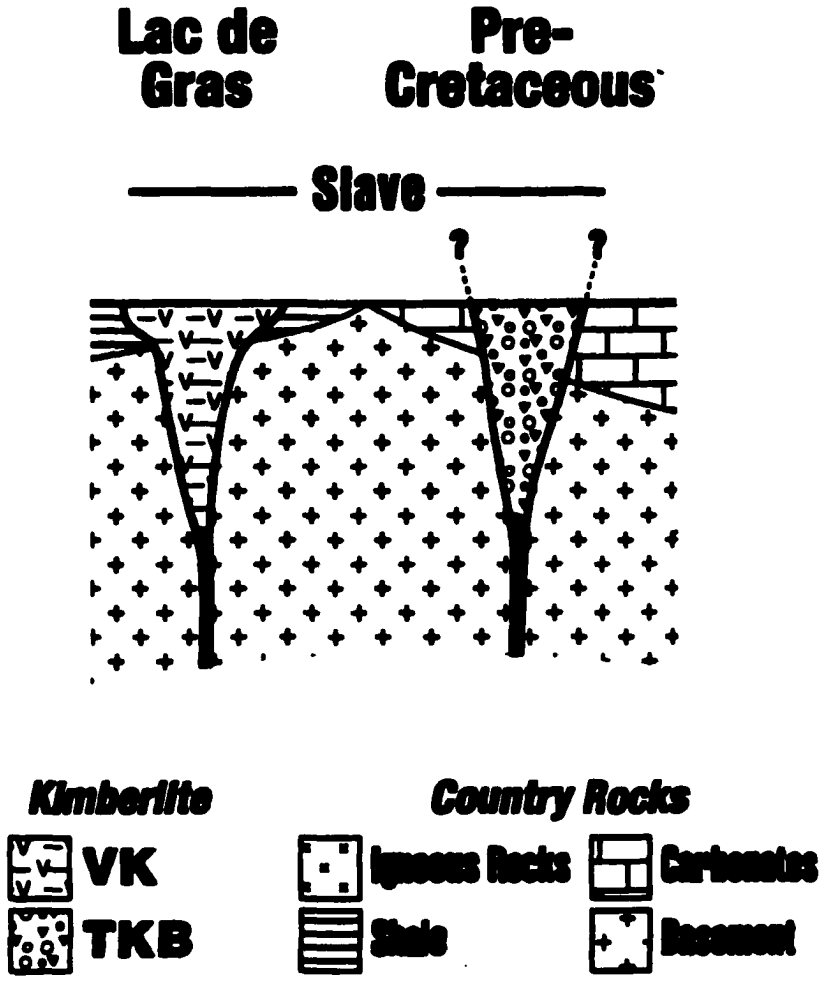

Figure 2.4. A schematic section showing the geological setting and infill characteristics of the Cretaceous kimberlites of Lac de Gras and the pre-Cretaceous kimberlites of the Slave province. VK=volcaniclastic kimberlite; TKB=tuffisitic kimberlite breccia (after Field and Scott Smith 1998).

CHAPTER 3. KIMBERLITES OF THE LAC DE GRAS AREA

3.1. INTRODUCTION AND LOCATION

Twenty separate kimberlite intrusions were examined in detail during this study. Nineteen of these kimberlite intrusions occurred on claims held by Diavik Diamond Mines Inc. (DDMI), Aber Resources Ltd., and SouthernEra Resources, on property located on southeastern Lac de Gras, approximately 300 kilometres northeast of Yellowknife (Figure 3.1). The Diavik claim block, originally encompassing 230 400 hectares, was staked by Aber Resources Ltd. and partners in late 1991 and early 1992. In 1992, a joint venture was formed between Aber and partners and Kennecott Canada Inc. (now Kennecott Canada Exploration Inc.) to explore the Diavik claims. DDMI was established in 1996 to develop the joint venture prospects. The property is held 60% by DDMI and 40% by Aber. The final kimberlite (DD39) is located on a mineral claim located on the western shore of Lac de Gras (refer to Figure 3.1), held by the DHK joint venture whose ownership consists of Kennecott Canada Exploration Inc. (KCEI), DHK (Dentonia Resources Ltd., Horseshoe Gold Mining Inc. and Kettle River Resources Ltd.) and SouthernEra.

Exploration on the Diavik claims has discovered over 50 kimberlite occurrences and dozens more have been discovered on adjacent claims held by DDMI or KCEI and partners. Exploration processes rely upon airborne and surface geophysical surveys and sampling of the glacial regolith for kimberlitic heavy mineral indicators and subsequent confirmation drilling.

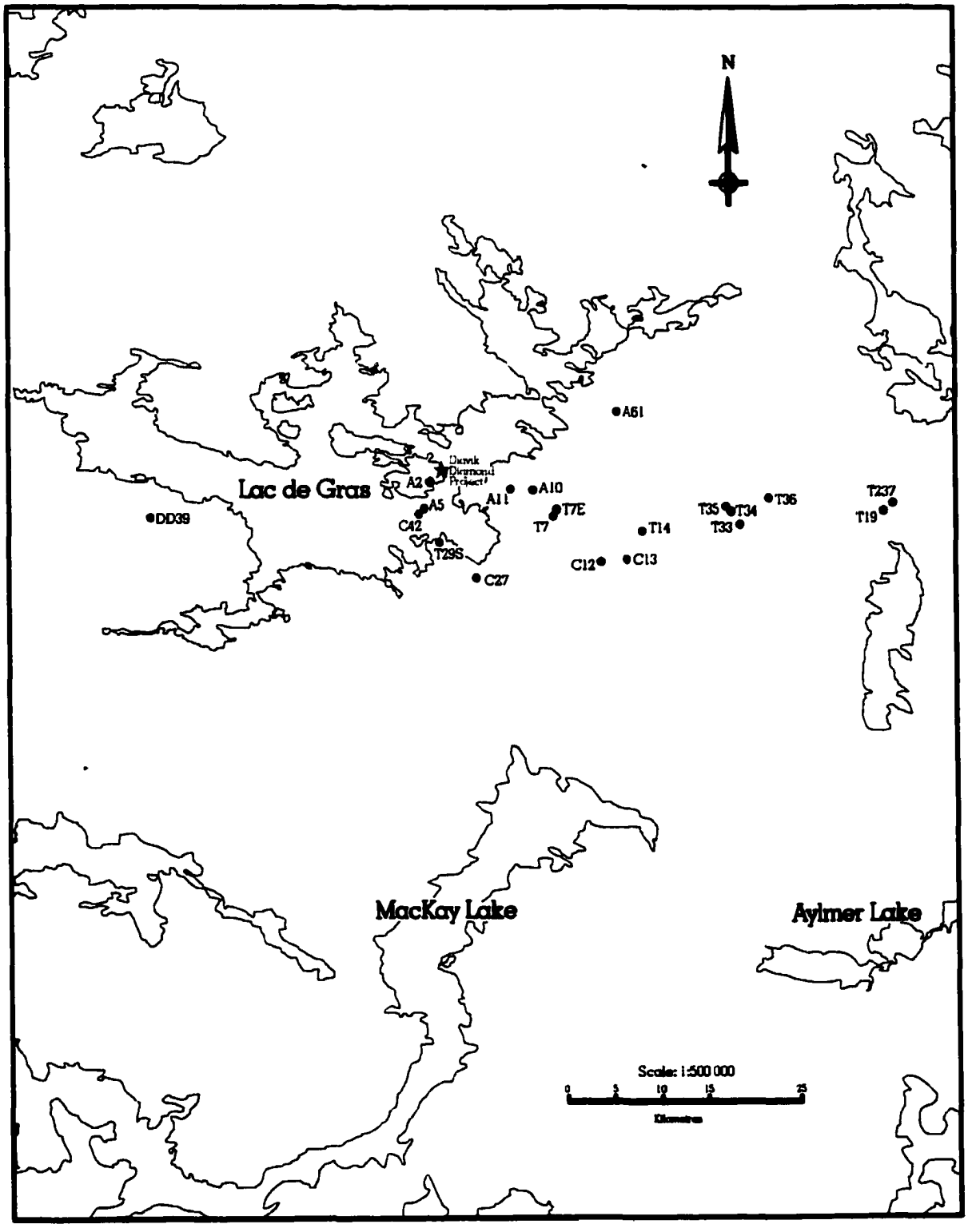

Figure 3.1. *Location of kimberlites reviewed in this study.*

3.2. PETROGRAPHY OF THE LAC DE GRAS KIMBERLITES

3.2.1. Kimberlite A5

Kimberlite A5 was discovered and drilled in 1994. A5, a bathymetric feature, is located beneath the waters of Lac de Gras, approximately one kilometre south of the Ekadi shoreline, the location of the Diavik Diamond Project (refer to location map, Figure 3.1).

Kimberlite A5 lies beneath nearly 20m of lake water and is overlain by up to 25m of glacial regolith. Ground magnetic surveys have revealed a 110x150m, nearly circular 40nT magnetic low. No significant electromagnetic signature is present. A5 intrudes Archean granite-granodiorites that are veined with pegmatites of granite-to-quartz syenite composition.

Data from two drill holes indicated that kimberlite occurs to a maximum depth of 171m below the present surface. Drill hole 94A5-1 was studied macroscopically and microscopically (refer to Appendix for a complete macroscopic drill hole log).

3.2.1.1 Macroscopic Observations

Macroscopically, kimberlite A5 is complex. Drill hole 94A5-1 is a vertical hole into the centre of the magnetic anomaly. The hole collared a volcaniclastic kimberlite unit (Unit#1), approximately 30m in vertical thickness. Much of this material is poorly consolidated and very incompetent; prevalent oxidation staining on open fracture surfaces suggests groundwater infiltration has occurred. The highly altered unit appears to be a matrix-supported kimberlite breccia with abundant rounded pseudomorphed macrocrystal olivines and numerous smaller, similarly altered microcrystal olivines. Rare macrocrysts of chrome diopside and garnet are present. Mudstone xenoliths (up to 5 cm in dimension) and large granodiorite fragments (up to 45 cm in length along the core axis) become more prevalent near the bottom of Unit#1. The volcaniclastic kimberlite overlies a unit or xenolith of 2.8 m in thickness (along the core axis) of dark gray.

massive, non-kimberlitic mudstone. Beneath the mudstone lies a large (inferred) granodiorite xenolith. This rock is quite incompetent, as it is highly oxidized and marginal carbonatization is extensive.

Beneath this large xenolith lies a normal-graded, volcaniclastic kimberlite unit containing common, large, highly altered granodiorite xenoliths. The bottom of this unit is marked by an abrupt increase in the concentration and size of olivine grains (Unit#2). Unit#2 may represent a small kimberlite sill of approximately 20 cm in thickness. Beneath Unit#2 lies another large granodiorite xenolith. This xenolith is approximately 20 m in thickness and shows minimal marginal alteration/reaction with host magma. A small, highly competent macrocrystal kimberlite dyke characterized by an olivine population of both fresh macrocrystal and microphenocrystal olivines cuts this xenolith. This inequigranular character imparts a "pseudoporphyritic" texture to the dyke.

The xenolith overlies approximately 10 m of "bedded" kimberlite. The unit is characterized by the alternation of two distinctly different kimberlite units ranging in thickness from 4 m to less than 30 cm. Both units in each "doublet" are of approximately the same thickness. The upper unit (Unit#4) in this pair is essentially identical macroscopically to Unit#3, that is, a very competent, probable hypabyssal kimberlite composed of approximately 15% fresh, rounded olivine macrocrysts and a distinct population of fresh subhedral-to-euhedral microphenocrystal olivines. No xenoliths or cognate fragments were observed. Unit#3 overlies a much darker, finer-grained volcaniclastic kimberlite (Unit#5) which is very similar to Unit#1. Unit#5 is altered and much less competent than Unit#4. It is characterized by the presence of approximately 10% rounded olivine pseudomorphs and common lithic and cognate fragments. The contacts between Unit#4 and Unit#5 are very sharp and range from 60-70 degrees to the core axis.

The final 15 m of kimberlite intersection within this hole consists of very competent, massive hypabyssal kimberlite (Unit#6) that is very similar to both Units#3 and #4. Abundant, relatively fresh, rounded olivine macrocrysts and numerous fresh-to-partially altered, subhedral-to-euhedral microphenocrystal groundmass olivines

characterize this unit. Oxidation staining on open fracture surfaces is common. Cognate and lithic fragments were not observed.

The drill hole exits kimberlite at a depth of 171.2 m and ends 28 m into the host granodiorite. This rock ranges widely in mineralogy and texture and may be considered locally a syenite, tonalite or a granite pegmatite.

3.2.1.2. Microscopic Observations

3.2.1.2.1. Unit #1

Unit #1 is comprised of numerous, lapilli-sized, well-rounded-to irregular-shaped cognate clasts (matrix-supported) (Figure 3.2). At their core, many clasts contain a spherical-to-ovoid macrocrystal olivine pseudomorph (calcite and serpentine after olivine) set in a groundmass consisting of many microphenocrystal olivines, euhedral-to-subhedral spinels in a tan matrix of serpentine and calcite. Elongated groundmass constituents may be tangentially oriented about the olivine macrocryst. One clast contains dark brown macrocrystal kimberlite at its core and is mantled by a rind of microporphyritic kimberlite as described above. This kimberlite mantle is a different colour than the core, however the mineralogy appears identical and resembles a chilled margin (refer to Figure 3.2). The margins of this clast are highly irregular. Some clasts to not contain a core. These microcrystal kimberlite clasts are irregular-to-amoeboid in shape and display irregular outlines. These fragments are considered to be juvenile lapilli.

The groundmass is characterized by the presence of numerous microphenocrystal olivine pseudomorphs. These olivines are commonly mantled by a relatively thick rind of fine-grained kimberlite, essentially identical to mantle material of the larger clasts. Microphenocrystal olivine, together with numerous subhedral-to-euhedral spinels (chromite, Ti-magnetite, spinel) and minor phlogopite are set in a sugary, granular-textured matrix that consists of very fine-grained, partially altered monticellite (serpentine after monticellite) set in an intergrowth of calcite and serpentine.

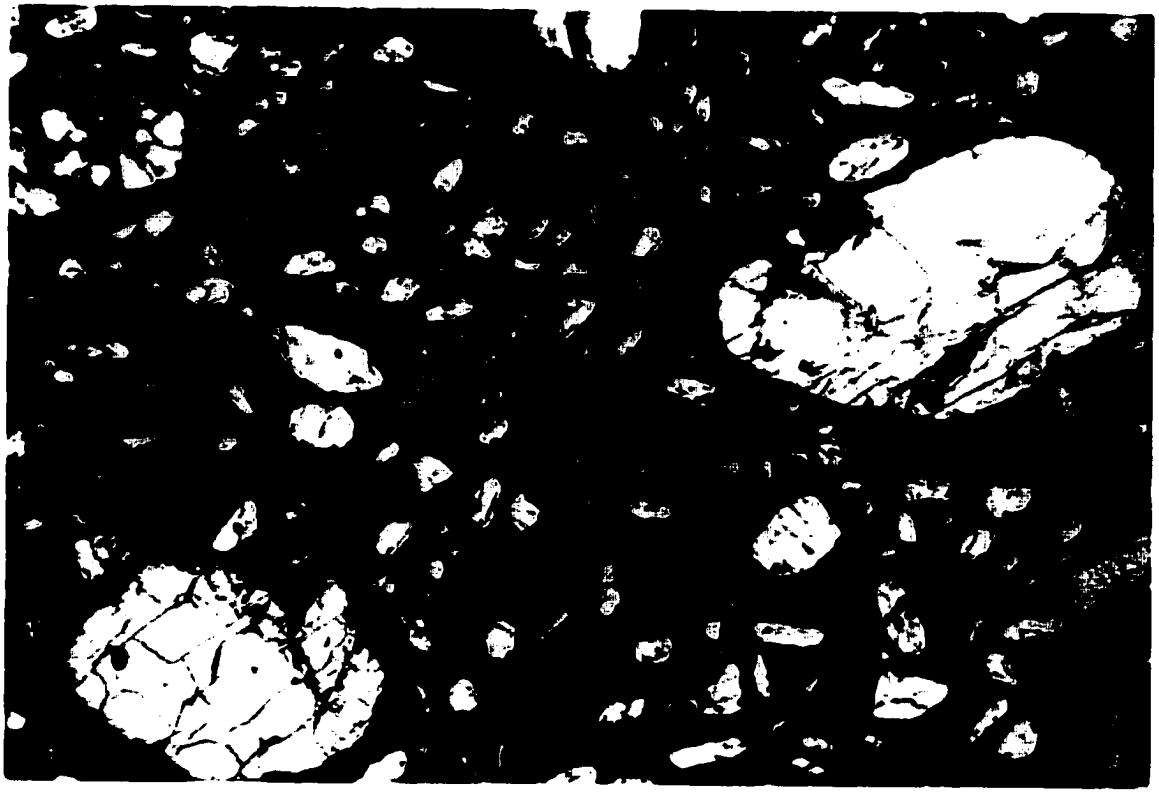

Figure 3.2. Kimberlite A5, Unit#1. Matrix-supported breccia consisting of numerous microphenocrystal juvenile kimberlite fragments (J). Note the large "zoned" fragments consisting of a dark core with a large subhedral olivine phenocryst (O) at its core mantled by a light coloured kimberlite nearly devoid of olivine. This rim appears to be a chilled margin (F.O.V. 6.0 mm).

Figure 3.3. Kimberlite A5, Unit#3. Segregation-textured macrocrystal hypabyssal kimberlite characterized by numerous small irregular-shaped segregations (S) filled with serpophitic serpentine (F.O.V. 6.0 mm).

Numerous calcite-filled cracks run through the section. No lithic fragments were observed on a microscopic level.

3.2.1.2.2. Unit #2

Unit #2 is an intensely and pervasively altered. This alteration eliminates nearly all of the primary texture.

The rock contains numerous large, rounded olivine macrocrysts altered to a yellow-brown (serpophitic) serpentine. A small relict core may remain. Calcite replacement is generally confined to cracks and margins.

The groundmass is characterized by numerous pseudomorphed microphenocrystal olivines. Microphenocrystal olivines are similarly altered to macrocrysts, *i.e.* replacement consists nearly entirely of yellow-brown serpophitic serpentine with calcite alteration confined to margins. Discontinuous spinel necklaces may mantle these olivines. Other groundmass constituents include euhedral-to-subhedral, discrete crystals, and complex atoll, abundant euhedral pyrite, and minor perovskite, set in a granular-textured matrix of fresh monticellite and minor phlogopite within a very fine-grained mesostasis of calcite and serpentine.

Lithic or cognate fragments were not observed at a microscopic level.

3.2.1.2.3. Unit #3

Unit #3 contains numerous large ovoid olivine macrocrysts. These are essentially unaltered by are veined by pale yellow serpentine. Minor marginal serpentinization is also common. Smaller, subhedral-to-rounded microphenocrystal groundmass olivines are abundant. These are generally fresh or partially serpentinized.

The groundmass consists of numerous, fine-grained opaque spinels (chromite, Ti-magnetite), perovskite, minor ilmenite, numerous sprays of prismatic apatite and common resorbed euhedral calcite. Groundmass phlogopite is not present. These are set

in a granular-textured mesostasis consisting of monticellite, which may be partially replaced by dolomite, set in a very fine-grained intergrowth of calcite and serpentine.

Numerous irregular segregations consisting primarily of yellow-brown serpophitic serpentine (Figure 3.3). Rhombs of euhedral calcite commonly occur at the margins of these segregations.

Cognate clasts, country rock xenoliths and xenocrysts are not present.

3.2.1.2.4. Unit #4

Unit#4 is nearly identical to Unit#3 and is characterized by numerous large, rounded olivine macrocrysts that are essentially unaltered. Minor replacement by pale yellow serpentine along cracks and margins is common. Numerous small, rounded, subhedral microphenocrystal olivines are abundant. As above, these are virtually unaltered, with minor replacement by pale yellow serpentine along small cracks. Microphenocrystal olivines appear to have a preferred orientation which is presumably the result of flow differentiation (Figure 3.4).

The groundmass is composed of numerous subhedral-to-euhedral discrete and complex atoll spinels. Discrete spinels include Mg-chromite, chromite, Ti-magnetite and spinel-hercynite. Atoll spinels are composed of a core of chromite and are mantled by Ti-magnetite. Other minor groundmass constituents include perovskite, apatite and small crystals of pyrite. The above mineral assemblage is set in a granular-textured mesostasis consisting of a fine-grained intergrowth of calcite and serpentine in which are set numerous crystals of phlogopite and many small crystals of partially altered monticellite. Monticellite is replaced at its core by serpentine and commonly poikilitically encloses small crystals of pyrite.

3.2.1.2.5. Unit #5

Contains common rounded-to-subrounded, ovoid olivine macrocrysts. These may have a small relict core, but are generally completely replaced by pale yellow and

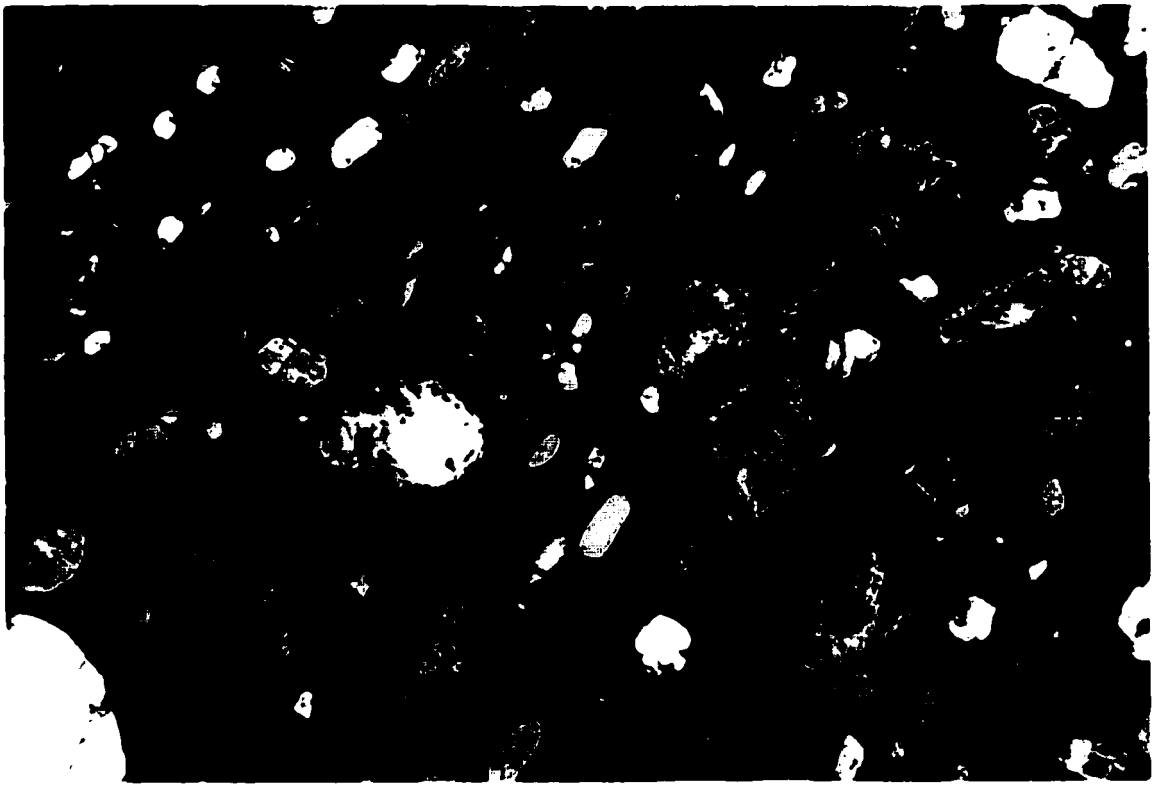

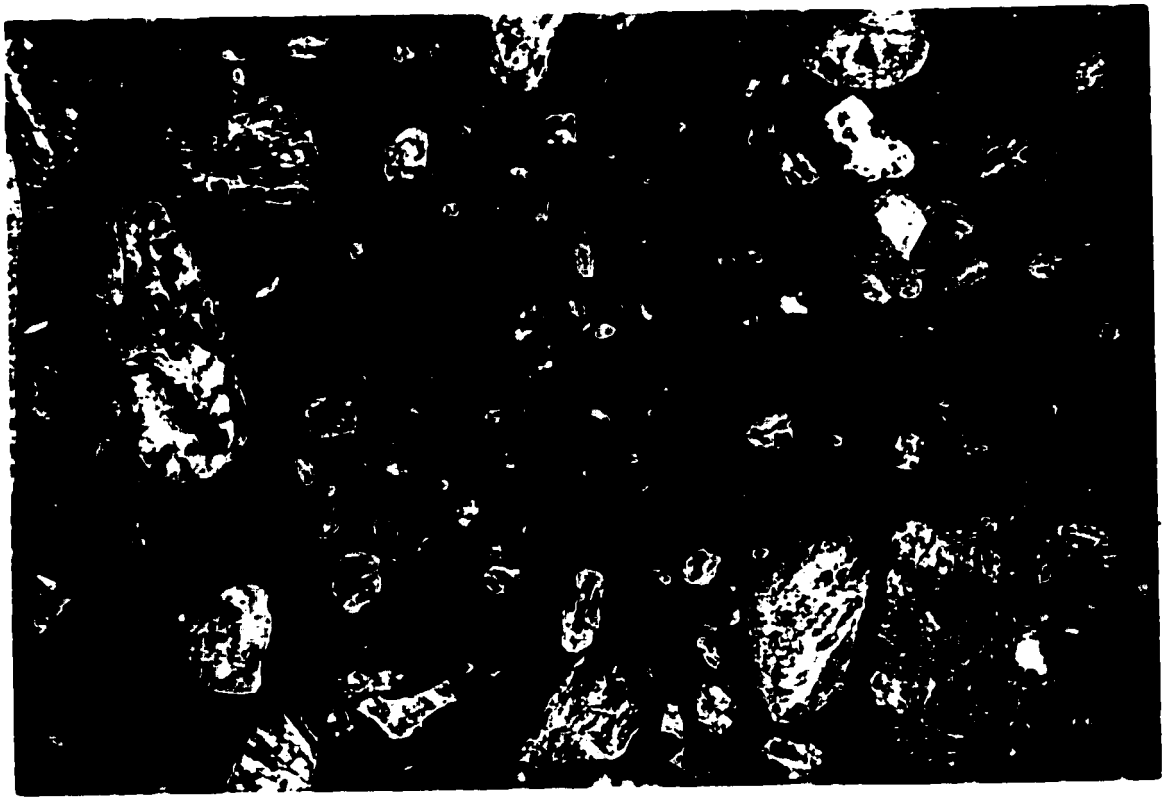

Figure 3.4. Kimberlite A5, Unit#4. Macrocrystal hypabyssal kimberlite showing flow alignment of primary microphenocrystal groundmass olivine (O) (F.O.V. 6.0 mm).

Figure 3.5. Kimberlite A5, Unit #5. Matrix-supported kimberlite breccia. Larger microphenocrystal fragments are considered to be autoliths (A) while small, dark-brown irregular fragments are juvenile lapilli (J) (F.O.V. 6.0 mm).

colourless serpentine. Smaller subhedral-to-subrounded olivines occur throughout the groundmass. These are completely replaced by serpentine. Olivine crystals commonly poikilitically enclose small crystals of magnesiochromite.

This section is characterized by abundant microporphyritic kimberlite clasts, typified by the presence of numerous microphenocrystal olivine and common, large, subhedral opaque Ti-magnetite. Smaller spinels and minor pyrite are set in a fine-grained, pale-green matrix of calcite and serpentine. Single, large olivine macrocrysts may core these clasts. The outer margins of the clasts are irregular-curvilinear and may contain broken crystal fragments, which suggests they were in fact solid upon incorporation into their current host. These clasts are considered to be autoliths of macrocrystal hypabyssal kimberlite (Figure 3.5).

A second group of subangular, dark brown, fine-grained kimberlite clasts characterize this unit (refer to Figure 3.5). These are smaller than the above-described kimberlite fragments and contain small, altered olivines, minor crystals of mica and subhedral, opaque spinels.

The groundmass consists of common discrete, subhedral-to-euhedral spinels, minor perovskite, rare xenocrystal biotite and minor apatite. These are set in a granular-textured matrix consisting of a very fine-grained intergrowth of calcite and serpentine and abundant crystals of phlogopite (which are commonly replaced by calcite) and many small crystals of monticellite, which may be partially replaced by serpentine and dolomite (Figure 3.6).

3.2.1.2.6. Unit #6

Unit #6 contains numerous large, rounded, relatively fresh olivine macrocrysts, which are veined and mantled by serpentine, and abundant smaller, subhedral-to-euhedral microphenocrystal olivine. The latter are fresh with minor serpentinization along cracks and margins. Olivine concentration throughout the section is not homogeneous and microphenocrystal olivines have an ill-defined preferred orientation, which is considered to be the result of flow differentiation.

Figure 3.6. Kimberlite A5, Unit#5. BSE-image of the groundmass of Unit#5, which consists of abundant monticellite (M) replaced by calcite and serpentine, common laths of phlogopite (P), perovskite (pink) and spinel (pink) set in predominantly calcite (F.O.V. 60 μm).

The oxide-rich groundmass consists of numerous subhedral-to-euhedral, discrete spinels, including abundant Ti-magnetite and resorbed, donut-shaped magnetite. Minor perovskite, apatite, xenocrystal biotite, prismatic pyrite and rare Fe-Ni-sulphides also occur throughout the groundmass. The groundmass is characterized by abundant, small, irregular-shaped segregations consisting of coarse calcite, which is commonly replaced by dolomite.

The above minerals are set in a granular-textured matrix consisting of a fine-grained intergrowth of calcite and serpentine in which are set numerous small crystals of monticellite (commonly partially replaced by calcite at its core and serpentine along its margins) and numerous intergrown crystals of phlogopite.

3.2.1.3. Discussion

Kimberlite A5 is quite complex. Unit#1 has a fragmental texture and contains *bona fide* juvenile lapilli and possible minor autolithic fragments. It is considered to be a resedimented volcaniclastic kimberlite that has undergone a moderate amount of reworking. The mudstone units that Unit#1 overlies may be a large xenolith of down-rafted Cretaceous sediment or may represent a laterally continuous bed of mudstone which was deposited during a hiatus in vent infill. Beneath this mudstone unit lies Unit#2. Although this unit contains common large granodiorite xenoliths on a macroscopic level, none were observed in thin section. This unit is difficult to classify due to the pervasive prograde carbonatization, however no features suggest that this rock is either a tuffisitic kimberlite of the diatreme facies or volcaniclastic kimberlite. It is likely to represent hypabyssal kimberlite.

Unit #3 is undoubtedly a segregation-textured macrocrystal hypabyssal monticellite kimberlite. This kimberlite dyke occurs at a relatively high structural level within the vent and likely represents a sill which intruded the vent subsequent to its emplacement and infilling.

Beneath these units bedded kimberlite in which Units#4 and #5 alternate. Unit#4, both macroscopically and microscopically appears nearly identical to Unit#3, however,

Unit#4 does not display a segregation-texture and minor, highly altered xenoliths do occur. Unit#5, conversely, is a resedimented volcaniclastic kimberlite containing abundant cognate fragments, both autoliths and juvenile lapilli. Unit#4 is either a large hypabyssal autolith or a post-eruptive kimberlite sill. Units#4 and #5 overlie massive macrocrystal hypabyssal segregation-textured monticellite kimberlite. Only 20m of this hypabyssal rock was intersected when the host rock, granodiorite was encountered.

The presence of numerous large granodiorite xenoliths within this vent suggests that emplacement was quite violent to dislodge and incorporate such large blocks of country rock.

In summary, kimberlite A5 represents a kimberlite vent infilled with resedimented volcaniclastic kimberlite, which contains abundant juvenile lapilli, common autolithic fragments and minor mudstone clasts. A hiatus in infill may have occurred in which a non-kimberlitic mudstone unit was deposited. Subsequent to emplacement and infill, the kimberlite vent was intruded by a small hypabyssal sill.

3.2.2. Kimberlite A2

Kimberlite A2 is located approximately five hundred metres south of Ekadi Island beneath the waters of Lac de Gras, just north of kimberlite A21 of the Diavik Diamond Project. A2 is characterized by a strong elongated electromagnetic anomaly, striking southwest-northeast with approximate dimensions 300 x 75 m. A coincident circular, weak magnetic low also occurs, with a diameter of approximately 140 m.

Kimberlite A2 lies beneath 15-20 m of water and is overlain by 5-10 m of glacial regolith. A2 is hosted by granite-granodiorite and biotite schist.

Two exploration diamond drill holes delineated the shape of A2. Both were vertical and intersected kimberlite to a maximum depth of 170m.

3.2.2.1. Macroscopic Observations

Drill hole A2-2 was investigated. This hole was drilled into the electromagnetic anomaly and was offset approximately 75m to the southwest of the magnetic anomaly. A2-2 collared granitic rock at a depth of 27m, intersecting kimberlite at 53 m. Two units are found to infill this vent: an intensely altered volcaniclastic kimberlite breccia (Unit#1) and a non-kimberlitic mudstone (Unit#2). Units #1 and 2 vary in thickness from less than one metre to approximately 34 m in vertical thickness. Few contacts are preserved; observed contacts were dipping at 45 degrees to the core axis.

The volcaniclastic kimberlite breccia occurs as relatively homogeneous units with vague bedding defined by the change in concentration of olivine macrocrysts. Unit#1 is intensely altered, consisting of 10-15% serpentinized, fragmental olivine together with approximately 10-20% lithic clasts (predominantly granitoids and less abundant biotite schists). Relatively fresh xenocrystal quartz and feldspar are ubiquitous, as are relatively fresh macrocrystal micas. The mica is considered to represent xenocrystal biotite derived from the disaggregation of country rock. Rare rounded-to-subrounded mudstone xenoliths and small angular wood fragments are present.

Unit#2 is a massive, featureless mudstone with no recognizable kimberlite constituents.

Granite is intersected at a depth of approximately 170 m, the lower contact of the kimberlite with the host rock is sharp at approximately 70 degrees to the core axis.

3.2.2.2. Microscopic Observations

3.2.2.2.1. Unit#1

Unit#1 is an intensely altered kimberlite containing little identifiable primary mineralogy. Indistinct, subrounded-to-subangular olivine relicts occupy approximately 5-15% of the rock and are replaced by a combination of serpentine and carbonate.

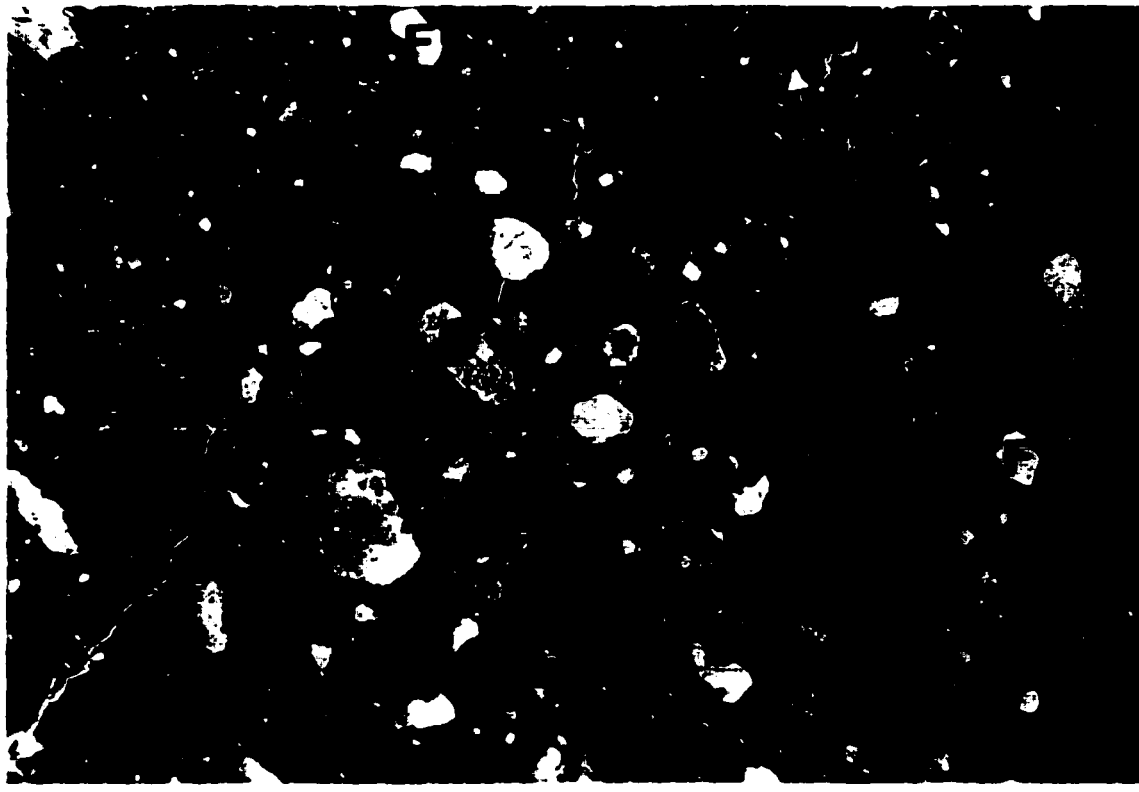

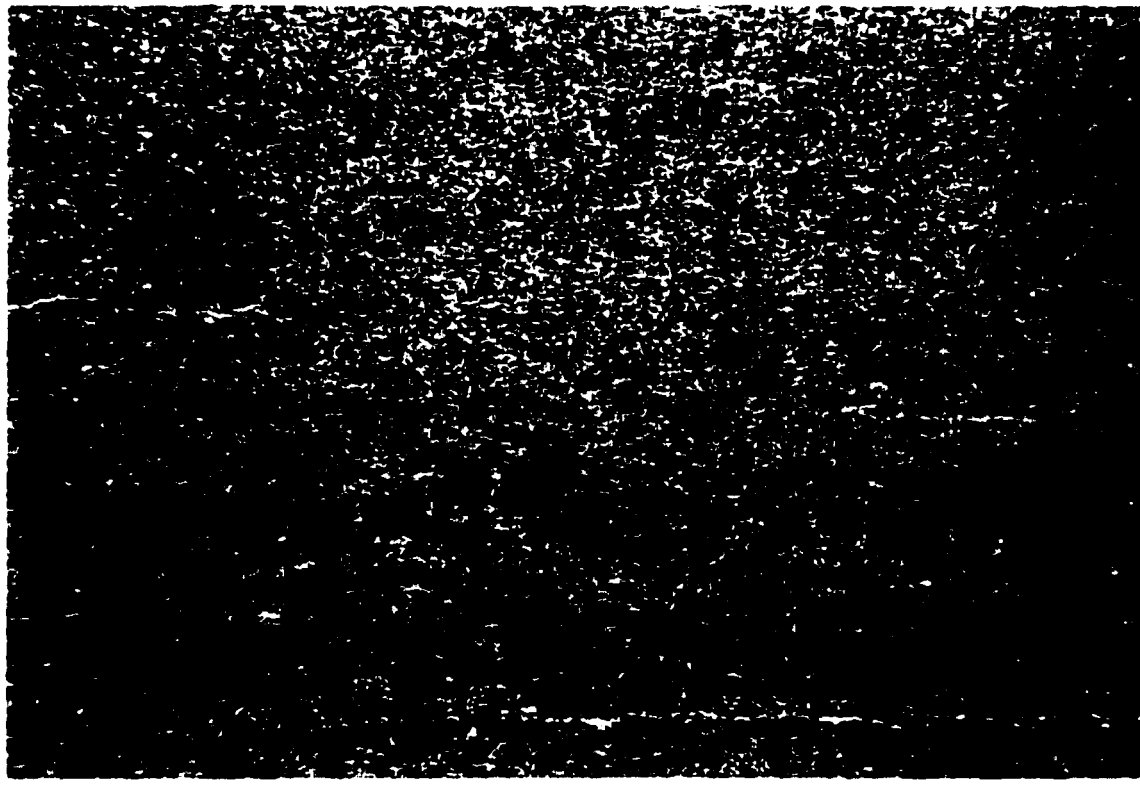

Reproduced with permission of the copyright owner. Further reproduction prohibited without permission.

Figure 3.7. Kimberlite A2, Unit#1. Resedimented volcaniclastic kimberlite consisting of kimberlitic juvenile fragments (dark brown), altered grains of olivine (O) and abundant xenocrystal feldspar (F) set in a turbid matrix (F.O.V. 6.0 mm).

Figure 3.8. Kimberlite A2, Unit#2. Well-laminated non-kimberlite mudstone (F.O.V. 6.0 mm).

Fragments, both lithic and kimberlitic are abundant. Lithic fragments include fresh-to-altered, subangular-to-subrounded clasts of mica schist. Xenocrystal fragments of feldspar, biotite and (less commonly) quartz are abundant and may occupy up to 10% of the rock. Rounded, very fine-grained brown clasts are abundant. No kimberlitic constituents are recognizable and some clasts may retain a vague lamination. These clasts are likely non-kimberlitic mudstone xenoliths. Kimberlite clasts are also quite common and occur as dark brown, very fine-grained, ash-to-lapilli-sized, amoeboid-shaped fragments containing small microcrystal olivine pseudomorphs, minor opaques and mica. Their morphology suggests that they are juvenile lapilli (Figure 3.7).

The above is set in a matrix containing relatively fresh mica (likely xenocrystal biotite), small crystals of feldspar, quartz, opaque spinels, sulphides and apatite. The mesostasis is a turbid mixture of calcite and serpentine.

Unit#1 is considered to be a resedimented volcaniclastic kimberlite breccia, or possibly a metachronous volcanogenic kimberlite.

3.2.2.2.2. Unit#2

Unit#2 is a well-laminated mudstone containing no kimberlite-derived constituents (Figure 3.8). Optical studies proved futile as few mineralogical constituents could be recognized other than mica. Unit#2 does not exhibit any grading or bedding and rather it is massive.

3.2.2.3. Discussion

Kimberlite A2 appears to be a relatively small kimberlite vent, which has erupted and subsequently been infilled with resedimented volcaniclastic kimberlite breccias and non-kimberlitic (possibly water-lain) sediments. Very little sorting can be detected within the resedimented volcaniclastic units suggesting they were deposited as a turbidity flow into the vent. This is further supported the inward-inclination of observed bedding contacts.

No *in situ* pyroclastic kimberlite or associated hypabyssal kimberlite was encountered, although the offset magnetic anomaly may be associated with the presence of hypabyssal kimberlite in another location within the vent.

3.2.3. Kimberlite A10

Kimberlite A10 is located approximately 3.5 kilometres off the eastern shore of Lac de Gras (refer to Figure 3.1) on a claim held by joint venture partners Diavik Diamond Mines Inc. and Aber Resources Ltd.

Kimberlite A10 lies beneath 2-3 m of lake waters and is overlain by 14-15m of glacial regolith. Ground magnetic and electromagnetic surveys have been conducted over A10. A10 is characterized by a 50nT EM low, 50x80 m in dimension. No magnetic signature is present. The ground EM survey suggests that A10 is an oval-shaped intrusion in plan and is approximately 0.2-0.5 ha in surface area.

A10 intrudes into biotite schists (metamorphosed sediments of the Yellowknife Supergroup) with common pegmatite veins of granitic composition. Four holes have been drilled into A10 to date, intersecting kimberlite to a maximum depth of 254.0 m below the present surface. Drill hole 95A10-1 was studied both macroscopically and microscopically (refer to Appendix for a complete drill log).

3.2.3.1. Macroscopic Observations

Macroscopically, kimberlite A10 appears to be a relatively incompetent, easily exfoliated, dark gray-green altered kimberlite characterized by the presence of 5-25%, relatively inequigranular, rounded-to-fragmented olivine macrocrysts which are intensely altered to pale green serpentine and minor calcite. Olivine concentration is not homogeneous throughout the hole. This sorting of olivine defines massive beds, however, these contacts are not sharp and units are gradational.

Lithic clasts are present, but occupy less than 5% of the kimberlite. Granitoid clasts are the most prevalent, followed by schist and rare mudstone fragments. Farther downhole, large granitic xenoliths of up to 1.5 m in length (along the core axis) are common. Reaction of country rock fragments with host-kimberlite appears to be minimal. Blackened wood fragments are rare, but present.

Subrounded-to-rounded cognate clasts are common reaching sizes of up to 7 cm. The content of cognate fragments gradually increased downhole. Relatively fresh crystals of xenocrystal biotite and muscovite are common within the groundmass.

3.2.3.2. Microscopic Observations

All sections are similar in both texture and mineralogy with the only obvious differences being olivine and clast (both lithic and kimberlitic) content (Figures 3.9 and 3.10).

Kimberlite A10 is an intensely and pervasively altered kimberlite characterized by abundant macrocrystal and small microcrystal and microphenocrystal olivines. Macrocrystal olivines are quite large (up to 10mm), rounded, spherical-to-ovoid crystals that are completely replaced by brown-green serpophitic serpentine and veined with colourless calcite. Macrocrystal olivine pseudomorphs may be mantled by dark brown, fine-grained microporphyritic kimberlite. Smaller groundmass olivines are subrounded-to-subhedral in nature and are similarly altered to their macrocrystal counterparts.

Kimberlitic clasts are common, but not abundant. Two different types of fragments occur within kimberlite A10: microporphyritic, ash-to-lapilli sized clasts characterized by highly altered microphenocrystal olivines, small crystals of relatively fresh xenocrystal mica and common opaque oxides set in a serpentine-calcite mesostasis. Their outlines are irregular-curvilinear resulting in amoeboid-shaped clasts (refer to Figure 3.10). These fragments are interpreted as juvenile lapilli. The second type of clasts noted are large, rounded microporphyritic autolithic fragments. These are not commonly seen in thin section but appear to be quite common within drill core.

Figure 3.9. Kimberlite A10. Highly fragmental kimberlite composed of abundant rounded-to-angular serpentinized olivine grains (O), minor kimberlitic fragments (F) (difficult to see) in a brown turbid matrix of serpentine and calcite (F.O.V. 6.0 mm).

Figure 3.10. Kimberlite A10. Tightly-packed fragmental heterolithic volcaniclastic kimberlite breccia composed of numerous serpentinized olivine grains (O), dark amoeboid-shaped juvenile lapilli (dark brown) and xenocrystal biotite (M) and feldspar (F) (F.O.V. 6.0 mm).

Despite the intense alteration of the kimberlite, relatively fresh crystals of brown-tan biotite and colourless muscovite are present as groundmass constituents. Partially altered feldspar crystals may also be present. These minerals are considered to be xenocrysts derived from the disaggregation of country rock (refer to Figure 3.10). Lithic fragments of biotite-bearing gneiss (Figure 3.11) and minor altered non-kimberlitic mudstone are present at a microscopic level.

The groundmass of A10 is characterized by the presence of abundant barite, which may occur poikilitically enclosed within olivine. The barite content of the kimberlite increases with depth. Numerous small plates of subhedral-to-anhedral calcite are present in the groundmass. Calcite commonly fills small, irregular-shaped "segregations" as interlocking plates. These irregular-shaped pods may represent pore spaces in the kimberlite which were later filled with fairly coarse-grained secondary calcite. Abundant chromite, Ti-magnetite, apatite (presence increases with depth) and minor ilmenite, brown perovskite and rare phlogopite and garnet also occur within the groundmass of A10. All of the above listed groundmass minerals are not present in every sample. This sorting also defines the various units within this kimberlite.

All of the above is set in a brown turbid mesostasis consisting of an intimate mixture of serpentine and calcite.

All of the aforementioned features are not present in each sample. Microscopic lithic fragments are not abundant within the upper units of the kimberlite. Similarly, groundmass barite is absent from samples obtained at higher structural levels within the kimberlite. Autolithic fragments are not recognized in samples A10-1-1 through A10-1-3. In these examples, small, poorly-formed and highly altered juvenile lapilli are present within the groundmass.

Macrocrystal olivines with thin kimberlitic mantles are only present in section A10-1-5. Furthermore, within increasing depth, kimberlite units may be described as lithic breccias as the presence of biotite- and feldspar-bearing gneiss and granites becomes more evident.

Figure 3.11. Kimberlite A10. Heterolithic volcaniclastic kimberlite breccia with numerous relatively fresh biotite- and feldspar-bearing basement xenoliths (X) and abundant relatively fresh feldspar (predominantly microcline) xenocrysts (F) (F.O.V. 6.0 mm).

3.2.3.3. Discussion

The presence of numerous anhedral crystals of relatively fresh xenocrysts, wood fragments, non-kimberlitic mudstone xenoliths and the intense alteration of the kimberlite suggests that all the units observed and described were reworked.

Kimberlite A10 is interpreted to represent a volcanic vent infilled with numerous units of resedimented volcaniclastic kimberlite that, with depth, becomes a resedimented volcaniclastic kimberlite breccia. Hypabyssal rocks were not encountered associated with, or underlying the volcaniclastic kimberlite.

3.2.4. Kimberlite A11

Kimberlite A11 was discovered and drilled in 1994 and is located approximately seven kilometres east-southeast of the Diavik Diamond Project, 2.5 kilometres off the eastern shore of Lac de Gras.

A11 intrudes biotite schist and is overlain by a small lake and 15-20m of glacial regolith. Ground geophysics reveals an elongated, northwest--trending weak magnetic low (A11) and an offset ellipsoidal north-south trending weak electromagnetic conductor (A11N), approximately 100x160 m in dimension. The electromagnetic response is located slightly east of the magnetic anomaly.

Eight holes were drilled into both A11 and A11N intersecting kimberlite to a maximum vertical depth of 160 m. Kimberlite 94A11-2 was observed macroscopically and microscopically.

3.2.4.1. Macroscopic Observations

Drill hole 94A11-2 collared kimberlite at a depth of 16.8 m. The upper 60 m of kimberlite consists of rubbley, incompetent dark brown, matrix-supported kimberlite (Unit #1) containing 5-30% subrounded-to-angular macrocrystal olivine (2-10mm in size). Olivine is generally completely replaced by yellow-green serpentine. Small relict

cores may remain. Microphenocrystal olivines are completely serpentinized. Olivine content varies greatly throughout the intersection, defining crude, sub-horizontal bedding. Rare macrocrystal garnet and chrome diopside occur. Garnets commonly exhibit kelphytic rims. Angular-to-subrounded biotite schist country rock fragments are common, but not abundant (<5% of rock) and are generally fresh, occasionally with a thin reaction mantle. Xenocrysts of biotite and feldspar from the disaggregation of country rock are strewn throughout the matrix. Lapilli-to-ash sized fragments occur throughout. Mudstone and wood fragments are prevalent. The above is set in a dark-brown, aphanitic matrix.

Unit#1 is interbedded with poorly consolidated, non-kimberlitic mudstones of up to 30 cm in thickness and numerous light gray-green, competent kimberlite (Unit #2) characterized by abundant (up to 50%), partially fresh to completely altered, rounded olivine macrocrysts. The later ranges in thickness from 15 cm to 6.6 m in thickness. Contacts, if preserved, are sub-horizontal.

At a depth of 95 m, a sharp contact defines a distinct change in the character of the kimberlite (Unit #3). Unit #3 is a light gray-green, very competent kimberlite (can only be broken with a hammer). Two populations of olivine, both macrocrysts and microphenocrysts, from less than 1 mm to 20 mm in size characterize this rock. Macrocrystal olivines are rounded with minor marginal serpentinization while microphenocrystal groundmass olivines are fresh-to-completely altered. Macrocrystal mica is common. Kelphytized garnets and fresh chrome diopsides are rare. The above together with rare dark brown cognate fragments sit in a gray-green aphanitic matrix. Open fracture surfaces are commonly coated with calcite. Dilational calcite veins are prevalent.

3.2.4.2. Microscopic Observations

3.2.4.2.1. Unit#1

Unit #1 consists of a widely varying percentage of olivine macrocrysts. Although single samples generally show a relatively restricted range of macrocrystal olivine sizes, the entire suite of samples shows quite a broad range of sizes, i.e., from 2-10 mm. Olivine macrocrysts are rounded-to-angular (Figure 3.12) and replaced by yellow-brown serpophite and pale green lizardite along cracks. Coarse, interlocking calcite crystals may replace cores, or a small relict core may remain.

Very small groundmass subhedral-to-euhedral microphenocrystal olivines are abundant and are completely replaced by yellow serpophite.

Small, partially altered (replaced by calcite) lithic fragments of biotite-bearing gneiss and schist are not very prevalent on a microscopic level. Small angular xenocrysts of biotite, microcline and quartz (in order of abundance), derived from their disaggregation occur throughout the groundmass.

Unit#1 is characterized by the presence of two types of cognate fragments. The presence of both of these clasts seems to be ubiquitous throughout the suite of samples observed. The two types of clast noted include:

1. Tan-coloured, amoeboid-shaped microporphyritic kimberlite fragments composed of subhedral-to-euhedral olivine. These crystals are replaced by very fine-grained, pale yellow serpophite. Relict cores commonly remain. Microphenocrysts are set in a groundmass composed of discrete subhedral-to-euhedral opaque spinels, common fresh mica and subhedral perovskites. The matrix has a distinct granular texture and is composed of a copious amount tightly packed "serpophitic" crystals. These likely represent pseudomorphed microphenocrystal olivines. Small circular-to-subcircular calcite-filled vesicles characterize these clasts (Figure 3.13).

2. Dark brown, irregular-shaped, fine-grained, aphanitic-to-microporphyritic kimberlite fragments composed of small subhedral-to-euhedral microphenocrystal olivine and pyroxene, which are pseudomorphed by serpophite. Small, relict cores rarely remain. Small "serpophitic" crystals are strewn throughout the matrix. These likely represent tiny microphenocrystal olivines. The groundmass further includes abundant spinels and minor perovskite set in a brown turbid, optically uniform mesostasis of calcite

Figure 3.12. Kimberlite A11, Unit#1. BSE-image showing large, rounded serpentinized macrocrystal olivine (O) and small grains of serpentinized groundmass olivine, common calcite (C), spinels (small, yellow) and minor small kimberlitic fragments (F) set in a serpentine-calcite matrix (F.O.V. 1.72 mm).

Figure 3.13. Kimberlite All, Unit#1. Volcaniclastic kimberlite containing small, irregular-shaped kimberlite fragments (J). Small, circular calcite-filled bodies are vesicles (V) indicating that these are *bona fide* juvenile lapilli (F.O.V. 1.0 mm).

and serpentine. Small irregular-shaped microporphyritic juvenile lapilli, as described above, are commonly enclosed within these clasts. Furthermore, a thin rind of microporphyritic kimberlite, as described in clast #1 may mantle these fragments. Broken crystals may occur along the margins.

Clast #1, based on its morphology and the presence of small vesicles, represent *bona fide* juvenile lapilli. Clast #2, however, is more complex. Although their morphology suggests that they were not consolidated upon incorporation into their current host, broken crystals along their margins suggests that they are autoliths. Because these fragments contain juvenile lapilli and are nearly identical in character to the host kimberlite, it is believed that these fragments represent poorly-consolidated resedimented volcaniclastic kimberlite which has been disrupted and incorporated into Unit#1.

The groundmass of Unit#1 consists of abundant discrete, subhedral-to-euhedral opaque spinels, including partially resorbed magnetite, subhedral perovskite, apatite, phlogopite, pyrite, and minor zircon and prismatic ilmenite. Chloritized xenocrystal mica is dispersed throughout the groundmass.

All of the above is set in a brown, turbid mesostasis of intimately intergrown calcite and serpentine.

3.2.4.2.2. Unit #2

Unit #2 is composed of large (up to 15 mm) ovoid macrocrysts of olivine and pyroxene. These crystals are relatively fresh, but commonly exhibit a relatively thick outer mantle of brown serpophite. Minor replacement by coarse-grained calcite occurs at their cores and along fractures.

Groundmass microphenocrysts olivines and less common pyroxene occur as euhedral-to-subhedral crystals, which have been partially-to-completely (in smaller crystals), replaced by serpophite and minor calcite. Subhedral-to-euhedral opaque spinels, apatite, minor perovskite and platy calcite are also strewn throughout the groundmass. The mesostasis is composed of blocky phlogopite, serpentine and calcite.

The matrix is composed of relatively small, essentially oxide-free "segregations" consisting of vermiculatized brown phlogopite and serpentine. Small euhedral rhombs of

calcite are dispersed throughout. These "segregations" may represent disrupted cumulates derived from earlier batches of magma.

3.2.4.2.3 Unit #3

Unit #3 contains abundant olivine (Figure 3.14), minor pyroxene macrocrysts and rare polycrystalline microxenoliths of lherzolite. The former are fresh and exhibit only minor marginal serpentinization. Large kelphytized xenocrystal garnets also occur.

Groundmass primary microphenocrystal olivines and minor pyroxene occur as relatively fresh crystals. Serpentinization is commonly confined to margins, however, smaller crystals may be completely replaced by yellow-brown serpophite. Within the silicate-oxide groundmass, opaque, subhedral-to-euhedral spinels are abundant. Resorbed donut-shaped magnetite is abundant. Atoll spinels are rare. Perovskite (enriched in Nd and Sr) is also common, as are sprays of acicular apatite and discrete crystals of apatite euhedra. The former may occur poikilitically enclosed within microphenocrystal olivines. Sprays of apatite poikilitically enclose small subhedral-to-euhedral crystals of serpentine after olivine. Monticellite may replace these crystals along their margins.

The mesostasis exhibits a sugary-granular texture and consists of a fine-grained intergrowth of serpentine, calcite and minor phlogopite. Small crystals of calcite after monticellite and scattered throughout the mesostasis.

The groundmass contains numerous irregular-to-amoeboid shaped, oxide-free segregations. These are filled with interlocking anhedra of calcite together with yellow-brown serpophite. Common euhedral rhombs of calcite occur along their margins. Euhedral prisms of apatite may occur within the segregations and sprays of acicular apatite may radiate from their margins. Apatite may be pseudomorphed by calcite. Smaller segregations may be filled only with serpophite. The margins of the segregations are commonly lined with botryoidal serpophite.

Figure 3.14. Kimberlite All, Unit#3. Macrocrystal hypabyssal kimberlite with partially altered olivine (O) (replaced by yellow serpophite and calcite) and small, irregular segregations (S) strewn throughout the groundmass (F.O.V. 6.0 mm).

3.2.4.3. Discussion

A11 represents a kimberlite vent infilled with a variety of different rocks. The fragmental texture and the presence of xenoliths and common xenocrysts of disaggregated country rock suggest that Unit #1 represents a resedimented volcaniclastic kimberlite. It is interbedded with small units of laminated, water-lain non-kimberlitic mudstone. The presence of the relatively thin beds of Unit#2 may represent one of the following:

1. Large autoliths of hypabyssal kimberlite, disrupted during kimberlite emplacement;
2. Small sills which were emplaced subsequent to kimberlite emplacement and vent infill.

The volcaniclastic vent-infill ends abruptly with a sharp contact. Below this contact lies oxide-rich macrocrystal apatite hypabyssal kimberlite (Unit#3). The proportion of macrocrysts varies throughout this intersection and is attributed to flow differentiation. Approximately 39 m of this hypabyssal kimberlite was intersected before the drill hole was terminated. Unit #3 may represent one of three possibilities:

1. a root zone-feeder system to the vent in which it underlies;
2. volcaniclastic kimberlite may underlie this unit and Unit #3 may represent a post-eruption sill which intruded the consolidated vent-infill;
3. a large autolith of hypabyssal kimberlite within the volcaniclastic infill.

3.2.5. Kimberlite A61

Kimberlite A61 is an isolated vent located nineteen kilometres east-northeast of the Diavik Diamond Project, five kilometres off the eastern shore of Lac de Gras. A61 is an ellipsoidal magnetic low, 200x175m in approximate dimension. The electromagnetic

response of A61 is weak. A61 is hosted within Archean granite and biotite schist and is overlain by approximately 10m of water and 15m of glacial regolith.

Four exploration drill holes attempted to delineate A61, only two of which intersected kimberlite. Drill hole A61-4 was investigated for this study. A –50 degree hole, A61-4 was drilled along the northeastern margin toward the middle of the magnetic low. After a 44m intersection of granite and biotite schist, 48 m of kimberlite was encountered before biotite schist was once again intersected and the hole ended.

3.2.5.1. Macroscopic Observations

A61 is composed of dark gray, fairly incompetent, bedded volcaniclastic kimberlite. Subtle variations in colour and proportions of clasts define crude bedding. Bedding contacts do not appear sharp within the core, a likely product of poor preservation.

At least three distinct volcaniclastic kimberlite units exist within A61. Unit#1 is a cognate, matrix-supported breccia composed of numerous ash-to-lapilli sized cognate fragments, commonly with relatively fresh olivine macrocrysts at their cores, set in a dark brown aphanitic matrix. Unit#2 is a crystal-rich kimberlite breccia consisting of numerous rounded, fresh olivine macrocrysts, minor macrocrystal pyroxene, abundant fresh crystals of mica and small opaque oxides, together with common kimberlitic clasts (both dark, aphanitic ash-sized fragments and larger, rounded microporphyritic kimberlite fragments) set in a green-brown serpentinized matrix. Unit#3 is a medium gray, competent breccia containing both cognate and lithic fragments, together with abundant fresh macrocrystal and microphenocrystal olivine and phlogopite set in a carbonate-rich matrix.

Units#1 and #2 alternate through the upper 43m of the kimberlite intersection giving way to a final three metres of Unit#3 at the end of the intersection. Thin beds of Unit#3 may be present and interbedded with Units#1 and #2.

Sample A61-4-1 (Unit#4) was taken from near the upper contact of the kimberlite and appears to be a macrocrystal hypabyssal kimberlite autolith composed of abundant macrocrystal and microphenocrystal olivine set in a brown, serpentinized matrix.

3.2.5.2. Microscopic Observations

3.2.5.2.1. Unit#1

This rock contains few large, rounded, commonly fragmented macrocrystal olivines. These crystals are relatively fresh and are veined and mantled by pale yellow-brown serpophitic serpentine.

The majority of the olivine population consists of relatively small (less than 4 mm), subrounded-to subhedral microphenocrystal olivines. The olivines typically exhibit a thick rim of pale yellow serpophite, giving the structure a "donut-like" appearance (Figure 3.15). Dark brown serpophite may partially replace the relict cores.

This unit is characterized by the presence of abundant, small amoeboid-to-irregular-shaped pelletal lapilli-like fragments, which have unusual textures (refer to Figure 3.15). The lapilli commonly have a kernel of fresh rounded macrocrystal olivine or small subhedral olivine microphenocrysts. These are mantled by a material which consists predominantly of very small, commonly tightly packed, rounded pale yellow amorphous serpophitic "crystals" which may be pseudomorphs after microphenocrystal olivine. Rare, small crystals of opaque spinels, apatite and altered mica are present in an optically unresolvable serpophitic material.

A second type of less common ash-sized kimberlite clast occurs within Unit#1. These fine-grained fragments consist of small, altered microcrystal olivines, small serpophite crystals and carbonate set in a very dark brown, unresolvable matrix. Their irregular shapes suggests they may be juvenile in nature, however, small broken crystals along their margins suggests that these fragments were consolidated, if not poorly consolidated, prior to their incorporation and are, in fact, autoliths.

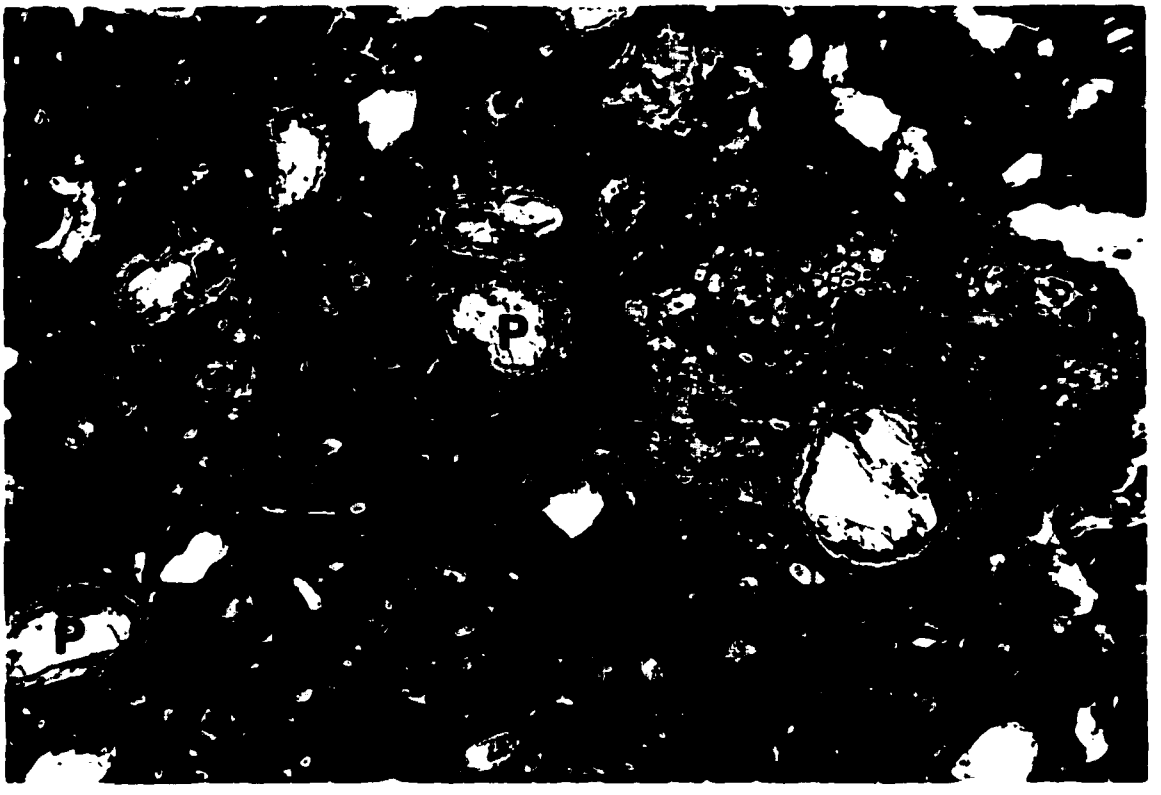

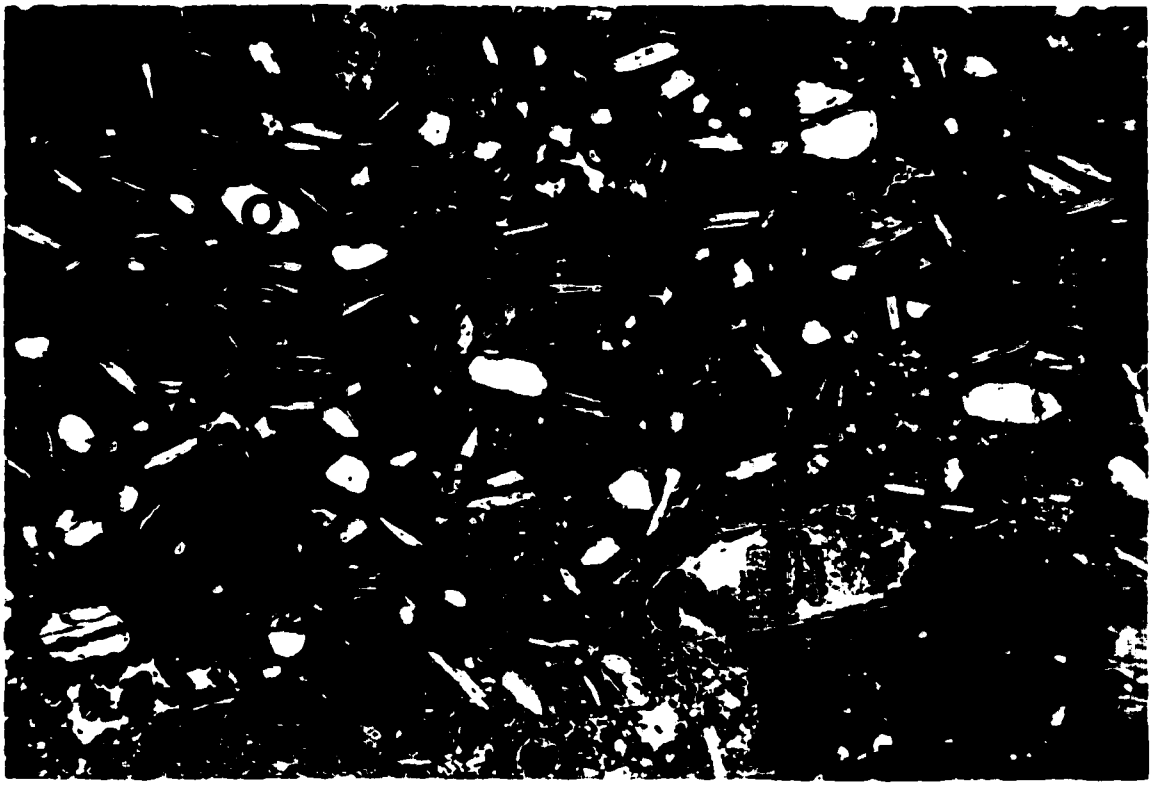

Figure 3.15. Kimberlite A61, Unit#1. Donut-like pseudo-pelletal lapilli (P) characterized by a thick outer margin of pale yellow serpophite. Larger, irregular-shaped fragment consists of a large, fresh phenocryst of olivine in a matrix composed predominantly of small serpophitized microphenocrystal olivine (J). Both of these fragments are juvenile lapilli (F.O.V. 2.5 mm).

Figure 3.16. Kimberlite A61, Unit#2. Pyroclastic kimberlite consisting of abundant laths of fresh phlogopite (P), microphenocrystal olivine (O) and common fine-grained, dark-brown, irregular-shaped juvenile lapilli (F.O.V. 6.0 mm).

The groundmass consists of abundant pale yellow serpophite crystals (microphenocrystal olivine pseudomorphs) together with minor altered mica, apatite and rare spinels. Primary carbonate appears abundant within the groundmass. The above is set in a turbid-brown serpophitic mesostasis.

Unit#1 is composed of volcaniclastic kimberlite breccia containing abundant kimberlitic fragments. These lapilli are considered to represent *bona fide* quenched magma droplets. Although the lithic component of Unit#1 is minor, it has likely undergone a significant amount of reworking.

3.2.5.2.2. Unit#2

Unit#2 contains common, fairly large (<6 mm), well-rounded olivine macrocrysts. These macrocrysts may be partially replaced at their cores by colourless calcite and minor lizardite and are mantled and veined by yellow-brown serpophite. Large macrocrystal olivines are not mantled by kimberlite. Rounded polycrystalline xenoliths of porphyroblastic lherzolite are also present.

Smaller euhedral-to-subhedral microphenocrystal olivines are fairly abundant. These crystals are typically partially altered-to-completely replaced by brown-yellow serpophite.

Two varieties of cognate fragments are present in Unit#2. The first type consists of microporphyritic fragments characterized by the presence of abundant fresh-to-partially altered microphenocrystal olivine (olivines may be tangentially oriented to clast margins) set in a groundmass of small euhedral amorphous serpophite crystals likely pseudomorphed microphenocrystal olivine), discrete opaque spinels and apatite set in a yellow brown mesostasis of calcite, phlogopite and serpentine. The larger of these clasts exhibit a darker core and lighter margin however core and margin are texturally and mineralogically identical. Small spherical calcite-filled "segregations" are rare, but may occur. These likely represent small vesicles. Smaller fragments may be cored by a single microphenocrystal olivine. The margins of these clasts are typically irregular suggesting they are juvenile lapilli.

A second group of distinctly different cognate clasts is also common within Unit#2. These clasts contain numerous partially altered microphenocrystal olivines. Alteration is limited to marginal replacement by yellow-brown serpophite, while smaller olivines may be completely replaced. Olivines, together with common small crystals of phlogopite and minor reddish-brown spinels are set in a very dark brown-black aphanitic, unresolvable serpophite. These fragments range from ash-size (<1 mm) to lapilli-sized (>10 mm). Their outer margins are highly irregular and often embayed (Figure 3.16). Their morphology suggests they are juvenile in origin but broken crystal fragments may occur along their margins, indicating they were likely disrupted from a poorly consolidated unit.

The interclast matrix consists of an unusual amount of fresh macrocrystal and groundmass of Ba-rich phlogopite, which contains 2-<10 wt.% BaO along crystal margins. Phlogopite often exhibits a pilotaxitic texture in which it crudely aligns itself around larger cognate clasts (typically the first group described above). Other groundmass constituents include subhedral-to-euhedral barite, apatite and perovskite. Back scattered electron images suggest that the groundmass of Unit#2 is composed of abundant small, welded juvenile fragments set in a matrix of dark brown serpophite and subhedral rhombs of calcite (Figure 3.17). These fragments commonly contain small partially-to-completely serpentinized microphenocrystal olivines at their cores and rarely phlogopite.

Unit#2 appears to be a pyroclastic phlogopite-rich volcaniclastic kimberlite tuff.

3.2.5.2.3. Unit#3

Unit#3 is characterized by the presence of numerous rounded olivine macrocrysts and minor macrocrystal orthopyroxene. Alteration is essentially absent, however, minor serpentinization along fractures in crystals does commonly occur. Some macrocrysts may be weakly strained suggesting they are in fact xenocrysts. Minor fresh polycrystalline, rounded lherzolitic xenoliths also occur (Figure 3.18).

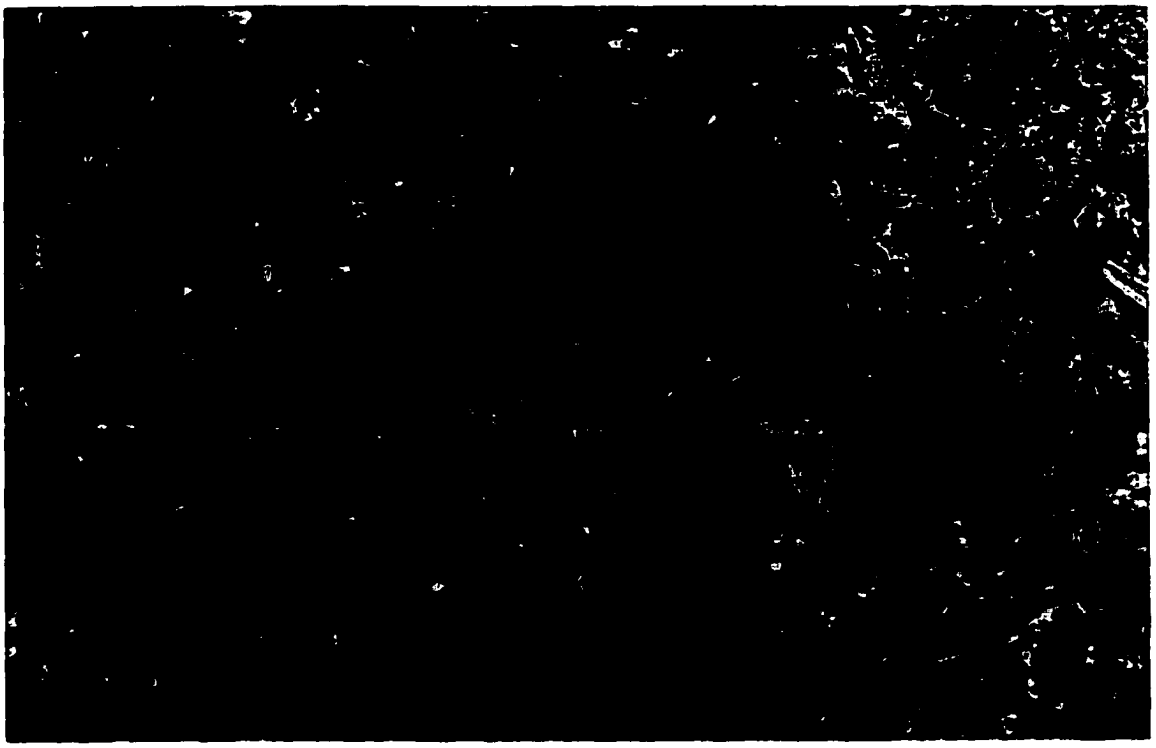

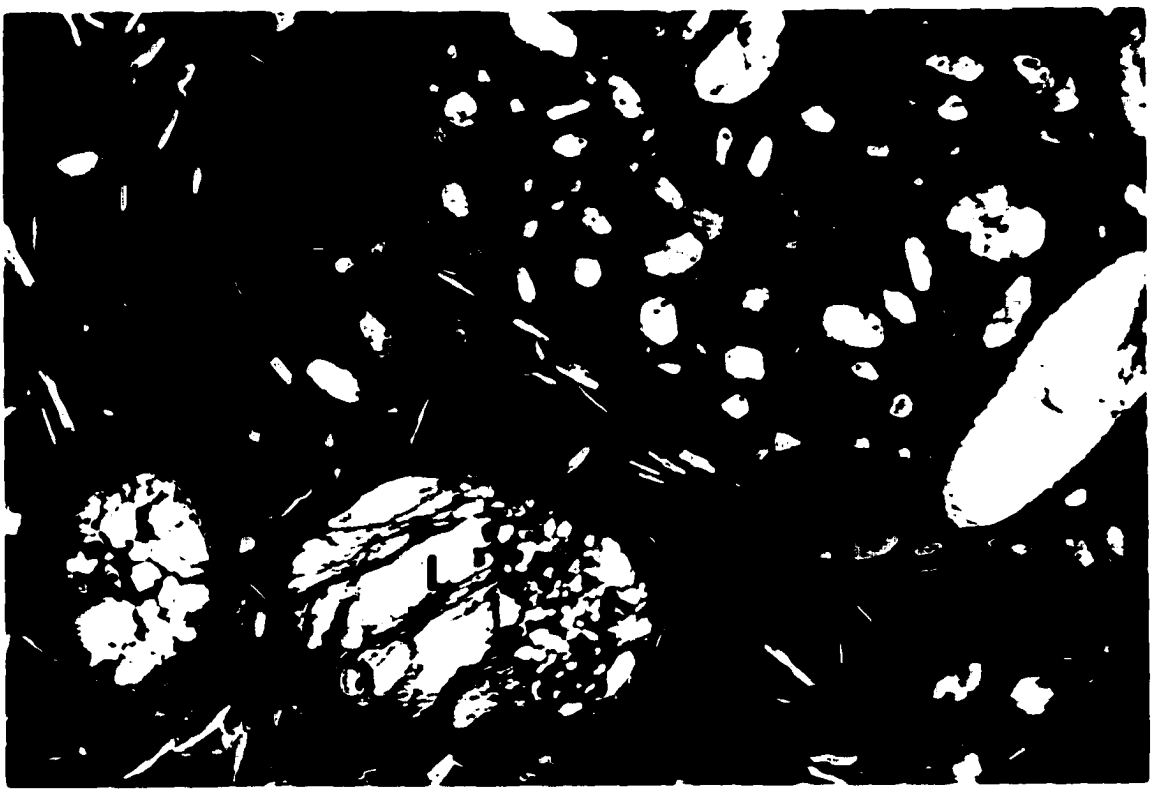

Figure 3.17. Kimberlite A61, Unit#2. BSE-image of small welded juvenile fragments within a pyroclastic kimberlite (F.O.V. 1.72 mm).

Figure 3.18. Kimberlite A61, Unit#3. Pyroclastic kimberlite consisting of rounded xenocrysts of mantle-derived lherzolite (L), a large microporphyritic juvenile fragment (J) and abundant laths of phlogopite. Phlogopite exhibits a pilotaxitic texture in which it crudely aligns itself around the larger kimberlite fragment (F.O.V. 6.0 mm).

The majority of the olivine population occurs as smaller (<5mm), rounded-to-euhedral, fresh microphenocrysts. Crystals of fresh, pale brown phlogopite are abundant (≈15%) throughout this unit. Phlogopite may exhibit a pilotaxitic texture in which it crudely aligns itself around larger cognate fragments.

Two distinct varieties of cognate fragments occur in Unit#3:

1. Dark-brown, fine-grained, amoeboid-shaped lapilli-sized fragments characterized by the presence of relatively fresh, rounded microcrystal olivine set in an optically unresolvable brown serpophite matrix. No evidence suggests that these clasts are autolithic.

2. Pale brown-yellow, lapilli-sized (generally larger than previous) microporphyritic kimberlite fragments characterized by the presence of relatively fresh subhedral-to-euhedral microphenocrystal olivines set in an oxide-poor groundmass consisting of minor perovskite, apatite and small "segregations" of coarse calcite. The above is set in a yellow-brown mesostasis consisting of calcite, phlogopite and serpentine. The margins of these clasts are frequently embayed. Such clasts are undoubtedly juvenile in origin (refer to Figure 3.18).

The oxide-rich groundmass consists of numerous opaque spinels (both discrete crystals and complex atoll structures), common perovskite, abundant apatite and small crystals of phlogopite set in a dark brown mesostasis of serpentine and calcite. Numerous pseudo-segregations of coarse anhedral-to-euhedral calcite occur throughout the groundmass (Figure 3.19). The oxide-rich groundmass is interpreted as representing small welded juvenile fragments, which are set in coarse secondary calcite cement. Some serpentinization of the cement occurs.

Unit#3 is interpreted as a primary pyroclastic volcaniclastic kimberlite tuff. This unit has undergone little alteration and may be a fresher example of Unit#2.

3.2.5.2.4. Unit#4

Unit#4 contains numerous large (<10mm) fresh ovoid olivine macrocrysts. The crystals are fresh with minor yellow-brown serpophite replacement along crystals fractures and commonly exhibit a thin mantle of serpophitic alteration.

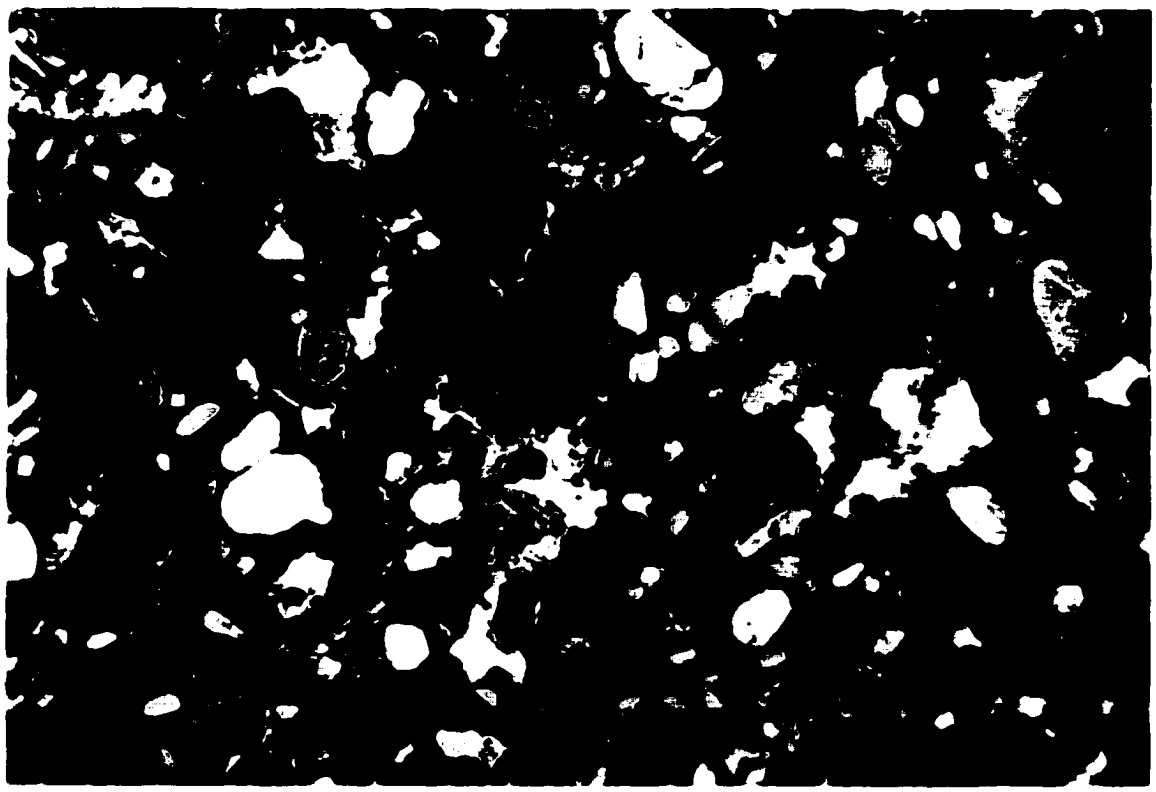

Figure 3.19. Kimberlite A61, Unit#3. Welded juvenile fragments, within a pyroclastic kimberlite, cemented with secondary calcite (F.O.V. 6.0 mm).

Figure 3.20. Kimberlite A61, Unit#4. BSE-image of the groundmass of hypabyssal kimberlite consisting of abundant laths of Ba-rich phlogopite (P) (F.O.V. 120 μm).

The majority of the olivine population consists of subrounded-to-euhedral, inequigranular (<1 to 5mm) relatively fresh microphenocrystal olivine. Larger olivines are generally exhibit minor marginal serpentinization; while smaller olivines typically exhibit a thick serpophitic margins and may be entirely replaced by serpophite. Alteration in both macrocrystal and microphenocrystal olivine is identical.

The groundmass of Unit#4 consists of numerous subhedral-to-euhedral opaque oxides, abundant prismatic apatite (which frequently occur in irregular-shaped aggregates), euhedral-to-subhedral discrete and complex atoll structures and minor subhedral perovskite. The most pervasive groundmass constituent is Ba-rich phlogopite (Figure 3.20). All of the above mineral constituents are set in a groundmass mesostasis of calcite and serpentine.

The oxide-rich groundmass consists of several small, irregular-shaped calcite-serpentine segregations. These segregations consist of coarse, interlocking calcite and minor yellow serpophite. Calcite may be partially replaced by serpophite. Irregular aggregates of prismatic apatite commonly partially fill the segregations. Aggregates emanate from the margins of the segregations, *i.e.*, margins acted as a substrate for the growth of apatite.

No evidence suggests that Unit#4 is volcaniclastic and can thus be appropriately termed a segregation-textured apatite phlogopite hypabyssal kimberlite.

3.2.5.3. Discussion

Kimberlite A61 represents a small kimberlite vent that has been infilled by both resedimented volcaniclastic and pyroclastic kimberlite. Segregation-textured hypabyssal kimberlite was encountered at a high structural level within the vent and may represent a post-eruptive kimberlite sill that intruded volcaniclastic kimberlite subsequent to vent infill. Large xenoliths of biotite schist wall rock have been incorporated within the vent near the end of the kimberlite intersection.

3.2.6. Kimberlite C13

Kimberlite C13 was discovered and drilled in 1994. It is located on the Commonwealth claim block, which adjoins the southern boundary of the Diavik Diamond project at the eastern end of Lac de Gras. C13 is located approximately 14 kilometres east of Lac de Gras, 4 kilometres southwest of kimberlite T14.

Kimberlite C13, a weak electromagnetic conductor, displays an irregular-sub-circular magnetic low, approximately 300x225m in dimension. It intrudes highly metamorphosed biotite schist of the Yellowknife Supergroup and is overlain by 25-30m of glacial regolith.

Available data from 10 diamond drill holes indicates that kimberlite has only been intersected to a maximum vertical depth of 103.5m. Drill hole 94C13-8 was investigated for this study.

3.2.6.1. Macroscopic Observations

Macroscopically, kimberlite C13 appears to be a bedded volcaniclastic rock. Beds differ with respect to the olivine-to-matrix ratio. Beds may vary in thickness from less than 10 mm to greater than 10m and, although many bedding contacts were not preserved due to the poor condition of the core, an angle of 55-60° to the core axis was consistently obtained for contacts that were preserved. Few units are distinctly reverse graded, other are normally graded, whereas most show no evidence of grading and are very sorted.

C13 is a dark gray-brown, incompetent and commonly poorly lithified kimberlite characterized by a paucity of lithic fragments. Small, subrounded, very fine-grained cognate clasts are common. Individual units may range from an entirely matrix supported kimberlite mudstone to a crystal-supported rock with greater than 40% olivine. Olivine crystals are typically well rounded-to-subangular, commonly broken and are intensely serpentinized to a yellow-brown colour. An individual sample from this kimberlite may yield a wide variety of olivine sizes, from less than 2 mm to greater than

10 mm. Small angular mudstone xenoliths (less than 2 cm in size) are rare, as are macrocrystal garnet and chrome diopside.

Near the end of the kimberlite intersection the above volcaniclastic kimberlite is interbedded with thin, competent units (<40 cm in thickness) that are characterized by abundant olivine grains (>40 vol.%).

3.2.6.2. Microscopic Observations

Kimberlite C13 contains anywhere from less than 5% to greater than 40 vol.% macrocrystal olivine pseudomorphs, subrounded-to-rounded in habit and commonly broken (Figure 3.21). Bedding and sorting may be distinguished on a microscopic scale (Figure 3.22). Olivine is replaced by yellow-brown serpophite and is commonly altered by calcite along cracks and margins. Small relict cores may remain in large crystals. Subrounded-to-subhedral microphenocrystal olivines are replaced by yellow-brown serpophite.

Although lithic fragments are rare, small xenocrysts of subangular-to-subrounded, partially altered feldspar and quartz and relatively fresh xenocrystal biotite are common groundmass constituents and may be copious in many units.

Kimberlitic clasts are present, but may be absent is some units. Fragments are composed of light brown, very fine-grained aphanitic kimberlite or microporphyritic kimberlite. Aphanitic clasts may contain a small rounded olivine macrocryst at its core. Broken crystal fragments along margins suggest that these clasts were solid at the time of their incorporation and therefore are considered to be autoliths. Microporphyritic kimberlite fragments are composed of subangular microphenocrystal olivine pseudomorphs, abundant subhedral-to-euhedral discrete spinels, rare garnets set in a nearly isotropic, optically unresolvable serpophitic matrix. These clasts have irregular-curvilinear margins are commonly amoeboid in shape. Their morphology suggests that they are juvenile lapilli.

The groundmass consists of abundant discrete, subhedral-to-euhedral spinels and rare preserved atoll spinels. Magnetite is abundant and shows evidence of extreme

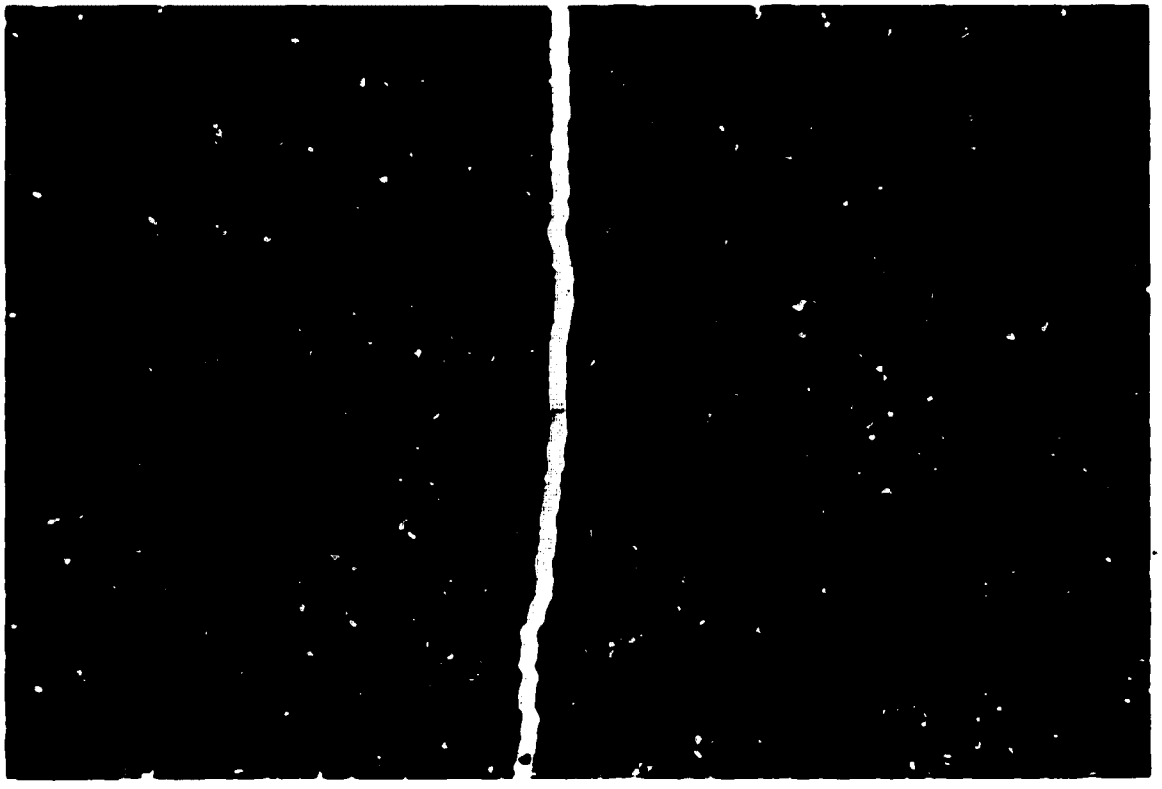

Figure 3.21. Kimberlite C13. Microphotograph showing the fragmental nature of C13. This rock is a matrix-supported, olivine-crystal rich, highly altered kimberlite (F.O.V. 6.0 mm).

Figure 3.22. Kimberlite C13. Microphotograph showing sorting on a microscopic scale. Individual units are defined by the proportion of olivine grains (F.O.V. 6.0 mm).

resorption. Other groundmass constituents included common subhedral perovskite (≈10μm), common rutile, barite, REE-bearing apatite, orthopyroxene (rutile exsolution not uncommon), minor garnet and anhedral shards of quartz. Anhedral-to-subhedral plates of calcite are strewn throughout the groundmass and may constituent a major groundmass phase in some units. Sulphides, including subhedral-to-euhedral pyrite and minor Fe-Ni sulphides are common. The above is set in a very fine-grained mesostasis of calcite and serpentine. Very small crystals (≈5μm) of fresh phlogopite are scattered throughout the mesostasis.

Two samples were taken from the olivine-rich units near the end of the kimberlite intersection. Superficially, these units resemble the resedimented volcaniclastic kimberlite described above, however, on closer examination using BSE-methods, the groundmass contains welded juvenile fragments (Figure 3.23) indicating that this rock is pyroclastic in origin.

3.2.6.3. Discussion

Although there is a scarcity of lithic clasts, abundant xenocrystal fragments of quartz, feldspar and biotite derived from the disaggregation of country rock suggests that C13 has been reworked. Kimberlite C13 represents a vent infilled with resedimented bedded volcaniclastic kimberlite, ranging from a dark gray, matrix-supported kimberlite mudstone to an olivine crystal-supported volcaniclastic kimberlite. Reverse grading and the poorly sorted nature of the kimberlite units, together with their inward-sloping bedding angles, suggest that debris flow may have been the mechanism of deposition. The presence of thin units of pyroclastic kimberlite at the end of the intersection suggests that pyroclastic activity may have contributed to the vent infill.

No hypabyssal kimberlite was intersected.

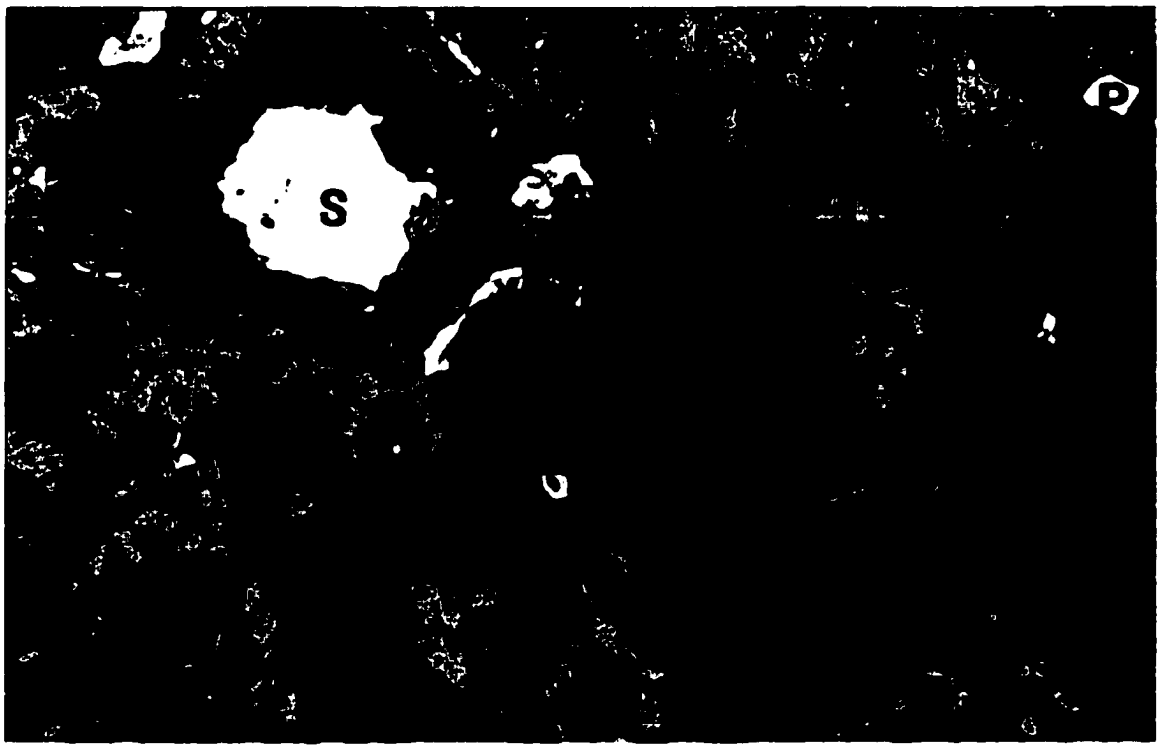

Figure 3.23. Kimberlite C13. BSE-image showing small, poorly develop, welded juvenile lapilli (J) together with spinel (S), subhedral perovskite (P) and primary calcite (C) set in a serpentine (blue) base (F.O.V. 86 μm).

3.2.7. Kimberlite C27

Kimberlite C27 is located 10 kilometres southeast of the Diavik Diamond Project, one kilometer off the southern shore of Lac de Gras. C27 is a strong ellipsoidal magnetic low, 130x70m in approximate dimension. It also shows a weak electromagnetic response. C27 is hosted within Archean biotite schists and granite gneiss and is overlain by approximately six metres of glacial regolith.

One exploration drill hole, drilled at an angle of –45 degrees, delineated this body. The drill hole collared biotite schist and intersected 65m of kimberlite at an approximate vertical depth of 40m before again intersecting 9m of schists and granite in which the hole was terminated.

3.2.7.1. Macroscopic Observations

Kimberlite C27 appears to be a rather massive volcaniclastic kimberlite (Unit#1) breccia with no distinct grading or bedding throughout most of the body. C27 is a dark gray-black, fine-grained, competent rock with common rounded, relatively fresh olivine macrocrysts and abundant fresh, subrounded microphenocrystal groundmass olivines. Many of the olivine crystals appear to be mantled by an aphanitic kimberlite ash. Rare macrocrystal garnet and pyroxene occur within the rock. The lithic component of C27 is high, containing a profusion of xenocrystal mica and feldspar in addition to abundant, rounded xenoliths of biotite schist and granite. The lithic component may vary from <15 to >20%. Their relative abundance and size may define crude bedding. Small fragments of Cretaceous mudstone are quite common and rare wood fragments occur.

Near the end of the kimberlite intersection (approximately the last metre), the rock becomes distinctly finer-grained and is quite poorly preserved (no contacts preserved). This dark gray-green rock (Unit#2) is highly altered and contains common rounded, serpentinized olivine macrocrysts, few altered microphenocrystal olivines, abundant xenocrystal mica and common small rounded country rock xenoliths set in an aphanitic matrix. This rock appears to be clast-supported.

Unit#2 marks the end of the kimberlite intersection where granite gneiss and biotite schist are encountered. This rock is quite brecciated and is intruded by a few small kimberlitic veinlets. It is likely this rock is merely a xenolith within the vent and does not mark the kimberlite-country rock contact.

3.2.7.2. Microscopic Observations

3.2.7.2.1. Unit#1

Unit#1 contains a few (<5%) angular clasts of fine-grained country rock and rather common single crystals of microcline (sericitized along margins), rare plagioclase and common relatively fresh crystals of xenocrystal biotite.

Ovoid olivine macrocrysts are relatively common. These are generally fresh, may be weakly strained and commonly exhibit serpophitization along cracks and margins.

The bulk of the olivine population consists of small, subhedral-to-subrounded microphenocrystal olivine. These are similarly fresh with minor serpophitic replacement along cracks and margins. Incomplete spinel necklaces may be present.

Both macrocrystal and microphenocrystal olivines, and less commonly microcline, form the cores of rounded lapilli-like clasts of very fine-grained kimberlite (Figure 3.24). The latter consists of minor, very small microphenocrystal olivines; abundant, relatively fresh monticellite, perovskite and rare Ti-magnetite set in a mesostasis of calcite and serpentine. These lapilli have an irregular margin and may not exhibit a coring mineral. These fragments are considered to represent non-vesiculated juvenile lapilli.

A second type of cognate fragment is also present in Unit#1. These fragments occur as small, amoeboid-shaped intensely altered structures that consist of pseudomorphed microcrystal olivine, opaque oxides and common xenocrystal constituents set in an optically unresolvable matrix. These fragments are commonly mantled by the above-described material. This type of clast is interpreted to represent a recycled autolith from a disrupted, poorly consolidated resedimented kimberlite.

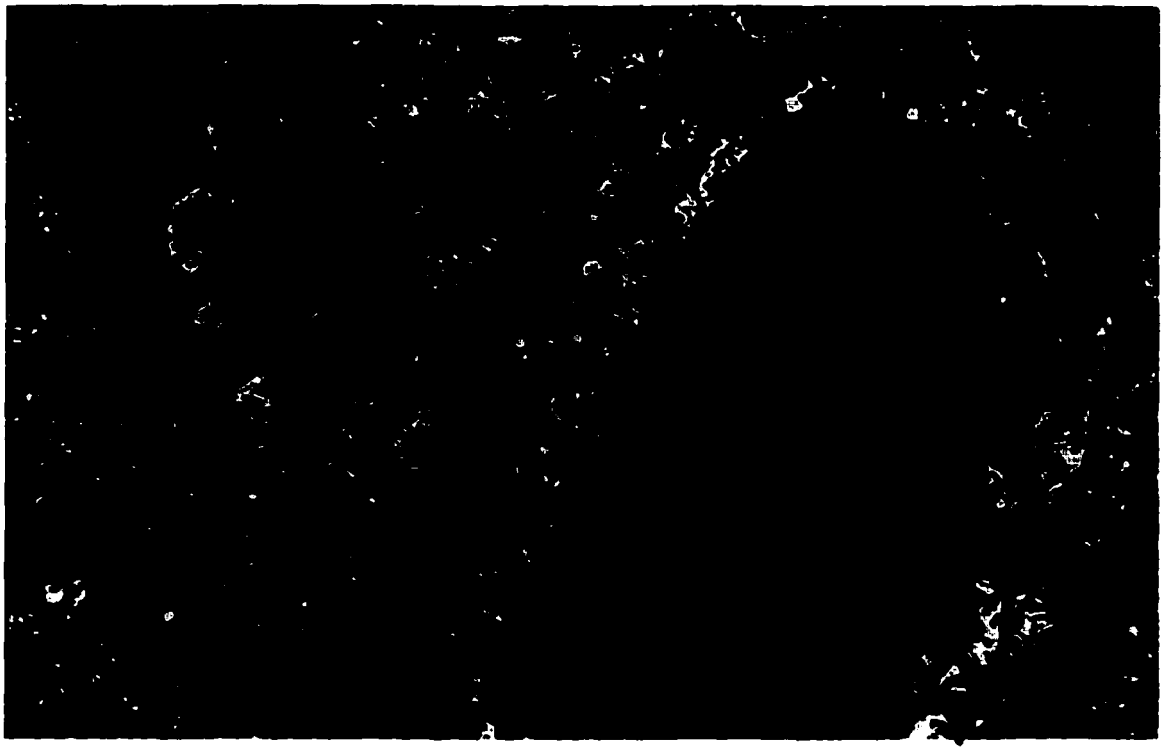

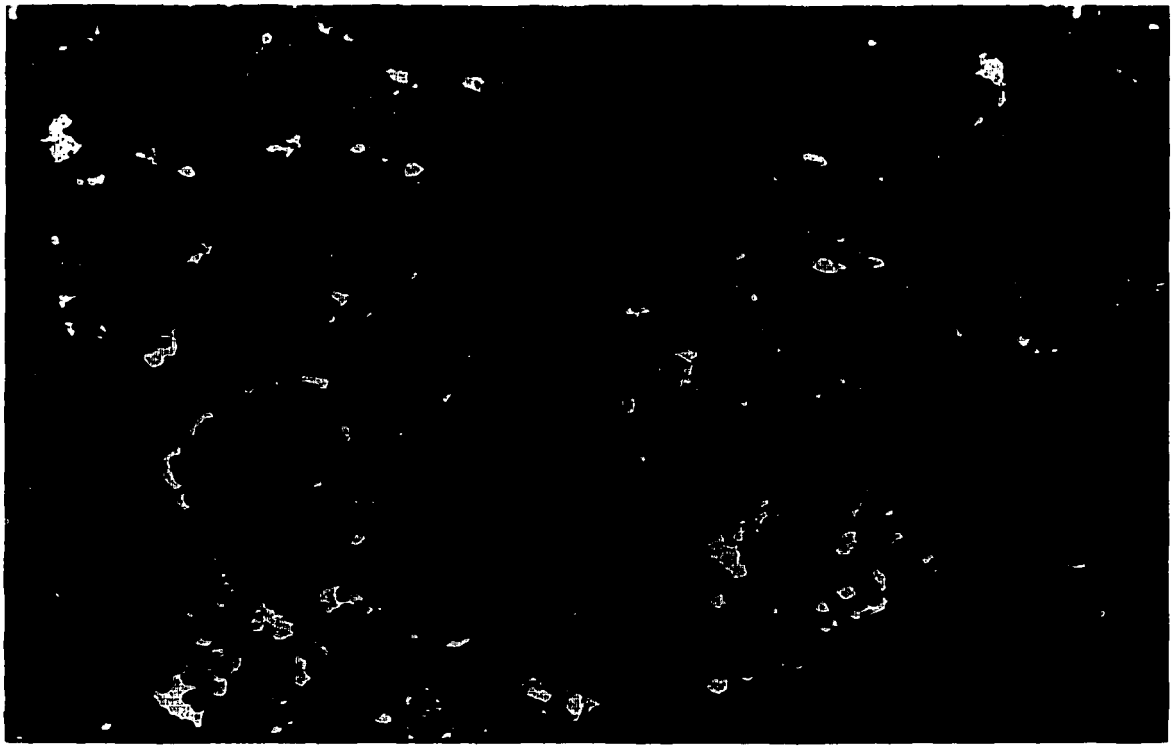

Figure 3.24. Kimberlite C27, Unit#1. BSE-image depicting a rounded lapillus (outlined) containing a kernel of fresh olivine (O) mantled by kimberlite consisting of microphenocrystal olivine, abundant fresh monticellite (M), perovskite (small, yellow crystals) and rare Ti-magnetite set in a matrix of calcite and serpentine. Note the similarities between the mineralogy of the lapillus and the surrounding kimberlite matrix in which it is set (F.O.V. 300 μm).

Figure 3.25. Kimberlite C27, Unit#2. BSE-image showing small, welded juvenile lapilli (J) within a pyroclastic kimberlite. Lapilli often contain a grain of olivine at their cores, which contain partial spinel (yellow) necklaces (F.O.V. 0.76 mm).

The above is set in a groundmass which consists of monticellite, perovskite, spinels, minor phlogopite, common globules of pyrite, apatite, minor prismatic rutile and rare zircon. Monticellite occurs as rather large (<30μm) subhedral crystals and may poikilitically enclose latter perovskites and spinels (refer to Figure 3.24). The groundmass is set in a fine-grained mixture of calcite and serpentine.

The groundmass is quite similar in character to the above-described lapilli-like juvenile clasts.

Unit#1 is a resedimented volcaniclastic kimberlite breccia.

3.2.7.2.2. Unit#2

Unit#2, distinctly different from Unit#1, is characterized by common, large (up to 7 mm) ovoid olivine macrocrysts. These crystals are completely pseudomorphed by brown-green serpentine. The bulk of the olivine population consists of microphenocrystal olivine pseudomorphs that are similarly completely replaced by serpentine. Rarely a relict core may remain and incomplete spinel necklaces may be present.

Xenoliths of biotite schist and single crystals of sericitized microcline are common. Relatively fresh biotite is abundant throughout this rock.

The above constituents are mantled by fine-grained kimberlite. This kimberlite ash is identical to the mantles described above in Unit#1. Small lapilli may contain a spinel at their cores or may be uncored. Unmantled olivines or single crystals of xenocrystal material are rare.

Unit#2 also contains common dark-brown, nearly aphanitic, amoeboid-shaped fragments of recycled, previously resedimented kimberlite. These fragments may be mantled by kimberlitic ash characteristic of the lapilli-like clasts.

The above-described fragments are tightly packed and sit within a secondary cement consisting of coarse calcite which has been nearly entirely replaced by dark brown serpophite. Smaller fragments appear to be welded (Figure 3.25).

Unit#2 is an intensely altered volcaniclastic kimberlite breccia, which may be an *in situ* pyroclastic lapilli tuff.

3.2.7.3. Discussion

C27 is a relatively small kimberlite vent, which has been evacuated, and subsequently infilled with predominantly resedimented volcaniclastic kimberlite breccia. Pyroclastic kimberlite appears to have contributed to vent infill.

No associated hypabyssal kimberlite was encountered within this vent.

3.2.8. Kimberlite C49

Kimberlite C49 is located nine kilometres south of the Diavik Diamond Projects, on the southern shore of Lac de Gras. It is characterized by an irregular-elliptical shaped magnetic low, approximately 145 x 115m in plan view. A coincident, slightly offset (to the northwest) strong electromagnetic anomaly is also present.

Kimberlite C49 intrudes well-foliated, porphyroblastic biotite schist and is overlain by approximately 10m of glacial regolith. Three holes have been drilled into C49, intersecting both hypabyssal and volcaniclastic kimberlite.

3.2.8.1. Macroscopic Observations

Drill hole C49-3 was drilled at an angle of –45 degrees, intersecting kimberlite at a vertical depth of approximately 30m. Kimberlite C49 appears to be a bedded volcaniclastic rock characterized by three distinct units from 1-10m in thickness. Contacts are not preserved and thus attitude could not be measured.

C49 consists of a brown-gray cognate kimberlite breccia (Unit#1) that consists of a greater number of cognate fragments, minor lithic clasts set in an earthy matrix. This breccia is in contact with a brown-gray, relatively competent heterolithic kimberlite breccia (Unit#2), which is characterized by numerous rounded, fine-grained cognate

fragments and abundant subangular lithic fragments (predominantly biotite schist and granite). These fragments together with approximately 10% pseudomorphed macrocrystal olivines are set in a matrix consisting of a variety of xenocrystal fragments. The above units appear to have been extensively reworked. .

Small distinctly different, competent beds lie in contact with both Units#1 and 2. Abundant kimberlitic fragments that have been cemented by a secondary carbonate characterize this kimberlite (Unit #3). Numerous varieties of cognate fragments are present, from nearly aphanitic brown-gray clasts resembling the rock seen in Units#1 and 2 and less altered coarser-grained microporphyritic kimberlite fragments. Lithic fragments are present.

The volcaniclastic kimberlite of C49 is cut by a relatively thin (approximately 1.5 m in vertical thickness) hypabyssal dyke (Unit#4). This gray, competent kimberlite in characterized by many large fresh macrocrystal olivines, small, dark cognate fragments and common altered granitic xenoliths.

The last ten metres of kimberlite intersection again marks a distinct change in the nature of the rock. Although the upper contact with the overlying volcaniclastic kimberlite is not preserved, a markedly different kimberlite occurs. This competent rock (Unit #5) is quite fine-grained, characterized by less than 15% of large olivine macrocrysts, together with far more numerous microphenocrystal groundmass olivines. This unit appears to be a segregation-textured hypabyssal kimberlite.

3.2.8.2. Microscopic Observations

3.2.8.2.1. Unit#1

Unit#1 is an intensely and pervasively altered rock characterized by the presence of quite numerous large, rounded macrocrystal olivine pseudomorphs. These olivines are replaced by yellow-brown serpophitic serpentine. Small cracks may be infilled with colourless calcite. Olivine macrocrysts may or may not be mantled by highly altered microporphyritic kimberlite. This kimberlite is dark brown with common small

completely replaced microphenocrystal olivines and common relatively fresh groundmass phlogopite and spinels set in an unresolvable matrix. The outer margins of these kimberlitic mantles are quite irregular in outline. The kimberlite mantles contain abundant tiny "serpophitic" serpentine crystals, which are likely very small pseudomorphed microphenocrystal olivines.

Microphenocrystal olivines are common in Unit#1 and are completely replaced by yellow serpophite. These crystals may also exhibit a thin mantle of kimberlite, as described above.

Identical microporphyritic kimberlite occurs as small clasts without olivine crystal cores, or may occur as a mantle on basement xenoliths (most commonly biotite schists) or relatively fresh xenocrysts or feldspar and quartz. These skins are commonly irregular in thickness and phlogopite may be tangentially oriented about the margins.

These fragments sit in a matrix of calcite and yellow brown serpentine. The serpentine looks to be replacing the calcite along margins of the clasts. The calcite is likely secondary (Figure 3.26).

The abundant lapilli and pelletal lapilli-like fragments within this unit are considered to be juvenile in nature. It is difficult to discern whether welding of the lapilli has occurred. This unit is considered to be a resedimented volcaniclastic kimberlite breccia.

3.2.8.2.2. Unit#2

This unit contains very few ovoid olivine macrocrystal (less than 10% of rock) pseudomorphs that underwent an initial stage of calcite replacement followed by subsequent veining and marginal replacement by brown serpophite. Small relict cores commonly remain. Microphenocrystal groundmass olivines are not present, but not abundant, and are replaced in a similar manner to their macrocrystal counterparts. Macrocrystal and microphenocrystal olivines may be mantled by fine-grained, microporphyritic kimberlite. This mantle is quite irregular in thickness, containing pseudomorphed microphenocrystal olivines, abundant groundmass spinels and rare mica

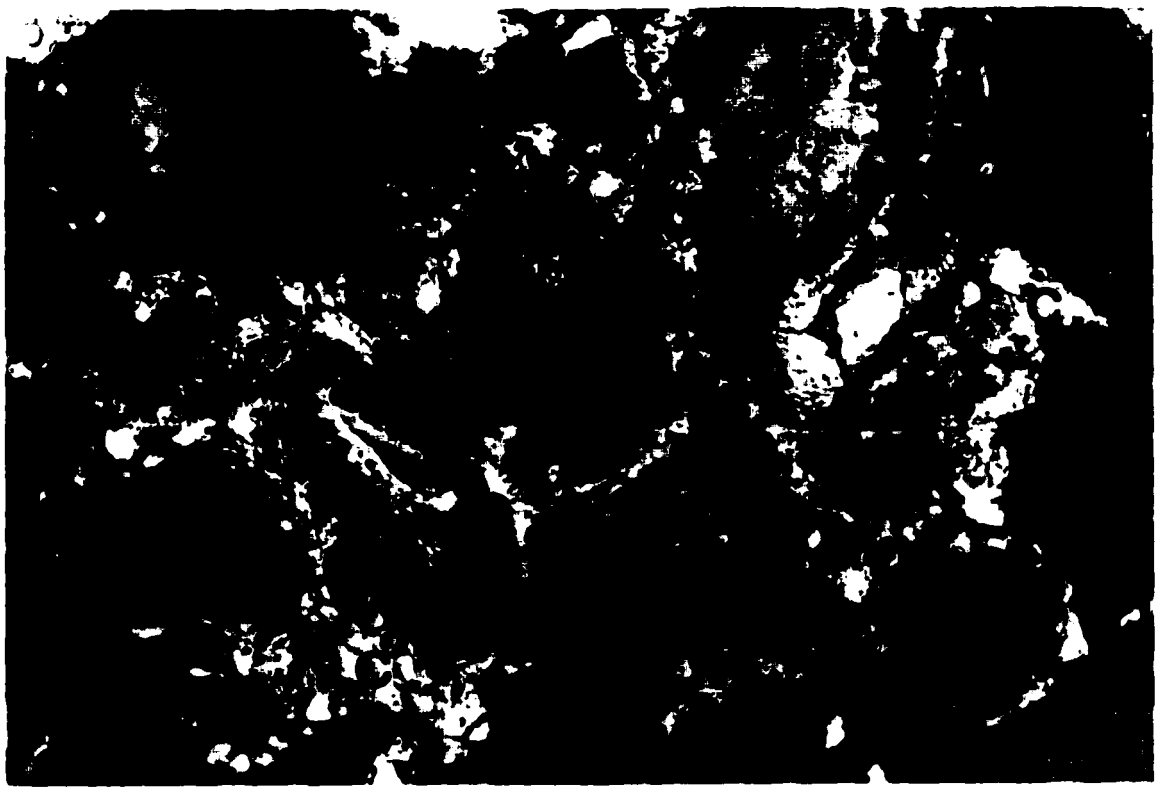

Reproduced with permission of the copyright owner. Further reproduction prohibited without permission.

Figure 3.26. Kimberlite C49. Unit#1. Densely-packed juvenile lapilli (J) set in a matrix of calcite (C) and serpentine (brown) (F.O.V. 1.0 mm).

Figure 3.27. Kimberlite C49, Unit#3. BSE-image showing irregular-shaped juvenile lapilli (J) cemented with a coarse, crystalline cement of calcite (C) and dolomite (D). Secondary pyrite (yellow) is strewn throughout the lapilli (F.O.V. 2.4 mm).

crystals set in a tan matrix of intimately intergrown calcite and serpentine. Xenolithic clasts of quartz mica schist are quite common within Unit#2 and are commonly mantled with the above-described microporphyritic kimberlite. These xenolithic cores are quite fresh, containing common Fe-Ni-sulphides and minor chloritization confined to their margins.

Cognate fragments of identical microporphyritic kimberlite lacking any central xenolithic or olivine kernel are also quite common. These ash-to-lapilli sized clasts are amoeboid in shape and are characterized by irregular-curvilinear margins. These fragments are considered to be juvenile in origin.

A second type of microporphyritic kimberlite clasts exists. These dark brown, very fine-grained fragments contain small pseudomorphed and are mantled by the microporphyritic kimberlite described above. This suggests that these clasts have been recycled, as they resemble small fragments of resedimented volcaniclastic kimberlite that has been poorly lithified and incorporated into this unit.

All of the above is set in a groundmass characterized by an abundance of rounded-to-subrounded, relatively fresh xenocrysts of alkali feldspar, biotite and quartz. Biotite is commonly altered by chlorite. Serpentines after monticellite pseudomorphs are common throughout the groundmass and subhedral-to-euhedral pyrite is abundant. The mesostasis consists of an unresolvable intimate intergrowth of calcite and serpentine (inferred).

3.2.8.2.3. Unit#3

Unit#3 is a clast-supported kimberlite breccia characterized by numerous tight-to-loosely-packed kimberlite clasts together with common quartz mica schist country rock fragments.

Two variety of kimberlite fragments occur is this rock: Dark brown, fine-grained subangular fragments containing numerous alkali feldspar xenocrysts, small ash-sized juvenile lapilli, minor pseudomorphed microphenocrystal olivines, euhedral-to-subhedral spinels, abundant anhedral calcite crystals and minor apatite and mica set in a very fine-

grained serpentine-calcite mesostasis. Broken crystals do occur at the margins, however their lobate-curvilinear nature suggests they were not well lithified upon incorporation into their current host. The second type of cognate clasts is composed of light brown, microporphyritic kimberlite, commonly with a large, partially serpentinized olivine macrocryst at its core. Less commonly large xenocrystal feldspars or small country rock fragments may form the kernel for these fragments. Kimberlite composing these clasts contains subhedral-to-euhedral olivine pseudomorphs (replaced by calcite, dolomite and secondary pyrite), abundant subhedral spinels, phlogopite, small rhombs of calcite, monticellite and rare rutile are set in a mesostasis of calcite and serpentine. These clasts commonly display a thin outer mantle, irregular in thickness, of a darker kimberlite, generally devoid of olivine, resembling a chilled margin suggesting that these cognate fragments were not solid upon their incorporation and likely juvenile in origin.

Smaller ash-sized, amoeboid-shaped, fine-grained kimberlite fragments occur interstitially to the larger-lapilli sized fragments, but share the same character as one of the above-described cognate clasts.

These clasts are cemented with coarse-grained, interlocking subhedral-to-euhedral plates of calcite and dolomite (Figure 3.27). All clasts are have an outer mantle of fine-grained, botroiydal calcite and dolomite. This cement is undoubtedly secondary.

No features of this rock suggest that it is an in situ pyroclastic kimberlite. Unit#3 is thought to represent a lapilli tuff that has been moderately reworked and subsequently redeposited and cemented by secondary carbonate.

3.2.8.2.4. Unit#4 and Unit#5

Unit#4 and Unit#5 are essentially identical and contain fresh, rounded (<10 mm) macrocrystal olivine (<10%), in which serpophitic replacement is generally confined to crack and crystal margins (Figure 3.28). Rare macrocrystal pyroxenes occur; these are altered in a similar manner to the olivines. Subangular biotite-bearing xenoliths of basement gneiss are present. These are not mantled by kimberlite. Unit#5 contains slightly fewer xenoliths. Subhedral-to-euhedral microphenocrystal olivines are abundant.

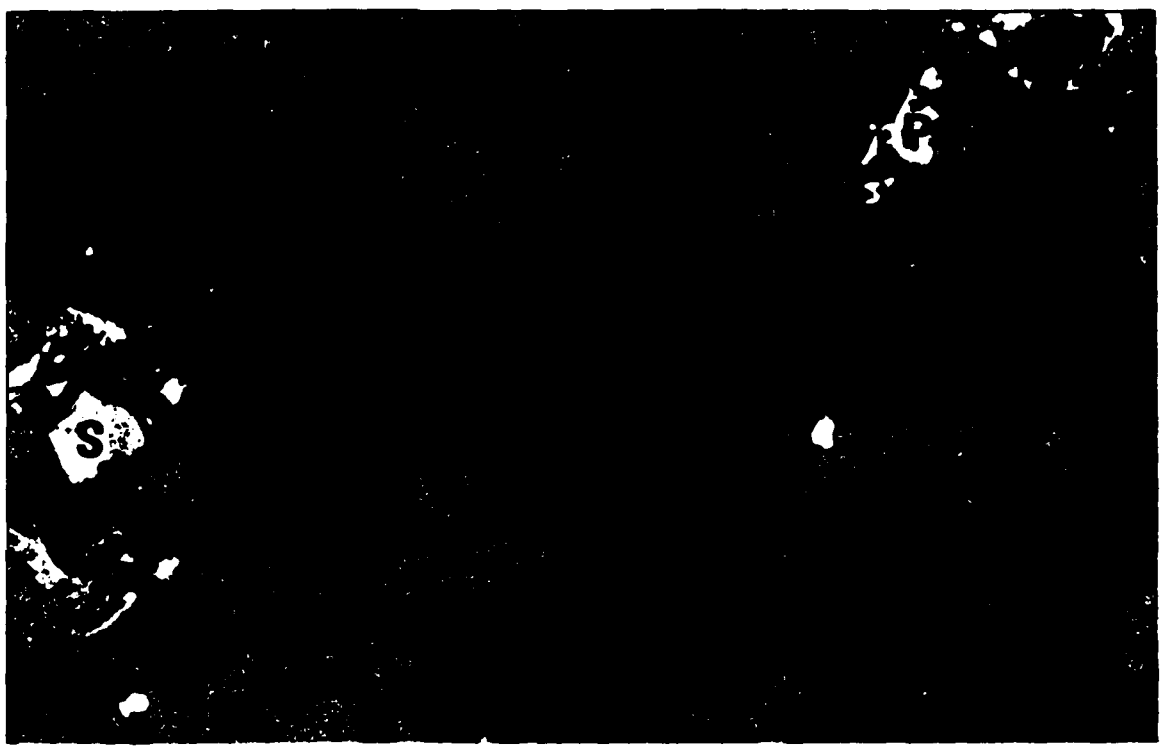

Figure 3.28. Kimberlite C49, Unit#4. Hypabyssal kimberlite containing few rounded macrocrystal olivine (O) and numerous small microphenocrystal groundmass olivine. The groundmass is characterized by small, amoeboid-shaped segregations (S) filled with calcite and serpentine (F.O.V. 6.0 mm).

Figure 3.29. Kimberlite C49, Unit #5. BSE-image of the groundmass of Unit #5, which consists of abundant laths of phlogopite (M), perovskite (P), spinel (S) set in a matrix of predominantly serpentine (blue) (F.O.V. 100 μm).

Larger crystals exhibit relict cores while smaller olivines may be totally replaced by yellow serpentine.

The groundmass contains common atoll spinels, subhedral-to-euhedral discrete opaque spinels, common brown perovskite (may be partially resorbed), apatite, abundant small subhedral crystals of calcite and small crystals of pseudomorphed monticellite. These pseudomorphs are commonly poikilitically enclosed by large crystals of phlogopite. These are set in a mesostasis consisting of abundant partially altered phlogopite, serpophite and calcite (Figure 3.29). Phlogopite crystals may contain up to 8wt% BaO.

The groundmass exhibits common, small irregular-shaped segregations of calcite and serpentine. Individual segregations may be filled entirely by calcite, or euhedral rhombs of calcite may be poikilitically enclosed within a serpentine-filled segregation.

This rock is a segregation-textured hypabyssal phlogopite calcite kimberlite.

3.2.8.3. Discussion

C49 is a small kimberlite vent that has been infilled by diverse resedimented volcaniclastic heterolithic kimberlite breccias and clast-supported volcaniclastic kimberlite breccias. Units#4 and #5 either represent rather large autoliths incorporated within the volcaniclastic kimberlites or the vent was intruded by a series of small sills subsequent to eruption and infill.

3.2.9. Kimberlite C42

Kimberlite C42 was discovered and in 1993. It is located two kilometres south of the southern shore of Ekadi Island beneath the waters of Lac de Gras. C42 is approximately one kilometre southwest of kimberlites A5 and A21.

Kimberlite C42 is overlain by 25-30m of lake water and 15-20m of glacial regolith. Ground magnetic surveys revealed no response, while the electromagnetic response of C42 was strong. The shape of C42 in plan view is unknown; ground EM

map was not observed. C42 presumably intrudes Archean granitoids as does nearby kimberlite A5, however only kimberlite was intersected in all drill holes and the host rock has not been observed.

Three vertical drill holes samples C42 and kimberlite was intersected to a depth of 326.0 m. Drill hole C42-3 was studied macroscopically and microscopically (refer to Appendix for complete drill log).

3.2.9.1. Macroscopic Observations

Drill hole C42-3 collared directly into volcaniclastic kimberlite and was also abandoned in volcaniclastic kimberlite at a depth of 326m. Kimberlite C42 is quite uniform throughout, that is, the vent is infilled with dark gray-brown, relatively incompetent, massive kimberlite characterized by abundant lithic fragments and xenocrysts. Lithic fragments comprise approximately 5-10% (predominantly granite with minor chlorite and biotite schists) of the kimberlite and have relatively sharp contacts with host.

Macrocrystal olivine pseudomorphs comprise 10-15% of the kimberlite and are altered by both calcite and serpentine. Macrocrystal chrome diopside is relatively common. Kimberlitic fragments are common and may be up to 1 cm in size.

The texture and mineralogy of the kimberlite remains quite uniform throughout the hole with only gradual and quite subtle changes in olivine grain size, xenolith proportion and alteration. Bedding contacts are not preserved. Thin beds of non-kimberlitic, massive mudstone, no greater than a few tens of centimetres in width, occur throughout the hole and appear to increase in abundance downhole. One small xenolith of metamorphosed shale occurs at a depth of 281m.

3.2.9.2. Microscopic Observations

All samples are very similar in mineralogy and texture with notable difference occurring in proportions of olivine macrocrysts, country rock xenoliths, xenocrysts and kimberlitic fragments.

Kimberlite C42 contains a wide variety of clasts, both cognate and accidental, which are not mantled by kimberlite. These highly altered ash-to-lapilli-sized microporphyritic clasts are tan in colour and contain numerous crystals of pseudomorphed subhedral-to-rounded olivine microphenocrysts, numerous euhedral-to-subhedral spinels, small crystals of mica and may contain tiny, rounded "segregations" of calcite. Based on their morphology, these rounded segregations probably represent small vesicles infilled with secondary calcite (Figure 3.30). Xenocrystal biotite and potassium feldspar (microcline) is commonly present. Zircon may be present as a groundmass constituent of these lapilli. The above are set in an optically unresolvable tan matrix presumably serpentine and calcite. The margins of these amoeboid-shaped lapilli are irregular-lobate. These lapilli are considered to represent juvenile material. These clasts may contain a rounded macrocrystal olivine at their cores. Elongated constituents (mica and feldspar) may be tangentially oriented about the margins of these juvenile pelletal lapilli (Figure 3.31).

A second type of ash-sized clast is present, but not common in this section. These very fine-grained clasts contain common, very small serpentinized olivine microcrysts and minor crystals of mica in a spinel-rich groundmass containing Ti-magnetite and chromite. These are set in a matrix of calcite and serpentine. It cannot be determined whether these small fragments are autoliths or true juvenile lapilli.

Macrocrystal olivine occur throughout the C42, and may comprise less than 5% to greater than 20% of the rock. Macrocrystal olivines are replaced by dark green serpophitic serpentine and are commonly mantled and veined by calcite. Coarse, crystalline calcite may also replace the core of some of the olivine macrocrysts. Microphenocrystal olivines are strewn throughout the groundmass and are completely pseudomorphed by dark green serpophite. A thin mantle of fine-grained kimberlite ash may mantle macrocrystal olivine.

Numerous xenoliths of country rock material (from less than 5% to greater than 30%) and a plethora of relatively fresh xenocrysts of potassium feldspar, quartz and biotite derived from the disaggregation of this material characterized this rock. Biotite schist and granite gneiss represent the bulk of the xenoliths within this vent.

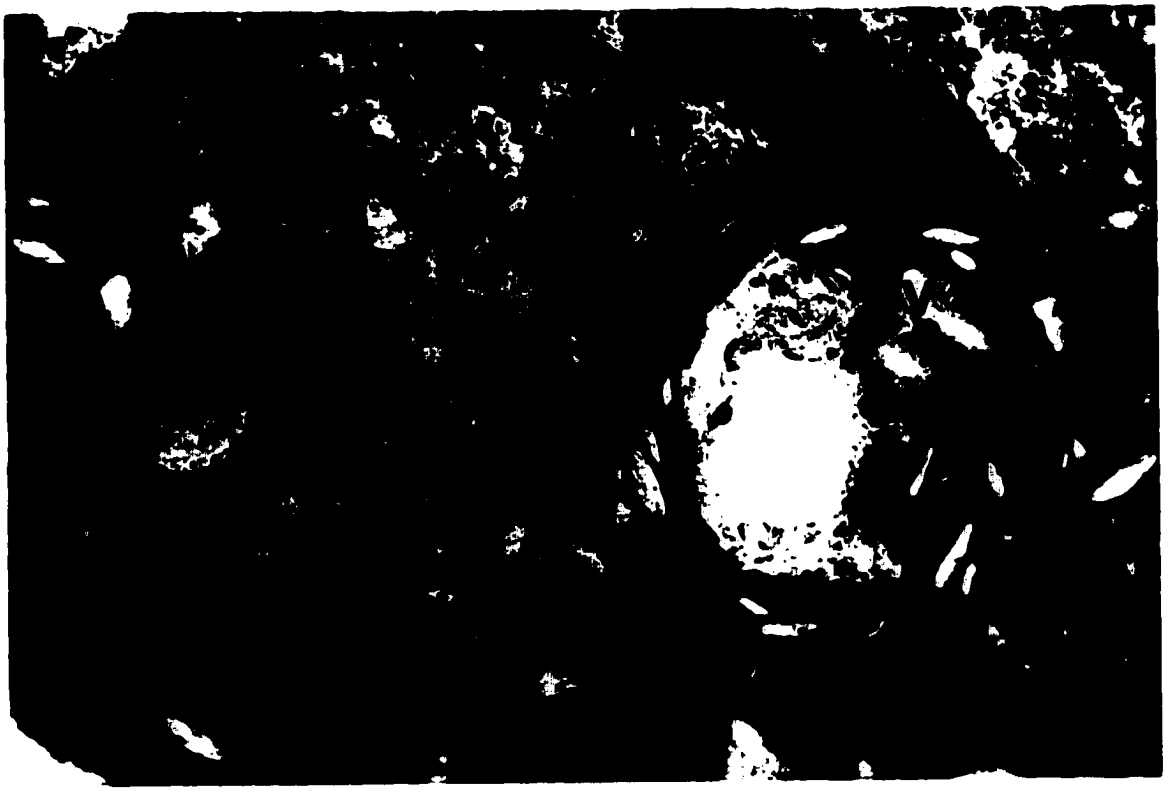

Figure 3.30. Kimberlite C42. Resedimented volcaniclastic kimberlite containing numerous juvenile lapilli (J) Larger lapilli (top of microphotograph) contain calcite-filled vesicles (V) (F.O.V. 2.5 mm).

Figure 3.31. Kimberlite C42. Juvenile lapillus with tangentially oriented feldspar (white) along its margin. Minor ellipsoidal and irregular-shaped calcite-filled vesicles (V) are present (F.O.V. 1.0 mm).

Replacement of margins by calcite and serpentine is common. Xenocrysts include subangular-to-subrounded relatively fresh laths of microcline and tan-brown biotite.

The above constituents are set in a groundmass numerous spinels (mainly chromite and Ti-magnetite), apatite, abundant euhedral pyrite, anhedral plates of calcite, minor phlogopite, zircon, Mg-ilmenite, diopside and rare garnets with kelphytic rims. The mesostasis consists of a very fine-grained intergrowth of calcite (commonly replaced by dolomite further downhole), serpentine and ± phlogopite. Dilational serpentine veins are very common throughout the rock.

3.2.9.3. Discussion

Due to the high proportion of country rock-derived xenocrysts and xenoliths, C42 is interpreted as representing a fairly large kimberlite vent infilled with crudely bedded resedimented volcaniclastic kimberlite breccia. No hypabyssal rock was intersected, either as sills or dykes at high structural levels or as a root zone-feeder system.

The mudstone units likely represent thin veneers of subaqueously-deposited sediment during hiatuses in vent infill, or may merely represent xenoliths of Cretaceous sediment that overlaid the Archean basement at the time of kimberlite emplacement.

3.2.10. Kimberlite DD39

DD39 is located thirty-one kilometres west of the Diavik Diamond Project, 4 kilometers off the western shore of Lac de Gras.

DD39 does not represent a single kimberlite body but numerous small circular-to-ellipsoidal magnetic lows approximately 0.4 hain size. These anomalies are approximately 200m apart and form a nearly straight line within a strike of northeast-southwest. Kimberlite was intersected in three of these anomalies; however, it is not known whether similar types of kimberlite characterize these bodies.

Drill hole DD39-1 was investigated, which is a vertical hole into the most westerly magnetic low. The anomaly is overlain by approximately 10m of glacial

regolith and is hosted within Archean biotite schist of the Yellowknife Supergroup. Nearly 100 m of bedded kimberlite was intersected and the drill hole was terminated at 107 m. No country rock was intersected.

3.2.10.1. Macroscopic Observations

Kimberlite DD39 is a relatively incompetent-to-competent bedded volcaniclastic kimberlite composed of numerous units of distinct kimberlite units ranging in thickness from 15 cm to 22m.

Kimberlite is intersected at a depth of eleven metres. The upper eight metres (Unit#1) is composed of gray-brown kimberlite containing common (≈5-10%) macrocrystal olivine. The top of this unit is highly altered and oxidized. This is presumably the result of groundwater inundation. These relatively large (<8 mm) rounded crystals may be fresh-to-altered and are commonly broken and angular. Rare, small green chrome diopsides are strewn throughout this unit. The majority of the olivine population occurs as small subrounded-to-subhedral fresh-to-altered groundmass microphenocrysts. These crystals together with minor dark brown-black, aphanitic cognate fragments and opaque spinels are set in a medium gray-brown, fine-grained matrix that is characterized by a plethora of small, irregular-shaped pods and small veins of carbonate. A small unit (40 cm in thickness) of dark brown-black reworked kimberlite has been deposited within Unit#1. It contains approximately 10% coarse, serpentinized olivine macrocrysts in a dark, earthy, featureless matrix. The uppermost contact of this unit with Unit#1 was measured at 60 degrees to the core axis. The lower contact was not preserved.

The next 16m is comprised of two alternating units of reworked and highly altered volcaniclastic kimberlite, ranging in thickness from less than one metre to greater than six metres.

The uppermost unit is this doublet (Unit#2) is an intensely altered dark brown-green kimberlite which contains partially altered, rounded olivine macrocrysts and abundant small subrounded groundmass microphenocrystal groundmass olivines. The

proportion of the later varies greater throughout the thin units (≈10%-40%). Olivine, together with abundant xenocrystal feldspar, mica and common subrounded cognate fragments which range from aphanitic to microporphyritic, are set in a dark, very fine-grained matrix of predominantly serpentine. Small segments of Unit#2 may be oxidized to an orange-brown colour. Elongated constituents may show a crude subhorizontal alignment.

Unit#2 is interbedded with a medium gray, moderately competent, pervasively altered kimberlite (Unit#3). Very few primary features are discernable. Small black, aphanitic fragments with thin reaction rims and few identifiable olivine macrocrysts are set in an intensely serpentinized matrix.

At a depth of 35m a thick (≈22m), massive dark gray-black unit of resedimented kimberlite breccia is encountered (Unit#4). This kimberlite contains approximately 10-15% serpentinized subrounded olivine macrocrysts. Many of these crystals are fragmented. Similarly altered microphenocrystal olivine are strewn throughout the groundmass together with abundant xenocrystal mica and feldspar and common ash-to-lapilli-sized aphanitic-to-microporphyritic kimberlitic fragments. The above is set in a dark brown, earthy, very fine-grained matrix.

Beneath this initial thick bed, Unit#4 is interbedded for 20-25m with a gray-green, competent kimberlite (Unit#5). Bed thickness ranges from <3 to >6m. Unit#5 contains abundant fresh-to-partially altered olivine macrocrysts and rare macrocrystal pyroxene and garnet. A thin rind of kimberlitic material commonly mantles these crystals. These pelletal lapilli-like fragments, together with uncored clasts, dark brown aphanitic cognate fragments and small fresh-to-partially altered microphenocrystal olivines are set in a carbonate-rich matrix. Unit#5 may vary with respect to the carbonate matrix and fragment proportion. The proportions of distinct varieties of fragments also varies throughout the various beds of Unit#5.

Through the last 25m of the intersection Units#4 and 5 regularly alternate but are intruded by a competent medium gray macrocrystal kimberlite. This fresh rock contains abundant fresh, rounded macrocrystal olivine, rare pyroxene and copious amounts of smaller, fresh microphenocrystal groundmass olivine. These together with abundant

opaque oxides are set in a gray matrix containing small irregular veins of calcite. This calcite may also be replaced by serpentine.

3.2.10.2. Microscopic Observations

3.2.10.2.1. Unit#1

Unit#1 is characterized by the presence of numerous large (<10 mm) well-rounded olivine macrocrysts and minor macrocrystal pyroxene, which may be weakly, strained. Rare rounded polycrystalline microxenoliths of lherzolite are present. All are similarly replaced by yellow-brown serpophite, which is generally confined to cracks and margins.

The groundmass contains numerous partially altered subhedral-to-euhedral microphenocrystal olivine. Larger crystals usually exhibit a relict core while smaller crystals are commonly completely serpentinized. This oxide-rich groundmass contains numerous subhedral-to-euhedral, discrete and complex atoll spinels, abundant apatite (common as late stage poikilitic, irregular masses), small subhedral perovskite (<20μm), minor Ba-rich phlogopite and accessory rutile. The mesostasis exhibits a sugary-granular texture due to the presence of small, partially serpentinized crystals of monticellite in an intimate mixture of calcite, dolomite and serpentine (Figure 3.32).

The groundmass of Unit#1 is characterized by the presence of numerous, small "segregations". These "segregations" are filled entirely with coarse, interlocking crystals of anhedral calcite. Minor replacement by serpentine is common. These calcite-filled bodies show sharp contacts with the oxide-rich groundmass (Figure 3.33).

The nature of these bodies suggests they are not "segregations" but secondary cement. Unit#1 is considered to represent an olivine-crystal rich volcaniclastic kimberlite. Whether Unit#1 has undergone resedimentation process is difficult to determine. However, the obvious lack of lithic constituents (no lithic xenocrysts or xenoliths were observed) and the lack of abrasion of fragile fragments suggest that very

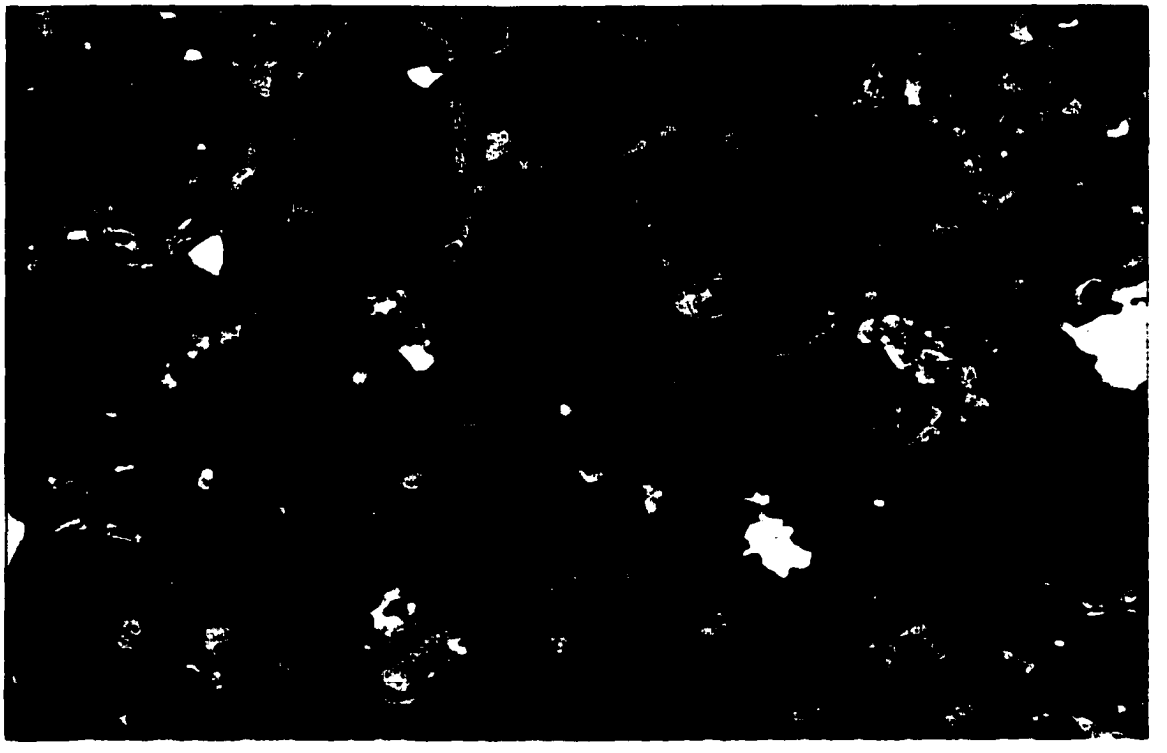

Figure 3.32. Kimberlite DD39, Unit#1. BSE-image depicting a sugary-granular textured matrix consisting of completely serpentinized crystals of monticellite (M) set in a mesostasis of calcite, dolomite and serpentine (F.O.V. 76 μm).

Figure 3.33. Kimberlite DD39, Unit#1. BSE-image of irregular-shaped calcite-filled bodies (C). These bodies represent secondary cement within this pyroclastic kimberlite (F.O.V. 0.54 mm).

little, if any reworking of Unit#1 occurred. It this case, Unit#1 can be termed an olivine crystal-rich volcaniclastic kimberlite tuff.

3.2.10.2.2. Unit#2

Most petrographic samples of Unit#2 are unsuitable for petrographic analysis, as intense and pervasive alteration has obliterated most primary textural and mineralogical features.

Unit#2 contains common macrocrystal olivine pseudomorphs, which are completely replaced by brown-green serpophite and veined and mantled by colourless calcite. A thin rind of microporphyritic kimberlite mantles many of these crystals, which is commonly discontinuous about the central core. This mantle contains small pseudomorphed microphenocrystal olivines, small subhedral spinels and rare brown perovskite set in an irresolvable matrix of presumably serpentine and calcite. Olivine crystals may be aligned tangentially along the margins of these fragments. Uncored fragments composed of identical kimberlite are common. These occur as subcircular bodies with microporphyritic kimberlite cores, which contain aphanitic margins. The fine-grained margins appear identical to the kimberlite core but are devoid of olivine. These rims resemble chilled margins suggesting that the fragments were not solid at the time of their incorporation into their current host and are *bona fide* juvenile lapilli.

Ash-sized dark brown, optically unresolvable, irregular-shaped clasts are also common throughout Unit#2. These do not appear to contain kimberlite-derived constituents and are likely derived from high stratigraphic levels (poorly consolidated Cretaceous sediments).

Many intensely altered fragments are difficult to distinguish from the similarly altered matrix.

Xenoliths of sericitized feldspar and biotite-bearing basement rock are common and are commonly mantled by a thin kimberlite rind.

The above is set in an intensely altered matrix which consists essentially of brown-green serpentine. The matrix seems to contain abundant ash-sized completely altered fragments of unknown origin.

Unit#2 represents an intensely altered resedimented volcaniclastic kimberlite.

3.2.10.2.3. Unit#3

Unit#3 represents a highly altered heterolithic breccia containing abundant cognate fragments and a profusion of xenocrysts.

Olivine macrocrysts are relatively common and occur as relatively large (<8 mm) rounded crystals replaced by both serpentine and calcite. Rare microxenoliths of rounded lherzolite occur. Macrocrystal olivines may be mantled by a thin, discontinuous rind of microporphyritic kimberlite containing altered microphenocrystal olivine, opaque spinels and brown perovskite in an unresolvable matrix. Uncored fragments of the above-described kimberlite are common. These lapilli-sized clasts exhibit highly irregular-curvilinear fine-grained margins that are generally devoid of olivine. Olivines present within these margins are usually tangentially oriented. These fragments are likely juvenile in origin.

Small, dark brown, fine-grained cognate fragments are strewn throughout this unit. These resemble recycled autoliths of poorly consolidated, disrupted volcaniclastic kimberlite.

The groundmass is characterized by the presence of abundant fresh quartz, feldspar and mica xenocrysts. These crystals are subangular-to-subrounded in nature and are not mantled by kimberlite. Small, subrounded-to-irregular-shaped, very fine-grained non-kimberlitic clasts are also present within the groundmass. These represent xenoliths derived from high stratigraphic levels, presumably poorly consolidated Cretaceous mudstone. Minor microphenocrystal olivines, apatite also occur within the groundmass. Numerous calcite-filled veinlets cut the groundmass.

All of the above is set in a brown, turbid mesostasis of calcite and serpentine.

Unit#3 is an intensely altered resedimented volcaniclastic kimberlite breccia. It is very similar to Unit#2 in most respects but contains far more abundant cognate fragments xenocrystal constituents.

3.2.10.2.4. Unit#4

Unit#4 is a fragmental rock, which contains numerous types of kimberlite fragments.

The first type of fragment is a dark brown, very fine-grained clast with abundant angular fragments of feldspar, mica and rarely quartz, small, rare subrounded microphenocrystal olivine pseudomorphs and common opaque oxides set in a brown, turbid matrix. Kimberlite-derived constituents only make up a small proportion of these ash-to-lapilli sized fragments. Their margins are commonly irregular in character and may contain broken crystals. These fragments are considered to represent xenoliths of poorly consolidated mudstone that overlaid the Archean basement at the time of kimberlite emplacement.

A second type of clast occurs as rounded, lapilli-sized circular microporphyritic kimberlite-derived fragments. These fragments are characterized by abundant relatively fresh subrounded-to-euhedral microphenocrystal olivine and less common large, rounded macrocrystal olivines together with subhedral-to-euhedral brown perovskite, numerous spinels, apatite, primary calcite, minor pyrite and ilmenite set in a granular matrix composed of pseudomorphed (by serpentine and dolomite) monticellite set in a mesostasis of calcite and serpentine. At their cores these lapilli commonly contain a single rounded, commonly serpentinized macrocrystal olivine or less commonly a rounded, partially kelphytized garnet or a small autolith. The kimberlite mantles may be continuous around the whole core or form discontinuous fringes of irregular thickness. The mantles may also graded into margins, which are poor in, or devoid of olivine. The outer rim of the clasts consists of two zones that differ in colour, but not in mineralogy. Poorly developed internal flow alignment may occur. Small subcircular calcite-filled

bodies may occur within these margins. This indicates that these lapilli are juvenile in origin.

Less abundant clasts of dark gray fine-grained microporphyritic kimberlite also occur within Unit#4. These fragments contain pseudomorphed microphenocrystal olivines, opaque oxides, perovskite and minor mica. The clasts are of very irregular shape and are characterized by lobate, embayed and curvilinear complex margins. Subcircular, calcite-filled vesicles may be present. The morphology of the clasts and the presence of vesicles indicates that they are juvenile fragments of kimberlite.

The above clasts, together with common rounded, unmantled pseudomorphed, commonly broken macrocrystal olivine and rare pyroxene are set in a groundmass consisting of common fresh-to-altered microphenocrystal olivine, rare fragments of garnet, common xenocrystal quartz, feldspar and mica, minor apatite, spinels and sulphides set in a brown-red mesostasis of serpentine and calcite.

The fragmental texture of this unit, the presence of juvenile fragments and relatively fresh xenocrystal constituents suggest this unit has undergone resedimentation processes and can thus be called a resedimented volcaniclastic heterolithic breccia.

3.2.10.2.5. Unit#5

Unit#5 is quite similar to Unit#4. It contains kimberlite fragments and minor xenoliths (as described above) together with minor rounded, relatively fresh, unmantled macrocrystal olivine (Figure 3.34). Interstitial to these larger fragments are tan-brown, very fine-grained ash-sized fragments which resemble the chilled margins that mantle some juvenile lapilli (Figure 3.35). These fragments are likely small juvenile clasts. Large fragments (up to 10 cm) of resedimented volcaniclastic kimberlite may occur within this unit.

The most notable difference is the clast-to-matrix ratio and the composition of the matrix. The fragments are set in an undoubtedly secondary coarse crystalline calcite cement. Minor dolomite is also present. This cement may be replaced by yellow-brown serpentine. No welding of the juvenile fragments is observed.

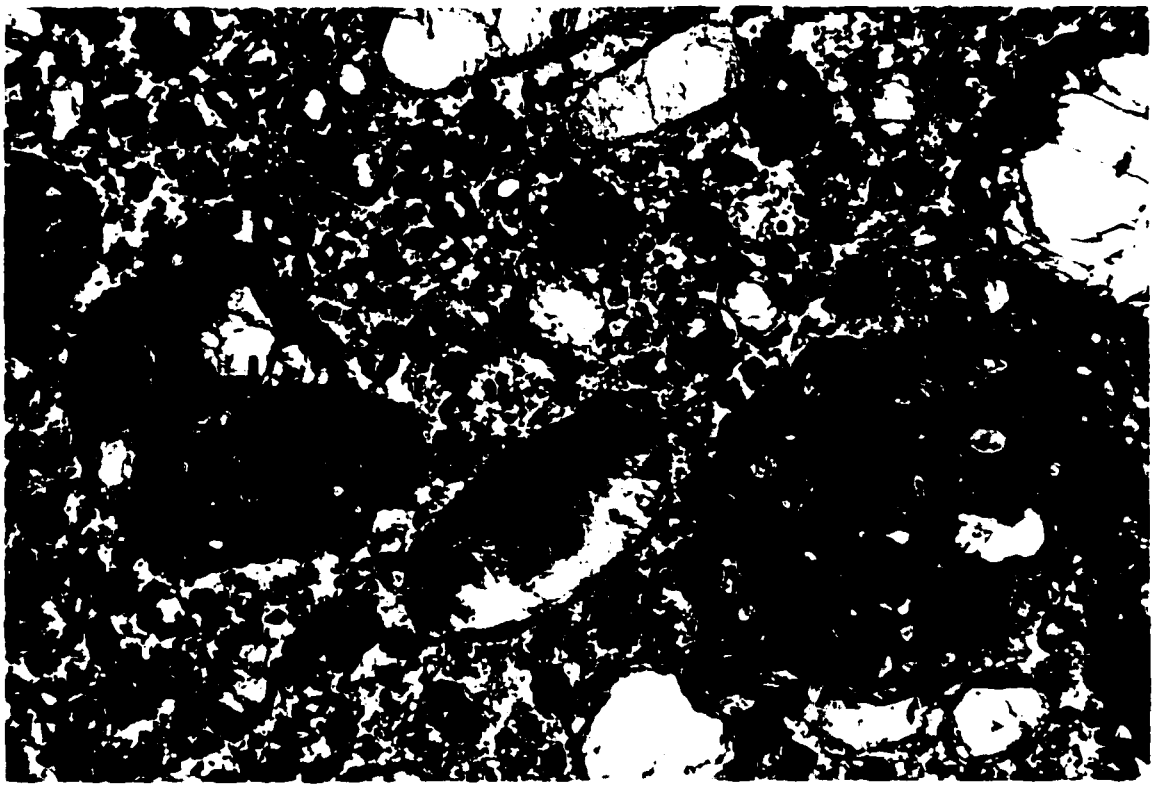

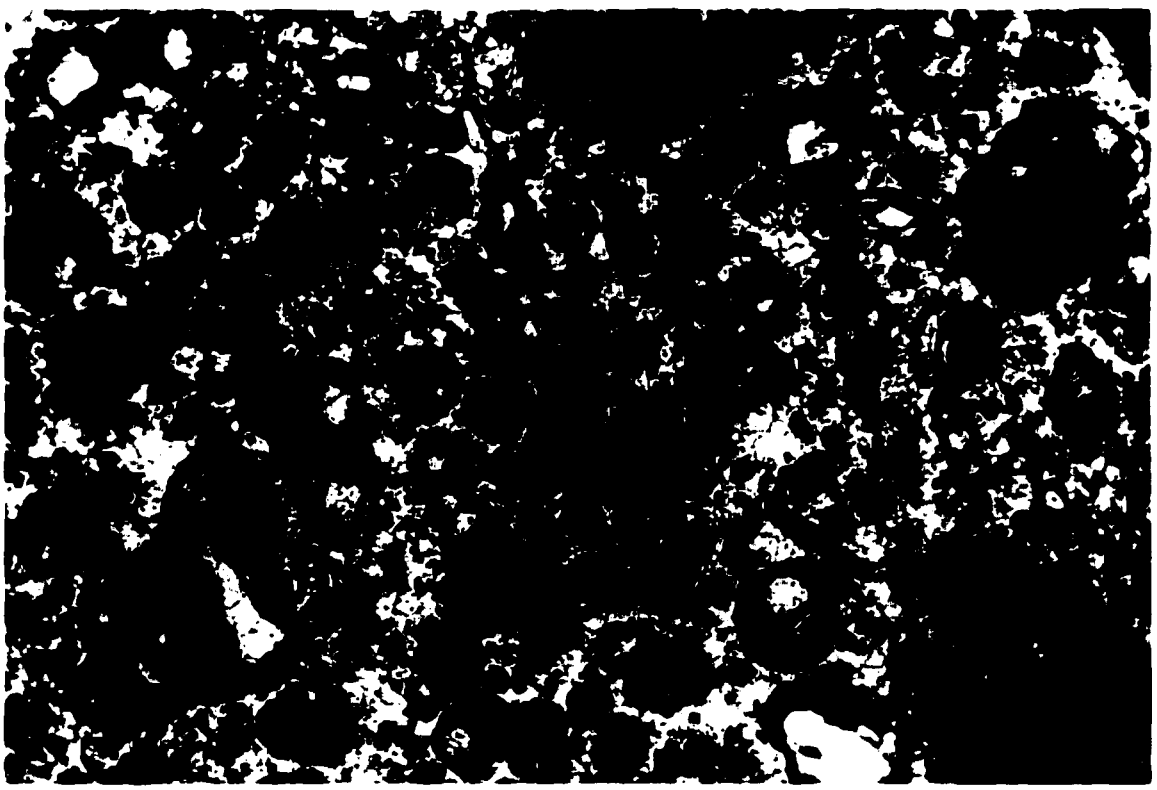

Figure 3.34. Kimberlite DD39, Unit#5. A pyroclastic lapilli tuff consisting of juvenile lapilli (J) and autoliths (A) cemented by a secondary calcite matrix. Single crystals of unmantled, rounded olivine are common (F.O.V. 6.0 mm).

Figure 3.35. Kimberlite DD39, Unit#5. Smaller groundmass juvenile fragments (J). Some minor welding (W) and molding has occurred (F.O.V. 2.5 mm).

These fragments were formed by pyroclastic processes, however, it is difficult to comment on whether reworking of this clastic deposit was significant. The paucity of extraneous and very fine-grained material and the lack of abrasion and breakage of the clasts suggest that reworking has not been important in their formation. In this case, this volcaniclastic kimberlite can be properly termed a pyroclastic lapilli tuff.

3.2.10.2.6. Unit#6

Unit#6 is characterized by the presence of numerous large, rounded spherical-to-ovoid, relatively fresh olivine macrocrysts (Figure 3.36). Alteration is confined to minimal serpentinization along the margins and cracks of individual crystals. Polycrystalline microxenoliths of lherzolite occur within Unit#6, but are comparatively rare. A second, distinct population of small subhedral-to-euhedral microphenocrystal olivine is characteristic of this unit. Larger microphenocrysts are partially altered by yellow serpophite while smaller crystals may be completely replaced. One lithic clast of altered muscovite-biotite schist is present in thin section.

The oxide-rich groundmass consists of numerous discrete and complex atoll crystals and partially resorbed magnetite, abundant apatite occurring as acicular sprays of radiating prismatic crystals or as euhedral-to-subhedral stout minerals, partially resorbed subhedral perovskite, phlogopite and minor pyrite. The mesostasis consists of an intimate mixture of Ba-rich phlogopite, calcite and serpentine. Few subhedral, partially altered crystals of monticellite are strewn throughout the mesostasis.

Numerous amoeboid-shaped bodies and irregular veins of calcite-serpentine segregations characterize the groundmass. These segregations are filled predominantly with interlocking calcite and are lined with botroiydal serpentine. Small, spherical masses of serpentine may be poikilitically enclosed within the calcite (refer to Figure 3.36). Euhedral rhombs of calcite and dolomite may occur along the margins of these segregations as well. Segregations may also be entirely filled with yellow serpophite with small crystals of calcite lining their margins. The margins of the segregations are gradational with the oxide-rich groundmass.

Figure 3.36. Kimberlite DD39, Unit#6. Segregation-textured macrocrystal hypabyssal kimberlite (F.O.V. 6.0 mm).

Unit#6 is considered to represent a segregation-textured macrocrystal hypabyssal oxide-rich phlogopite apatite kimberlite occurring at high stratigraphic levels within the kimberlite vent, in direct contact with volcaniclastic kimberlite.

3.2.10.3. Discussion

Kimberlite DD39 is a small volcanic vent that was evacuated and subsequently infilled predominantly with resedimented volcaniclastic kimberlite. Short-lived, primary pyroclastic activity, which appears to have disrupted earlier deposited kimberlite units, may have also contributed to vent infill resulting in relatively fresh, thin lapilli tuffs. The vent infill was than intruded by numerous late stage, small subhorizontal sills at high stratigraphic levels.

3.2.11. Kimberlite T29S

Kimberlite T29S was discovered and drilled in 1992 and is located just off of the southeastern shore of Lac de Gras, 6 kilometres south of the Diavik Diamond Project.

Kimberlite T29S is overlain by less than 5 m of glacial regolith and occurs adjacent to a north-south trending diabase dyke of the Mackenzie swarm. Ground magnetic surveys reveal a 50x250m, 1200 nT oval-shaped magnetic low, which is the southern portion of a north-south trending echelon shaped dyke system which includes both T29N and T29S. The elongated 30x110m form of T29N is slightly offset to the east of T29S. Both have an identical strike of about N15°W. Both T29N and S have no electromagnetic signature.

Kimberlite T29S intrudes Archean two mica granite. The host rock of T29N is biotite schist, a metamorphosed sediment of the Yellowknife Supergroup.

Only one hole was drilled into T29S at an angle of –55 degrees. Twenty metres of kimberlite was intersected.

3.2.11.1. Macroscopic Observations

Kimberlite T29S is a dyke probably no more than 10-12m in thickness. It is relatively homogeneous (no evidence of flow differentiation) lithic breccia consisting of approximately 15% (varies locally) subangular-to-subrounded xenoliths of granite and minor biotite schist. Xenoliths are commonly bleached and may have thin reaction margins.

Macrocrystal olivines occupy about 10% of the dyke and are generally fresh-to-partially serpentinized. Serpentinization is generally confined to the margins of the macrocrysts. Groundmass microphenocrystal olivines are partially fresh-to-completely replaced by serpentine. Oxides are abundant, including rare macrocrystal oxides similar in size to microphenocrystal olivines. Prominent, rounded segregations are common throughout the kimberlite.

The margins of the host granite are brecciated and oxidized (confined to within 50 cm of the kimberlite). Minor bleaching of the granite is evident.

No associated volcaniclastic rocks occur at T29S.

3.2.11.2. Microscopic Observations

Kimberlite T29S contains relatively few large, ovoid, fresh olivine macrocrysts (Figure 3.37). Minor replacement by yellow-brown serpophitic serpentine along cracks and margins is common. Microphenocrystal groundmass olivines are common, many are fresh or have relict cores, others are completely pseudomorphed by yellow-brown serpophite. Thin pale green rims chlorite may mantle some groundmass olivines. Discontinuous spinel necklaces may decorate the microphenocrystal olivines.

Groundmass spinels occur as subhedral-to-euhedral, discrete opaque crystals. Macrocrystal magnetite up to 300 μm in size are common. Atoll spinels are not common. Spinels, perovskite (up to 100 μm) and individual euhedral prisms and numerous sprays

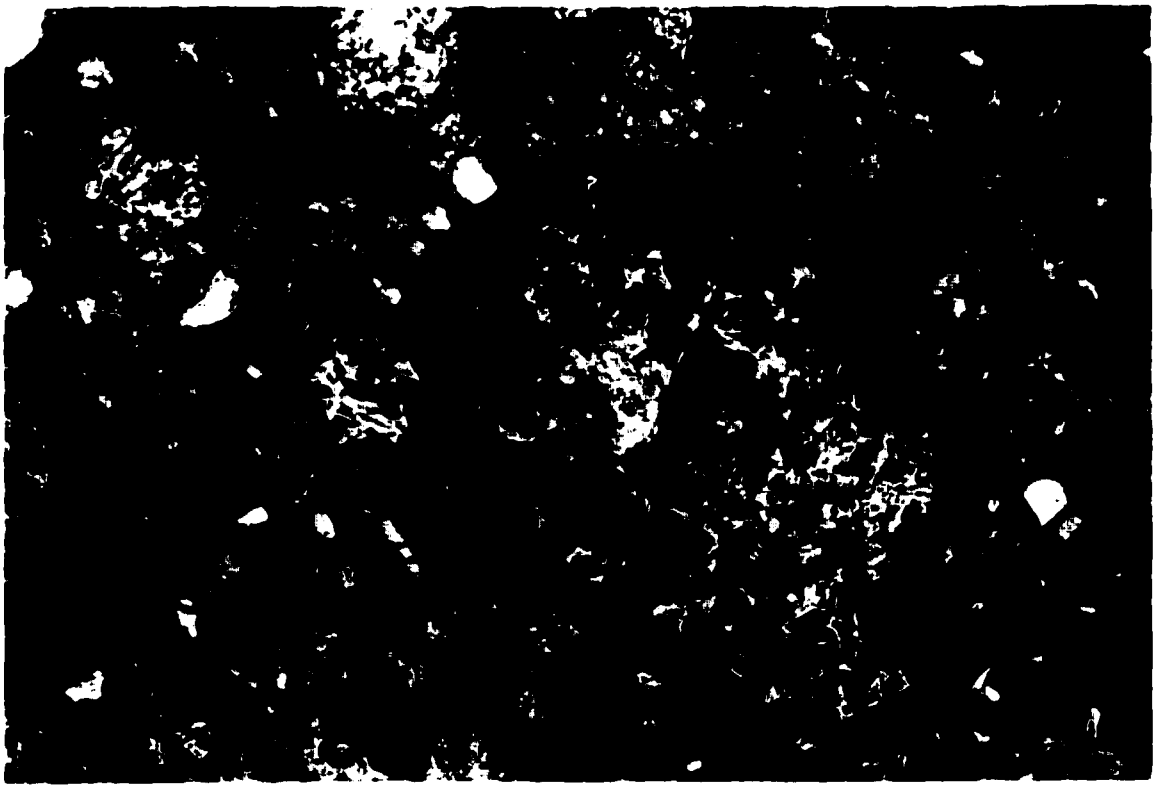

1114

Figure 3.37. Kimberlite T29S. Oxide-rich segregation-textured hypabyssal kimberlite characterized by relatively few macrocrystal olivine (O) (F.O.V. 6.0 mm).

Figure 3.38. Kimberlite T29S. Small clast-like segregation (outlined) infilled with colourless, prismatic pectolite (white) and interstitial serpentine. Orange-red mineral along the margin of the body is phlogopite (F.O.V. 6.0 mm).

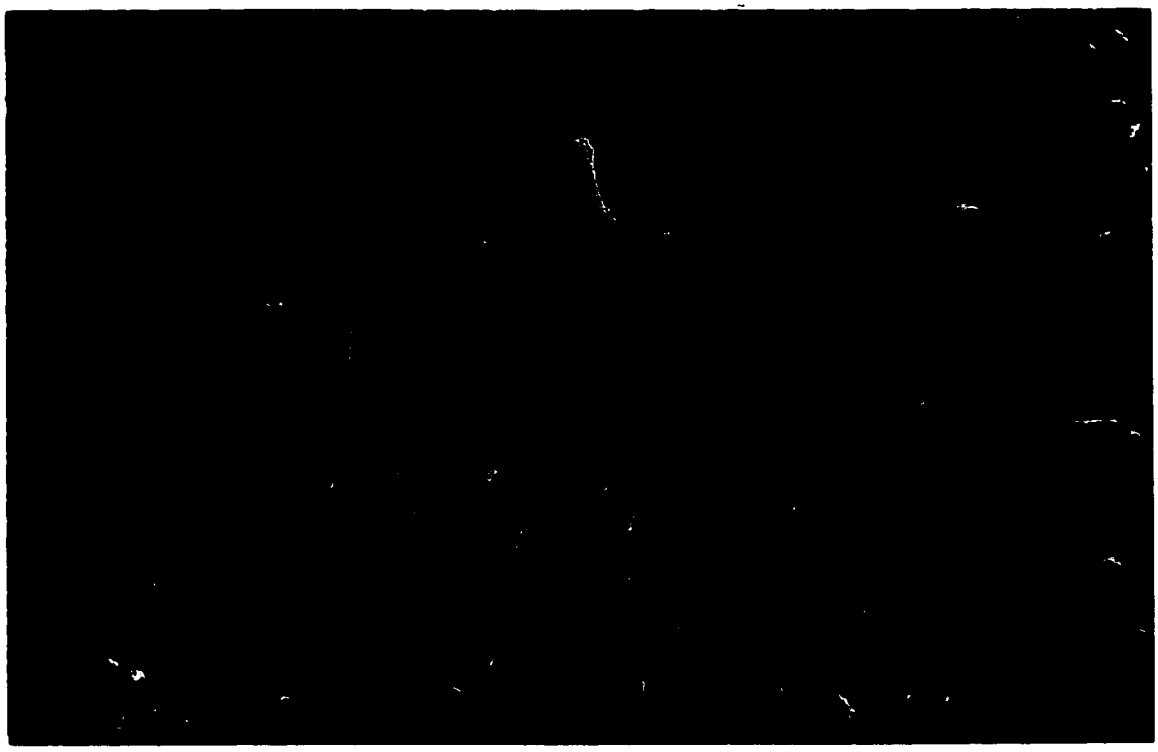

Figure 3.39. Kimberlite T29S. BSE-image depicting prismatic sprays of pectolite (P) within oxide-poor segregations (F.O.V. 462μm).

of acicular hydrous calcium silicate (perhaps pectolite) are set in a matrix consisting of reddish mica, serpentine and abundant relatively fresh monticellite.

This rock is characterized by the presence of numerous clasts-like bodies (Figure 3.38). These are relatively coarse-grained rounded-to-ovoid segregations consisting of sprays of prismatic hydrous calcium silicate (pectolite) and common reddish phlogopite enclosed by dark brown serpophite (Figure 3.39).

3.2.11.3. Discussion

T29S is an oxide-rich segregation textured monticellite phlogopite hypabyssal kimberlite. The texture of the colourless radiating aggregates of acicular calcium silicate within the matrix suggests that it occurs as a primary groundmass phase. The composition of the kimberlite may have been modified by the partial digestion and reaction with an unusual xenolith which contaminated the magma.

Pectolite has been identified in several kimberlites (Scott Smith *et al.* 1983; Agee *et al.* 1982; Akella *et al.* 1979; reviewed in Mitchell 1986)). It occurs as a groundmass phase as radiating aggregates of colourless acicular or fibrous crystals set in a base of serpentine. Textural relationships suggest that the pectolite is primary, however, the pectolite is only developed adjacent to altered xenoliths. Scott Smith *et al.* (1983) proposed two possible origins. Pectolite may occur as an apparently primary where the composition of the kimberlite has been modified by the partial digestion of and reaction with Na-bearing xenoliths, or it may occur as a secondary mineral, in veins, formed by the metasomatic introduction of Na-bearing fluid.

Because T29S contains significant xenoliths of wall rock (granite and biotite schist) that have reacted with the host kimberlite, it is quite probable that partial digestion of this substantial xenolithic material resulted in the contamination of the magma and the subsequent crystallization of pectolite. Na-rich metasomatic fluids were likely not introduced, in this case.

3.2.12. Kimberlite T237

Kimberlite T237 was discovered and drilled in 1996 and is located on the Tenby claim block. T237 is located approximately fifty kilometres east of the Diavik Diamond Project in a small cluster of kimberlites which includes T19, C53, T21 and T18 four kilometres to the west.

Ground magnetics reveals T237 to be a 50x150m (0.5-0.7ha) oval-shaped, east-west trending strong magnetic low. T237 intrudes biotite schist and is overlain by 8-12m of glacial regolith.

Two holes have been drilled into T237, intersecting kimberlite to a maximum depth of 126 m. Drill hole T237-2, a -45 degree hole drilled perpendicular to the strike of the anomaly, suggests the kimberlite is a narrow dyke, intersecting less than twenty metres on the angle.

3.2.12.1. Macroscopic Observations

Kimberlite T237 is a relatively competent, greenish-gray rock with abundant calcite-filled veinlets cutting the core at various angles. The upper contact with host biotite schist is preserved at 35° to the core axis. Subangular-to-subrounded xenoliths, which comprise less than 5% of the rock, consists of both granite and biotite schist, generally no larger than 5 cm in size. Xenoliths are generally altered and display reaction rims.

Macrocrystal olivines are fresh, partially replaced by serpentine along cracks and margins, comprise from 5-10% of the rock and range in size from 0.5-3 mm in size. Locally, olivine macrocrysts show a preferred orientation (from 40-55 degrees to the core axis), presumably due to flow differentiation. Microphenocrystal groundmass olivines are common and may be fresh-to-completely serpentinized. Rare macrocrystal garnets are present.

Small, irregular-shaped pods, predominantly filled with calcite represent segregations.

Biotite schist host rock, near contacts (within 50 cm) with the kimberlite dyke is slightly brecciated and altered. Small veinlets of kimberlite may penetrate up to 10 cm into the host schists.

3.2.12.2. Microscopic Observations

Kimberlite T237 is a relatively uniform rock that displays a paucity of olivine macrocrysts and locally may be considered aphanitic. Olivine and rare pyroxene macrocrysts tend to be rounded, circular-to-ovoid in shape. Macrocrysts may be slightly strained and are partially replaced by small, interlocking calcite crystals are their cores. No microxenoliths of lherzolite are present. Serpophitization along crystal margins and cracks is common.

Microphenocrystal olivines are abundant. They occur as subhedral-to-euhedral, relatively fresh crystals. The margins of these microphenocrysts commonly appear irregular at high magnifications indicating partial resorption. Partial mantles of opaque spinels are prevalent. Flow alignment of olivine crystals is not uncommon. (Figure 3.40).

Large euhedral-to-subhedral (some nearly as large as microphenocrystal olivines) macrocrysts and abundant small euhedral-to-subhedral opaque spinels and donut-shaped, partially resorbed magnetite and Ti-magnetite are abundant. Complex atoll structures are commonly preserved. The above opaques, together with common sprays of acicular and individual stout prisms of apatite, small subhedral (1-5 μm) perovskite constitute the silicate-oxide groundmass.

The above is set in a "sugary"-granular mesostasis consisting of partially altered Ba-rich phlogopite (up to 10 wt% BaO), fresh-to-altered monticellite, calcite and serpentine (Figure 3.41). Phlogopite commonly poikilitically encloses crystals of monticellite and small spinels.

Numerous small, irregular-to-amoeboid shaped serpentine-calcite segregations are scattered throughout the groundmass. These consist of coarse, interlocking calcite with botryoidal serpophite occurring along margins, in which may be set euhedral crystals of

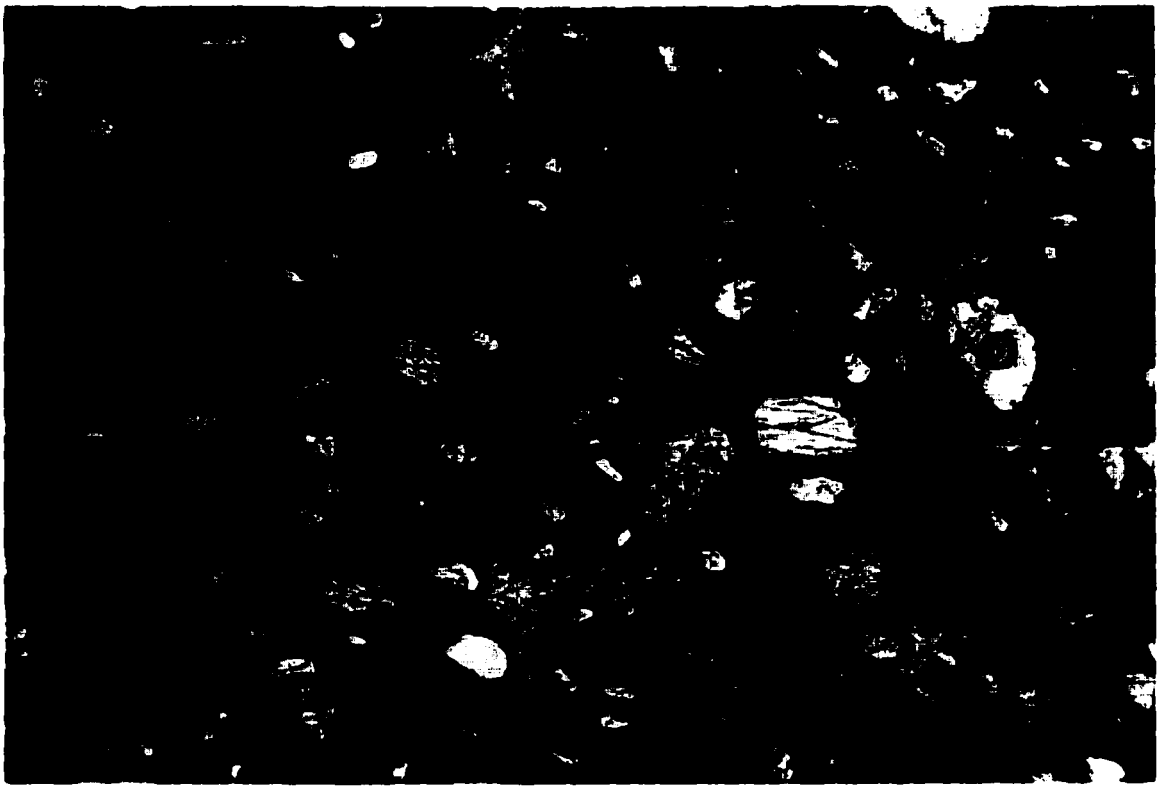

Figure 3.40. Kimberlite T237. Oxide-rich segregation-textured hypabyssal kimberlite containing relatively few macrocrystal olivine (O) abundant microphenocrystal groundmass olivine (which show a vague flow alignment) and opaque oxides (F.O.V. 6.0 mm).

Figure 3.41. Kimberlite T237. BSE-image depicting a groundmass containing monticellite (dark gray), spinel (S) and perovskite (P) in a mesostasis of altered Ba-rich phlogopite (M) and minor calcite (C) (F.O.V. 76 μm).

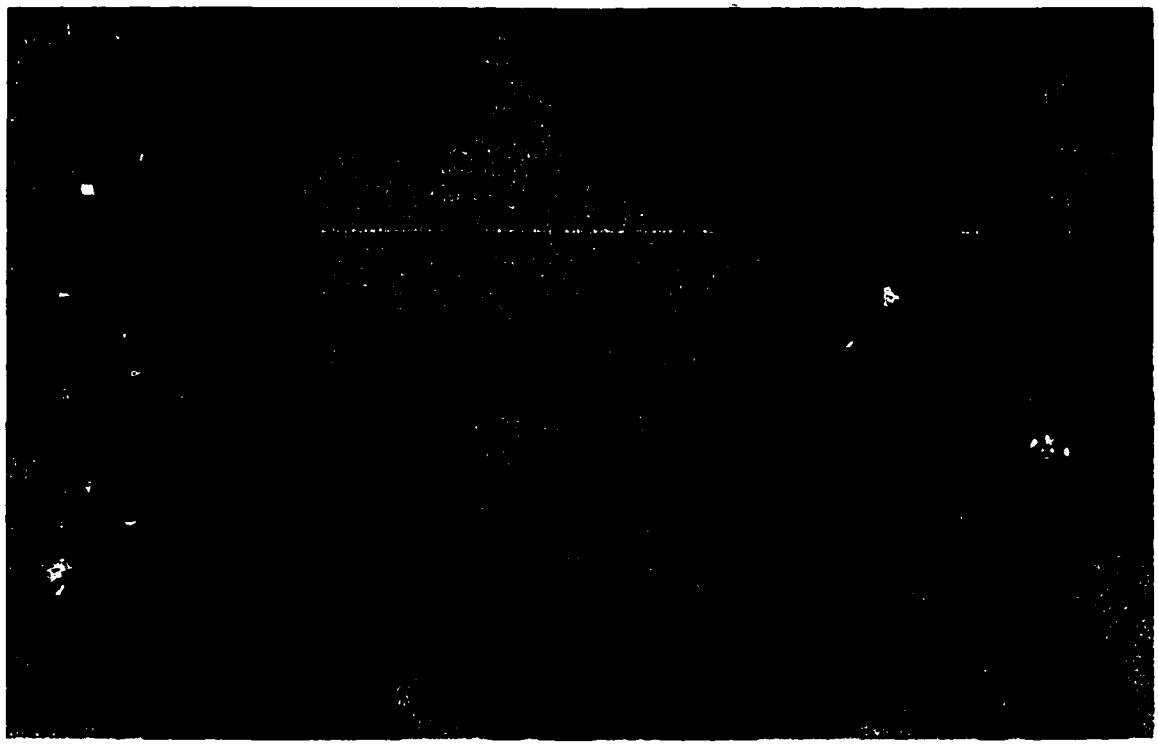

Figure 3.42. Kimberlite T237. BSE-image of irregular-shaped segregations. These segregations are infilled with calcite (C) and botryoidal serpentine (S) along their margins. Euhedral, zoned crystals of dolomite (D) are strewn throughout the segregations (F.O.V. 500 μm).

zoned dolomite (Figure 3.42). The walls of the segregations, in several instances, have acted as a substrate for the growth of inward-projecting sprays of acicular apatite.

3.2.12.3. Discussion

Kimberlite T237 is an oxide-rich segregation-texture monticellite phlogopite hypabyssal kimberlite. T237 occurs as an isolated dyke segment with no associated volcaniclastic kimberlite. Minor effects of flow differentiation can be seen, such as preferred orientation of olivine crystals and local variation is olivine proportions. The relationship of T237 to the other kimberlites within this small cluster in unknown.

3.2.13. Kimberlite T36

Kimberlite T36, discovered and drilled in 1993, lies approximately 34 kilometres east of the Diavik Diamond Project, approximately 4 kilometres east of a small cluster of five kimberlites, T32, T33, T34, T35 and T706 (refer to Figure 3.1).

T36 intrudes into biotite schist of the Yellowknife Supergroup and intersects a small northwest-trending diabase dyke of the Mackenzie dyke system (refer to Chapter 1). T36 is overlain by approximately 8-9 m of glacial regolith. Ground geophysics conducted over the area reveal an elliptical, 160x75 m, approximately northeast-trending strong magnetic low, which disrupts a continuous, northeast-trending, narrow magnetic low which represents the diabase dyke. No electromagnetic signature is present.

Two holes have been drilled into T36, revealing kimberlite to a depth of at least 87.5 metres below the present-day surface. Drill hole 93T36-1 was studied macroscopically and microscopically.

3.2.13.1. Macroscopic Observations

Drill hole 93T36-1 initially intersected less than a metre of biotite schist before passing through the highly magnetic diabase dyke. This dyke is narrow, only 70

centimetres along the core axis. Kimberlite was intersected at a depth of 10.2 metres and the hole was abandoned while still in kimberlite at a depth of 87.5 metres.

T36 is a very competent, extremely hard, gray-green rock whose dominant feature is the presence of abundant large, bleached granitoid xenoliths. These xenoliths are angular and commonly have thin reaction mantles with the host rock. Further downhole, intersections of large biotite schist xenoliths become common and xenoliths increase in abundance until they equal that of the host kimberlite. Numerous dilation calcite veins cut the core and coat open fracture surfaces.

Kimberlite T36 contains approximately 10% large (<10 mm) rounded olivine macrocrysts. These crystals are fresh-to-partially serpentinized. Microphenocrystal olivines are abundant completely replaced by serpentine. Fairly large (<2 mm) macrocrystal and smaller subhedral-to-euhedral primary spinels are profuse.

Although most features of the kimberlite are homogeneous throughout the intersection, the number of olivine macrocrysts and microphenocrysts and the intensity of their alteration appear to increase near the centre of the intersection. This can be explained by flow differentiation.

No associated volcaniclastic kimberlite occurs.

3.2.13.2. Microscopic Observations

Kimberlite T36 contains large (<10 mm) rounded, commonly broken olivine macrocrysts and rare pyroxene. These are relatively fresh and slightly strained. Subcircular patches of brown serpophite may replace macrocrysts along cracks and margins. Some macrocrysts are polycrystalline porphyroclastic aggregates of microxenolithic lherzolite and contain predominantly olivine and pyroxene. Macrocrysts are mantled by a thin rim of yellow, fine-grained serpophite.

The microphenocrystal olivine population consists of abundant relatively small, subhedral-to-euhedral crystals. These are pseudomorphed by brown, fine-grained

Figure 3.43. Kimberlite T36. Segregation-textured macrocrystal hypabyssal kimberlite with abundant fresh-to-altered groundmass olivine (O) and profuse opaque spinels. Olivine grains are replaced by fine-grained brown serpophite (F.O.V. 6.0 mm).

Figure 3.44. Kimberlite T36. Rounded oxide-poor segregation (S) composed of calcite and pale brown serpophite. Note that microphenocrystal olivine (O) are mantled by pale green chlorite (F.O.V. 2.5 mm).

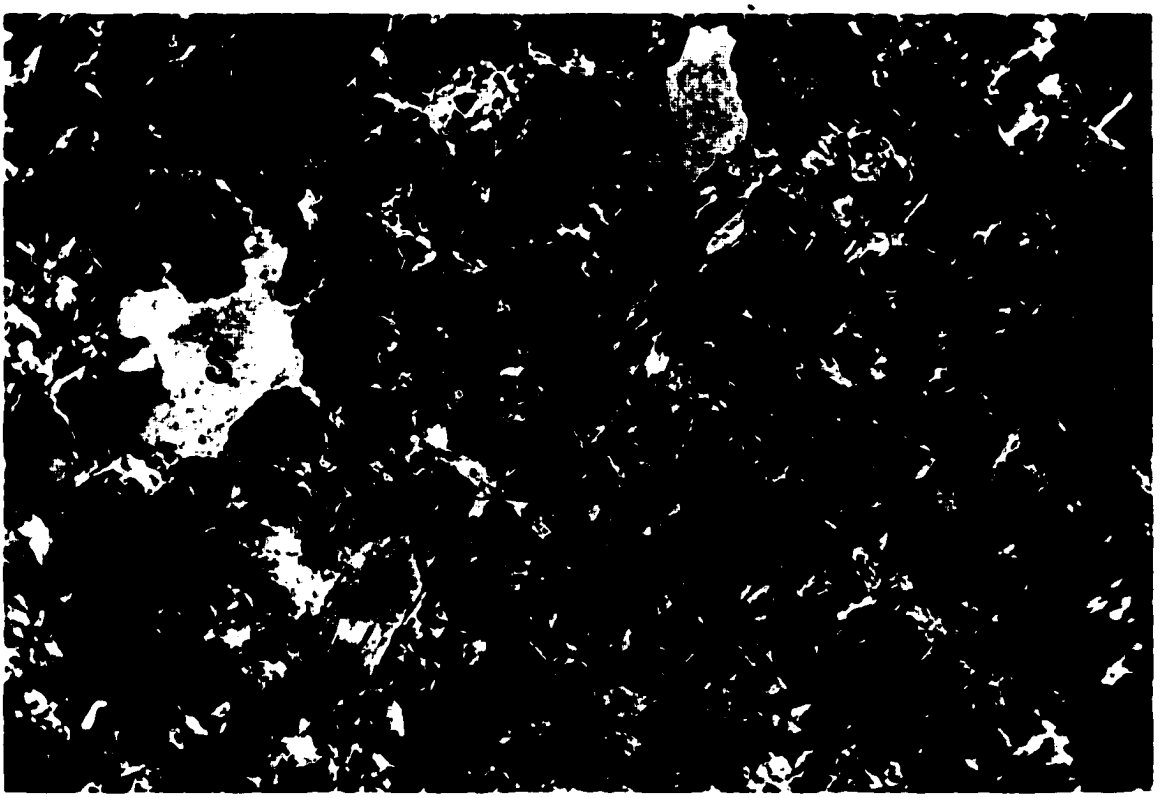

Figure 3.45. Kimberlite T36. Microphotograph of the groundmass of T36, which consists of olivine (O) opaque spinels and irregular-shaped segregations (S) of calcite set in a mesostasis of interlocking mica (white laths), serpentine and calcite (F.O.V. 2.5 mm).

serpophite. In larger crystals fresh cores commonly remain (Figure 3.43). Pale green chlorite may form a relatively thick mantle about smaller microphenocrysts (Figure 3.44). Discontinuous spinel necklaces mantle many microphenocrysts.

Large, subhedral-to-euhedral opaque spinels are abundant; many are similar in size to the microphenocrystal olivine and pyroxene. Perovskite occurs as small subhedral, reddish-brown crystals in the groundmass. Complex atoll spinels are rare.

The above is set in a very fine-grained mesostasis of interlocking mica, serpentine and calcite (Figure 3.45). Some acicular sprays and single crystals of apatite are scattered throughout the mesostasis. The mesostasis is not homogeneous with respect to its contents, certain areas may be rich in phlogopite and serpentine, while lacking calcite.

Small, irregular-to-subrounded segregations of calcite and pale brown serpophite are not common, but do occur with more prevalence towards the middle of the kimberlite intersection (Figure 3.44). Alteration of olivine macrocrysts increases downhole.

Rare, highly altered, partially assimilated country rock xenoliths do occur on a microscopic level. Intense alteration does not permit conclusive determination of their parentage. No cognate clasts are noted.

3.2.13.3. Discussion

Kimberlite T36 is a segregation-textured macrocrystal hypabyssal phlogopite kimberlite with no associated volcaniclastic kimberlite. Ground geophysics suggests it is an isolated dyke segment. The emplacement of this dyke was likely controlled by a regional fracture pattern related to the diabase dyke into which it was emplaced. No conclusions can be made about the size, strike and dip of T36, as the kimberlite has not been properly investigated by delineation drilling for these purposed.

3.2.14. Kimberlite T35

Kimberlite T35, discovered and subsequently confirmed by a single drill hole in 1992, lies approximately 30 kilometres east of the Diavik Diamond Project in a small

cluster of five kimberlites, which includes T32, T33, T34 and T706. Kimberlite T36 lies 4 kilometres to the east of T35 (refer to Figure 3.1).

T35 intrudes biotite schist of the Yellowknife Supergroup and is overlain by approximately seven metres of glacial till. Ground geophysics conducted over T35 reveals a small, relatively weak ellipsoidal magnetic low. No electromagnetic signature is present.

One vertical hole, 92T35-1 delineates this intrusion. The drill hole collared into kimberlite and an intersection of 22.2 m was obtained.

3.2.14.1. Macroscopic Observations

T35 is a gray-green, competent kimberlite characterized by an overall paucity of large olivine macrocrysts (these account for about one percent of the rock and are 1-3 mm in dimension). Olivine macrocrysts are partially-to-completely replaced by a combination of calcite and olivine. Subhedral microphenocrystal olivines are common (less than 1 mm in size) are similarly altered.

Highly altered granitoid and schistose xenoliths are present, but uncommon. These fragments may be up to 5 cm in length, along the core axis, with thin white reaction mantles.

T35 appears to be a homogeneous throughout the intersection with respect to olivine and xenolithic content and alteration. No flow differentiation textures are observed. What appear macroscopically to be small rounded, serpentinized nodules are probably a segregation-textured matrix.

No associated volcaniclastic kimberlite was encountered.

3.2.14.2. Microscopic Observations

Kimberlite T35 is very similar both mineralogically and texturally to kimberlite T34. It contains relatively few spherical-to-ovoid pseudomorphed olivine macrocrysts.

Figure 3.46. Kimberlite T35. Macrocrystal hypabyssal kimberlite composed of numerous grains of fresh olivine (O) and abundant opaque spinels. Groundmass microphenocrystal olivine are often decorated with partial spinel necklaces (F.O.V. 6.0 mm).

Figure 3.47. Kimberlite T35, mesostasis. BSE-image consisting of partially resorbed Ti-magnetite (S) and minor perovskite (P) set in a matrix composed of phlogopite (M), calcite (C) and serpentine (SP) (F.O.V. 60 μm).

Pseudomorphing minerals included coarse, interlocking calcite grains and minor green-yellow serpophitic serpentine. Small, irregular-shaped relict cores commonly remain.

The bulk of the olivine population consists of smaller, subhedral-to-euhedral microphenocrysts. The majority of these olivines are completely replaced by coarse calcite. Many microphenocrystal olivines have partial spinel necklaces (Figure 3.46). Thus, larger macrocrystal and smaller microphenocrystal olivines have been similarly replaced.

Groundmass spinels are prevalent, occurring as either subhedral-to-euhedral, discrete crystals or complex atoll or skeletal structures. Resorbed, donut-shaped magnetite is strewn throughout the groundmass. Small (5-10 μm) subhedral groundmass perovskite is common. Acicular sprays of apatite are abundant. These may poikilitically enclose small subhedral-to-euhedral crystals of serpentine after monticellite. The above is set in a mesostasis containing abundant phlogopite, calcite and serpentine (Figure 3.47).

Calcite segregations characterized the groundmass. These amoeboid-to-irregular shaped patches host aggregates of coarse-grained calcite and acicular sprays of a pale yellow-green-to-colourless, prismatic apatite. Yellow-brown, botryoidal serpophite may mantle these segregations.

3.2.14.3. Discussion

Kimberlite T34 is an oxide-rich segregation-textured apatite phlogopite hypabyssal kimberlite. This intrusion is a small dyke with no associated volcaniclastic rock. Because only one hole was drilled into T35, no conclusions can be made as to its size, strike or dip.

3.2.15. Kimberlite T33

Kimberlite T33 occurs within a small cluster that includes kimberlites T32, T31, T706, T34 and T35. T33 is located approximately 30 kilometers east-southeast of the

Diavik Diamond Project, 25 kilometers off the eastern shore of Lac de Gras (refer to Figure 3.1).

T33, an ellipsoidal, strong magnetic low has an approximate strike of northwest-southeast and is 150x70 m in dimension. It intrudes biotite schist and is overlain by 5 to 8 m of glacial regolith.

Two exploration drill holes attempted to delineate kimberlite T33. T33-1, a vertical hole, along the northeastern margin of the anomaly failed to intersect kimberlite, while T33-2, a -45° hole drilled along the northeast margin of the anomaly parallel to its strike. This drill hole intersected approximately 25 m of kimberlite (on the angle) at a vertical depth of 53 m and a small intersection of one metre at a vertical depth of 79 m.

3.2.15.1. Macroscopic Observations

After a 70 metre intersection of biotite schist, a kimberlite dyke was intersected. The dyke shows rather profound effects of flow differentiation, ranging from a medium-gray macrocrystal, segregation-textured hypabyssal kimberlite (Unit#1a) to an aphanitic rock (Unit#1b) with less than 5% small, rounded macrocrystal olivines. Both of the above varieties of kimberlite display relatively fresh olivine macrocrysts.

T33 also comprises another distinctly different variety of kimberlite, which appears to be a second batch of magma unrelated to the first. This rock (Unit#2) is a dark gray, very competent kimberlite composed of altered, rounded "clasts" and abundant large, rounded olivine pseudomorphs (both macrocrystal and microphenocrystal) set in a fine-grained, aphanitic matrix. Within the core, Unit#2 appears to be "bedded" with Unit#1a and 1b, with "beds" of up to 4 m in thickness. Spatial data would likely reveal that these "beds" are indeed irregular-shaped bodies composed of different magma types.

Ten metres of country rock was traversed before a final one metre of relatively fine-grained, competent kimberlite was intersected (Unit#3). Macroscopically, Unit#3 is quite similar to Unit#2 although the former exhibits some fresh olivines, while the latter appears quite profoundly altered.

3.2.15.2. Microscopic Observations

3.2.15.2.1. Unit#1a

Unit#1 is characterized by numerous rounded pelletal-sized clasts. At their cores, these clasts may contain fairly large (<5 mm), rounded olivine macrocrysts. These macrocrysts are relatively fresh and are mantled by an orange-brown alteration rim of iron oxide. Xenocrystal garnets, derived from the disaggregation of lherzolite, may also core these clasts.

The bulk of the rock consists of small, rounded clasts cored by rounded-to-subhedral microphenocrystal olivines. The thickness of the mantles may range from a skin to the approximate thickness of the olivine core. These olivine cores may be relatively fresh, with a small relict core and are also characterized by orange-brown alteration necklaces of iron oxide. Commonly, the microphenocrystal olivines are completely replaced by this substance. Many small, subrounded clasts lack central kernels, but are otherwise identical to above.

The kimberlite mantle of these clasts consists of tan-coloured, fine-grained kimberlite composed of partially fresh-to-altered microphenocrystal olivines, small subhedral-to-euhedral discrete spinels, common partially resorbed atoll spinels, perovskite, apatite and common hydrous calcium silicate, which may enclose serpentinized monticellite. Larger clasts may contain concentrically oriented microphenocrystal olivine along their margins. The above is set in a mesostasis consisting of an abundant phlogopite and serpentine. Mantling kimberlite of both the microphenocrystal and macrocrystal olivines are essentially identical, however the former rarely contains microphenocrystal olivines within it.

The margins of these rounded clasts are interpreted as representing globular segregations. These segregations are set in a matrix, which consists of coarse subhedral interlocking calcite with a margin of botroiydal yellow-brown serpophite and vermeculitized phlogopite. Small segregations may be filled entirely with serpophite. The margins of these segregations have also acted as a substrate for the growth of

acicular sprays of prismatic apatite. Calcite and serpentine commonly replace apatite. Euhedral rhombs of calcite, replaced along their margins by yellow-brown serpentine, commonly occur along the boundaries of segregations and may poikilitically sprays of acicular apatite.

The margins of these globular segregations exhibit irregular-gradational margins with the serpentine-calcite matrix, suggesting consanguinity, *i.e.*, segregation of late stage fluids.

Unit#1 is considered to be a globular-segregation-textured macrocrystal phlogopite apatite hypabyssal kimberlite.

3.2.15.2.2. Unit#1b

Unit#1a is nearly devoid of any olivine and contains less than 5% subrounded olivine macrocrysts (Figure 3.48). The macrocrysts are essentially unaltered with minor serpophitic alteration confined to the margins.

These olivine macrocrysts are set in a groundmass consisting of numerous subhedral-to-euhedral crystals of calcite, abundant perovskite (<5μm), spinels (both discrete euhedral magnetite and complex atoll structures), apatite and prismatic crystals of calcium silicate, which may enclose small serpentinized pseudomorphs of monticellite and subhedral perovskites. The mesostasis consists of a very intimate intergrowth of phlogopite and serpentine.

Small irregular-shaped segregations are strewn throughout the groundmass. They are filled predominantly with interlocking plates of calcite.

This rock is considered to be a segregation-textured aphanitic phlogopite perovskite hypabyssal kimberlite. The paucity of olivine macrocrysts is likely the result of differentiation.

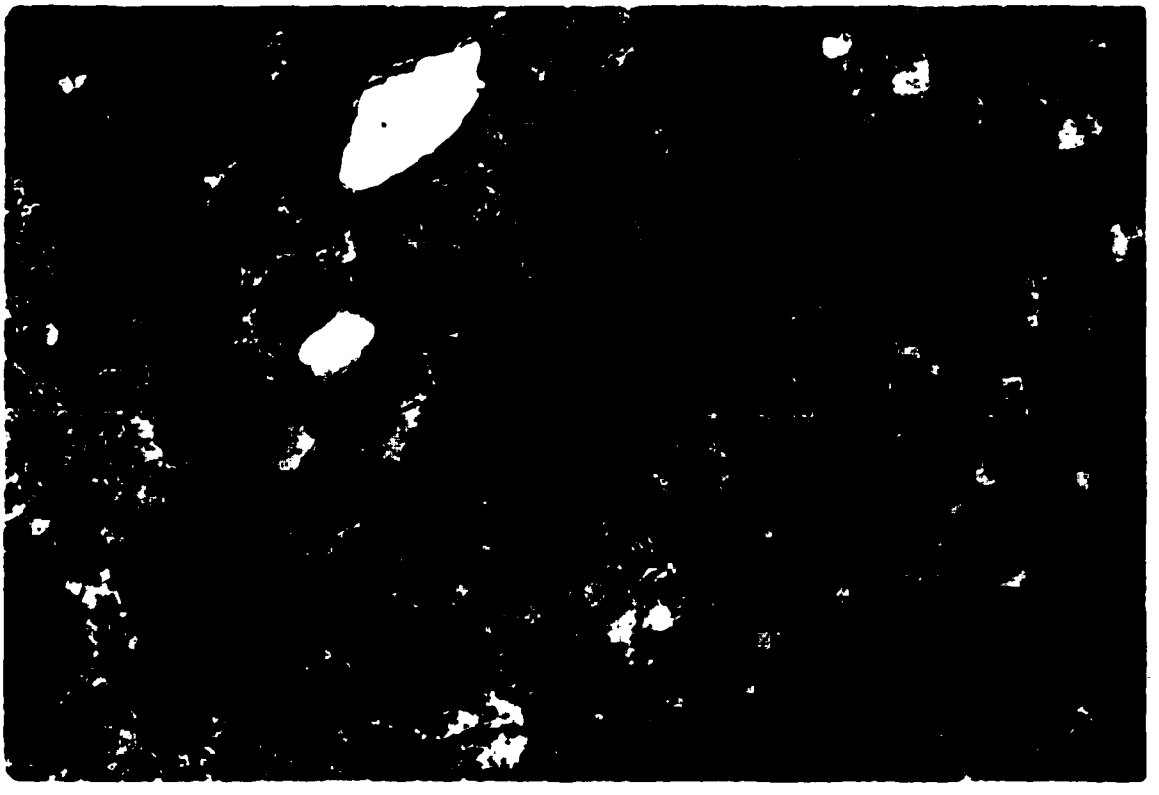

Figure 3.48. Kimberlite T33, Unit#1b. Segregation-textured aphanitic hypabyssal kimberlite. Segregations (S) are predominantly filled with interlocking calcite (F.O.V. 6.0 mm).

Figure 3.49. Kimberlite T33, Unit#2. Groundmass of a globular segregation consisting of altered grains of olivine (O) set in matrix of phlogopite (M), Ti-magnetite (yellow), perovskite (yellow) and apatite. The mesostasis in composed of predominantly serpentine and calcite (C) (F.O.V. 200 μm).

3.2.15.2.3. Unit#2

Unit#2 lacks any large macrocrystal olivines and is predominantly composed of small (<2 mm) subhedral-to-euhedral pseudomorphed microphenocrystal olivines. Olivines are replaced by brown serpophitic serpentine, veined by calcite and are commonly mantled by an alteration necklace of opaque iron oxides. Smaller groundmass olivines are replaced by a fine-grained intergrowth of calcite and serpentine. Opaque alteration necklaces are still present, but are commonly discontinuous. Microphenocrystal olivines form the core of rounded-to-irregular-shaped kimberlite clasts. Larger clasts may consist of numerous microphenocrystal olivines, with no single core.

The groundmass of these clasts consists of a plethora of apatite, numerous small subhedral perovskite (1-5um), resorbed magnetite, poorly preserved atoll spinels and rare crystals of calcium silicate set in a mesostasis of abundant platy phlogopite, calcite and interstitial serpentine (Figure 3.49). These kimberlite clasts probably represent globular segregations. Segregations are set in an oxide-free matrix consisting of coarse-grained, interlocking calcite, with dark brown serpophitic margins. Euhedral rhombs of calcite may emanate from the margins of the matrix.

Unit#2 likely represents a globular-segregation-textured phlogopite apatite hypabyssal kimberlite.

3.2.15.2.4. Unit#3

Unit#3 contains few large (<5 mm), rounded olivine macrocrysts. These are replaced by yellow-brown serpophitic serpentine. A small relict core commonly remains.

The bulk of the rock consists of small (<1 mm) subrounded-to-subhedral microphenocrystal olivines. Yellow-brown serpophite commonly entirely replaces the olivines, and discontinuous spinel necklaces may decorate their margins, however, fresh cores commonly remain in larger crystals.

Figure 3.50. Kimberlite T33, Unit#3. Globular segregation-textured hypabyssal kimberlite. Segregations are filled with calcite (C) and pale brown serpophite (S). Sprays of prismatic apatite (A) are emanating from the margins of the segregations (F.O.V. 6.0 mm).

Olivines form the cores of what are considered to be globular segregations. The mantling kimberlitic material consists of numerous subhedral-to-euhedral discrete Ti-magnetite crystals, complex atoll spinels, small subhedral crystals of perovskite and numerous subhedral, discrete crystals and radiating sprays of acicular apatite. Apatite commonly poikilitically encloses pseudomorphed monticellite.

The globular segregations are set in an oxide-free matrix consisting of coarse interlocking plates of calcite and marginal yellow serpophite. Prismatic sprays of acicular apatite commonly emanate from the margins of these segregations and may be replaced by serpophite (Figure 3.50). Smaller segregations are entirely filled with serpophite, lacking both calcite and apatite.

Unit#3 is considered to be a globular-segregation-textured apatite phlogopite hypabyssal kimberlite.

3.2.15.3. Discussion

T33 is represents a small dyke segment composed of at least two injections of kimberlite that have consolidated to give the dyke a well-defined layering within the core. Units#1a and b appear to represent the same batch of kimberlite and the contrast within the proportions of cumulous phases (*i.e.* macrocrystal olivine) and in mineral grading (*i.e.* changes in the ratio of perovskite and apatite) is the result of magmatic differentiation. Units#2 and 3, representing a second injection of magma, have essentially identical mineralogy and texture and only differ in alteration.

The dimensions of the dyke are unknown as the drill hole was drilled parallel to its strike and thus reveals little information.

3.2.16. Kimberlite T7

Kimberlite T7 is located approximately 12-13 kilometers east-southeast of the Diavik Diamond Project, about 10 kilometers off the southeastern shore of Lac de Gras.

T7 occurs within a small cluster of kimberlites, which includes T7 and T7N. All three of these small bodies lie within a few hundred metres of one another.

Kimberlite T7 is characterized by a relatively small, north-south striking elongated magnetic low, 160x40 m in approximate dimension. Host rock includes both biotite schist and Archean granite and T7 is overlain by 5 m of glacial regolith.

One exploration drill hole delineated kimberlite T7. It was drilled at an angle of -45 degrees, perpendicular to the strike of the anomaly. Slightly less than 12 m of kimberlite was intersected, coinciding with the centre of the magnetic low.

Very little core was remaining in the boxes, less than a quarter of the original kimberlite. However, two samples were taken for petrographic study, but the exact depth a relationship of the rock is unknown.

3.2.16.1. Macroscopic Observations

Drill hole T7-1 intersected approximately 12 m kimberlite at a vertical depth of 45 m. Two distinct varieties kimberlite were noted and sampled.

The first distinct unit encountered, Unit#1 is a relatively competent, clast-supported kimberlite breccia containing a plethora of mica-bearing basement gneiss fragments (<1 cm to >5 cm) and prevalent, relatively large (up to 8 mm) laths of xenocrystal feldspar. Both xenoliths and xenocrysts are mantled by very fine-gained kimberlite ash. Rounded, completely serpentinized olivine macrocrysts and microphenocrysts (from <1 mm-7 mm) are common and generally mantled by kimberlitic ash. The above, together with common crystals of relatively fresh mica (likely xenocrystal biotite) are set in a gray matrix containing a high proportion of carbonate.

Unit#2, the second distinct unit within T7 is a very competent, dark gray rock characterized by large amoeboid-to-bulbous-shaped yellow "segregations" composed of predominantly serpentine. These bodies display a preferred orientation of approximately 45° to the core axis. Pseudomorphed, subrounded olivines are common and are generally less than 2 mm in size. Replacing constituents include carbonate and yellow serpentine (identical to serpentine within the "segregations"). The above together with common

small opaque oxides and very sparse (less than 5 mm) lithic fragments are set in a dark gray, aphanitic matrix.

3.2.16.2. Microscopic Observations

3.2.16.2.1. Unit#1

Unit#1 is characterized by the presence of numerous non-vesiculated spherical-to-ovoid lapilli of kimberlite. Lapilli are most commonly cored by a rounded olivine macrocrysts (Figure 3.51). Olivine crystals, yellow-green in plane polarized light, are completely replaced by a mixture of serpentine and calcite. Less commonly, a xenolith of surrounding country rock (biotite schists and gneisses) or a partially altered lath of potassium feldspar may core these pelletal lapilli (refer to Figure 3.51). Large xenocrysts of unmantled biotite and feldspar are present.

A fine-grained, altered, microporphyritic kimberlite ash comprises the mantling kimberlite. This kimberlite is comprises of tangentially flow aligned (Figure 3.52) pseudomorphed microphenocrystal olivines together with numerous subhedral spinels, subhedral-to-euhedral apatite, common poorly preserved atoll spinels and minor perovskite set in a matrix of very fine-grained aluminous serpentine and abundant phlogopite. Commonly the outer margins of these mantles are composed of a very fine-grained material, which appears essentially identical to the kimberlite mantle, devoid of microphenocrystal olivines or large oxides, resembling a chilled margin (refer to Figure 3.52)

Small, rounded-to-amoeboid-shaped ash and lapilli fragments of kimberlite lacking central kernels are also present within Unit#1. No flow textures can de discerned in these clasts. These smaller clasts which occur interstitially to the larger pelletal lapilli may be welded.

The above fragments and pelletal lapilli are considered to be *bona fide* juvenile lapilli and juvenile pelletal lapilli as no conclusive evidence suggests a diatreme origin.

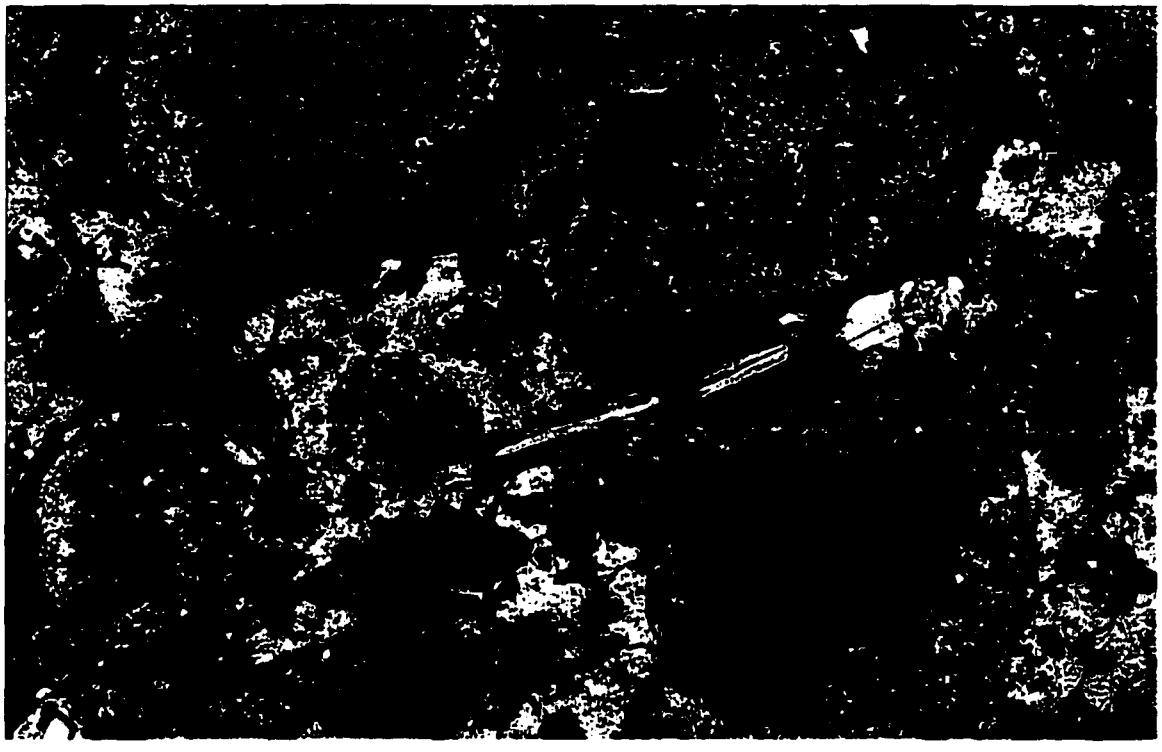

Figure 3.51. Kimberlite T7, Unit#1. Juvenile lapilli, (J) which superficially resemble pelletal lapilli of diatreme facies kimberlite. Lapilli are cored by serpentinized olivine (O), country rock xenolith or xenocrystal feldspar (F) and mantled by kimberlite ash composed of apatite, perovskite and spinel set in a matrix of blocky phlogopite and serpentine. Large, unmantled laths of xenocrystal biotite (M) are strewn throughout the rock (F.O.V. 1.0 mm).

Figure 3.52. Kimberlite T7, Unit#1. Clast-supported pyroclastic kimberlite composed of abundant rounded-to-irregular-shaped juvenile fragments (J). The outer mantle of the large kimberlite fragment is fine-grained and darker in colour than the core (difficult to see), resembling a chilled margin (F.O.V. 6.0 mm).

All of the above constituents are set in a secondary cement consisting predominantly of interlocking plates of calcite and serpentine. The serpentine within the cement is mineralogically identical to that in the lapilli (*i.e.* aluminous).

Unit#1 appears to be an *in situ* primary pyroclastic airfall volcaniclastic kimberlite lapilli tuff breccia.

3.2.16.2.2 Unit#2

Unit#2 is a pervasively altered rock that resembles a segregation-textured hypabyssal kimberlite. It is characterized by numerous subrounded-to-amoeboid-shaped yellow "segregations", commonly with coarse, interlocking plates of calcite at their cores (Figure 3.53). Small subhedral-to-euhedral opaque oxides may occur at their margins. Their margins are gradational (over <1 mm) with the oxide-rich groundmass. Some of these "segregations" may be serpentinized olivines or small cognate fragments.

Unit#2 contains two distinct populations of olivine: large, rounded macrocrystal olivines (<5%) completely replaced by yellow serpentine, identical to that forming the "segregations" and minor calcite. Calcite commonly occurs as coarse, interlocking plates at the core of the macrocrysts. Small relict cores rarely are preserved. The second, more prevalent, population of olivines occurs as subrounded-to-subhedral, partially-to-completely altered microphenocrystal olivines, replaced by yellow serpentine identical to above and common interlocking calcite at their cores.

Olivines, together with sparse subrounded micaceous xenoliths, one noted, relatively fresh autolith are set in a groundmass containing abundant subhedral-to-euhedral apatite, skeletal and atoll (partially resorbed) Ti-magnetite, euhedral-to-subhedral primary chromite and common perovskite set in a mesostasis of abundant phlogopite (with Ba-rich margins), calcite and serpentine.

Unit#2 is a difficult rock to classify as its contacts and field relationship to the rest of kimberlite is not preserved. The preservation of atoll spinels and the lack of any fragmental texture suggest that it is a segregation-textured apatite phlogopite hypabyssal kimberlite.

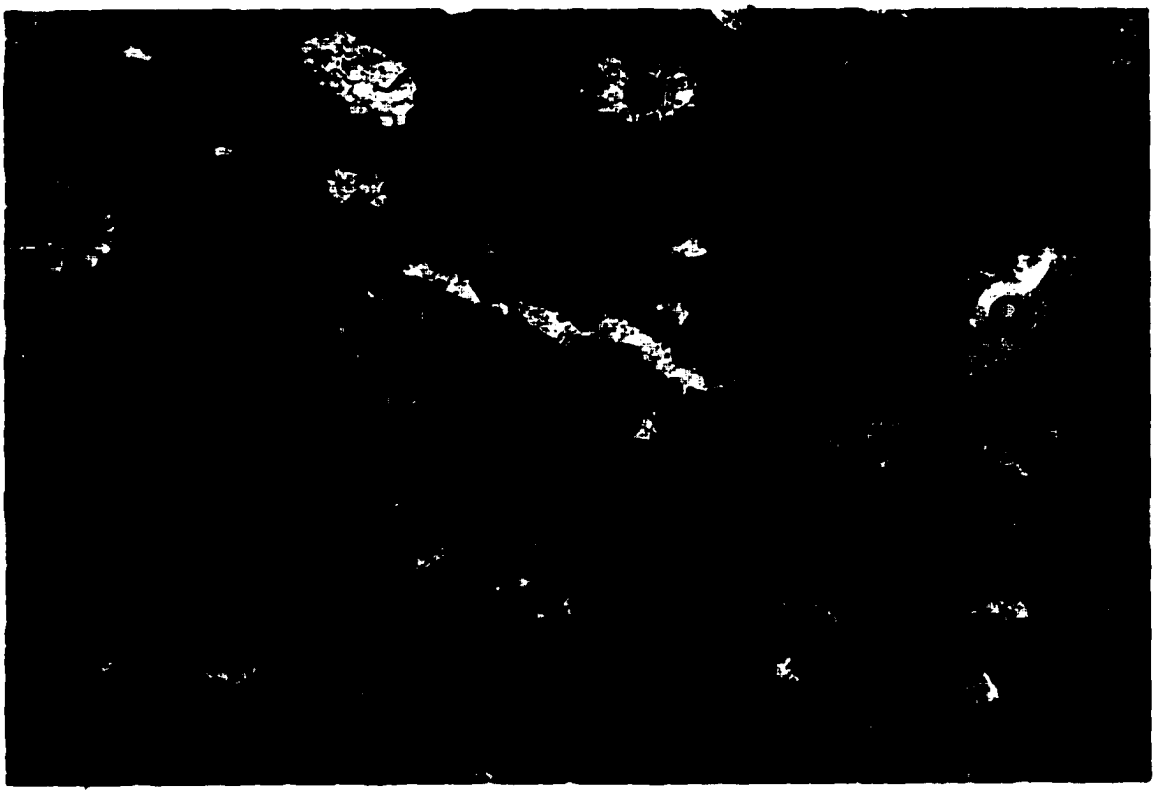

Figure 3.53. Kimberlite T7, Unit#2. Segregation-textured hypabyssal kimberlite composed of abundant partially-to-completely altered groundmass olivine (O) and opaque spinels (F.O.V. 2.5 mm).

3.2.16.3. Discussion

Kimberlite T7 is a very small satellite(?) vent which contains both pyroclastic and hypabyssal rock. Unit#1 may represent a down rafted block of volcaniclastic material within hypabyssal kimberlite or Unit#2 may represent an autolith within volcaniclastic kimberlite, or a post-eruptive kimberlite sill which intrudes into volcaniclastic kimberlite. However, the relationship between these two units is impossible to discern and any conclusion is mere speculation

3.2.17. Kimberlite T34

Kimberlite T34 was discovered and drilled in 1992 and is located approximately 25 kilometres east of the eastern shore of Lac de Gras in a small cluster of five kimberlite intrusions (T32, T33, T34, T35 and T706). Kimberlite T36 lies four kilometres to the east of T34 (refer to Figure 3.1).

Kimberlite T34 intrudes biotite mica schist and Archean granites and is overlain by approximately 7m of glacial regolith. Both ground and air magnetic and electromagnetic surveys have been conducted over this intrusion. T34 is characterized by a relatively strong, ellipsoidal magnetic low, 180x80 m in dimension in plan, with a strike of N26°W. No electromagnetic signature is present. One hole has been drilled to delineate kimberlite T34.

3.2.17.1. Macroscopic Observations

Kimberlite T34 is a gray-green, competent rock with numerous olivine crystals that are fresh-to-partially altered to a yellow-green colour. This alteration appears to be confined to the margins of the olivine. The bulk of the olivine population consists of small subhedral-to-euhedral microphenocrystal minerals, generally less than 1 mm in dimension. These microphenocrystal olivines are commonly completely replaced by a combination of serpentine and olivine. The groundmass of the kimberlite appears to be

quite micaceous. No kimberlitic clasts were noted, however, large xenoliths of quartz mica schist with fine-grained white alteration rims are quite common. The upper 50 cm of the kimberlite intersection displays a rusty oxidation staining which is probably the result of ground water induration. Numerous veinlets of calcite cut the kimberlite at various angles to the core axis.

3.2.17.2. Microscopic Observations

T34 is a relatively fresh, segregation-textured to globular-segregation-textured apatite phlogopite hypabyssal kimberlite dyke (Figures 3.54 and 3.55). The samples taken across the kimberlite intersection were all very similar in both texture and mineralogy and only the proportion of macrocrystal olivine varied throughout the kimberlite. This is presumably the result of flow differentiation.

Kimberlite T34 contains relatively few, large, rounded olivine macrocrysts (<5 mm). These macrocrysts are fresh at their cores, with serpentinization confined to their margins.

The bulk of the olivine population consists of small (<2 mm) subhedral-to-euhedral microphenocrysts. Small relict cores and marginal serpophitization characterized the larger microphenocrystal olivine. Alteration consists of an initial stage of marginal serpentinization followed by the replacement of the core with coarse-grained calcite. Microphenocrystal olivines may be nearly entirely replaced by serpentine, with calcite replacement confined to cracks. Many microphenocrysts have a relatively thick mantle of yellow–brown (serpophitic) serpentine and are decorated by a necklace of subhedral-to-euhedral spinel. Spinel necklaces may not be continuous.

Macrocrystal and microphenocrystal olivines are set in an oxide-rich groundmass consisting of abundant subhedral-to-euhedral discrete spinels, complex atoll spinels, profuse resorbed donut-shaped magnetite and common perovskite. These oxides, together with groundmass chalcopyrite are set in a fine-grained matrix of abundant apatite, phlogopite, Ba-rich phlogopite, serpentine, calcite and dolomite. Apatite commonly occurs as acicular sprays of prismatic crystal. Larger plates of groundmass

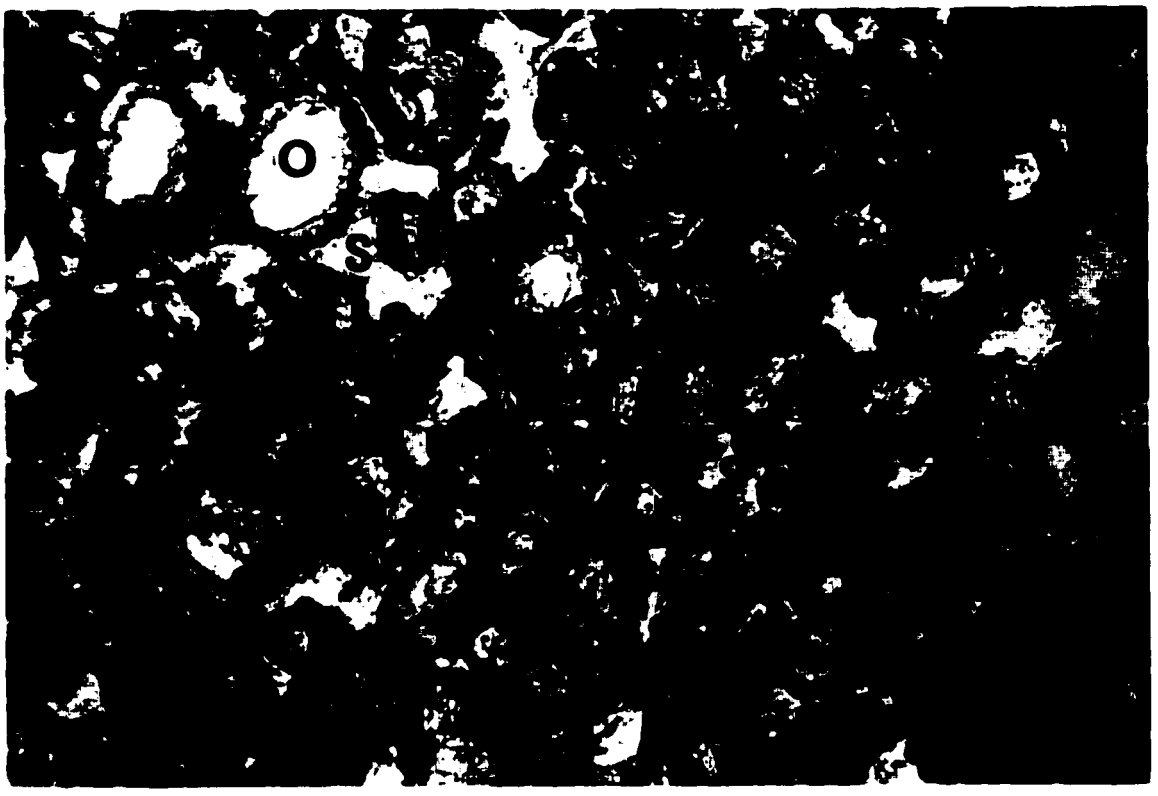

Figure 3.54. Kimberlite T34. Segregation-textured hypabyssal kimberlite composed of abundant microphenocrystal olivine (O) set in an oxide-rich matrix. Irregular-shaped segregations (S) are filled with calcite (F.O.V. 6.0 mm).

Figure 3.55. Kimberlite T34. Globular-segregation-textured hypabyssal kimberlite. Olivine grains (O) are replaced by serpophite and mantled by discontinuous spinel necklaces (F.O.V. 2.5 mm).

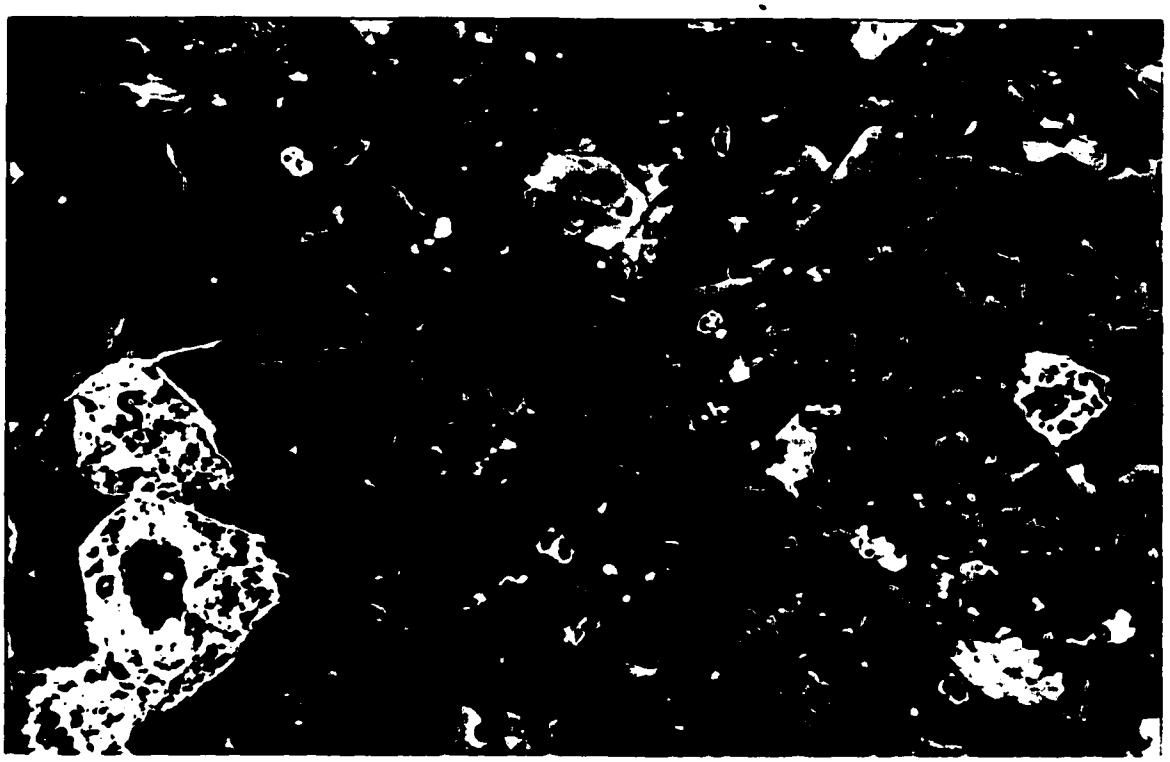

Figure 3.56. Kimberlite T34. BSE-image showing a relatively large lath of phlogopite poikilitically enclosing small serpentinized crystals of monticellite (black). The groundmass consists of donut-shaped, partially resorbed magnetite (S), spinel (white) and perovskite (white) set in a matrix of phlogopite (M), calcite (C) and serpentine (SP) (F.O.V. 120 μm).

phlogopite, and less commonly apatite, may poikilitically enclose small serpentinized subhedral crystals of monticellite (Figure 3.56).

The groundmass is characterized by numerous amoeboid-to-irregular-shaped segregations. These segregations are filled with coarse, interlocking plates of calcite and lack opaque oxides. Colliform textures are common; outer margins are commonly replaced by dolomite. Small sprays of prismatic apatite may emanate from the margins of the segregations.

No kimberlitic fragments or lithic xenoliths or xenocrysts are present.

3.2.17.3. Discussion

Kimberlite T34 is a segregation-textured to globular-segregation-textured apatite phlogopite hypabyssal kimberlite. No associated volcaniclastic kimberlite was intersected and T34 represents a small kimberlite dyke segment. Because only one hole was drilled into T34, the thickness, orientation or lateral extent of the dyke is unknown.

3.2.18. Kimberlite T7E

Kimberlite T7E is located approximately 12-13 kilometres east-southeast of the Diavik Diamond Project, approximately ten kilometers off the southeastern shore of Lac de Gras. T7E occurs in a small cluster including known kimberlites T7 and T7N. Kimberlite T7E occurs as a small circular magnetic low, approximately 100 m in diameter or, 0.8 ha. T7E intrudes into Archean granite and is overlain by approximately 15 m of glacial regolith.

Two exploration drill holes delineate this small vent, intersecting volcaniclastic kimberlite to a maximum vertical depth of 96 m (drill hole abandoned in kimberlite). Drill hole T7E-1, a -55 degree hole drilled from the centre of the magnetic low towards its eastern margin, was investigated in this study. Sixty metres of volcaniclastic kimberlite was intersected on the angle, suggesting an approximate radius of 40 m for the vent.

3.2.18.1. Macroscopic Observations

Drill hole T7E-1 collared bedded volcaniclastic kimberlite at a vertical depth of 17.5 m. Two distinct varieties of volcaniclastic kimberlite alternate throughout the vent. The first unit (Unit#1) may range in thickness from 4-10 m and occurs as a dark gray-green, fairly incompetent rock. Unit#1 is characterized by numerous subrounded-to-rounded cognate fragments and common small (generally less than 1 mm) green-yellow microcrystal olivine pseudomorphs. Rare large, rounded, pseudomorphed olivine macrocrysts are observed. The above is set in a gray-brown earthy matrix, aphanitic in nature. Unit#1 tends to be quite massive with little or no observable sorting.

The second distinct unit within the vent (Unit#2) occurs as beds from approximately one to greater than ten meters in thickness and occurs in relatively sharp contact with Unit#1. Bedding contacts, however, are not preserved. Unit#2 is a pale gray-green, relatively competent volcaniclastic kimberlite displaying a distinct "pocked" appearance. It is characterized by more abundant (5-10%), coarser, rounded, partially-to-completely altered (predominantly by carbonate) olivine macrocrysts. These macrocrysts together with sparse (less than 5%) lithic clasts of schist and granite occur in a carbonate-rich matrix.

Host rock granite is intersected at a depth of approximately 75 meters. The lower contact of the kimberlite is highly fractured.

3.2.18.2. Microscopic Observations

3.2.18.2.1. Unit#1

Unit#1 is a dark brown, matrix-supported rock containing a variety of cognate clasts. Abundant small, pale yellow clasts with irregular-lobate margins characterize Unit#1 (Figure 3.57). These clasts are elongated-to-bulbous in habit and consist of pale yellow "serpophite" crystals with irregular patches of dark brown serpophite.

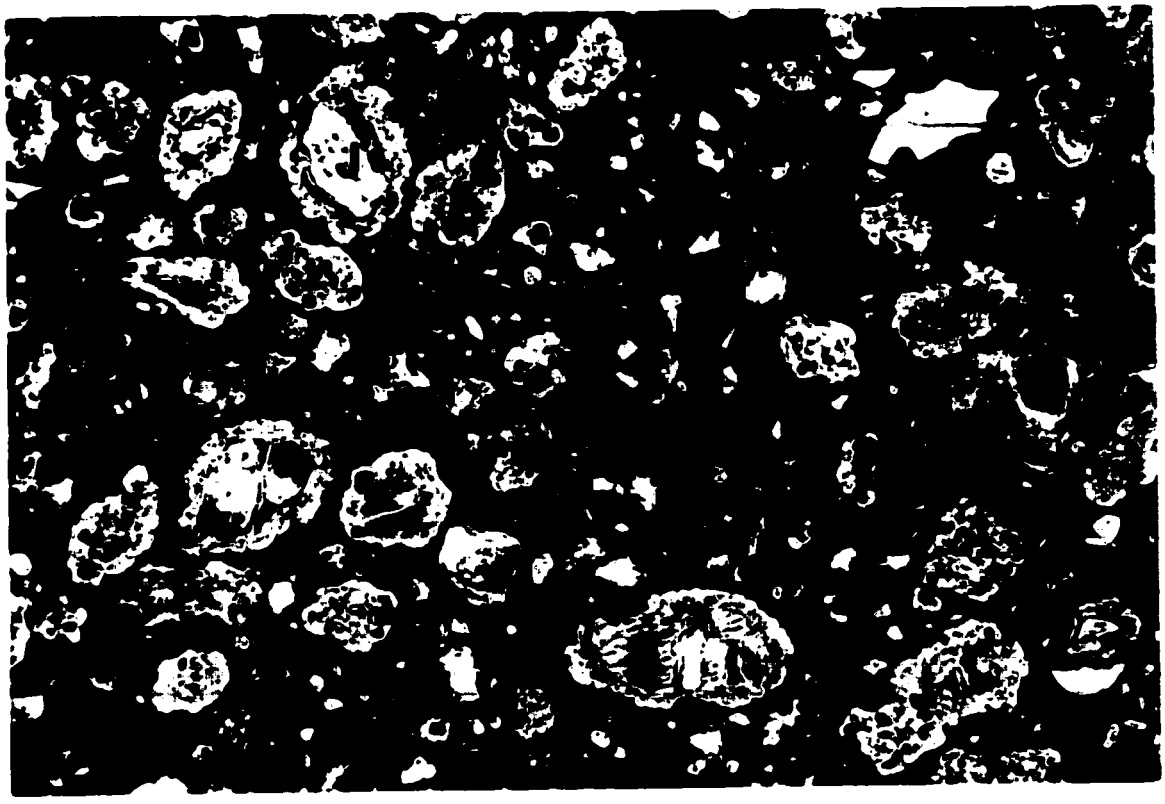

Figure 3.57. Kimberlite T7E, Unit#1. Resedimented volcaniclastic kimberlite breccia characterized by pale yellow, amoeboid-shaped, bulbous juvenile clasts (J) (F.O.V. 2.5 mm).

Figure 3.58. Kimberlite T7E, Unit#1. Amoeboid-shaped microporphyritic juvenile lapilli (J) within a resedimented volcaniclastic kimberlite breccia (F.O.V. 2.5 mm).

Pseudomorphed olivines (pseudomorphed by the same yellow serpophite and dark brown serpophite), discrete atoll spinels or single, complex atoll structures may form the core of the clasts. The former may form chain-like structures around the margins of the clasts. The "serpophitic" crystals may represent pseudomorphed microphenocrystal olivines. The distinct irregular habit of these clasts indicates that they are juvenile in origin.

Ash-to-lapilli sized, tan coloured microporphyritic clasts are common throughout this unit (Figure 3.58). These clasts contain abundant small, subhedral-to-rounded microphenocrystal olivines that are replaced with brown serpophite. Olivine and abundant euhedral-to-subhedral atoll and discrete spinels are set in a very fine-grained matrix consisting of predominantly calcite with small patches of dark brown serpophite. Small sub-spherical "segregations" are strewn throughout the matrix of these clasts. They are infilled with calcite and likely represent small vesicles, indicating that they are undoubtedly juvenile lapilli. Oftentimes these clasts contain small, ash-sized dark brown, amoeboid-shaped juvenile lapilli, as described above. The shape of these clasts is quite irregular, commonly amoeboid and margins are embayed and lobate. Smaller fragments of this nature may at their cores contain a single serpentinized microcrystal olivine. Commonly a thin, irregular, dark brown kimberlitic material mantles these microporphyritic clasts. This kimberlite appears to be of essentially the same composition as its core, however it is devoid of olivine. Such mantles may represent chilled margins.

A third type of clast common to Unit#1 is an ash-to-lapilli-sized, dark brown, optically uninformative clast, which contains small microphenocrystal olivine which appear to be replaced by predominantly calcite. Small angular xenocrysts of quartz or feldspar may be incorporated in this amoeboid-shaped, irregular fragment. The above-described juvenile material may mantle this type of fragment. These clasts may represent a recycled fragment of poor consolidated reworked volcaniclastic kimberlite which has been incorporated and redeposited within Unit#1

The above lapilli, together with sparse pseudomorphed olivine microcrysts are set in a groundmass of abundant serpophitized microphenocrystal olivines, copious anhedral barite, broken atoll spinels and subhedral-to-euhedral discrete spinels, apatite, small

euhedral rhombs of primary calcite and minor dolomite, subhedral perovskite, minor rutile and anhedral masses and discrete euhedral sulphides. Small xenocrysts of relatively fresh biotite, feldspar and quartz are profuse. The mesostasis consists of a very fine-grained intergrowth of altered phlogopite, serpentine and minor calcite.

The abundance of xenocrystal material within the groundmass suggests that Unit#1 is a resedimented volcaniclastic kimberlite breccia.

3.2.18.2.2. Unit#2

Unit#2 is a clast-support cognate breccia that contains numerous juvenile fragments and juvenile pelletal lapilli. These clasts are similar to the first type of clasts described in Unit#1, however pseudomorphing serpophite is a much darker brown.

These fragments are highly variable in size and shape, from ash-to-lapilli, elongated-to-bulbous. They consists of aggregates of small pseudomorphed microphenocrystal olivines (described previously as "serpophite" crystals) that are replaced by dark brown serpophite at their core with an outer mantle of yellow serpophitic alteration. Many resemble a donut structure (Figure 3.59). These crystals are set in irregular-to-subspherical patches of dark brown serpophite and a groundmass which contains subhedral perovskite, spinels (after small groundmass olivine), anhedral-to-euhedral apatite, poorly preserved atoll spinels and minor pyrite associated with the alteration of groundmass olivines. These clasts may or may not be cored by an olivine or spinel. Single crystals of these donut-like pseudomorphed microphenocrystal olivines are strewn throughout, commonly welded, the rock. A fine-grained serpophitic material commonly mantles them.

The above clasts appear to be welded and are set in a secondary cement of coarsely crystalline calcite (Figure 3.60).

Unit#2 is a pyroclastic kimberlite lapilli tuff that has been subsequently cemented by secondary calcite cement.

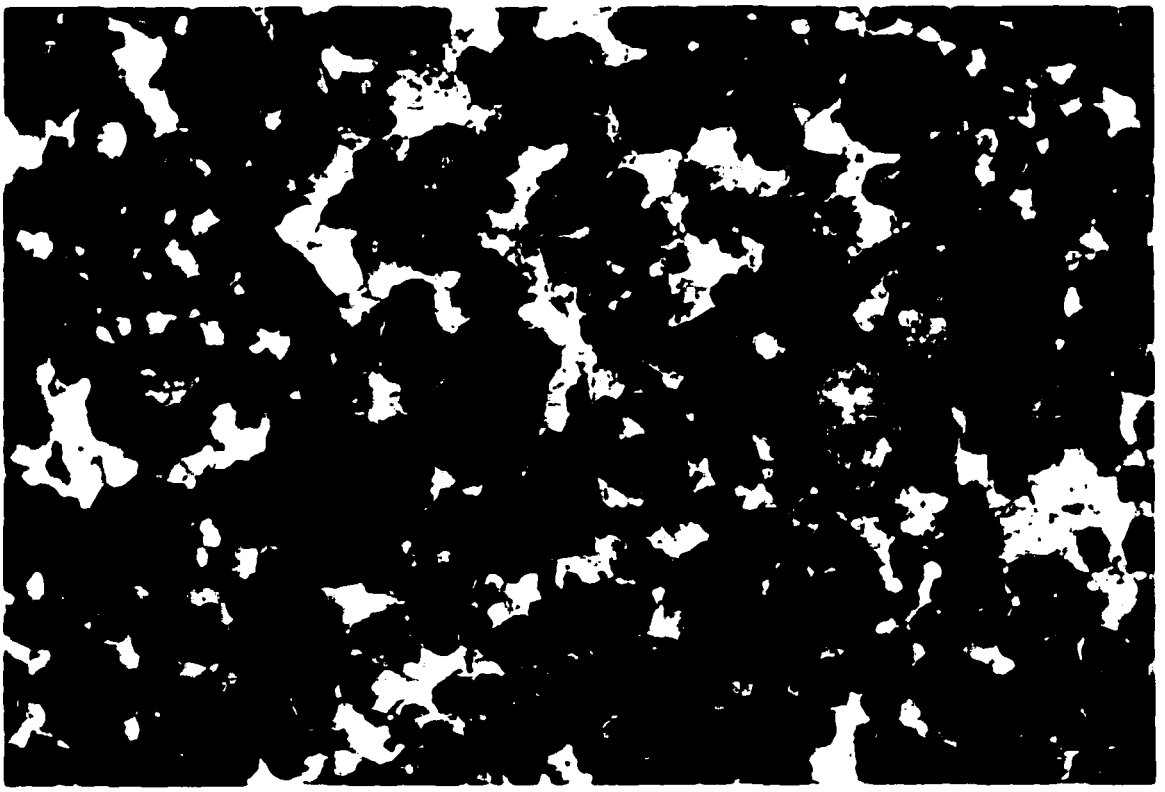

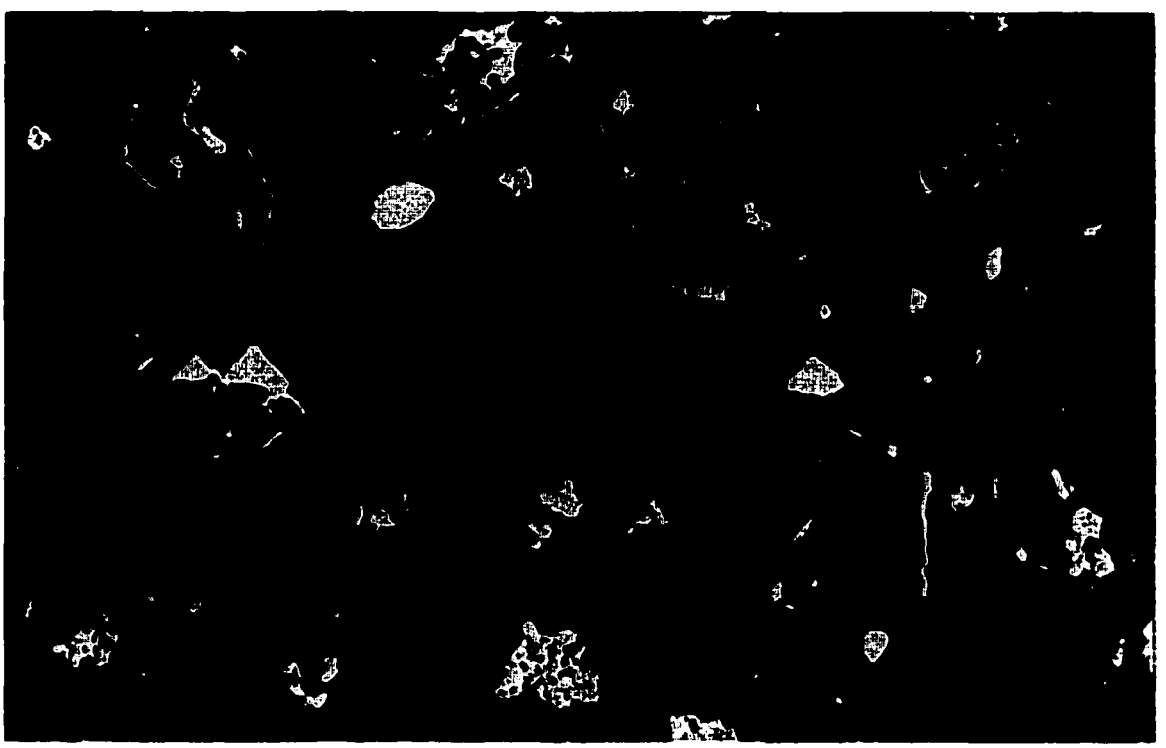

Figure 3.59. Kimberlite T7E, Unit#2. Small ash-to-lapilli-sized welded juvenile clasts (J) cemented with interlocking calcite (C). Many small fragments are composed of microphenocrystal serpentinized olivines that have a donut structure consisting of a dark core and a light-coloured mantle (F.O.V. 2.5 mm).

Figure 3.60. Kimberlite T7E, Unit#2. BSE-image showing small, welded groundmass juvenile fragments. Fragments are cemented with secondary calcite and minor serpentine (F.O.V. 120 μm).

3.2.18.3. Discussion

Kimberlite T7E represents a small kimberlite vent that has erupted and been infilled predominantly resedimented volcaniclastic breccias and intermittent, minor primary pyroclastic activity. No associated hypabyssal kimberlite was encountered.

3.2.19. Kimberlite T14

Kimberlite T14 was discovered and drilled in 1993. T14 is located 15 kilometres east of Lac de Gras, four kilometres northeast of C13 on the Tenby claim block which adjoins the eastern boundary of the Diavik Diamond Project.

Ground geophysics reveals a moderate electromagnetic response and a small, subtle sub-circular magnetic low, approximately 150x150 m in dimension. A single drill hole, 93T14-1, a vertical hole drilled near the centre of the magnetic anomaly, confirmed the presence of kimberlite.

Kimberlite T14 is overlain by approximately 9-10 m of lake water and 20 m of glacial regolith. The host rock of T14 is not known as the drill hole failed to intersect country rock. The drill hole collared directly into kimberlite and reached a vertical depth of 124.7 m.

3.2.19.1. Macroscopic Observations

Kimberlite T14 is an intensely altered, incompetent and highly friable dark gray-brown kimberlite. The kimberlite is massively bedded, however bedding contacts were not preserved and therefore could not be measured. Bedding is defined by the olivine-to-matrix ratio, which may range from approximately 5-15%. Units with higher olivine proportions tend to be more competent. Single samples from T14 have relatively restricted olivine grain sizes, while the entire suite of samples display a wide range of grain sizes (from less than 0.2 cm to greater than 1 cm). Olivine is completely replaced

by a yellow-brown serpentine. Xenocrystal fragments (mica and feldspar) are abundant and lithic fragments prevalent. Most lithic clasts are intensely altered making determination of their parentage impossible on a macroscopic scale. The proportion of lithic fragments increases with depth. Cognate clasts are common and occur as small, competent, very fine-grained rounded fragments.

The above volcaniclastic kimberlite is interbedded with dark gray, massive aphanitic siltstone. No kimberlitic constituents are identifiable macroscopically and these units appear to be non-kimberlitic sediments.

3.2.19.2. Microscopic Observations

Volcaniclastic kimberlite of T14 is intensely and pervasively altered. Alteration in the upper thirty metres of the intersection obliterates much of the primary texture and mineralogy leaving some samples optically uninformative.

T14 is characterized by an abundance of anhedral, subrounded xenocrystal feldspar, quartz and mica (predominantly biotite with minor muscovite). These crystals are usually relatively fresh, but may be replaced by calcite and serpentine along cracks and margins. Xenolithic fragments are present, but not abundant. Intense alteration prevents conclusive determination of their parentage. Minor, relatively fresh, subrounded non-kimberlitic siltstone fragments are present.

Macrocrystal olivines are well rounded and highly altered. Very fine-grained, optically uniform serpophite and fine-grained calcite replace macrocrystal olivine. Groundmass microphenocrystal olivines are similarly altered by a combination of brown serpophite and calcite. Many olivine crystals have a discontinuous mantle of euhedral opaque spinels and may poikilitically enclose discrete spinel or perovskite crystals. Fine grained, microporphyritic kimberlite mantles commonly surround olivines and are composed of kimberlite containing small relict microphenocrystal olivine and subhedral-to-euhedral discrete spinels.

T14 is comprised of numerous lapilli-to-ash sized kimberlitic fragments.
Two distinct varieties exist:

1. Microporphyritic kimberlite comprised of highly altered microphenocrystal olivine, which are mantled by spinels and broken atoll crystals (Figure 3.61). Olivine is set in a matrix of essentially calcite, minor serpentine with abundant perovskite. Broken crystals along at the margins of some of these fragments suggest they were solid at the time of their incorporation into their current host and therefore are autoliths.

2. Highly altered amoeboid-shaped microporphyritic kimberlite clasts (Figure 3.62) comprised of small, serpentinized euhedral-to-subhedral microphenocrystal olivine commonly poikilitically enclosing abundant spinels. Spinel appears to replace olivine along margins. The matrix is composed of spinel and perovskite in a mesostasis of calcite and serpentine. Small circular-to-ovoid calcite-filled vesicles are rare. The morphology and presence of vesicles suggest these clasts are *bona fide* juvenile lapilli. This identical kimberlite may contain at its core a single macrocrystal or microphenocrystal olivine or a discrete or atoll spinel (as described previously).

The groundmass consists of abundant subhedral-to-euhedral discrete and disrupted atoll spinels, common prismatic pyroxene, profuse anhedral-to-subhedral perovskite (<5um to 50um), apatite and subhedral-to-euhedral sulphides. Small resorbed crystals of barite are rare. Xenocrystal quartz, feldspar and biotite are abundant throughout the groundmass.

All the above is set in a mesostasis of intimately intergrown serpentine and calcite. Small crystals of phlogopite are strewn throughout the mesostasis.

Within these volcaniclastic units are discrete beds (from less than 10 cm to nearly 15m in thickness) of non-kimberlitic siltstone. These siltstones are brownish-red, massive, vaguely laminated and optically uniform units. They contain small crystals of mica that show a preferred orientation parallel to the lamination (depositional feature), abundant small crystals of quartz, feldspar (predominantly potassium feldspar), pyrite and minor prismatic pyroxene. Contacts with volcaniclastic kimberlite units were likely sharp.

3.2.19.3. Discussion

Presence of abundant xenocrystal material derived from the disaggregation of country rock indicates that kimberlite T14 is undoubtedly a vent infilled by resedimented

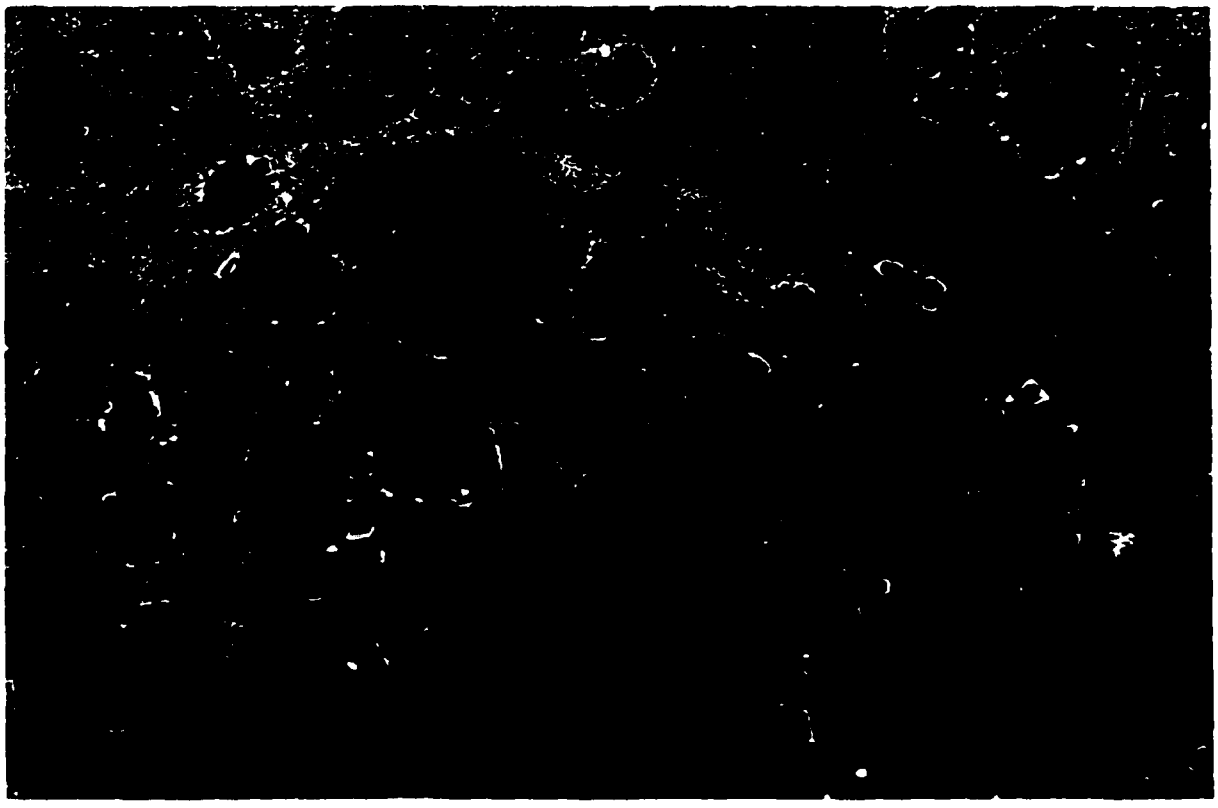

Figure 3.61. Kimberlite T14. BSE-image showing a relatively fresh autolith (outlined) of microporphyritic kimberlite (F.O.V. 1.72 mm).

Figure 3.62. Kimberlite T14. Small amoeboid-shaped juvenile lapilli composed of serpentinized microphenocrystal olivine (O) ± magnetite (black) set in a matrix of serpentine and calcite (F.O.V. 1.0 mm).

volcaniclastic kimberlite. Volcaniclastic kimberlites with such shale matrices have been reported (Graham *et al.* 1998, McKinlay *et al.* 1998, Doyle *et al.* 1998) and a similar conclusion was reached for the origin of kimberlite T14. The presence of thinly laminated, water lain crater infill substantiates this conclusion. T14 appears to lack hypabyssal rock.

3.2.20. Kimberlite T19

Kimberlite T19 was discovered in 1992 and is located approximately 46 kilometres east of the Diavik Diamond Project in a small cluster of three kimberlite intrusions including T237 and T21 1.5 kilometres and 2.5 kilometres to the northeast, respectively.

Kimberlite T19 is overlain by approximately 2 to 25 m of glacial regolith. Ground magnetic surveys reveal an elongated ovoid-shaped intrusion, 75x350 m in dimension, striking east-west. T19 intrudes biotite schists of the Yellowknife Supergroup.

This narrow vent was poorly sampled by two drill holes. Both holes were drilled at angles of –55° across the strike of the intrusion and as this kimberlite is quite narrow (no greater than 30 m); very little kimberlite was intersected. No information regarding the depth extent of T19 is available.

3.2.20.1. Macroscopic Observations

Drill hole T19-2 collared into 61 m of biotite schist host rock and kimberlite was intersected at 98 m at an angle of –55°. Five distinct units of reworked rock, both volcaniclastic kimberlite and non-kimberlitic siltstone and mudstone, occur in this vent. Two separate units (2 to 6 m in thickness) of hypabyssal kimberlite have cut these units.

The uppermost unit (Unit#1) intersected is an "earthy", incompetent dark brown massive non-kimberlitic siltstone approximately 4.5 m in thickness. This unit overlies a veneer of light brown non-kimberlitic mudstone (not sampled). The mudstone unit lies a

volcaniclastic clast-supported kimberlite breccia (Unit#2). This contains approximately 10-15% highly serpentinized, rounded macrocrystal olivine which commonly form the cores of cognate fragments. Below Unit#2 lies a highly altered, matrix-supported volcaniclastic kimberlite (Unit#3) that contains numerous cognate fragments and approximately 10-15% macrocrystal olivine pseudomorphs, set in a dark brown, aphanitic matrix.

The above units are intersected within this drill hole by two separate units of hypabyssal kimberlite (Units #4 and #5), separated by a three metre intersection of highly incompetent reworked volcaniclastic kimberlite. The very competent hypabyssal kimberlite is characterized by the presence of abundant rounded and fragmented macrocrystal olivines, which have been replaced by calcite. Similarly altered microphenocrystal olivine are numerous, imparting a pseudoporphyritic texture to the rock. Numerous dilational calcite veins cut the core at diverse angles.

3.2.20.2. Microscopic Observations

3.2.20.2.1. Unit#1

This optically uninformative rock contains abundant small, subangular-to-rounded crystals of quartz and feldspar (approximately 20%), common tan-coloured mica crystals, and numerous subhedral opaque oxides and sulphides. These together with altered brown relicts of minerals of unknown parentage are set in a brown, optically unresolvable matrix. No kimberlite-derived constituents are present.

3.2.20.2.2. Unit#2

Numerous rounded-to-irregular-shaped microporphyritic cognate fragments characterize this clast-supported rock. These fragments are dark brown in colour and contain abundant subhedral-to-euhedral microphenocrystal olivine pseudomorphs. Olivine is replaced by dark green retrograde serpophitic serpentine and are mantled by a

thin rind a pale yellow serpentine. Olivine, together with minor subhedral-to-euhedral opaque oxides, small crystals of mica and apatite are set in a very fine-grained, dark-brown, optically unresolvable matrix. These clasts may be cored by a single large, rounded macrocrystal olivine. Margins of these clasts are quite irregular and are probably juvenile lapilli (Figure 3.63).

Xenoliths of microcline-bearing syenite are present, but not common. These are commonly replaced at their margins by serpentine and carbonate.

The juvenile lapilli are cemented together with a coarsely crystalline, undoubtedly secondary, calcite cement.

3.2.20.2.3. Unit#3

Unit#3 is characterized by the presence of very few rounded and commonly broken olivine macrocrystal pseudomorphs. The olivines are replaced by dark brown-green serpophitic serpentine and are commonly veined and mantled by calcite.

Lapilli-to-ash-sized cognate fragments are common. They are composed of microporphyritic kimberlite as described in Unit#2. These amoeboid-shaped fragments are not cored by olivine and are probably juvenile lapilli.

The groundmass contains numerous highly altered microphenocrystal olivines that are completely pseudomorphed by dark brown serpophite. These crystals are commonly difficult to distinguish from a similarly coloured matrix. Microphenocrystal olivine, together with abundant angular fragments of xenocrystal feldspar, minor quartz and common subhedral-to-euhedral opaque oxides, fresh-to-partially altered mica and minor apatite are set in a very fine-grained, homogeneous matrix of serpophite and calcite.

3.2.20.2.4. Unit#4 and Unit#5

These units contain common rounded, spherical-to-ovoid olivine macrocrysts, completely replaced by relatively coarse-grained, interlocking calcite and are mantled by

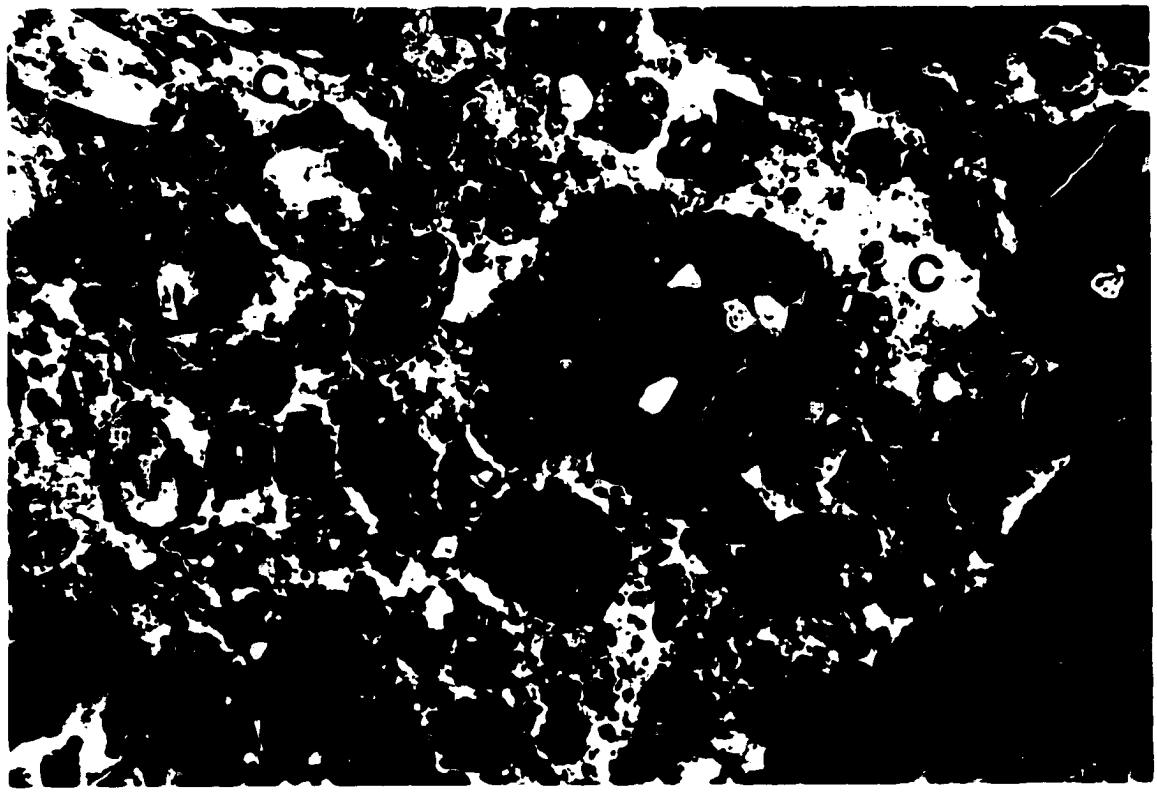

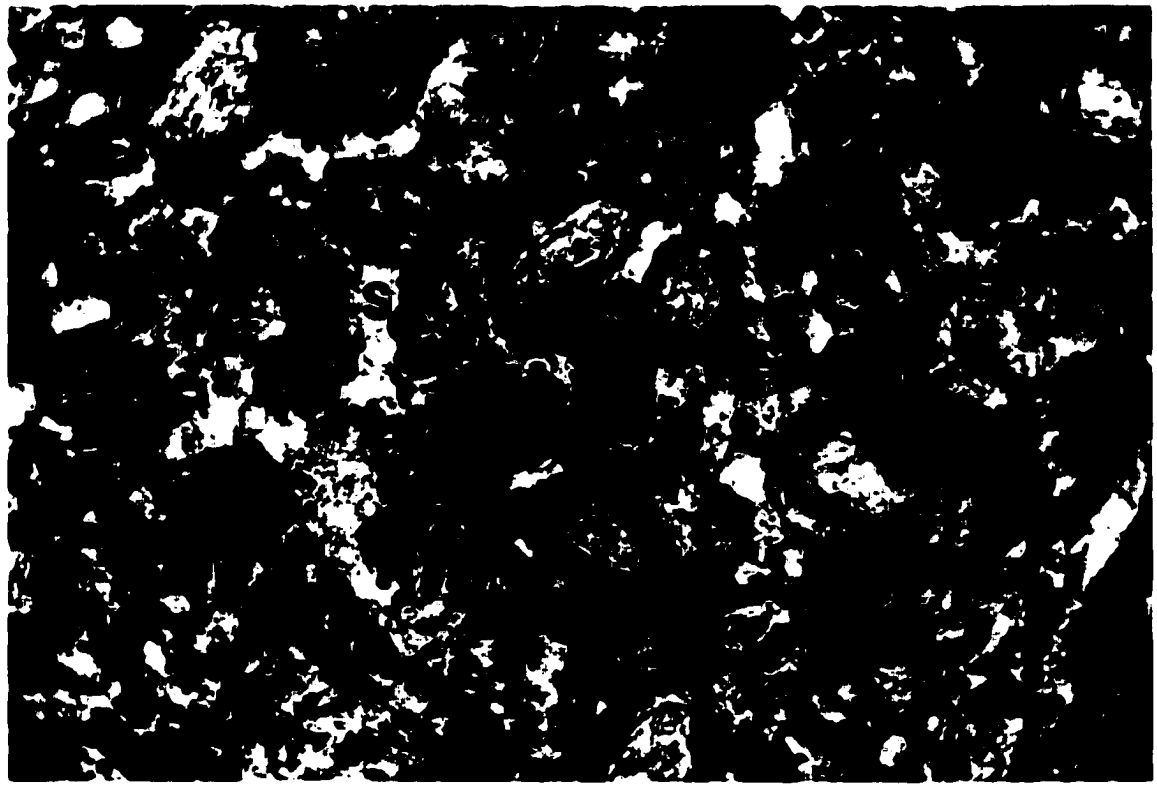

Figure 3.63. Kimberlite T19, Unit#2. Volcaniclastic kimberlite breccia composed of abundant juvenile fragments (J) cemented with a secondary calcite cement (C) (F.O.V. 6.0 mm).

Figure 3.64. Kimberlite T19$_{n}$ Unit#4. Segregation-textured hypabyssal kimberlite composed of numerous groundmass olivine (replaced by calcite and marginal serpentine) and common atoll spinels. Segregations (S) are filled predominantly with calcite and minor serpentine (F.O.V. 6.0 mm).

a thin margin of pale yellow serpentine. Small relict cores may remain. The majority of the olivine population consists of fine-grained, subhedral-to-euhedral microphenocrystal olivine (Figure 3.64). These are also replaced by crystalline calcite and have thin margins of pale yellow serpentine. Both populations of olivine have been altered in a similar fashion. Groundmass olivines may poikilitically enclose REE-bearing euhedral apatite.

Groundmass spinels are prevalent and occur as discrete euhedral-to-subhedral crystals or as complex atoll structures. Resorbed crystals of magnetite are strewn throughout the groundmass. Crystallization of primary magnetite around microphenocrystal groundmass olivines as "necklaces" is common phenomenon. Perovskite occurs as rare, small, subhedral crystals and minor sulphides including sphalerite, chalcopyrite and pyrite are noted. The above are set in a very fine-grained, heterogeneous matrix consisting of well-crystallized mica together with calcite and serpentine. Mica occurs short blocky colourless-to-orange crystals of phlogopite that poikilitically enclose abundant monticellite (pseudomorphed by serpentine). Apatite is common as prisms and irregular masses of anhedral crystals that appear to have crystallized prior to the groundmass mica.

Calcite-rich segregations are common. These irregular-shaped patches consist of coarse-grained, interlocking calcite. Apatite, which belongs to the initial stages of segregation crystallization, form sprays of acicular crystals at the margins of the segregations. These are now replaced by calcite.

3.2.20.3. Discussion

T19 is an elongated kimberlite vent infilled with interbedded non-kimberlitic mudstones and siltstones (*i.e.* Unit#1) and volcaniclastic kimberlite (Unit #2 and #3). Unit#2 appears to be a highly altered lapilli tuff that has been subsequently cemented with secondary calcite, while Unit#3 is a resedimented volcaniclastic kimberlite containing common juvenile lapilli and abundant xenocrysts of disaggregated country rock. Thin sills of segregation-textured apatite phlogopite monticellite hypabyssal

kimberlite have intruded the vent at high structural levels, subsequent to eruption and infill.

CHAPTER 4. ORAPA A/K1 KIMBERLITE, BOTSWANA

4.1. INTRODUCTION

After extensive exploration by a De Beers team of geologists in the western part of Botswana's Central District, the Orapa B/K1 and A/K1 kimberlites were discovered 240 km west of Francistown, Botswana (Figure 4.1). The later is the largest (118 hectares), of over 50 kimberlites discovered in the area. The economic potential of A/K1 was evaluated and by 1 July 1971 Orapa began production. The production created excellent exposures that permitted detailed mapping to take place allowing further insight into kimberlite emplacement within southern Africa.

Orapa A/K1 intrudes Archean basement granite-gneiss and tonalite as well as the sedimentary rocks and lavas of the Karoo Supergroup. The Karoo Supergroup, which comprises the wall rock at Orapa, can be subdivided into five formations: Tlapana, Tlhabala, Mosolotsane, Ntane and Stromberg (Smith 1984). The Permian Tlapana Formation unconformably overlies basement granite-gneiss and is composed of interbedded sandstones, carbonaceous mudstones and thin coal measures. The Triassic Tlhabala formation consists of massive gray mudstones, the Late Triassic Mosolotsane Formation comprises red mudstones and minor interbedded sandstones, the Late Triassic Ntane Formation comprises predominantly aeolian sandstones (an aquifer), with minor fluviatile sandstones at its base and the Stromberg Formation is compose of tholeiitic basalt lavaflows of Jurassic age. Because A/K1 and other kimberlites of close proximity intrude into a graben-like structure, thicker Karoo sequences are preserved (Field *et al.* 1995, 1997; Kilham *et al.* 1998; Figure 4.2). An age of 92.1 Ma, using U-Pb methods on zircons, for the A/K1 kimberlite was established by Davis (1977).

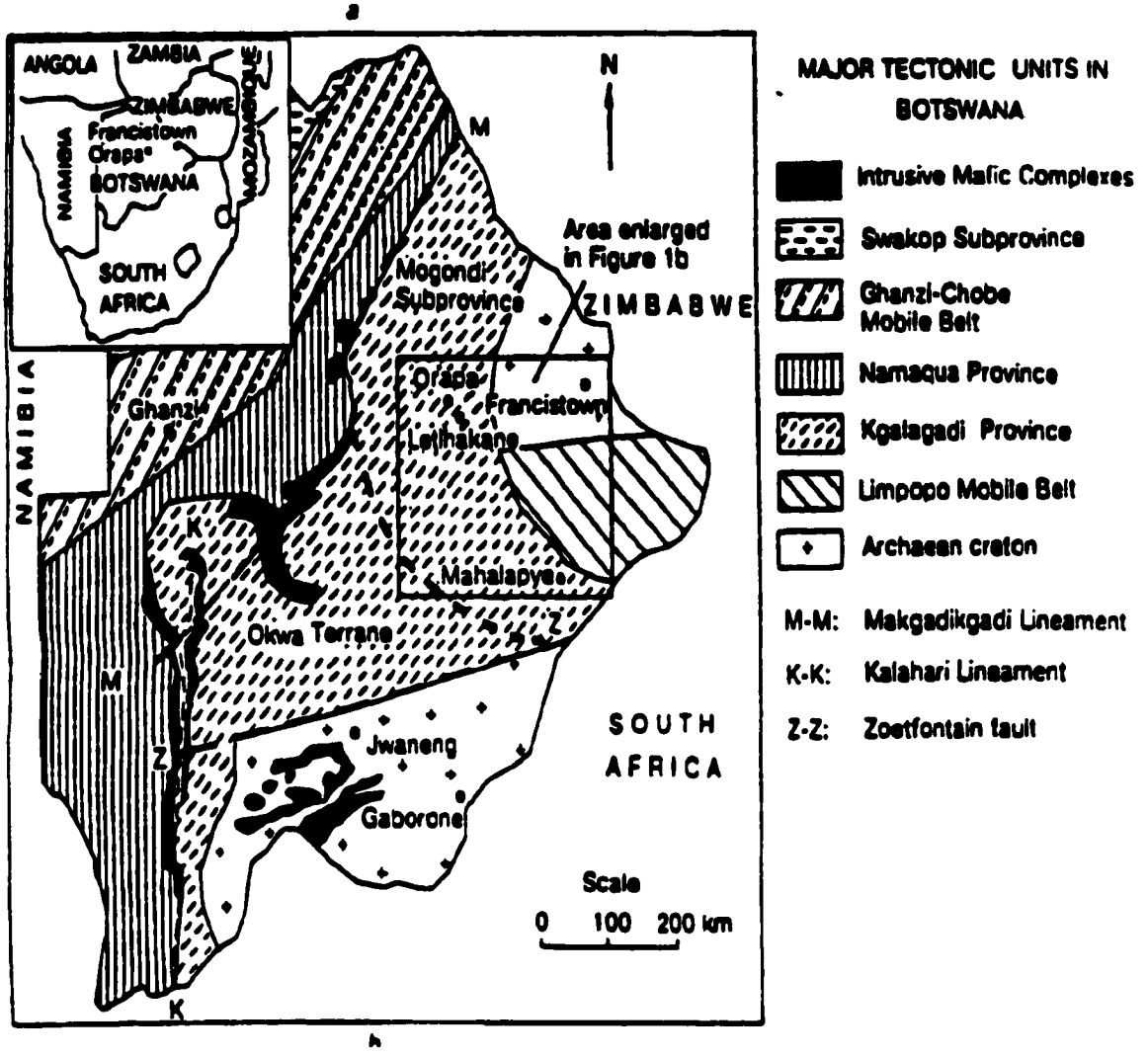

Figure 4.1. Map showing the location of Orapa in Botswana relative to the underlying tectonic framework (Field *et al.* 1997).

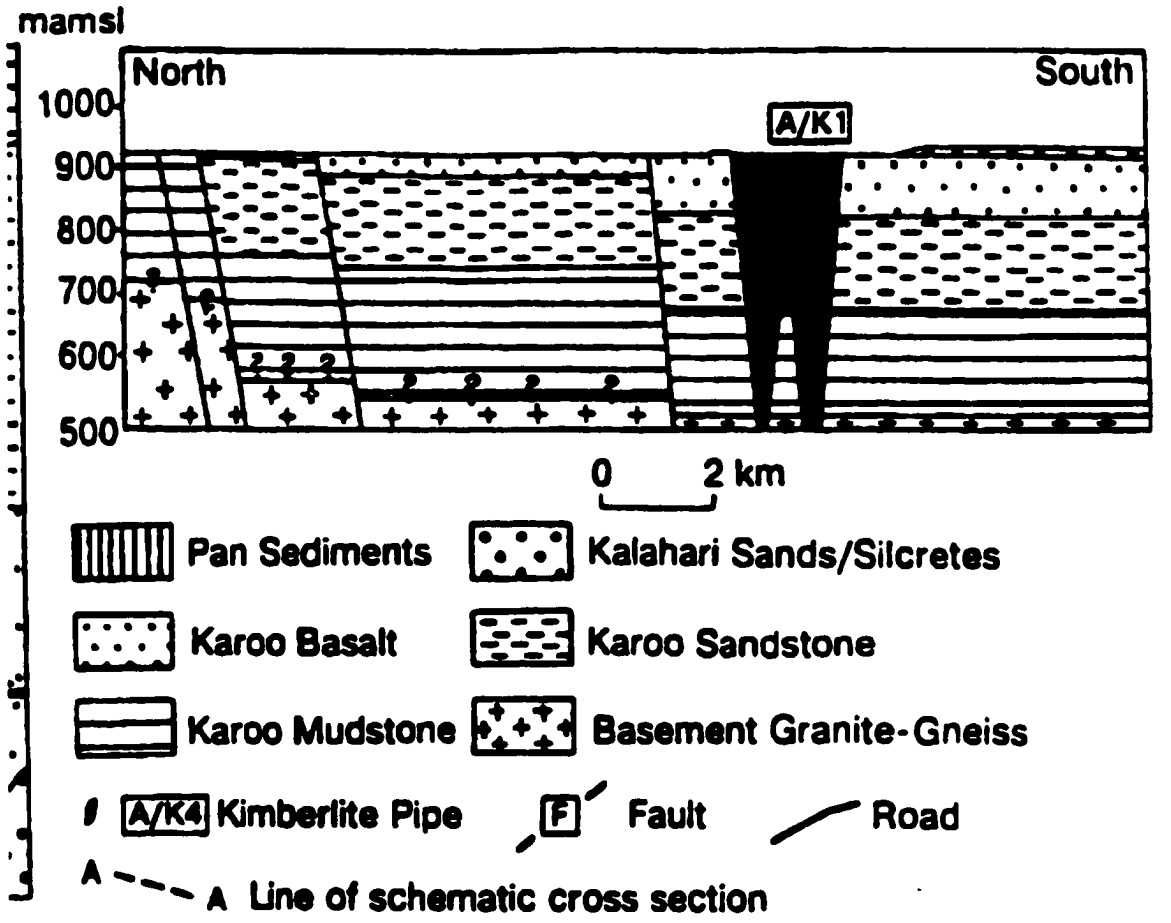

Figure 4.2. Detailed geological setting of Orapa A/K1 in cross-sectional view. There is a 7x vertical exaggeration (Field *et al.* 1997).

4.2. GEOLOGY OF THE ORAPA A/K1 KIMBERLITE

The Orapa kimberlite comprises two diatremes that intruded the Archean basement and Phanerozoic Karoo sediments, coalescing into a single crater at surface. The two vents have been named the "northern" and "southern lobes" respectively (refer to Figures 4.3 and 4.4). The northern lobe was initially emplaced and subsequently disrupted and truncated by the subsequent emplacement of the southern lobe (Field *et al.* 1995, 1997; Kilham *et al.* 1998).

Mining operations have exposed the upper 100 m of the A/K1 kimberlite; consequently the rock comprising this zone has been extensively studied. Rock types occurring below this exposure have been studied in far less detail through a combination of precision and core drilling, accordingly, far less is known about these unexposed rocks, particularly below the 200-metre depth (Field *et al.* 1995, 1997; Kilham *et al.* 1998).

Kimberlite belonging to all three facies (Dawson 1971; Hawthorne 1975; Clement and Skinner 1979, 1985; Clement 1982; Mitchell 1986 and Clement and Reid 1989), *i.e.*, crater, diatreme and hypabyssal, have been recognized within the A/K1 kimberlite body (Field *et al.* 1995, 1997; Kilham *et al.* 1998).

4.2.1. Northern Lobe

The northern-lobe is a steep-sided vent that extends to a known vertical distance of 600 m (refer to Figure 4.4). At depth, the northern-lobe is infilled with massive, monotonous tuffisitic kimberlite breccia, which gives way to grossly layered pyroclastic kimberlite (northern pyroclastic kimberlite). These two rock types are virtually indistinguishable on hand specimen or even petrographic scale; the two units are distinguished only based on the gradual transition from grossly-layered to massively-layered kimberlite at depths greater than 230 m (Field *et al.* 1995, 1997; Kilham *et al.* 1998). No hypabyssal rock, to date, has been intersected in the northern lobe of the A/K1 kimberlite.

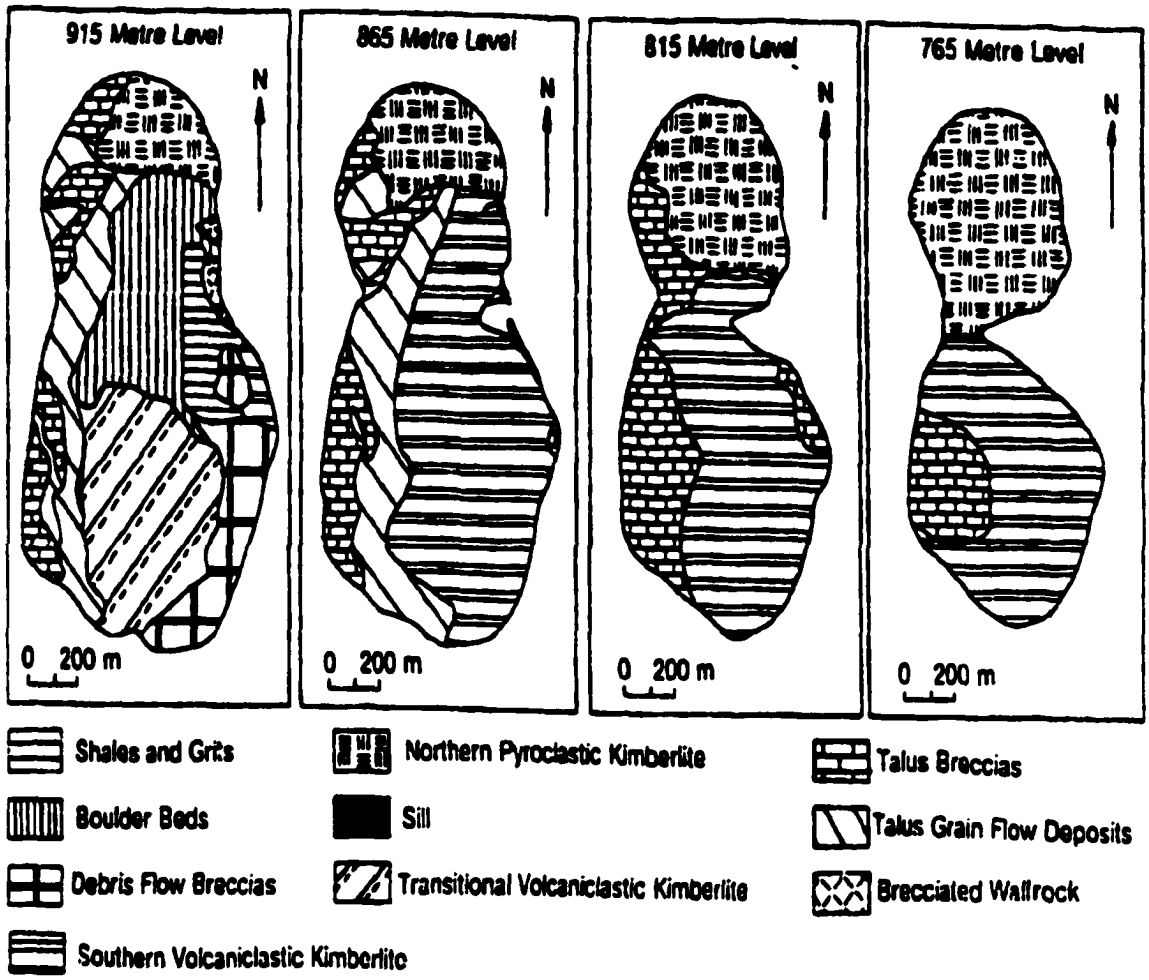

Figure 4.3. The internal geology of Orapa A/K1 showing the distribution of geological units on four different elevation levels. The present-day surface is approximately 960 metres above mean sea level (Field*et al.* 1997).

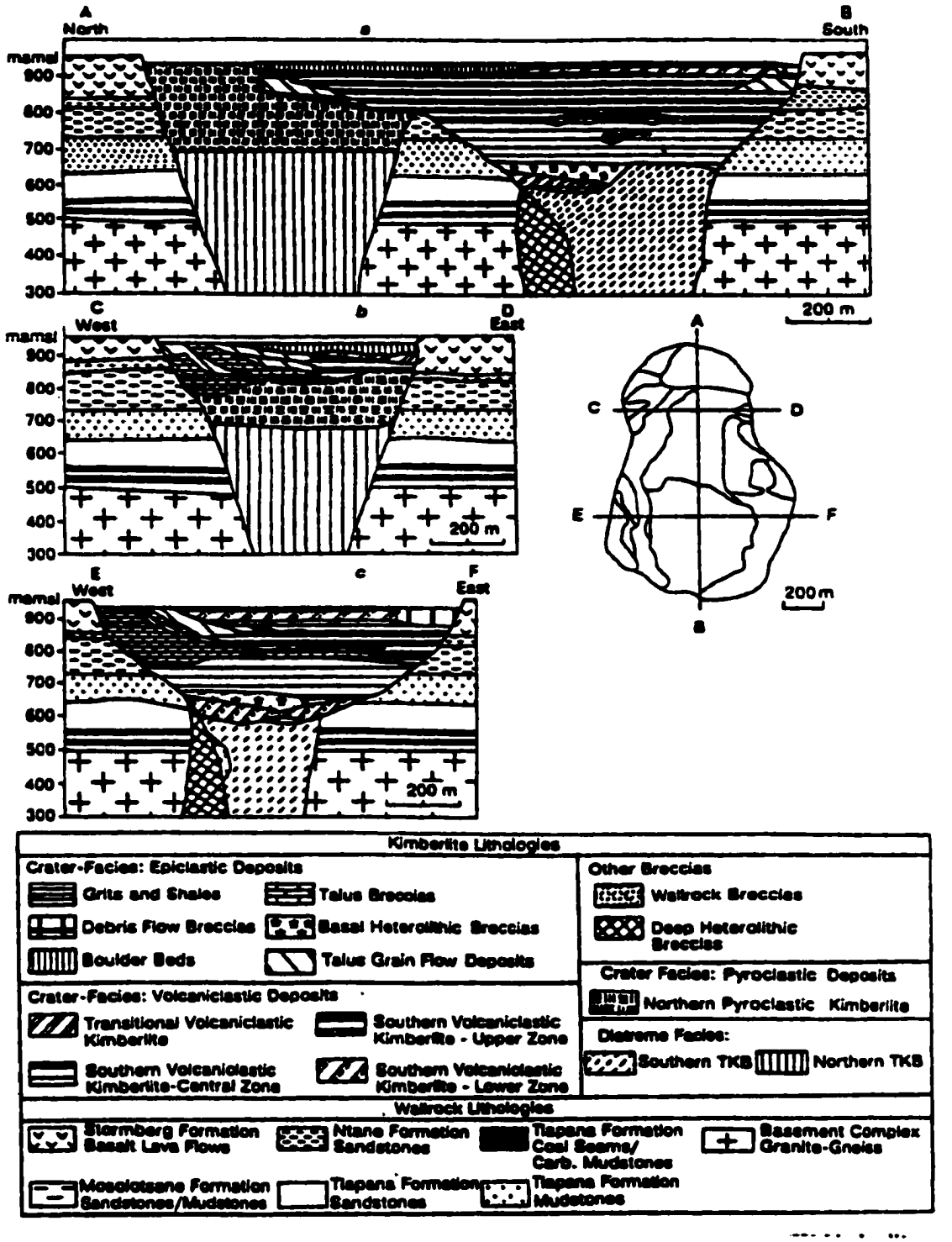

Figure 4.4. North-south (a) and east-west (b and c) cross sections through the Orapa A/K1 kimberlite (Field *et al.* 1997).

4.2.1.1.1. Petrographic Features of the Northern Pyroclastic Kimberlite

The northern pyroclastic kimberlite (NPK) contains abundant poorly developed juvenile lapilli, which are essentially identical to the pèlletal lapilli found in the underlying tuffisitic kimberlite breccia, together with common basement-derived lithic fragments and basaltic clasts (Figure 4.5) in a matrix rich in microlitic diopside, also identical to that which characterizes to diatreme infill below. The NPK deposit is crudely graded, both reverse and normally and many of the basaltic and basement fragments show ballistic impact structures. Layering in not obvious near the centre of this unit and clast-rich layers are confined to edges of the deposits (*i.e.* near the wall rock contacts) suggesting that the central parts of the deposit represented a feeder zone for pyroclastic activity (Field *et al.* 1997; Kilham *et al.* 1998). The bedded deposits contain small pipe-like structures which are interpreted to represent degassing structures.

Grading within the NPK is defined by either the concentration of large basalt and basement clasts, or by size-grading of finer-grained constituents, or by variations in packing density.

On a microscopic scale, the NPK is a moderately-to-tightly-packed heterolithic kimberlite breccia that is characterized by abundant, relatively large (<5mm) rounded and commonly broken, serpentinized macrocrystal olivine. A thin mantle of kimberlitic ash may rim these grains. Olivine, together with smaller, subrounded macrocrystal ilmenite and abundant lithic fragments are suspended with two types of kimberlite juvenile lapilli in a matrix which is dominated by globular clusters and individual laths of microlitic diopside set in a groundmass mesostasis of serpentine (Figure 4.6). Other groundmass constituents include phlogopite, subhedral-to-euhedral apatite and stout crystals of subhedral-to-euhedral diopside.

The first type of juvenile lapilli (Figure 4.7) consists of a microgranular intergrowth of spinel, perovskite, and serpentinized monticellite and microphenocrystal olivine in a serpentine base. This intergrowth forms thin rinds about macrocrystal olivine grains or lithic fragments. Microlitic diopside is strewn throughout these mantles. Small crystals of apatite are also common throughout these ash rinds. Field *et al.* (1997)

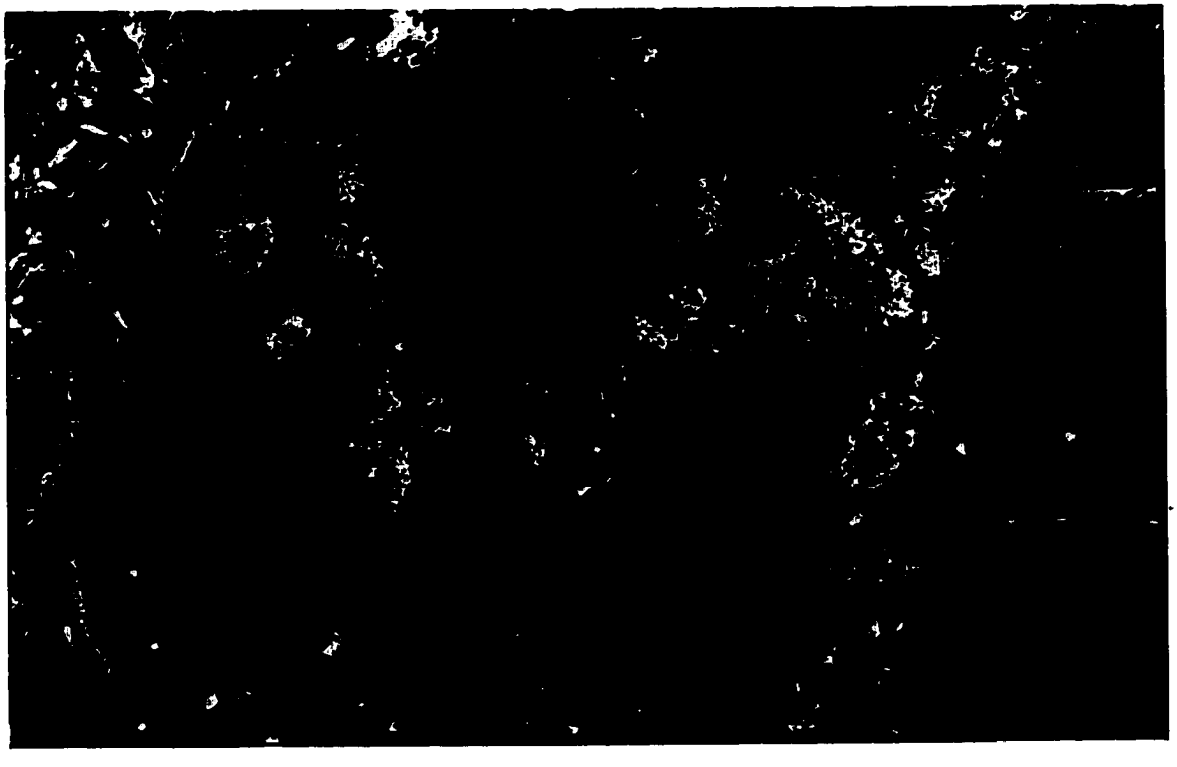

Figure 4.5. Northern pyroclastic kimberlite. Clasts of wall rock (X), serpentinized olivine macrocrysts (O) and numerous poorly-developed juvenile lapilli (J) set in a very fine-grained, diopside-rich matrix (F.O.V. 2.5 mm)

Figure 4.6. Backscattered electron image of the northern pyroclastic kimberlite. Larger serpentinized olivine macrocrysts, subhedral-to-euhedral serpentinized microphenocrystal olivine (O) (which may be mantled by microlitic diopside) are set in a matrix dominated by globular clusters and individual laths of microlitic diopside (yellow). All of the above is set in a serpentine mesostasis (F.O.V. 500 μm).

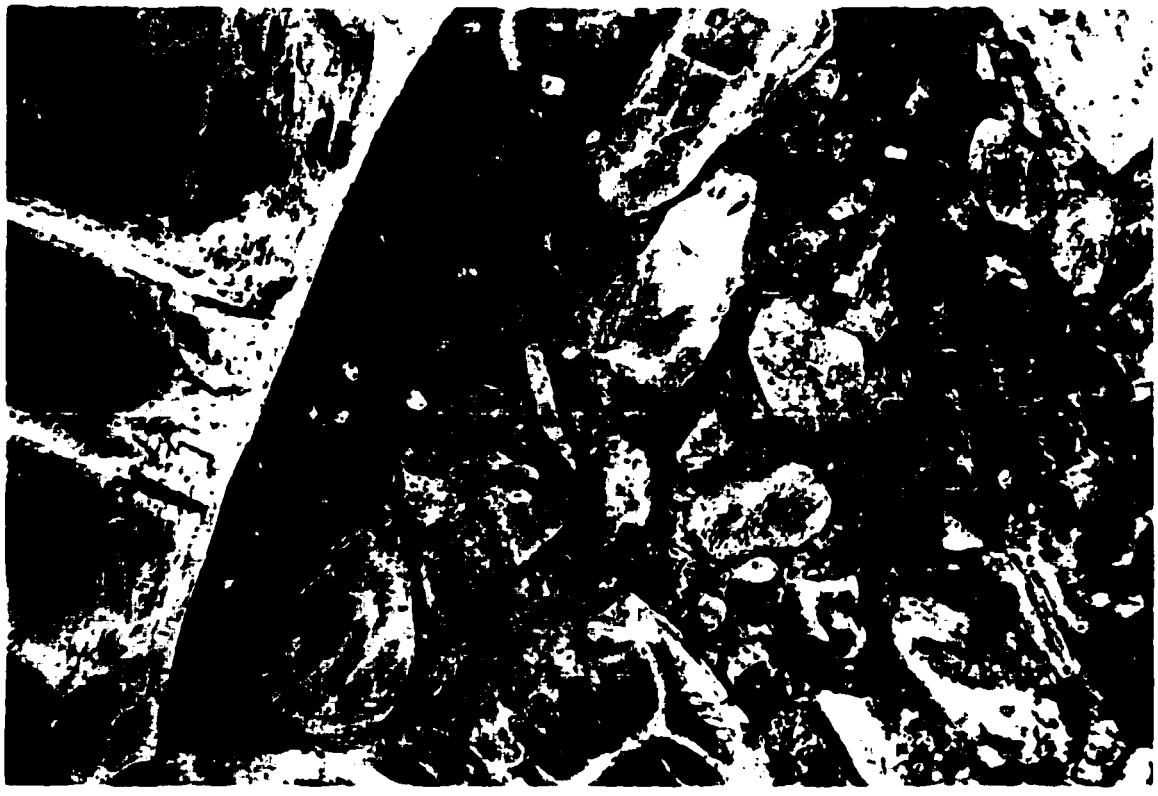

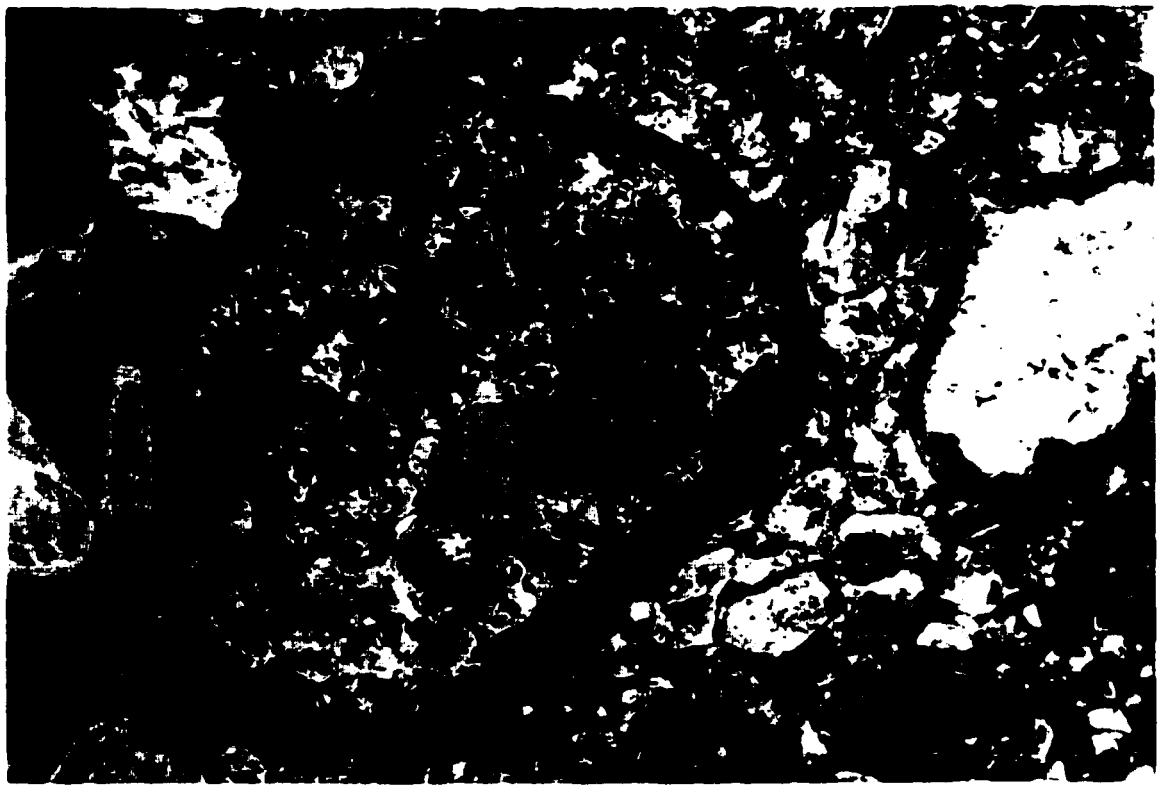

Figure 4.7. Partial view of a "crystalline lapilli" as defined by Field *et al.* (1997) within the northern pyroclastic kimberlite (F.O.V. 2.5 mm).

Figure 4.8. Microcrystalline lapilli, as defined by Field *et al.* (1997) within the northern pyroclastic kimberlite. These juvenile lapilli are indistinguishable form the pelletal lapilli characteristic of the northern tuffisitic kimberlite breccia (F.O.V. 2.5 mm).

suggest the matrices of these rounded-to-subrounded fragments have crystallized to an advance stage before being incorporated into the NPK unit and has thus termed them "crystalline" lapilli. The second, more common, type of juvenile lapilli recognized within the NPK are termed "microcrystalline lapilli" by Field *et al.* (1997) and consist of intimately intergrown subrounded aggregates of microlitic diopside laths which may form discrete, rounded bodies or may mantle macrocrystal of xenolithic constituents (Figure 4.8). Less common spinel, perovskite and apatite grains may occur within these fragments.

Odd-shaped laths of mica have overgrown some olivine macrocrysts. These are secondary in nature.

Field *et al.* (1997) suggest that the microlitic diopside was formed by rapid quench crystallization from a hot vapour phase. Field *et al.* (1997) further believe their origin is similar to the microlites found in tuffisitic kimberlite breccia, that is, trapped gases from the degassing vent (Clement 1982), with the exception that gases were trapped within the subaerially deposited NPK. The combination of this hot crystallization, reverse-to-normally graded beds and the presence of fumarole pipe-like structures provide convincing evidence for a pyroclastic origin for this unit. The NPK is thought to have been deposited under high temperatures of emplacement by a flow-type mechanism (Field *et al.* 1997).

4.2.1.1.2. Emplacement of the Northern Lobe

The model presented by Field *et al.* (1997) suggests that the northern lobe was emplaced by a single, short lived catastrophic event that resulted in the deposition of both the NPK and the underlying northern tuffisitic kimberlite breccia.

Field *et al.* (1997) envisions an eruption that is similar to the high-energy eruptions, which occur in silicic volcanoes in which conduits are blocked with the crystallization of highly viscous magmas. The case of the A/K1 kimberlite, competent basaltic country rock acts as the plugs. A catastrophic eruption results in the breakthrough of magma and an eruption column was produced. The outer part of the

NPK is deposited by fallout and possibly pyroclastic flow mechanisms resulting in the periodic collapse of the high, CO_2-rich eruption column.

4.2.2. Southern Lobe

The southern lobe, which is also comprised of tuffisitic kimberlite breccia (TKB) at depth occurs as a steep-sided diatreme with an overlying, flaring crater. The overlying crater infill overlies, in sharp contact, the TKB. Crater infill consists of early basal heterolithic breccias (BHB) that are overlain by thick, monotonous deposits of juvenile-rich volcaniclastic kimberlite [Southern Volcaniclastic Kimberlite (SVK) and Transitional Volcaniclastic Kimberlite (TVK)] that are covered by extensive fans of epiclastic rock composed largely of basaltic fragments [talus grain flow deposits (TGF), talus breccias, debris flow breccias, boulder beds and shales] (Field *et al.* 1997; Kilham *et al.* 1998; Field and Scott Smith 1998). In contrast to the northern lobe, hypabyssal facies kimberlite has been encountered both at depth and within the crater deposits in the form of a sill (Field *et al.* 1997; Kilham *et al.* 1998).

4.2.2.1. Petrographic Features of the Southern Lobe

4.2.2.1.1. Talus Deposits

Talus deposits of the southern lobe, which are best developed along the western margin, can be subdivided into two units: talus breccias and talus grain flow deposits.

4.2.2.1.1.1. Talus Breccias

Talus breccias, as described by Field *et al.* (1997) and Kilham *et al.* (1998) are massive breccias composed of crudely stratified, closely-packed, poorly-sorted, angular basaltic fragments, ranging in size from a few millimetres to a few metres, set in a matrix composed predominantly of secondary carbonate, ferrous oxides and minor serpentine.

Minor kimberlite-derived minerals occur within these beds. At least six individual units have been recognized. Basaltic fragments are generally fresh and kimberlite constituents consist mainly of large, rounded serpentinized olivines, minor ilmenite, phlogopite, garnet and primary calcite and dolomite.

4.2.2.1.1.2. Talus Grain Flow Deposits

Talus grain flow deposits occur as well-sorted, well-layered beds composed of resedimented kimberlite debris and lesser amounts of xenolithic fragments. Size grading of clasts is common and Field *et al.* (1997) and Kilham *et al.* (1998) note reverse grading. Six individual units have been identified within the southern lobe; these units occur as overlapping fans in close association with the talus breccias.

Talus grain flow deposits are clast-supported heterolithic breccias with a closely-packed array of well-sorted juvenile and lithic fragments (Figure 4.9). Poorly-developed juvenile lapilli, serpentinized, rounded olivine macrocrysts, rare autoliths, distorted macrocrystal phlogopite, rare garnet, ilmenite and lithic fragments of predominantly basalt (rounded, abraded and intensely altered by calcite) and rare mudstone (only one observed) are set in a base of predominantly serpentine which contains amoeboid-shaped calcite-filled bodies. It is commonly difficult to discern juvenile lapilli from a similarly altered matrix. Calcite-filled bodies may represent vesicles within the lapilli. Sulphides are also present within the groundmass of the talus grain flow units.

Intense alteration has obliterated much of the primary texture and mineralogy of these rocks.

4.2.2.1.2. Debris Flow Breccias

Debris flow breccias, which occur along the eastern crater margin of the southern lobe, are heterolithic breccias characterized by abundant basaltic fragments. This unit can be distinguished from the talus breccias by their matrix-supported textures and

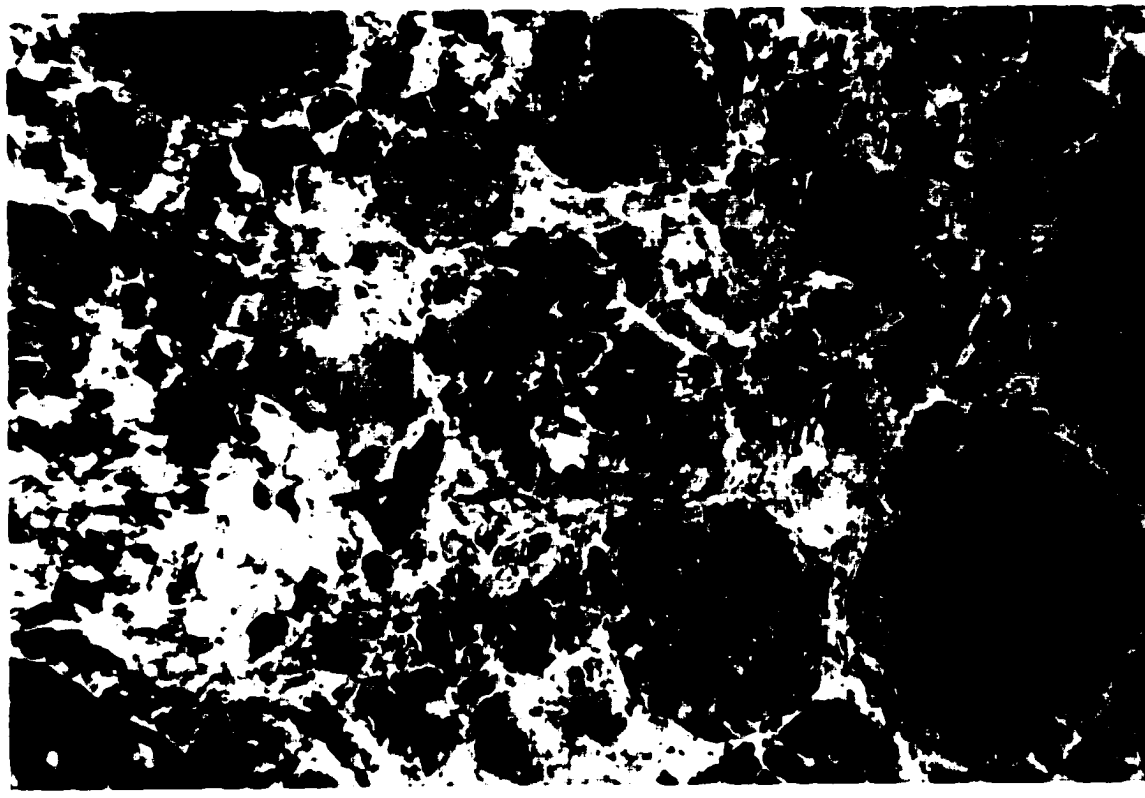

Figure 4.9. Closely-packed array of olivine grains (O), minor lapilli (L) and lithic fragments. Intense alteration has destroyed most of the primary mineralogy and texture of the talus grain flow deposits (F.O.V. 2.5 mm).

bounding surfaces at lower angles. Normal and reverse grading is noted (Field *et al.* 1997; Kilham *et al.* 1998).

The basaltic clasts together with kimberlite-derived constituents, which include relict olivine macrocrysts, chloritized phlogopite are set in a highly altered matrix of clays and carbonates. Mantle xenoliths have also been recognized within this unit (Field *et al.* 1997).

4.2.2.1.3. Boulder Beds

Boulder beds range from a matrix-supported to a clast-supported texture in which lithic clasts (basalt, mudstone and basement fragments) are set in a matrix of serpentine, clay and carbonate. Small juvenile lapilli have been noted; these generally consist of kimberlite-derived or lithic constituents that are mantled by thin rinds of kimberlitic ash (Field *et al.* 1997; Kilham *et al.* 1998).

4.2.2.1.4. Volcaniclastic Deposits

A sharp contact at an approximate depth of 60 m separates the epiclastic units from the underlying, more massive kimberlite. This unit is referred to as the Southern Volcaniclastic Kimberlite (SVK) and although it also overlies the NPK deposits of the northern lobe, it appears to be a feature particular to the southern lobe. A transitional unit between the SVK proper and the overlying epiclastic deposits, the Transitional Volcaniclastic Kimberlite (TVK), has been identified within the central portions of the southern lobe of AK/1. The TVK is considered to represent weathered SVK that was likely reworked and redeposited within the overlying epiclastic basin (Field *et al.* 1997; Kilham *et al.* 1998).

The SVK is characterized by both coarse massive, matrix-supported units and well-sorted, bedded, sub-horizontal and fine-grained zones. Concentrations of lithic fragments impart a grossly layered appearance to the SVK. Field *et al.* (1997) and Kilham *et al.* (1998) have subdivided the SVK into three distinct zones:

1. Upper Zone: This unit is a massive, matrix-supported breccia that occurs between the epiclastic deposits (above) and talus breccias (below). The upper zone consists of serpentinized olivine crystals, juvenile lapilli, lithic fragments and mantle-derived xenoliths and xenocrysts set in a mesostasis of serpentine, clays and occasional irregular-shaped carbonate-rich pools. Both crystalline and microcrystalline varieties of juvenile lapilli are present.

2. Central Zone: The central zone, which occurs between the underlying basal heterolithic breccias (BHB) and the overlying talus breccias is characterized by fewer layered horizons and more abundant basement fragments. Microlitic juvenile lapilli are present as are carbonate degassing structures.

3. Lower Zone: This zone comprises layers of volcaniclastic kimberlite interbedded with the BHB. A further increase in basement clasts and microlitic lapilli is noted within this unit and microlite diopside laths may occur within the interclast matrix. The lower zone strongly resembles the NPK.

Figure 4.10 shows the microscopic features present within the SVK. Within these samples macrocrystal ilmenite is common and the discrete carbonate-rich pools common to the interclast matrix may contain a significant amount of dolomite. Carbonate alteration of basaltic wall rock fragments may be prolific. Groundmass constituents include minor spinels and relatively large (<0.1mm) rounded grains of apatite. As is evident in Figure 4.10, the SVK has been intensely altered and much of the primary mineralogy and textures have been eradicated.

4.2.2.1.5. Basal Heterolithic Breccia

The base of the crater zone within the southern lobe of A/K1 is marked by unique heterolithic breccias. These deposits are unique in that they contain a significant amount of wall rock clasts derived from lithologies other than basalt. The BHB is not dispersed across the entire crater floor and appear to be absent in the southern half of the southern lobe.

These breccias consist of a profuse amount of lithic fragments (sandstone, mudstone, carbonaceous mudstone, basalt, granite-gneiss, amphibolite), minor amounts of quartz grains, together with kimberlite-derived constituents set within a variable

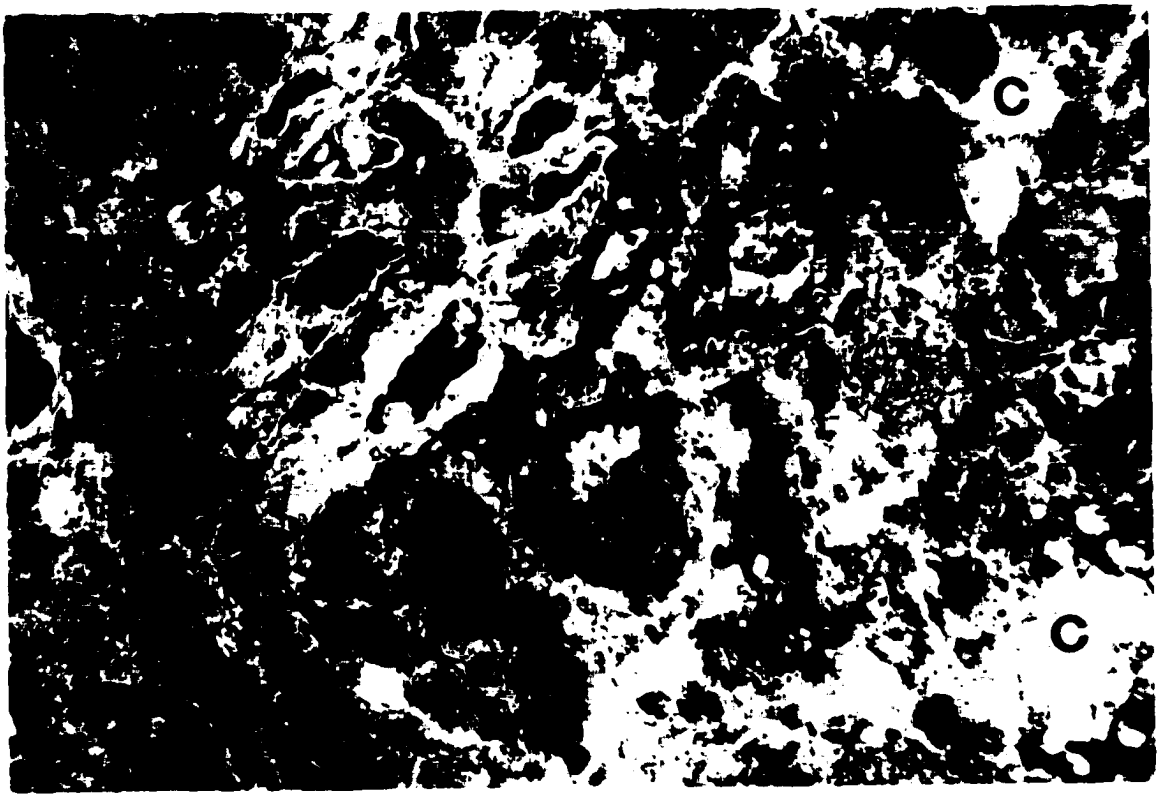

Figure 4.10. Intensely altered southern volcaniclastic kimberlite. Note the numerous carbonate-rich pools (C) throughout the groundmass (F.O.V. 6.0 mm).

matrix. Individual units are identified by their dominated clast-types. Kimberlite constituents include rare juvenile lapilli, single grains of altered olivine and phlogopite macrocrysts and mantle xenocrysts (garnet, ilmenite, and clinopyroxene). BHB has only been encountered at depth and their distribution and origin remains uncertain (Field *et al.* 1997; Kilham *et al.* 1998).

4.2.2.1.6. Diatreme Facies Kimberlite

Diatreme facies kimberlite intersected within the southern lobe occurs in sharp contact with overlying SVK or BHB. This tuffisitic kimberlite breccia, in contrast to above volcaniclastic kimberlite, is dark and fresh. It consists of lithic fragments (basalt, granite-gneiss, mudstone), single crystals of macrocrystal olivine and abundant pelletal lapilli (both of the crystalline and microcrystalline varieties) set in a matrix of serpentine and abundant microlitic diopside. Considerable interstitial carbonate may be present and in some cases secondary serpentine and clay has obliterated the microlitic diopside. Petrographic variations within the TKB suggest that more than one phase of diatreme facies kimberlite is present within the southern lobe uncertain (Field *et al.* 1997; Kilham *et al.* 1998).

Along the northern and western edges of the southern lobe diatreme, complex heterolithic breccias are encountered that are characterized by xenolithic fragments derived from basement rocks and the basal part of the Karoo Formation *(i.e.* Tlapana Formation). Minor kimberlite material is present within the matrices of these breccias (Field *et al.* 1997; Kilham *et al.* 1998). A floating reef of BHB occurs at depth with the diatreme facies kimberlite of the southern lobe.

4.2.2.1.7. Hypabyssal Facies Kimberlite

Hypabyssal kimberlite, which occurs at depth within the southern lobe, is macrocrystal kimberlite with a slight segregationary-texture. Two mineralogical varieties have been identified: spinel perovskite phlogopite monticellite kimberlite and apatite

perovskite spinel monticellite kimberlite. Both are archetypal kimberlites (Field *et al.* 1997; Kilham *et al.* 1998).

Mining exposed a hypabyssal kimberlite sill within the southwestern corner of the southern lobe associated with the talus grain flow deposits of the crater. It occurs as a steeply dipping sheet, paralleling the volcaniclastic kimberlite in which it is hosted. This sill is a segregation-textured macrocrystal kimberlite consisting of spinel, phlogopite and relict monticellite (Field *et al.* 1997; Kilham *et al.* 1998). Mining activities have since removed this sill.

4.2.2.2. Emplacement of the Southern Lobe

The southern lobe is smaller in diameter and surface area than the northern lobe and presumably represents a less explosive event. In contrast to the northern lobe, whose crater was infilled primarily by syn-eruptive primary pyroclastic activity, scant evidence exists to support to presence of primary pyroclastic kimberlite and instead the upper portions of the southern lobe was infilled primarily by post-eruptive resedimentation processes.

On the northern and western sides of the diatreme of the southern lobe a precursor breccia body has been identified. The clasts within it are locally derived and displaced slightly downward; clasts from higher stratigraphic levels are absent. Field and Scott Smith (1998) and Field *et al.* (1997) and Kilham *et al.* (1998) feel that this feature can be easily explained by the "embryonic pipe" stage within the Clement (1979, 1982; Clement and Reid 1989) model (refer to Section 4.3). Scott Smith (1998) and Field *et al.* (1997) and Kilham *et al.* (1998) feel that the southern lobe diatreme was emplaced as described within the Clement model (1979, 1982; Clement and Reid 1989) and provides further validation of this model.

4.3. EMPLACEMENT MODEL FOR THE A/K1 KIMBERLITE

The emplacement model, outlined below is taken from Field *et al.* (1997) and Kilham *et al.* (1998). It accounts for the features present within the A/K1 kimberlite and follows the "embryonic pipe" model of Clement and Reid (1989) and Clement (1979, 1982). The model is illustrated in Figure 4.11. Clearly, the hydrovolcanic model of kimberlite emplacement can be as easily applied to the A/K1 diatreme formation (Section 4.4). The outline model, presented below, does however, serve to shed light on the post-breakthrough crater infill processes which occur within kimberlite vents.

Stage 1: The intrusion of archetypal kimberlite magma. Early stage magma batches serve to seal fractures within the country rock.

Stage 2: The development of an embryonic pipe following the model of Clement and Reid (1989) and Clement (1979, 1982).

Stage 3: Explosive breakthrough resulting from a gradual build up of gas pressure under the competent cap rock provided by the Stromberg basalts.

Stage 4: Formation of a small, unstable eruption column with intermittent collapse episodes, producing small pyroclastic flows within the crater.

Stage 5: Concomitant emplacement of the northern diatreme by short-lived fluidization and draw down during eruption.

Stage 6: Embryonic pipe development for the southern diatreme.

Stage 7: Explosive breakthrough forming the southern crater. This larger crater cuts the northern diatreme. A large, poorly sorted tuff ring is deposited around the crater rim.

Stage 8: Concomitant emplacement of southern diatreme by fluidization processes.

Stage 9: Spalling of exposed wallrock fragments, which collect of the crater floor to form the BHB. Slumping of exposed walls of NPK to form the lower zone of the SVK, which occurs interleaved with the BHB.

Stage 10: Collapse of a large portion of relatively unaltered tuff cone and deposition largely by mass flow processes, thus forming the central SVK. These deposits fill up the crater to a level corresponding to the middle of the Mosolotsane formation in the wall rock cliffs, thus preventing further spalling of lower Karoo fragments.

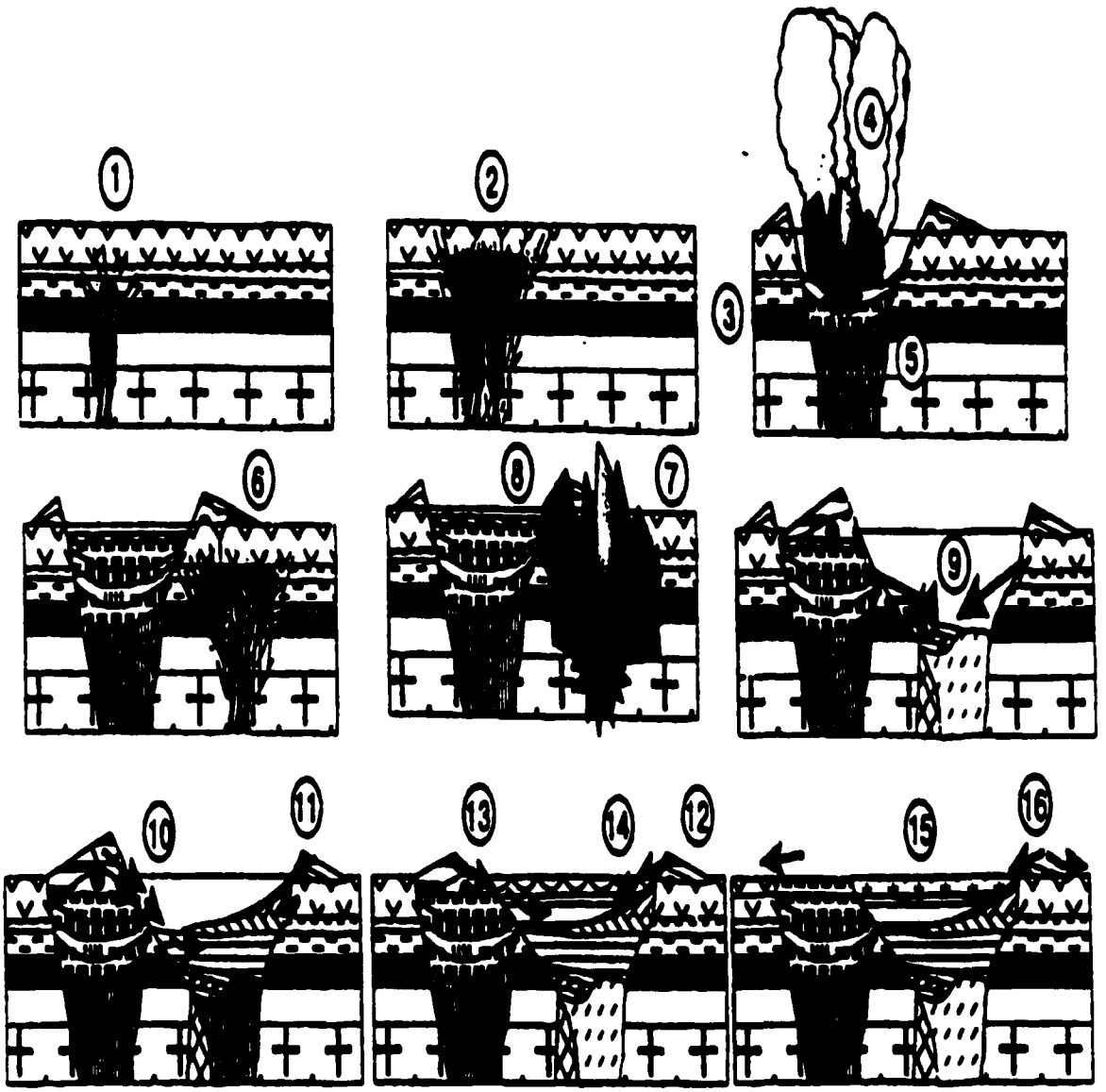

Figure 4.11. A schematic representation of the emplacement for the Orapa A/K1 kimberlite. The circled numbers refer to the stages of emplacement as described in section 4.3. The symbols used to represent wall rock and kimberlite varieties is the same used in Figures 4.3 and 4.4 (Field *et al.* 1997).

Stage 11: Spalling of basalt to form extensive talus breccias. Spalling eventually leads to undercutting of the surrounding tuff cone and the establishment of scree slopes along which fragments from the tuff cone move by grain flow mechanisms. These processes establish six individual talus fans around the crater rim.

Stage 12: A further episode of collapse of more weathered tuff cone material leads to the deposition of the upper SVK.

Stage 13: An extended quiescent period in which the remaining tuff cone materials become highly weathered (oxidized), a crater lake is established in an off-centre position and continued, slow talus fan development occurs.

Stage 14: Periodic collapse of the tuff cone and wall rock producing sub-aqueous debris flows which form boulder beds, debris flow breccias and produce fines for incorporation in shale beds.

Stage 15: A gradual reduction in collapse episodes resulting in an increase in shale deposition and a reduction in debris flow events.

Stage 16: Gradual erosion of the tuff cone and later possibly part of the crater infill itself.

The southern lobe crater appears to represent a long-lived opening that was gradually filled with secondary post-eruption infill processes. The infilling of the upper part of the northern diatreme by primary syn-eruptive processes is in direct contrast to the southern lobe. Field and Scott Smith (1998) suggest that the emplacement processes involved in the emplacement of the northern and southern lobes of the AK/1 kimberlite represents two extremes of the Clement (1979, 1982; Clement and Reid 1989) diatreme emplacement model which is driven by juvenile gases. The contrast in size and shape of the two lobes is envisioned to be the result of restricted post-breakthrough fluidization process with less modification of the initial crater. The southern lobe, whose diatreme is smaller, is predicted to have been emplaced by a less explosive event than the larger northern diatreme.

4.4. THE SOUTHERN AFRICAN KIMBERLITE EMPLACEMENT MODEL

Clement (1979, 1982) recognized that no single process can account for the geological diversity and petrographic characteristics observed within a kimberlite vent. Clement (1979, 1982) further proposed a model in which kimberlite root zones are considered to represent "embryonic pipes" that are subsequently modified by post-surface breakthrough fluidization in to diatremes. Great emphasis is placed upon the occurrence of contact, permeation and intrusion breccias, blind extensions roofed by breccias, and structural control of intrusion. Root zones are believed to develop as a result of subsurface processes which include hydraulic fracturing and wedging, magmatic stoping, intermittent explosive and/or implosive brecciation, spalling, slumping and rock bursting.

Clement (1979, 1982; in Mitchell 1986) and Clement and Reid (1989) believe kimberlite dykes rising from depth develop a precursor volatile phase due to CO_2 exsolution. The CO_2 is liberated due to the pressure decrease with magma ascent. The path of the advancing magma is controlled by pre-existing structures. High pressure causes the volatile phase to penetrate fractures and joints in the wall rocks (hydraulic ramming) above and at the margins of the intrusive kimberlite magma. Implosion and shattering of the country rock occurs as a result of gas expansion. The expansion is controlled by the fluctuations in magma flow rate, which leads to pressure reduction. Wall rock spalling and burst may also occur. This advancing front of contact brecciation is followed by magma, which penetrates the breccia, and any fractures or joints present within the wall rock. Intrusion breccias are formed and wall rocks are wedged into the conduit. With ascent, magma will change in character from fissure filling to root zone development. This may be due to an increase in volatile exsolution as pressure falls with ascent and the intersection of the kimberlite dyke with a fracture within the wall rock which can be exploited or which contains groundwater. Once formed the initial root zone "bud" will self-propagate and will act as a focus for ensuing activity. During root zone development, successive cycles of shattering and erosion caused by the surging and churning of the magma, in effect, permits the magma to etch upward through the country rock.

The production of complex root zones and "embryonic pipes" is the result of the influx of several batches of kimberlite magma. Earlier buds (incipient diatremes) are cut off as blind extensions or cored out by later intrusions (refer to Figure 4.12). This process is thought to continue until the magma reaches a level where explosive surface-breakthrough is possible (300-400 m) and may be promoted by magma-groundwater interaction. Subsequent diatreme formation is a result of post-surface breakthrough modifications of the basal portions of the crater zone and the upper levels of the root zone (refer to Figure 4.12). Breakthrough results in pressure release; the magma in the root zone is envisioned to de-gas rapidly and to form a vapour-liquid-solid fluidized system. The vapour exsolution surface is thought to migrate rapidly downward as a consequence of expansion and further pressure release. During this period of fluidization, pre-existing root zone hypabyssal kimberlite, high level contact breccias and degassing magma are thoroughly mixed. Lack of rounding of the country rock clasts indicates that the fluidized system only briefly existed. Vent enlargement by plucking of joint bounded blocks may occur during this stage of diatreme development, however, no widening of the gas-tuff fluxion is envisaged. Following degassing, activity ceases and during the waning stages of vent evolution activity is restricted to the emplacement of root zone intrusions. Repetition of the entire process will produce diatremes with several distinct varieties of diatreme facies kimberlite and highly complex root zones.

Clement's (1979, 1982) and Clement and Reid's (1989) hypothesis accounts for most of the features of kimberlite vents, particularly the complex root zones which cannot be fully explained by fluidization or hydrovolcanism. Evidence exists within kimberlite diatreme of the existence of an upper level root zone which was subsequently destroyed by diatreme formation (*i.e.* brecciated mega-xenoliths, high level contact breccias) and Clement's (1979, 1982; Clement and Reid 1989) model has fully accounted for this phenomenon. However, significant drawbacks exist with this model, particularly the proposal that fluidization plays a major role in the final stages of diatreme formation (Mitchell 1986). This process is introduced by Clement (1979, 1982) and Clement and Reid (1989) to account for the mixing of autoliths and xenolithic material, the formation

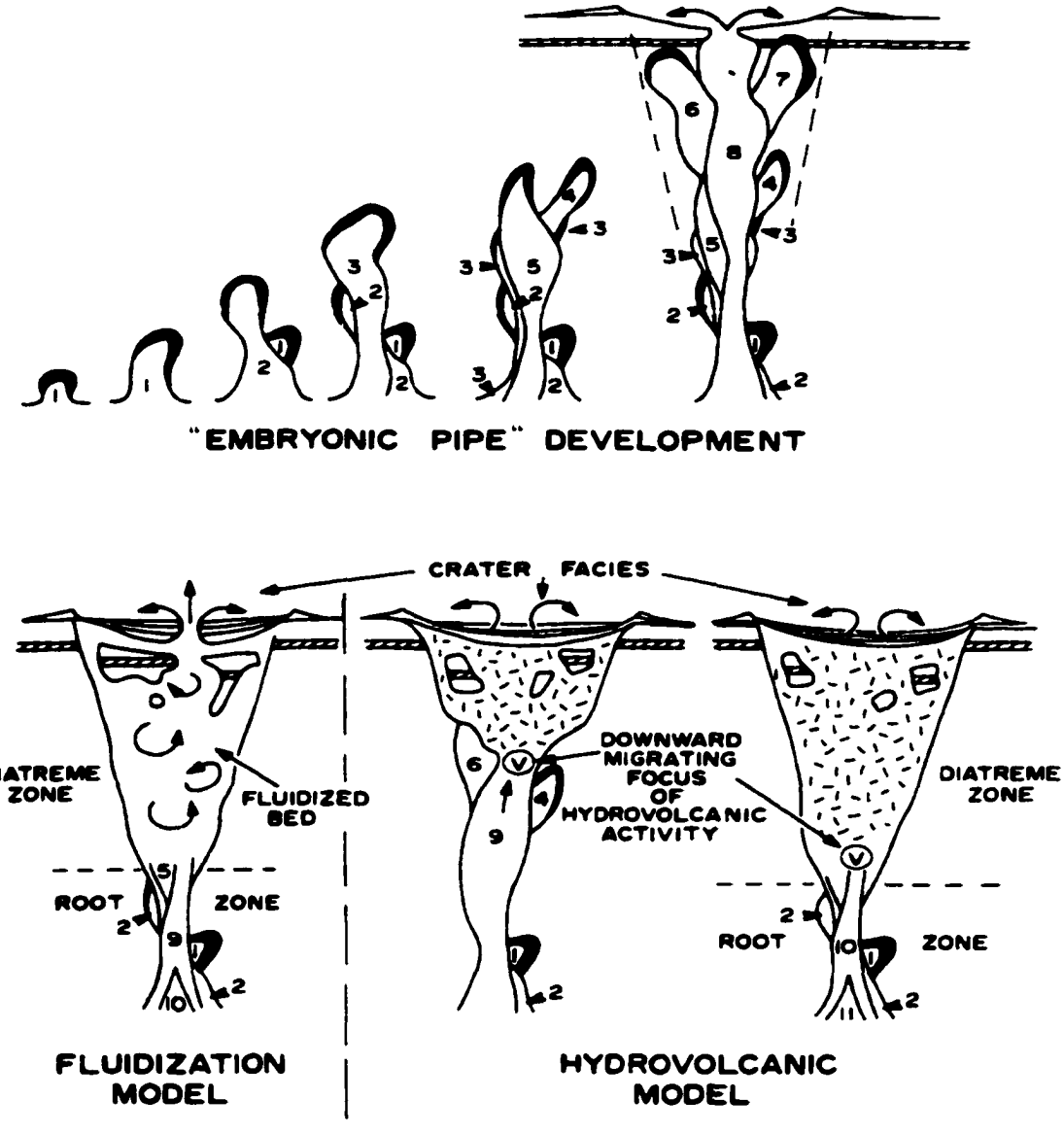

Figure 4.12. Stages in diatreme development as envisioned by Clement (1982). The period of "embryonic pipe" development is followed by either fluidization (Clement 1982) or hydrovolcanism (Mitchell 1986). Figure taken from Mitchell (1986).

and presence of pelletal lapilli and the significant displacement of xenolithic material within the diatreme.

Mitchell (1986) notes numerous persuasive arguments against Clement's (1979, 1982; Clement and Reid 1989) fluidization model. These include the absence of tuffisitization features within the kimberlite diatreme, problems of generating sufficient volumes of volatiles to support a 1-2 km long fluidized system and the unlikelihood that decompression and explosive degassing of the magma will result in the formation of a bubbling fluidized bed within the diatreme. Moreover, Lorenz (1979) suggests the low viscosity magma may inhibit explosive devolitization.

Mitchell (1986) discusses an alternative emplacement model for southern African kimberlites which combines hypotheses from both Clement's (1979, 1982; Clement and Reid 1989) fluidization model and Lorenz's (1973, 1975, 1979, 1984, 1985) hydrovolcanic model of diatreme formation.

Mitchell (1986) suggests that the geology and morphology of the crater zone of a kimberlite is consistent with a hydrovolcanic origin and it is therefore appropriate to suggest that such processes operated in diatreme formation (refer to Figure 4.12). These processes can account for the formation of pelletal lapilli, xenolith mixing and lack of thermal metamorphism without recourse to fluidization processes.

Within Mitchell's (1986) hydrovolcanic "embryonic pipe" model, root zone development is considered to occur as outlined by Clement (1979, 1982) and Clement and Reid (1989), with the role of hydrovolcanism becoming more important as the "embryonic pipe" advances towards the surface where it can encounter groundwater. At high levels hydrovolcanic activity may be interspersed with subsurface brecciation. At shallow levels load pressures decrease sufficiently to allow formation of hydrovolcanic explosion craters or maars, and with continuing activity leading to the development of tuff rings or cones. The maar will act as a focus for the accumulation of groundwater and this water will seep into the underlying "embryonic pipe" and encounter new batches of magma. The explosive interaction between the water and the magma will lead to the formation of new breccias and will disrupt pre-existing ones.

Mitchell (1986) suggests that pelletal lapilli, characteristic of diatreme facies tuffisitic kimberlite breccia, are produced by fuel-coolant interactions wherever magma and water come into contact. Residual coolant condenses as the interclast matrix. Mega-xenoliths are thought to be the remnants of the roofs of root zone buds or down-slumped wall rocks.

After breakthrough, repeated hydrovolcanic explosions will modify the "embryonic pipe". This process results in well-mixed breccias. Declining magmatic activity (which is indicated by the lack of formation of lava pools or central conduit plugs) induces the downward migration (refer to Figure 4.12) of the focus of hydrovolcanic explosion resulting in the destruction of the upper levels of the root zone, incorporating autoliths of the hypabyssal kimberlite into the diatreme. Slumping and mixing is thought to be responsible for the downward creep of high-level wall rock fragments.

The balance between the water supply and magma will determine the axial lengths of the diatremes; diatreme formation and modification will cease once impermeable layers are reached. The repetition of the magmatic cycle will result in the formation of highly complex diatreme and root zones. After magmatic activity ceases, the resultant diatreme infill will consists of highly porous breccias. These breccias will be subject to slumping and the circulation of groundwater resulting in extensive secondary alteration.

The study of the Orapa A/K1 kimberlite by Field *et al.* (1997) and Kilham *et al.* (1998) provides further insight into the near surface syn- and post-eruptive processes, which operate during kimberlite emplacement. Contemporaneous with break through and "embryonic pipe" modification, juvenile and xenolithic material is ejected from the crater and forms an eruption cloud. The kimberlite crater will be infilled with pyroclastic fragments, which may be well-to-poorly bedded. Depressions within the crater are infilled by post-eruption resedimentation processes; subsequent resedimented volcaniclastic kimberlite will be further deposited on top of the crater (Field and Scott Smith 1998).

It is evident that no single process is responsible for kimberlite formation and southern African (and southern African-type) kimberlite vents are likely secondary structures formed by the subsequent modification of the underlying root zone (or "embryonic pipe") by fluidization (Clement 1979, 1982; Clement and Reid 1989) or downward migrating hydrovolcanism (Mitchell 1986).

CHAPTER 5. FORT À LA CORNE KIMBERLITES

5.1. INTRODUCTION

Kimberlites were first discovered in Saskatchewan in 1987 at Sturgeon Lake. Here were found two glacially-transported megablocks of Cretaceous volcaniclastic kimberlite of unique character which did not conform to the southern African "classic" diatreme model (Scott Smith 1995, Scott Smith *et al.* 1996). The volcaniclastic kimberlite contained amoeboid-shaped, glassy, vesicular juvenile constituents that had not been previously recognized in kimberlite. The nature of these clasts showed that they were extrusively-formed pyroclastic juvenile lapilli. These features together with the presence of common size-grading and plane parallel bedding suggests that these bodies were deposited by primary subaerial pyroclastic airfall processes derived from a distinctly different style of eruption to that which is suggested to occur in the diatreme-bearing kimberlite vents of southern Africa (Field and Scott Smith 1998).

Subsequent to the discovery at Sturgeon Lake, a large Cretaceous (98-94 Ma) kimberlite field in the vicinity of Fort à la Corne, 80 km east of Sturgeon Lake, was discovered (Lehnert-Thiel *et al.* 1992, Figure 5.1). The Fort à la Corne kimberlites are composed of volcaniclastic kimberlite similar to that observed in the Sturgeon Lake megablocks. The Fort à la Corne bodies are shallow, saucer-to-champagne glass-shaped vents, with near-surface diameters of up to 1300 m and depths up to 200 m below the present-day sub-glacial surface (Field and Scott Smith 1998). No evidence of diatreme or root zone formation has been found within these bodies and no associated diatreme or hypabyssal facies kimberlite has been intersected at Fort à la Corne. Hence, the vent shape and the infill within the Saskatchewan kimberlites clearly demonstrates that the classic southern African diatreme emplacement processes (refer to Section 4.4) did not operate within the Saskatchewan kimberlites (Field and Scott Smith 1998).

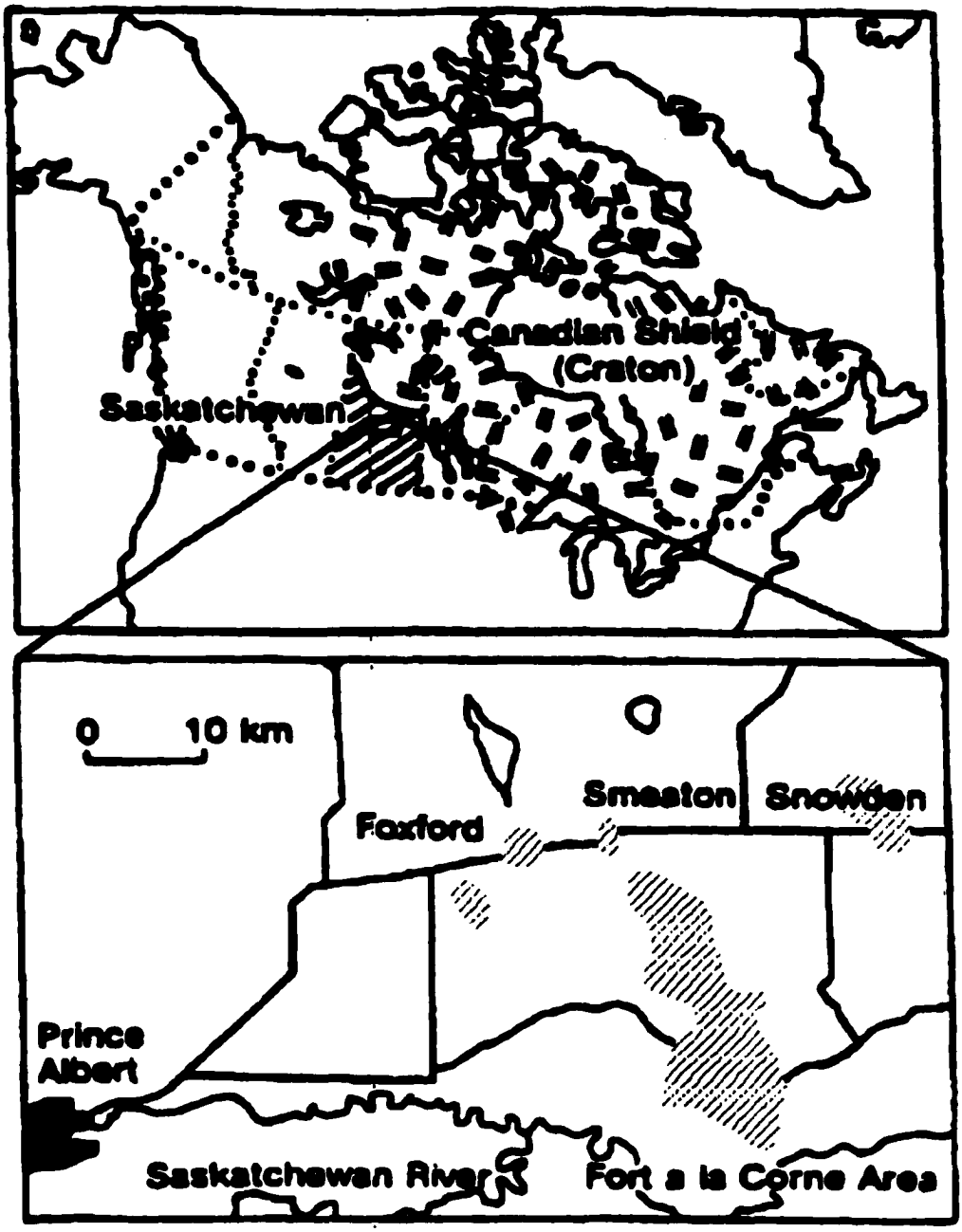

Figure 5.1. Map of Saskatchewan showing locations of major kimberlite fields. These kimberlites intrude Cretaceous sediments and Archean basement rock of the Canadian Shield Shaded zones indicate aeromagnetic anomalies produced by the kimberlite intrusions (after Nixon and Leahy 1997).

5.2. GEOLOGY OF THE FORT À LA CORNE KIMBERLITES

5.2.1. Geological Setting

The Fort à la Corne kimberlites, which have been stratigraphically constrained as being late Cretaceous in age, were emplaced into poorly consolidated Cretaceous sediments. The sediments comprise ±100m of clays, silts and sandstone of the Mannville Formation (±119-100 Ma), formed in coastal marine, subaerial flood plain and/or lacustrine environments, and ±100m of marine shales of the Ashville Formation (±100-91 Ma, Scott Smith *et al.* 1995). The Ashville shales were deposited towards the edge of the Western Interior Seaway. The Mannville structurally overlies 400m of Paleozoic sediments that are dominated by indurated carbonate, which structurally overlies the Precambrian basement. The Cretaceous sediments into which the kimberlites have been emplaced correlate with regional stratigraphy indicating they are *in situ* and undisturbed (Scott Smith *et al.* 1995).

5.2.2. Petrographic Features

Thin sections of ten drill core samples of kimberlite were examined from the Fort à la Corne area. Each of the samples was obtained from different kimberlite intrusions. A list of the various thin sections and their corresponding textural classification is given in Table 5.1. The nature of the alteration of individual samples is variable. Many samples are now composed of mainly serpentine, calcite and secondary magnetite; each of which occurs in various proportions in different samples.

Four types different types of fragmental volcaniclastic kimberlite are discernable within these vents: matrix-supported, non-welded lapilli tuff; clast-supported welded lapilli tuff; olivine crystal tuff; volcaniclastic kimberlite. Non-welded lapilli tuffs appear to be the most common unit.

Table 5.1. Samples Obtained from the Fort à la Corne Area.

Sample Number	Textural Classification
H3	Olivine crystal tuff and Non-welded matrix-supported lapilli tuff
H14	Non-welded matrix-supported lapilli tuff
H19	Volcaniclastic kimberlite
H20	Volcaniclastic kimberlite
H32	Welded clast-supported lapilli tuff
H33	Non-welded matrix-supported lapilli tuff
H41	Non-welded matrix-supported lapilli tuff
H50	Non-welded matrix-supported lapilli tuff
V89	Olivine crystal tuff
V102	Non-welded matrix-supported lapilli tuff

5.2.2.1. Matrix-Supported Non-Welded Lapilli Tuff

These samples are fragmental rocks composed of single crystals of macrocrystal olivine, less common pale-brown phlogopite, relatively common xenocrystal ilmenite and rare, kelphytized garnets. Macrocrystal olivines occur as relatively large (less than 8 mm. commonly less than 2 mm) rounded, commonly broken crystals which are partially-to-completely replaced by serpentine, magnetite and minor calcite. Many crystals are nearly entirely replaced by secondary magnetite. Most olivine crystals are a part of the macrocrystal suite. Larger subhedral phenocrysts are not uncommon. Phlogopite occurs

as sub-rounded, commonly distorted crystals that have been replaced by serpentine and chlorite along cleavage planes.

These rocks are characterized by the presence of abundant kimberlite fragments (generally less than 2 mm, maybe as large as 8 mm, Figure 5.2). The small, commonly turbid fragments are generally highly irregular in outline, commonly exhibiting embayed and curvilinear margins and are distinctly amoeboid in habit. Some smaller clasts appear to be somewhat rounded. These medium-to-dark brown fragments are composed of abundant euhedral-to-subhedral, slightly rounded microphenocrystal groundmass olivines. These grains are invariably replaced by a combination of pale yellow serpophite and magnetite. Larger phenocrystal olivines may have small relict cores. Olivines, together with phlogopite, subhedral-to-euhedral groundmass spinels, minor perovskite, apatite rutile and primary calcite are set in a mesostasis of calcite and serpentine. No evidence of monticellite was observed. The fragments may contain at their core a large, rounded, altered macrocrystal olivine, or less commonly, phlogopite or xenocrystal ilmenite. Small (<0.5 mm), fragmental garnets, with kelphytic rims, are rare. Broken crystals along the margins of some of the fragments indicate that they were solid upon incorporation into their current hosts and are in fact autoliths (refer to Figure 5.2). Many larger fragments have thin margins that are slightly darker in colour than their cores. These margins seem to contain fewer microphenocrystal olivines, which are tangentially oriented about the margins of the clasts, but are otherwise texturally and mineralogically identical to the kimberlite, which they mantle and may represent. Fragments, with identical constituents to the above are set in a clearer base composed of pale green isotropic serpentine. Some composite fragments, containing a darker, vesiculated core with a pale green, clearer margins do occur within these units.

Smaller, ash-sized fragments occur in juxtaposition to the above. These irregular-curvilinear fragments are essentially identical to the larger fragments but are composed of fewer olivine microphenocrysts, usually pseudomorphed and xenocrystal garnet in a groundmass of spinels, secondary magnetite and minor phlogopite in a mesostasis of cryptocrystalline serpentine and calcite (Figure 5.3).

Figure 5.2. Matrix-supported non-welded lapilli tuff with juvenile lapilli of various sizes (L), one unmantled garnet (G) in a calcite-serpentine cement. Some fragments contain broken crystal fragments at their margins indicating they are autoliths (F.O.V. 6.0 mm).

Figure 5.3. Small, irregular-curvilinear, non-vesiculated juvenile fragments within a matrix-supported non-welded lapilli tuff (F.O.V. 1.0 mm).

The hallmark characteristic of these fragments is the presence of spherical, vesicle-like structures that are now infilled with fine-grained secondary calcite and minor serpentine, indicating that these kimberlite fragments are *bona fide* juvenile lapilli (Figure 5.4). Larger, amoeboid-shaped structures filled with calcite and commonly lined with fine-grained serpentine occur in some fragments.

Within these units, single crystals are generally less common than the kimberlite fragments, but the reverse may also be true, indicating sorting occurs within this kimberlite. Xenolithic material is not common and occurs as separate fragments. One mica-bearing, intensely altered (by carbonate and chlorite) basement fragments was observed as a core for a kimberlite fragment. Kimberlitic fragments do not appear to be abraded.

The interclast matrix, when fresh, is composed of predominantly calcite as a coarse-grained mosaic, whereas pale yellow serpentine is the dominant cement in more intensely altered samples.

These units are generally matrix supported, although degree of packing does vary. Flattening along interfaces between juvenile lapilli that are in contact does occur, suggesting these beds are likely primary pyroclastic kimberlites and have not been subjected to resedimentation processes.

5.2.2.2. Clast-Supported Welded Lapilli Tuffs

These units, which are far less common than the above are clast-supported volcaniclastic kimberlites containing abundant, welded, microporphyritic juvenile fragments and rare, rounded macrocrystal olivine pseudomorphs (up to 10 mm), which may or may not be mantled by kimberlite. Smaller, mantle-free phenocrystal olivines are also common. Olivine crystals are replaced by a combination of calcite, serpentine and magnetite.

The highly irregular-to-amoeboid kimberlite fragments are ash-to-lapilli in size and are composed of abundant subhedral-to-euhedral microphenocrystal olivine. Colourless calcite, pale yellow serpentine and magnetite replace these crystals. Smaller

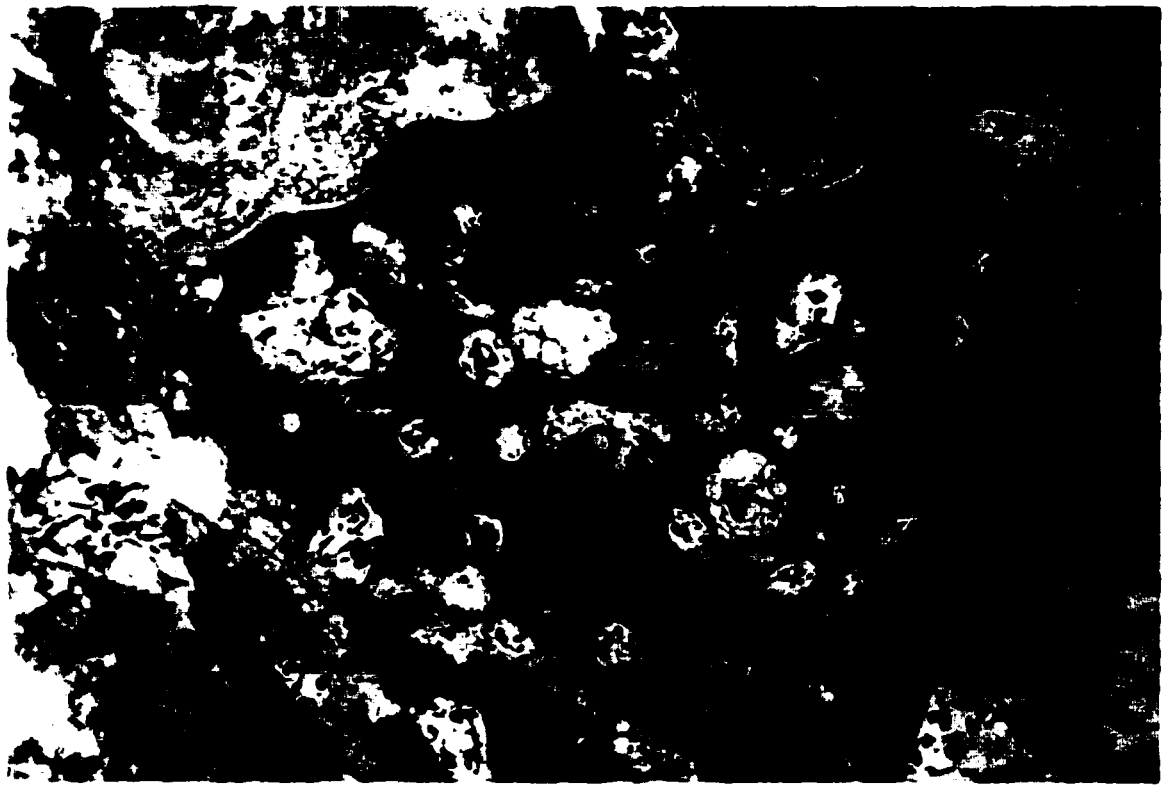

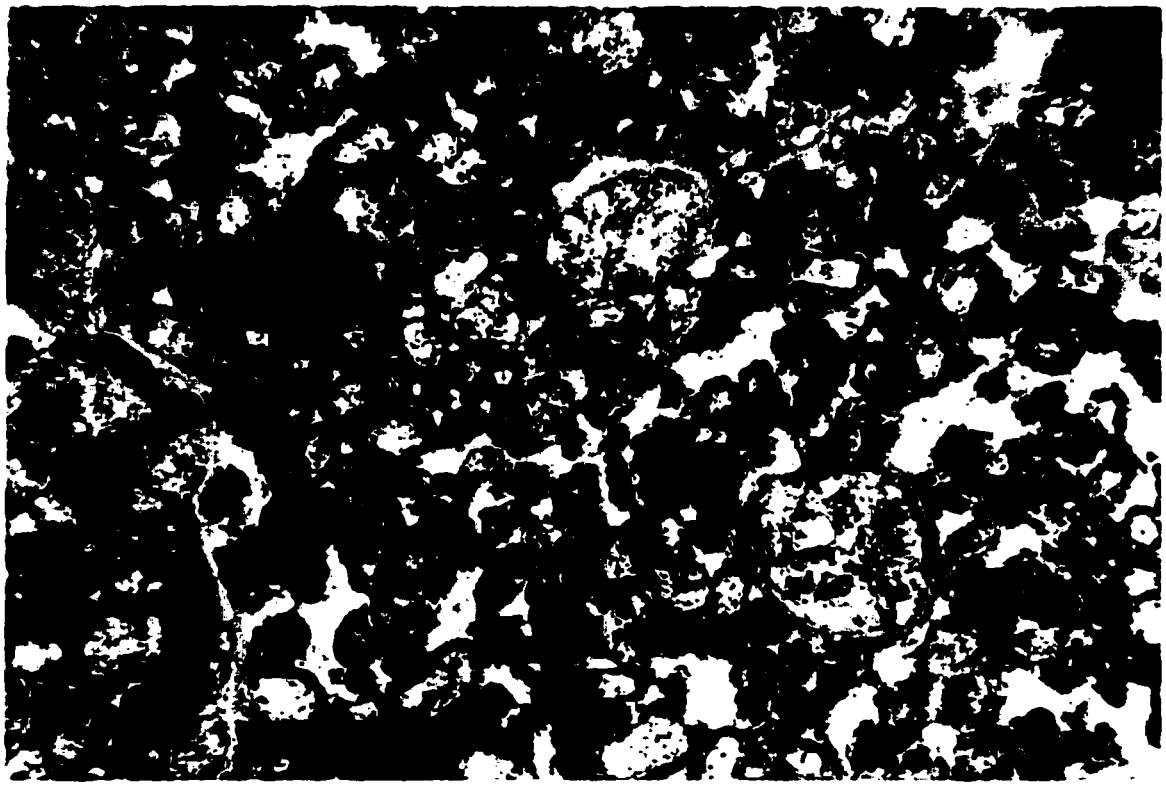

Reproduced with permission of the copyright owner. Further reproduction prohibited without permission.

Figure 5.4. Vesiculated juvenile lapillus. It has an irregular-curvilinear outline and is comprised of altered microphenocrystal olivine (O) and abundant fine-grained opaque spinels. It is characterized by spherical-to-subspherical calcite-filled vesicles (V) (F.O.V. 1.0 mm).

Figure 5.5. Welded lapilli tuff with abundant altered microphenocrystal olivine. Note the clast-supported texture with obvious welding and molding of the juvenile fragments (F.O.V. 6.0 mm).

crystals may be entirely replaced by relatively pure, secondary magnetite. The olivine crystals are set in a groundmass containing partially resorbed perovskite, small crystals of ilmenite, spinel and minor apatite in a "sugary"-granular matrix of serpentine, calcite and serpentinized monticellite. A thin, pale green rim of amorphous serpophite mantles many of these fragments.

These clasts, which are clearly juvenile in origin, differ markedly from the juvenile lapilli described in the non-welded lapilli tuffs in that they contain no vesicles, *i.e.*, their formations is a result of a different mechanism. No evidence of sorting is apparent on a microscopic level. Plastic deformation, good molding and flattening as well as amoeboid-shaped welded constituents indicates a higher temperature of deposition (Figure 5.5). Elongated constituents do not show a preferred orientation however the significant reduction of pore space when compared to the non-welded units suggests mechanical compaction.

The welded fragments are cemented together with medium-grained, interlocking crystals of calcite. This cement is undoubtedly secondary.

5.2.2.3. Olivine Crystal Tuffs

When compared to the above lapilli tuffs, these units are finer-grained and dominated by clasts of olivine crystals with subordinate kimberlite juvenile lapilli (Figures 5.6 and 5.7). The olivine crystal tuffs are dominated by small (<0.5 mm) microphenocrystal olivines surrounded by thin mantles of brown-to-pale green serpentine. Kimberlite juvenile lapilli are fairly uncommon and occur as relatively large (1-4 mm) non-vesiculated amoeboid-shaped fragments. Large, altered, rounded macrocrysts are relatively uncommon within these crystal-rich units. Single crystals of altered olivine macrocrysts and relatively fresh phlogopite do occur. One fragmented garnet with a kelphytic rim and a rounded xenocrystal ilmenite were noted.

The above is cemented with, when fresh, with a mosaic of relatively fine-grained calcite. In more altered units, serpentine replaces much of the interstitial calcite cement.

Rare crustal xenoliths occur within these beds.

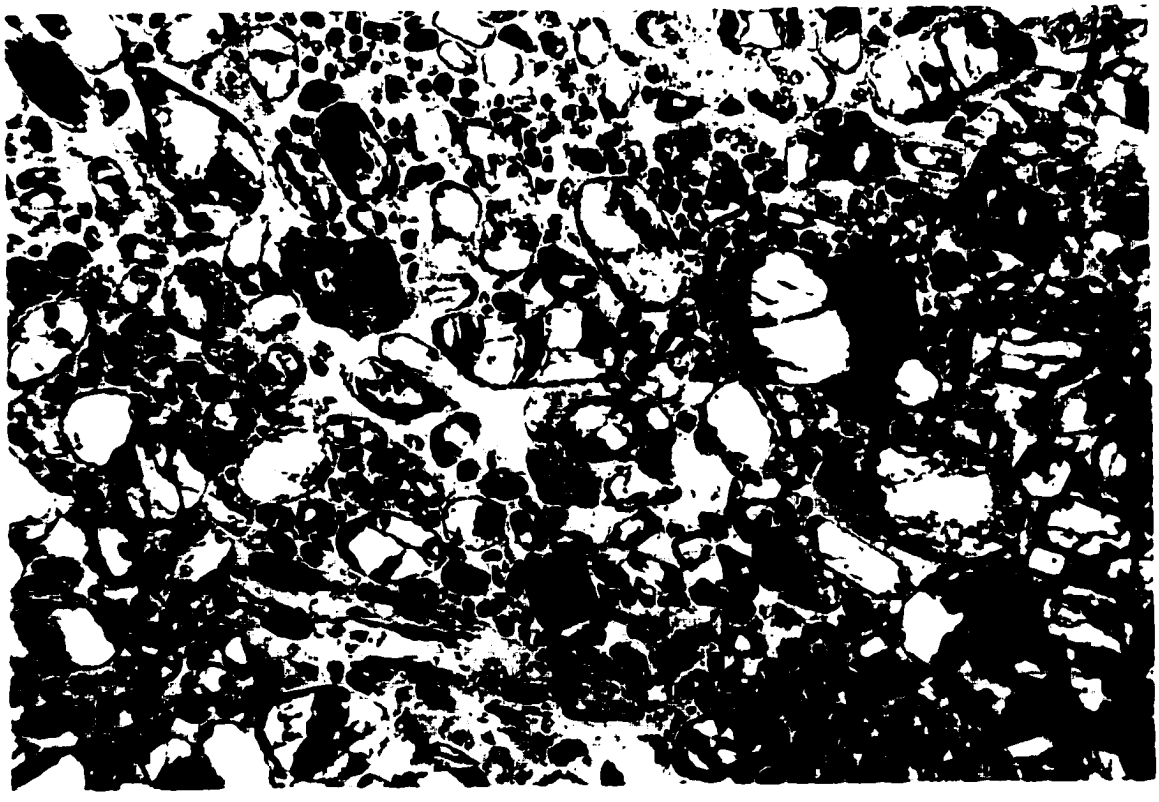

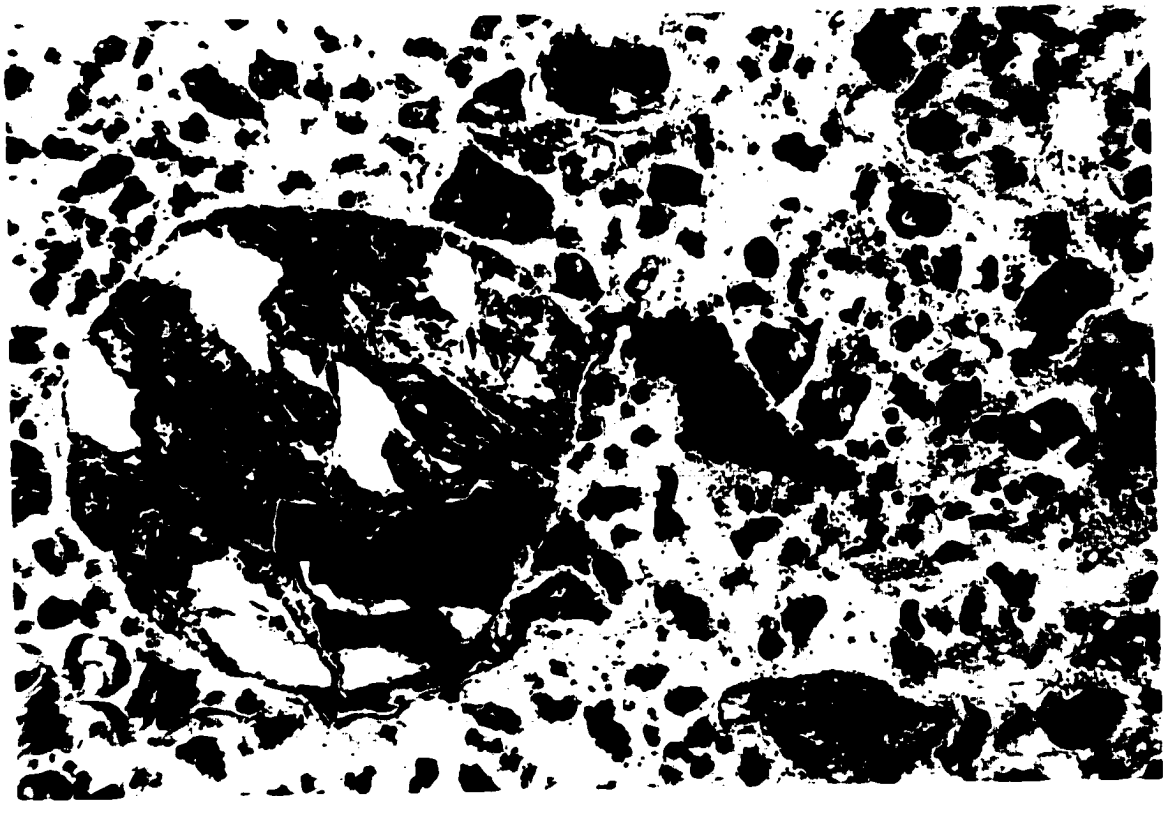

Figure 5.6. Relatively fresh olivine crystal tuff dominated by partially serpentinized primary olivines with thin yellow mantles of serpentine. Note the small juvenile fragments (F.O.V. 6.0 mm).

Figure 5.7. Olivine crystal tuff with small serpentinized microphenocrystal olivines and larger rounded macrocrystal olivines mantled with yellow-green serpentine and cemented with calcite (F.O.V. 6.0 mm).

5.2.2.4. Volcaniclastic Kimberlite

These matrix-supported beds contain common, but not abundant kimberlite juvenile lapilli as described in the non-welded lapilli tuffs as well as composite lapilli. All lapilli are microporphyritic fragments composed of abundant altered microphenocrystal olivine, replaced by calcite, magnetite and less commonly serpentine and minor mica set in a groundmass of spinel, perovskite, ilmenite and apatite. Both vesiculated and non-vesiculated juvenile lapilli are found. Common subspherical-to-amoeboid bodies are filled with cryptocrystalline (quenched?) brown serpentine. Most appear to resemble vesicles however the larger, amoeboid-shaped bodies, which contain subhedral-to-euhedral grains of calcite, resemble segregations found in hypabyssal kimberlite. Numerous lapilli appear to be composite structures, containing up to three distinct types of kimberlite (Figure 5.8). The inner cores are commonly composed of a dark brown-green microporphyritic kimberlite which is mantled by a lighter coloured (pale green-yellow) kimberlite which appears nearly identical in mineralogy and texture to the core. The contact between the two varieties of kimberlite is distinct in thin section. Many of these composite structures are mantled by a fine-grained, medium-brown, turbid kimberlite ash, which is essentially devoid of microphenocrystal olivine. The contact is sharp and this outer ash coating is irregular in thickness. Lapilli within these beds are difficult to detect, as they are similar in colour, mineralogy and texture of the matrix in which they are set (Figure 5.9). Some kimberlite fragments contain broken crystals along their margins indicating that they are autoliths.

Single crystals of rounded, altered olivine macrocrysts, smaller phenocrystal and microphenocrystal olivine, macrocrystal mica, kelphytized garnet, rounded ilmenite and rounded mantle and crustal xenoliths are also common within these beds. These may or may not be mantled by kimberlite. Many grains may be broken and subangular.

The groundmass consists of abundant subhedral-to-euhedral spinels, mica, minor perovskite and apatite set in a groundmass mesostasis of calcite and serpentine. Primary groundmass calcite is strewn throughout the groundmass.

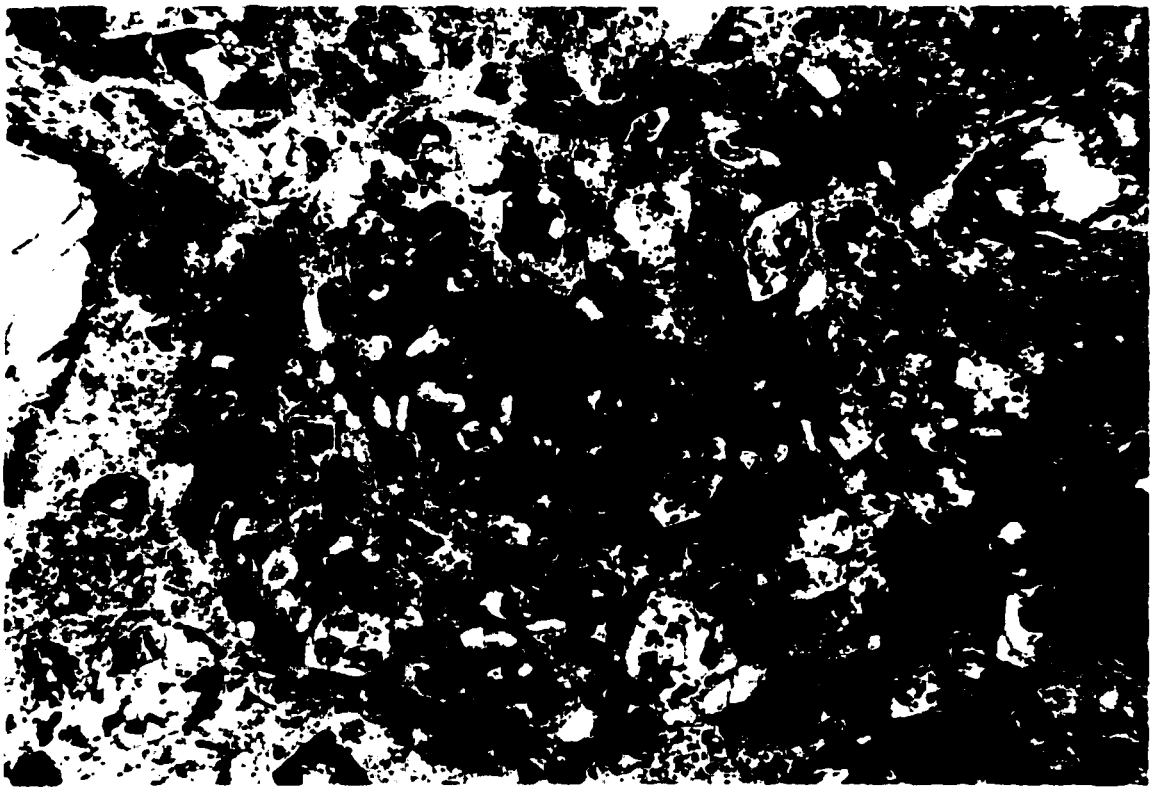

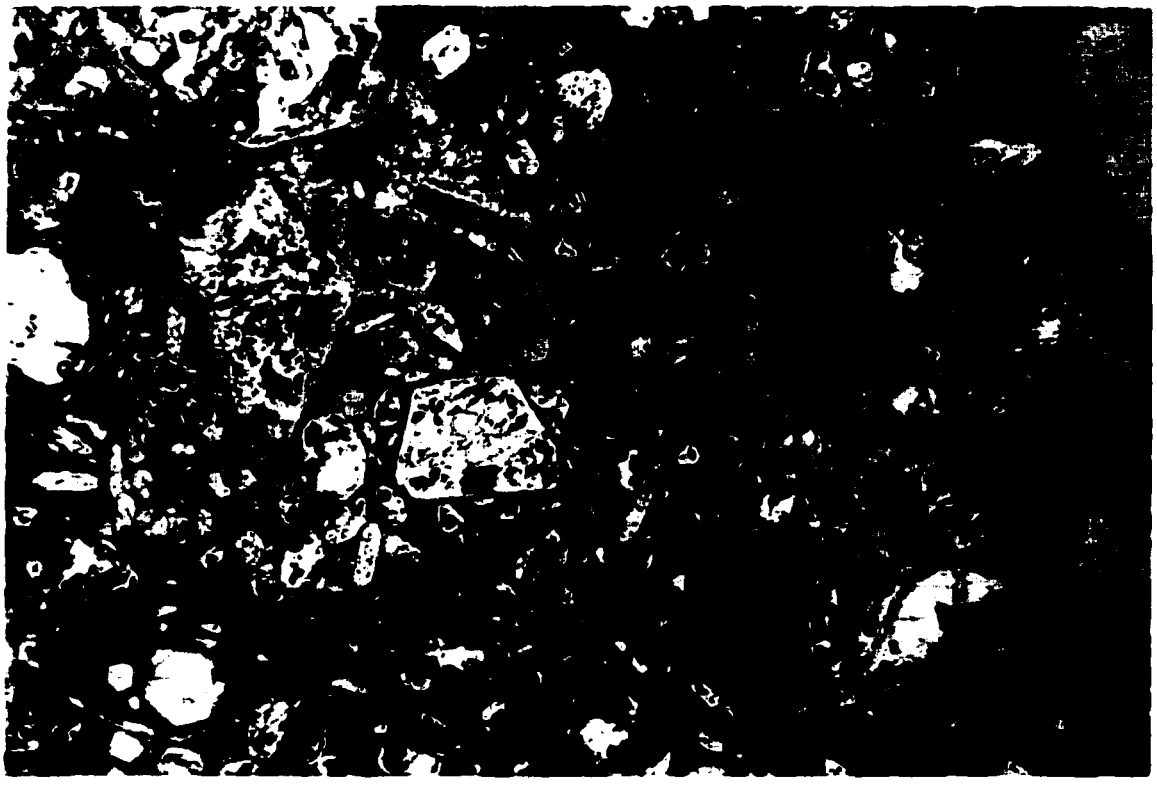

Reproduced with permission of the copyright owner. Further reproduction prohibited without permission.

Figure 5.8. Composite lapilli within volcaniclastic kimberlite containing three distinct types of kimberlites: dark green microporphyritic core mantled by green microporphyritic kimberlite and an outer mantle of fine-grained kimberlite ash of irregular thickness (F.O.V. 2.5 mm).

Figure 5.9. Volcaniclastic kimberlite with common juvenile lapilli (L) which are often difficult to detect in a matrix of similar texture and colour (F.O.V. 2.5 mm).

These beds contain common juvenile lapilli, most of which are composite structures and some appear abraded. No compelling evidence suggests that primary pyroclastic processes deposited these units. The fragmental, abraded and turbid mature of this kimberlite and the relative abundance of wall rock xenoliths indicate that this volcaniclastic rock may have been subjected to resedimentation processes.

5.3. DISCUSSION

Primary features observed within these units, which include anhedral macrocrysts and smaller euhedral microphenocrysts of pseudomorphed olivine, defining two generations of olivine. Other macrocrysts present include phlogopite, ilmenite and less common garnet. Primary phlogopite is also present. Other primary groundmass minerals include serpentine, spinel, apatite, perovskite, probable monticellite and calcite. The cryptocrystalline nature of the matrix suggests some degree of quenching characteristic of juvenile fragments. All of these features are characteristic of, but not exclusive to kimberlites (cf. Mitchell 1994). However, no features observed would preclude these rocks from being classified as archetypal kimberlite, although many petrographic features observed may be atypical for kimberlites from elsewhere.

Both primary pyroclastic and volcaniclastic kimberlite (perhaps resedimented) are present within the Fort à la Corne kimberlite field. Hypabyssal or diatreme facies kimberlite were not encountered in this study, or any other.

The units described above are similar to many of those described within the literature (Leckie *et al.* 1997, Leahy 1997, Field and Scott Smith 1998) and thus modes of emplacement are not different from those currently believed to have operated at Fort à la Corne. It is clear that primary pyroclastic activity was responsible for the bulk of the infill of these kimberlites. Non-welded, matrix-to-lapilli-supported lapilli-rich tuffs show no evidence of resedimentation and are likely primary pyroclastic units. Moreover, welded, lapilli-supported lapilli-rich tuffs are clearly pyroclastic in origin. These beds are similar to air-fall lapilli tuffs described in the literature (Leckie *et al.* 1997). Variable matrix-to-lapilli ratios, welding of units and lapilli grain sizes is the likely result of

variable kimberlite magma vent discharge rates and melt fragmentation (Leckie *et al.* 1997). Leckie *et al.* (1997) further suggest that these lapilli-rich units owe their origin to violent Strombolian forming highly fragmented tephra that has a limited areal dispersion. Non-vesiculated kimberlite lapilli likely owe their derivation from a more explosive, kimberlite-specific eruption.

The olivine crystal tuffs, which are considered to originate as air falls (Leckie *et al.* 1997), are generally depleted in fines, suggests eolian sorting during air fall. The presence of other juvenile kimberlite material, such as lapilli, crystals of phlogopite are also consistent with an air-fall origin (Leckie *et al.* 1997, Scott Smith *et al.* 1994). The small average grain size (<2 mm) suggests higher fragmentation during eruption. These observations are consistent with explosive volcanic eruptions of crystal-rich kimberlite magma (Leckie *et al.* 1997).

The volcaniclastic kimberlite described in Section 5.2.2.4. differs significantly from the pyroclastic kimberlite units. If these units are resedimented volcaniclastic kimberlites, their origin is likely similar to other reworked units from the Fort à la Corne area described within the literature (Leckie *et al.* 1997; Leahy 1997), *i.e.* debris flows from slumping and aqueous modification of tuff piles.

5.3.1. Mode of Emplacement of Fort à la Corne Kimberlites

As no new conclusions can be drawn from the kimberlite reviewed in this study, the currently accepted emplacement model presented in the literature will be reviewed here.

The Fort à la Corne kimberlites are formed by two distinct processes: crater excavation and crater infilling (Field and Scott Smith 1998). The shapes of these craters are superficially similar to those of maars, *i.e.*, rapidly flaring edifices with low depth-to-diameter ratios formed by phreatomagmatic processes. Hence craters at Fort à la Corne appear to represent explosion craters excavated into the soft overlying Cretaceous sediment (Figure 5.10)

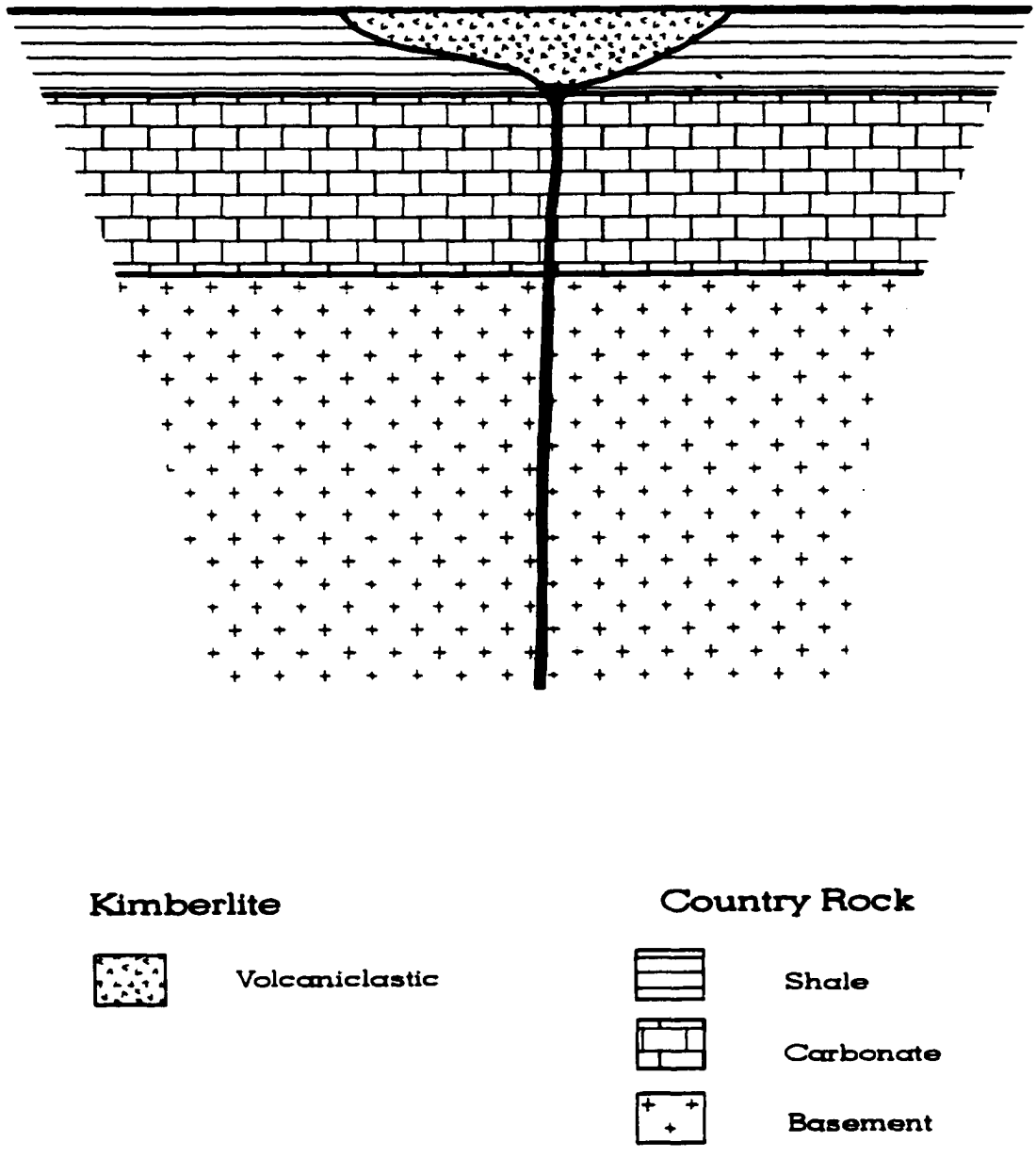

Figure 5.10. Simplified model of the Fort à la Corne kimberlites (after Scott Smith 1996 and Field and Scott Smith 1998).

The resulting excavated material was likely deposited mainly as extra-crater deposits, and the craters were subsequently infilled by subaerial primary pyroclastic magmatic processes ranging from violent Strombolian to a much more explosive, kimberlite-specific eruption style (Field and Scott Smith 1998; Leckie *et al.* 1997). Resedimented volcaniclastic kimberlite also contributed to vent infill in many kimberlite bodies (it appears to be entirely absent in others); some of this reworked material described from Smeaton core was suggested by Leckie *et al.* (1997) to represent subaqueous air-fall deposits, some of which may have been reworked by waves. Resedimented extra-crater deposits do not appear to contribute to vent infill.

As previously noted no evidence for the formation of a southern African-style diatreme has been uncovered at Fort à la Corne, or any Canadian Prairie kimberlite intrusion. This supports suggestions made by Scott Smith *et al.* (1996) and Field and Scott Smith (1998) that kimberlite eruption style and resultant deposits are controlled by the near-surface geology of the erupting environment. Therefore it can be surmised that the lack of diatreme formation is directly related to the lack of a competent barrier or cap rock. This feature is characteristic of the Western Canadian sedimentary basin, and is in direct contrast to the Karoo sedimentary basin of southern which is typified by abundant igneous rocks forming barriers and cap rocks to rising kimberlite magmas (Field and Scott Smith 1998). Moreover, the presence of many long-lived aquifers within the Western Canadian sedimentary basin during the Cretaceous provides further circumstantial evidence that the Fort à la Corne craters are explosion craters formed by phreatomagmatic processes. Clearly, additional work needs to be carried out to constrain this model further.

CHAPTER 6. MINERALOGY

6.1. MINERALOGY OF THE LAC DE GRAS KIMBERLITES

6.1.1. Spinel

6.1.1.1. Introduction

Spinels are ubiquitous throughout the Lac de Gras kimberlites, in both hypabyssal and volcaniclastic facies, and occur as:

1. macrocrysts;
2. primary groundmass minerals;
3. reaction or replacement products formed during the serpentinization of olivines.

6.1.1.1.1. Macrocrystal Spinel

Macrocrystal spinels, ranging in size from 0.1-0.5 mm (Mitchell 1986) are somewhat sparse within Lac de Gras kimberlites. They are generally rounded and vary from translucent reddish-brown to opaque crystals.

6.1.1.1.2. Primary Groundmass Spinel

Primary groundmass parageneses account for most of the spinels within the Lac de Gras kimberlite field. Small (0.001-0.1mm) subhedral-to-euhedral spinels comprise a significant proportion of the groundmass mineral assemblage in most kimberlite vents. The abundance of these spinels can range from less than 5 to approximately 30 volume percent. Their proportion may vary widely on a centimetre or even a millimetre scale as a result of their concentration by flow differentiation, preferential nucleation about pre-existing crystals (most commonly olivine) or the presence of oxide-free serpentine-calcite segregations that are abundant in most hypabyssal rocks (Mitchell 1986).

Groundmass spinels occur as discrete homogeneous or as continuously and complexly zoned and epitaxially mantled crystals. Resorption, ranging from minor corrosion to nearly complete dissolution, has altered the habit of many of these crystals. Resorption of epitaxially mantled spinels results in an atoll-textured crystal.

6.1.1.1.3. Atoll Spinels

Atoll spinels are relatively abundant, occurring as subhedral-to-euhedral cores separated by a small but distinct gap from a narrow rim of magnetite. Within the Lac de Gras kimberlites, this rim may not be relatively pure magnetite and can contain significant amounts of MgO and TiO_2. The gap between the core and rim of the crystal is occupied by a fine-grained intergrowth of calcite and serpentine, identical to that composing the groundmass mesostasis in which the spinels are set. Small anhedra of perovskite and less commonly rutile occur along the outer margins of the thin rims. The atoll structure is usually disrupted by resorption.

6.1.1.1.4. Reaction Product Spinels

During the retrograde serpentinization of olivine under relatively oxidizing conditions iron is released as tiny (<1μm) euhedral magnetite crystals scattered throughout an iron-poor serpentine matrix. These crystals are extensively resorbed resulting in a "skeletal" appearance. Moreover, as a consequence of prograde replacement of serpentinized olivine by deuteric fluids, pseudomorphs of calcite and magnetite can be produced (Mitchell 1986). The magnetite formed, in both cases, is a relatively pure Ti-free magnetite. Marginal serpentinization of primary groundmass olivines also causes the crystallization of primary groundmass spinels. The groundmass olivines act as nucleation centres around which "necklaces" and discontinuous necklaces of spinels form.

Table 6.1. Representative Compositions of Spinel from the Lac de Gras Kimberlites[a].

	1	2	3	4	5	6	7	8	9	10	11	12	13	14
TiO_2	1.63	0.68	0.59	0.81	0.84	7.84	7.02	7.04	7.13	8.14	8.14	1.80	13.01	6.07
Al_2O_3	50.64	53.69	56.90	44.52	54.73	17.05	17.96	19.16	23.58	17.73	17.73	21.73	16.13	16.50
Cr_2O_3	3.79	1.12	0.67	9.12	0.65	0.00	0.00	0.27	0.14	0.13	0.13	34.93	4.11	26.12
FeO[b]	20.90	21.74	18.76	22.88	21.31	57.72	56.21	54.12	46.44	53.04	53.04	24.01	46.10	30.10
MnO	0.15	0.12	0.08	0.02	0.16	0.53	0.25	0.39	0.47	0.50	0.50	0.36	0.48	0.35
MgO	22.12	21.71	22.82	22.67	21.76	13.58	14.53	14.35	16.49	15.06	15.06	16.85	16.89	16.03
	99.23	99.06	99.82	100.02	99.45	96.72	95.97	95.33	94.25	94.60	94.60	99.68	96.72	95.17
Recalculated analyses														
$Fe^{2+}O$	7.53	7.77	6.74	5.45	8.07	20.16	18.16	18.26	15.25	17.58	17.58	11.12	19.45	14.01
$Fe^{3+}{}_2O_3$	14.86	15.52	13.35	19.38	14.71	41.74	42.28	39.86	34.67	39.40	39.40	14.33	29.62	17.88
	100.72	100.62	101.16	101.96	100.92	100.90	100.21	99.32	97.72	98.55	98.55	101.12	99.69	96.96

	15	16	17	18	19	20	21	22	23	24	25	26	27	28
TiO_2	1.48	1.75	1.10	1.37	1.51	1.25	1.15	3.25	11.87	11.38	2.49	5.57	0.70	0.23
Al_2O_3	5.21	4.90	6.41	5.84	7.59	6.33	6.15	0.89	9.31	1.05	0.25	0.00	0.30	0.28
Cr_2O_3	58.61	56.92	58.42	56.97	53.91	58.18	58.91	0.52	0.34	1.01	0.12	0.11	0.33	0.34
FeO[b]	19.52	20.46	18.84	20.86	19.67	18.18	18.64	81.12	57.32	65.52	87.03	83.26	87.36	87.95
MnO	0.36	0.17	0.30	0.27	0.04	0.38	-	1.54	0.63	0.66	1.18	0.90	0.02	0.15
MgO	13.03	13.32	14.68	14.38	14.25	15.00	14.52	4.75	14.53	13.38	2.03	1.35	2.55	2.75
	98.21	97.52	99.75	99.69	96.97	99.32	99.37	92.07	94.00	93.00	93.10	91.19	91.26	91.70
Recalculated analyses														
$Fe^{2+}O$	13.47	13.22	11.38	12.03	11.96	10.79	11.79	24.84	20.13	19.96	28.94	32.25	27.16	26.46
$Fe^{3+}{}_2O_3$	6.72	8.05	8.29	9.82	8.56	8.21	7.61	62.55	41.33	50.65	64.56	56.68	66.90	68.33
	98.88	98.33	100.58	100.67	97.83	100.14	100.13	98.34	98.14	98.07	99.57	96.87	97.96	98.54

[a]1-5 pleonaste; 6-10 titanian fempleonaste; 11-14 titanian magnesian alminous chromite; 15-18 titanian magnesian chromite; 19-21 macrocrystal magnesian aluminous chromite; 22-24 magnesian ulvospinel-ulvospinel-magnetite; 25-26 ulvospinel-magnetite; 27-28 magnetite
[b]Total Fe calculated as FeO

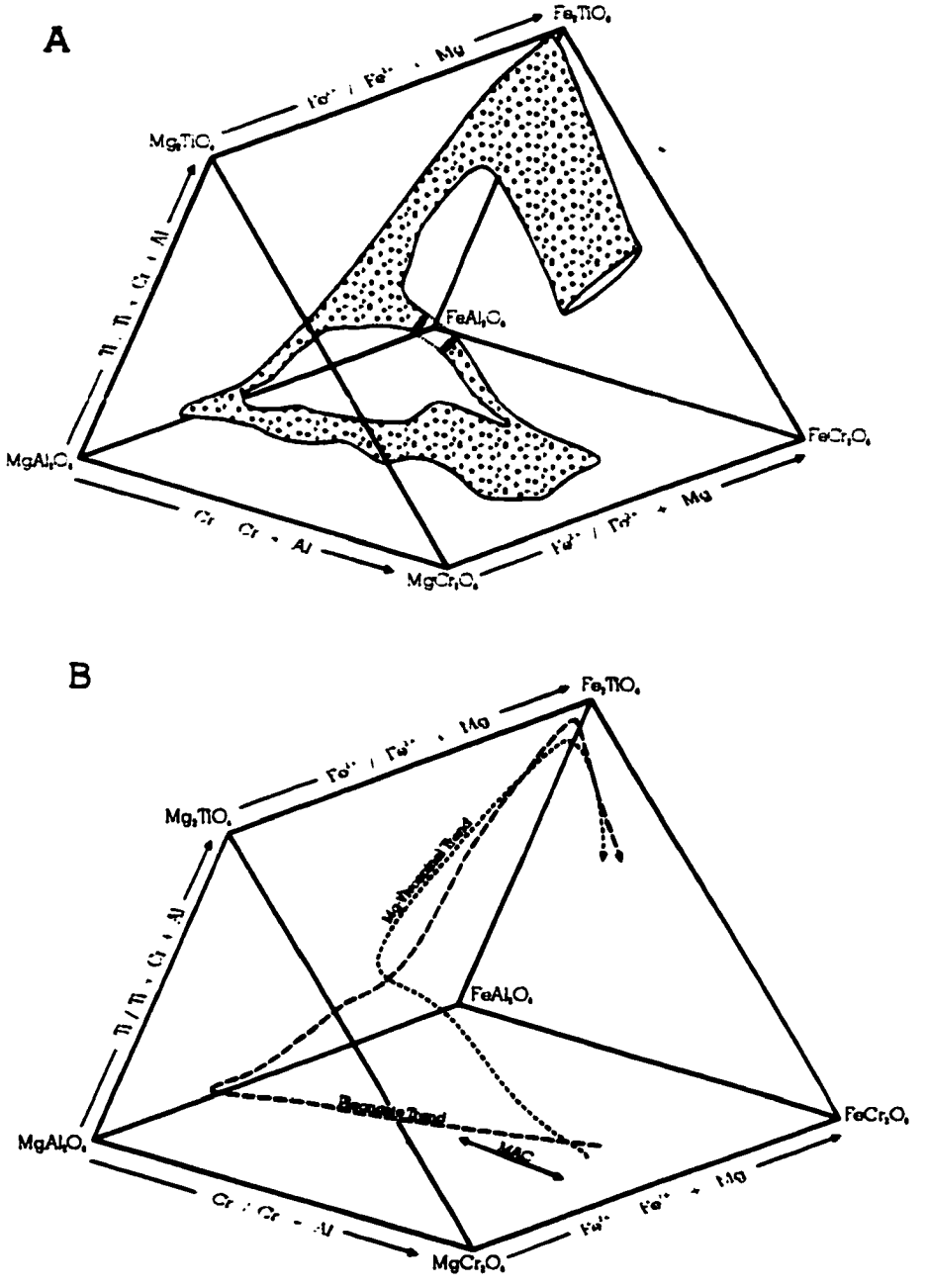

Figure 6.1. Overall compositional trends of spinels from the Lac de Gras kimberlite field (A) and schematic representation of the various trends present within this field (B).

6.1.1.2. Composition of Macrocrysts and Primary Groundmass Spinel within the Lac de Gras Kimberlite Field

The composition of the Lac de Gras kimberlite spinels, in common with most other kimberlite spinels, fall within the 8-component system $MgCr_2O_4$ (magnesiochromite)-$FeCr_2O_4$ (chromite)-$MgAl_2O_4$ (spinel)-$FeAl_2O_4$ (hercynite)-Mg_2TiO_4 (magnesian ulvöspinel)-Fe_2TiO_4 (ulvöspinel)-$MgFe_2O_4$ (magnesioferrite)-Fe_3O_4 (magnetite). Manganese contents are typically low (<1 wt % MnO, typically <0.5) and the Mn_2TiO_4 (manganoan ulvöspinel) or $MnFe_2O_4$ (jacobsite) end members are absent. Representative composition of spinels analyzed from the Lac de Gras field are given in Table 6.1.

End-member spinel molecules are calculated as outlined by Mitchell and Clarke (1976) and the data are plotted in a reduced iron spinel prism in Figure 6.1. This type of projection, in which total iron is calculated as FeO is useful for many kimberlite spinels which are known to have formed under relatively reducing conditions. The projection, however, fails to illustrate variations in Fe_3O_4 or $MgFe_2O_4$ content, but has the merit that all major elements present are included in the prism. Illustrating spinel compositions from the Lac de Gras kimberlites within the "oxidized" spinel prism would have proved superfluous.

Textural relationships indicate that at least three parageneses of spinel are present within the Lac de Gras kimberlite field. Overall compositional trends for the spinels from the Lac de Gras kimberlite field are shown in Figure 6.1.

6.1.1.2.1. Macrocrystal Trend

These spinels primarily plot near the basal plane of the spinel prism, belonging essentially to the quaternary system $MgAl_2O_4$-$MgCr_2O_4$-$FeCr_2O_4$-$FeAl_2O_4$ (refer to Figure 6.1). Most contain less than 2 wt.% TiO_2 (refer to Table 6.1) and exhibit a fairly wide range in their Cr/(Cr + Al) [0.6-0.91; rarely as low as 0.5] and Fe/(Fe + Mg) [≈0.3-0.55] ratios. These spinels are best described as magnesian aluminous chromites (MAC) (*sensu* Mitchell 1986) as MgO is always greater than Al_2O_3 in individual crystals.

Individual crystals are typically homogeneous. The compositional trend of the MAC macrocrysts overlaps the compositions of the least evolved (Ti-poor, Cr-rich) cores of primary groundmass spinels.

6.1.1.2.2. Magnesian Ulvöspinel Magmatic Trend

This compositional trend, illustrated in Figure 6.2, traverses the spinel prism from the base near the $MgCr_2O_4$-$FeCr_2O_4$ join [Cr/(Cr + Al) = 0.8-0.9, Fe/(Fe + Mg) = 0.3-0.5] toward the rear rectangular face, upward toward the Mg_2TiO_4-Fe_2TiO_4 apex [Ti/(Ti + Cr + Al) = 0.2-0.5]. Spinel evolution is from titanian magnesian aluminous chromite (TIMAC) or titanian magnesian chromite (TMC) containing <1-4% TiO_2 toward members of the magnesian ulvöspinel-ulvöspinel-magnetite (MUM) spinels (>10% TiO_2). These mantles plot along the $FeCr_2O_4$-$FeAl_2O_4$ join. The magnesian ulvöspinel trend is one of increasing Ti, total Fe and decreasing Cr at approximately constant $Fe^{2+}/(Fe^{2+}+ Mg)$. Aluminum commonly increases.

Each kimberlite within the Lac de Gras field appears to be characterized by a slightly different range of $Fe^{2+}/(Fe^{2+}+ Mg)$ within this trend, that is, their placement is displaced slightly along the basal plane of the spinel prism (refer to Figure 6.2B, variation 1). The Fe-enrichment culminates with the development of Ti- and Mg-free magnetite (Mitchell 1986); however, within the Lac de Gras kimberlites, extensive resorption of groundmass spinels has usually resulted in the elimination of this phase or its occurrence as an incomplete, fretted rim. When this phase is present, it does not occur as pure magnetite as in most archetypal kimberlites but contains significant amounts of TiO_2 (generally <5wt.% TiO_2) and MgO (<3wt.% MgO, may be as high as 4.5wt.%; refer to Table 6.1). Cr_2O_3 contents are generally low, *i.e.*, less than 1 wt.% Cr_2O_3. These rims are commonly intimately intergrown with anhedra of perovskite. The presence of Ti-rich spinels containing substantial proportions of the magnesian ulvöspinel molecule is the hallmark of spinels belonging to this trend.

A variation of the magnesium-ulvöspinel trend within the Lac de Gras field occurs within kimberlites A11, T7 and DD39 (refer to Figure 6.2B, variation 2).

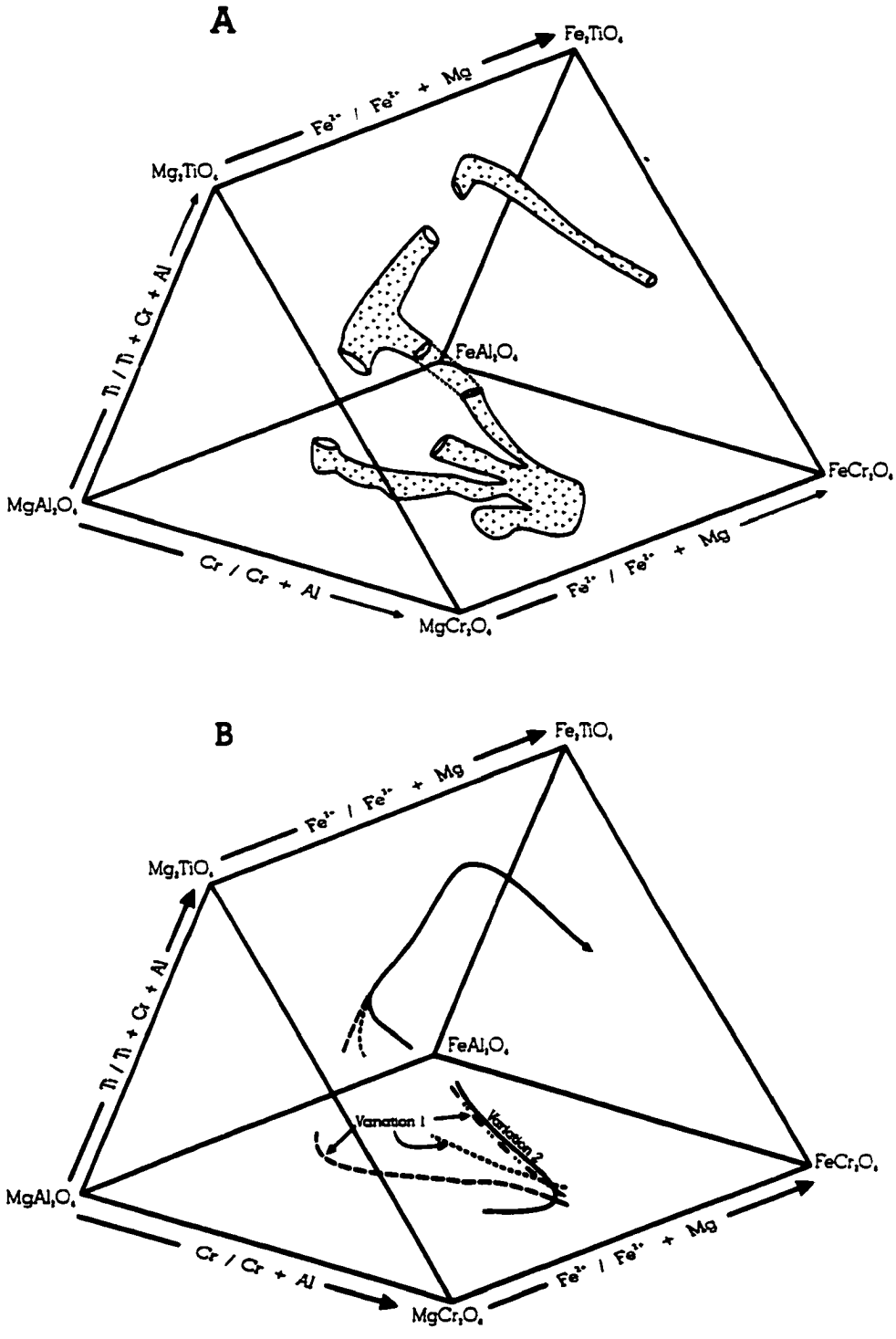

Figure 6.2. Compositional field of the magnesian ulvöspinel trend (A) and a schematic representative of the variations seen within the magnesian ulvöspinel trend (B).

Mantling relationships within these kimberlites indicate a compositional trend from a moderately aluminous titanian magnesian chromite (Ti-bearing Al- Mg-rich spinel) to a titanian magnesian chromite (Ti-bearing, Fe-Cr-rich spinel). This trend reflects an initial increase in the Cr / (Cr + Al) and $Fe^{2+}/(Fe^{2+}+ Mg)$ ratio of the magma. Following these initial increases, the composition of the spinels than follows the above-described TMC/TIAMC-MUM evolutionary trend.

In most kimberlites (T35, DD39, C49, A61-9) characterized by the magnesian-ulvöspinel trend a complete series of compositional variation is not present and individual crystals in spinel consist of early crystallizing TIMAC or TMC mantled by discrete rims of MUM (A61-9). Other kimberlites contain spinels belonging primarily to the initial or final portions of this trend and in some intrusions TIMAC or TMC spinels occur as homogeneous crystals without MUM-spinel (DD39, T35). Rare examples exist of kimberlites that are characterized predominantly MUM spinels and titanian and magnesian-enriched magnetite (A61-9).

It is clear from Figure 6.2 that there is a distinct hiatus in the crystallization sequence of spinel and there is not a continuous series of solid solutions between TIAMC/TMC and MUM compositions. Mitchell (1986) also noted this hiatus within Trend 1 (magnesian ulvöspinel trend) spinels. Mitchell (1986) suggests this hiatus may represent a solvus in this spinel system, as demonstrated experimentally by Muan *et al.* (1972).

6.1.1.2.3. Pleonaste Trend

Al-rich groundmass spinels that do not belong to either of the above-described trends occur as homogenous subhedral-to-euhedral crystals (T33, A5, T29S) or as epitaxial mantles upon Trend-1 spinels in some kimberlites (T34, T7, A61-1, T33, A5, T29S, Figure 6.3).

Within this trend, the composition of spinels initially traverse the prism from near the base at the $MgCr_2O_4$-$FeCr_2O_4$ join [Cr/(Cr + Al) = 0.8-0.9, Fe/(Fe + Mg) = 0.3-0.5] toward the $MgAl_2O_4$-$FeAl_2O_4$ join with a decreasing $Fe^{2+}/(Fe^{2+}+ Mg)$ and Cr/(Cr + Al)

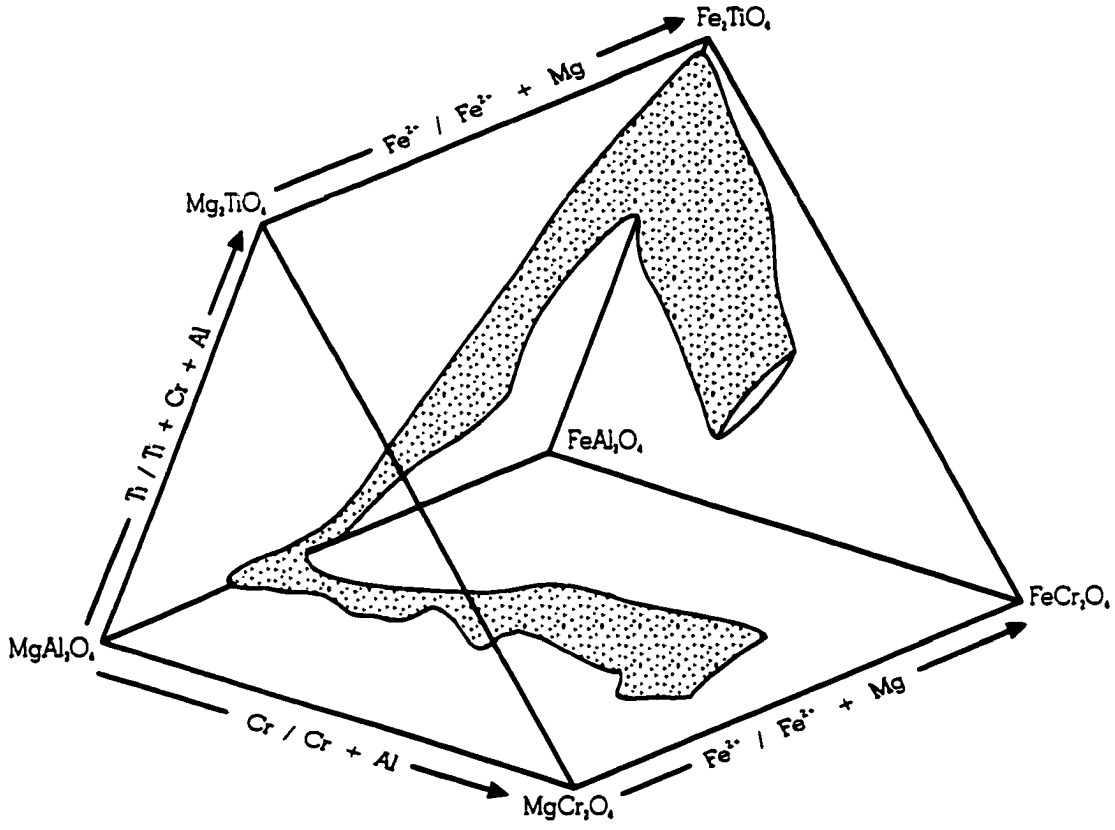

Figure 6.3. Compositional field of the pleonaste trend.

ratios. During this initially traverse, the Ti/(Ti + Cr + Al) ratio may increase or decrease. Aluminum contents significantly increase within single crystals of spinel and generally contain greater than 50 wt.% Al_2O_3. The compositions of the spinels then follows the $MgAl_2O_4$-$FeAl_2O_4$ join, and are characterized by continually increasing $Fe^{2+}/(Fe^{2+}+ Mg)$ and Ti/(Ti + Cr + Al) ratios at a relatively constant Cr/(Cr + Al) ratio (generally <0.01), toward the Fe_2TiO_4 apex. In general, this trend ranges in composition from TMC-TIAMC-Pleonaste-Titanian ferripleonaste (TFP)-MUM (not usually present)-ulvöspinel magnetite-magnetite. TFP are similar to MUM spinels but are distinctly more aluminous. Thin outer mantles of magnetite are usually present as thin, irregular, extensively resorbed rims. Extensive resorption of these rims commonly precludes an accurate analysis. Individual spinel crystals in which the outer mantle of magnetite is preserved plot along the $FeAl_2O_4$-$FeCr_2O_4$ join. These magnetite crystals are commonly rich in MgO (<3wt.% MgO) and TiO_2 (<5wt.% TiO2). Cr_2O_3 proportions within these magnetite rims is generally low (<1wt.% Cr_2O_3) but will displace the composition along the $FeAl_2O_4$-$FeCr_2O_4$ join toward the $FeCr_2O_4$ apex with increasing Cr_2O_3 contents (refer to Figure 7.4). Groundmass crystals of homogeneous magnetite similarly plot along the $FeAl_2O_4$-$FeCr_2O_4$ join.

A complete compositional trend, as described above, is not present in most of the kimberlite intrusions, but can only be delineated when all the data are viewed together (refer to Figure 6.3). Instead, fragments of this trend characterize individual kimberlites (Figure 6.4).

Kimberlite A5 is characterized by discrete rims of pleonaste followed by TFP mantling cores of earlier crystallizing TMC and TIAMC; the MUM series never appears to have crystallized. Spinels within A5 may lack cores of TMC or TIAMC; pleonaste cores are mantled by TFP, lacking a MUM outer mantle. Moreover, homogeneous groundmass TFP spinels are not uncommon within A5. Spinels analyzed from kimberlites T33 and T7 show cores of TMC of TIAMC mantled by TFP with no evidence of the pleonaste or MUM series crystallizing. Spinels in kimberlite A61 are characterized by cores of TMC and TIAMC, following a complete evolutionary trend to pleonaste. TFP is not present and may have been resorbed. An outer rim of MUM and Ti-. Mg-

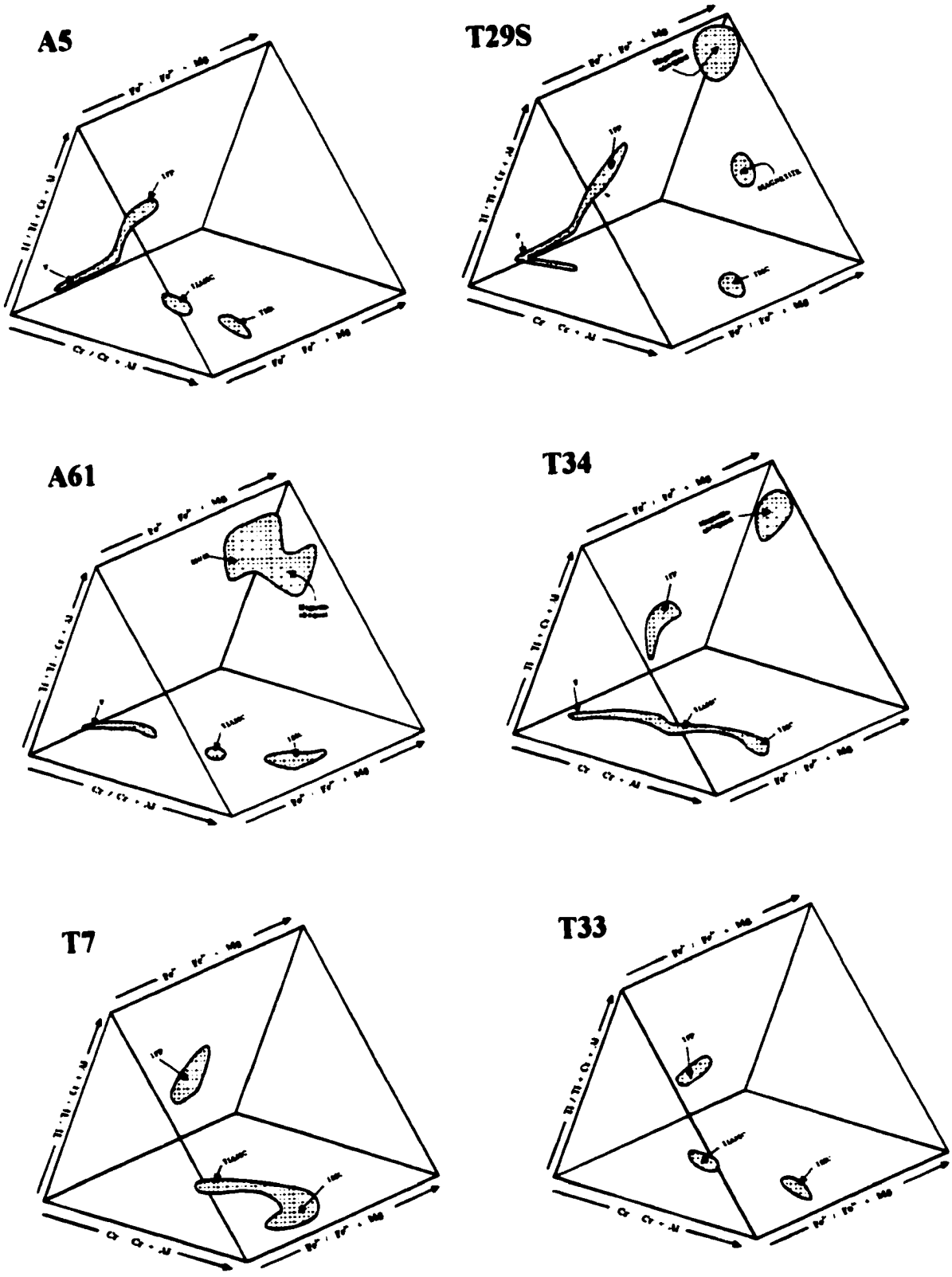

Figure 6.4. Pleonaste-trend spinel compositions from the Lac de Gras kimberlites.

bearing magnetite (not often preserved) mantles the pleonaste. Kimberlite T29S contains spinels cored by TMC, which are mantled by a discrete rim of pleonaste that evolves into TFP and is mantled by the ulvöspinel-magnetite series with a thin, partially resorbed outer margin of Ti- and Mg-bearing magnetite. Finally, kimberlite T34 is cored by TMC, which is successively mantled by TIAMC, TFP and ulvöspinel-magnetite. Pleonaste is not present and has likely been resorbed.

It is important to note that the spinel Trend 2 (*sensu* Mitchell 1986), which is a common trend in spinels from orangeites, lamproites and a wide variety of "basaltic" rocks is not present in the Lac de Gras kimberlite field. This trend is characterized by an initial evolution along the prism acid [increasing $Fe^{2+}/(Fe^{2+}+ Mg)$] followed by a rapid Ti and Fe^{3+} (titanian chromite) increase toward the Fe_2TiO_4 apex.

Pasteris (1980, 1983) described chromites (TIAMC) and MUM spinels epitaxially mantled successively by pleonaste and magnetite. When pleonaste is not present in atoll spinels, Pasteris (1980, 1983) belives that it has been resorbed due to the subsequent increase in fo_2 in the late stages of crystallization. However, in many kimberlites within the Lac de Gras field, pleonaste and TFP are preserved. Pasteris (1980, 1983) suggests that rapid cooling prevents the resorption process from being complete.

6.1.1.3. Discussion

The magnesian ulvöspinel trend appears to be present in both hypabyssal kimberlite and resedimented volcaniclastic kimberlite. The hypabyssal kimberlite occurs in association with volcaniclastic vent infill as either autoliths or late-stage sills. The pleonaste trend seems to be confined to hypabyssal kimberlite occurring as isolated dyke segments or as large autoliths or late-stage sills within volcaniclastic vent infill. Extensive wall rock contamination in these later kimberlites may have resulted in an enhancement of Al within the melt resulting in the crystallization of pleonaste and titanian ferripleonaste. However, the relative enrichment of Al within nearly all of the spinels analyzed within the Lac de Gras kimberlite field suggests that most of the intrusions have been contaminated, to some degree, by the country rock during intrusion.

Rapid cooling within the small hypabyssal intrusions may have prevented the pleonaste and TFP from being resorbed.

6.1.2. Phlogopite

6.1.2.1. Introduction

Phlogopite within the Lac de Gras kimberlites are divisible into two broad groups: macrocrystal micas and microphenocrystal groundmass micas. Very rare parageneses are as rims upon olivines and as metasomatic replacements of xenoliths.

Macrocrystal phlogopites are not overly abundant within the Lac de Gras kimberlites, ranging from rare scattered crystals to abundant plates that may be oriented about fragments giving the rock a pilotaxitic texture (*eg.*, A61). Macrocrystal phlogopite is typically rare in highly evolved calcite-serpentine kimberlites. The phlogopites occur as bronze single crystals ranging from 2-8 mm in length. Commonly they are rounded, broken, distorted, or kink banded and show undulose extinction. Calcite, chlorite and serpentine replacement, particularly along cleavage planes, is common. The margins of many macrocrysts are corroded and embayed and may be mantled by small secondary spinels.

Groundmass phlogopites commonly occur as a closely packed mosaic of tabular-to-lath shaped microphenocrysts, typically less than 0.5 mm in length. Some kimberlites may display flow aligned groundmass micas. Many groundmass crystals are distorted and corroded. Groundmass micas often contain inclusions of spinel and perovskite and often poikilitically enclose monticellite. Phlogopite may also occur within calcite-serpentine segregations of segregation-textured hypabyssal kimberlite, having nucleated at the margins of bounded segregations.

6.1.2.2. Composition of Phlogopite within the Lac de Gras Kimberlite Field

Representative compositions of phlogopite from the Lac de Gras kimberlites are given in Table 6.2. Kimberlite micas are essentially phlogopites and barian phlogopite (>2-9.4 wt.% BaO). Most phlogopites show a distinct enrichment in BaO and can be considered to be members of the phlogopite-kinoshitalite solid solution series. Tetraferriphlogopite appears to be absent.

Barian phlogopites have moderate, but variable SiO_2. Groundmass micas range from 32.5-36.2 wt.%, but typically have less than 35 wt.% SiO_2. Conversely, macrocrystal micas have a slightly greater amount of SiO_2, ranging from 34.4-38.6 wt.% (most have >36 wt.% SiO_2). SiO_2 content may increase or decrease from the core to the mantle of individual micas. FeO contents of groundmass mica range from 0.35-6.2 wt.%, and are usually less than 4 wt.%, while macrocrystal micas typically have FeO contents greater than 4 wt.%, ranging from 2.83-5.99. Al_2O_3 and MgO range from 14.5-17.5 wt.% and 22.1-27.6 wt.% respectively. K_2O content of macrocrystal phlogopite, which shows a distinct correlation with BaO, ranges from 7.3-10.5 wt.% K_2O and groundmass phlogopite has significantly lower K_2O contents, ranging from 4.8-7.9 wt.% K_2O. Na_2O and CaO content is usually less than 0.5 wt.%, CaO is commonly entirely absent. Na_2O does not appear to correlate with BaO while samples enriched in BaO typically have higher CaO contents.

Although many of the analyzed phlogopite grains are heterogeneous, no systematic zoning patterns have been detected with respect to the major elements (refer to Figures 6.5 and 6.6).

Barium is the only element that displays an obvious zonation pattern; BaO shows a systematic increase from the core to the mantle of individual crystals (BaO contents of crystal cores ranges from 0.67-8.5 wt.% BaO, whereas mantle values range from 1.2-9.4 wt.% BaO). Furthermore, groundmass micas typically display a higher BaO content than their macrocrystal counterparts and the increase in BaO content from core to mantle is more subtle (Figure 6.6).

Table 6.2. Representative Compositions of Barian Phlogopite[a]

Wt.%	1	2	3	4	5	6	7	8	9	10	11	12	13	14	15	16
SiO_2	33.91	34.04	33.53	34.36	32.91	33.92	37.33	35.67	36.92	38.21	38.22	35.10	37.51	35.49	34.95	32.50
TiO_2	0.50	0.45	0.31	0.51	0.38	0.69	1.32	1.50	1.02	1.35	1.14	1.27	1.32	1.22	1.86	0.70
Al_2O_3	16.41	15.58	15.18	15.32	16.37	14.96	15.41	15.98	14.71	15.21	14.43	15.59	14.43	15.18	16.15	17.85
Cr_2O_3	0.00	0.10	0.00	0.02	0.00	0.02	0.79	0.76	0.14	1.39	1.26	0.22	1.14	0.19	0.03	0.00
FeO[b]	3.51	3.23	3.30	3.56	3.38	3.91	4.88	5.44	4.68	4.36	4.51	4.63	3.14	4.25	2.83	6.18
MnO	0.06	0.00	0.15	0.03	0.07	0.16	0.07	0.01	0.09	0.03	0.01	0.02	0.12	0.08	0.30	0.25
MgO	27.33	25.81	26.72	26.17	26.09	25.98	23.46	22.87	23.82	24.56	24.70	24.72	24.68	24.16	24.80	23.20
CaO	0.06	0.09	0.00	0.00	0.02	0.42	0.00	0.00	0.00	0.00	0.00	0.00	0.00	0.00	0.00	0.42
Na_2O	0.14	0.17	0.21	0.20	0.06	0.14	0.33	0.24	0.14	0.13	0.10	0.21	0.31	0.18	0.57	.28
K_2O	7.42	7.18	7.52	7.24	7.20	6.91	10.25	9.90	8.31	10.07	10.39	8.86	9.76	9.24	8.10	5.64
BaO	8.48	8.11	8.41	7.35	7.95	7.76	1.58	1.70	5.15	0.90	0.96	5.51	1.25	3.09	5.65	8.49
NiO	n/d	n/d	n/d	n/d	n/d	n/d	n/d	n/d	n/d	0.08	0.00	0.00	0.14	0.09	0.37	0.18
	97.82	94.76	95.33	94.76	94.43	94.87	95.42	94.07	94.98	96.29	95.72	96.13	93.80	93.17	95.61	95.41
Structural Formula based on 22 oxygens																
Si	4.988	5.143	5.074	5.167	4.996	5.128	5.423	5.280	5.469	5.450	5.500	5.193	5.482	5.316	5.156	4.918
Ti	0.055	0.051	0.035	0.058	0.043	0.078	0.144	0.167	0.114	0.145	0.123	0.141	0.145	0.137	0.206	0.080
Al	2.846	2.775	2.708	2.716	2.930	2.666	2.639	2.789	2.569	2.557	2.448	2.719	2.486	2.681	2.809	3.185
Cr	-	0.012	-	0.002	-	0.002	0.091	0.089	0.016	0.157	0.143	0.026	0.132	0.023	0.003	-
Fe	0.432	0.408	0.418	0.448	0.429	0.494	0.593	0.673	0.580	0.520	0.543	0.573	0.384	0.532	0.349	0.782
Mn	0.007	-	0.019	0.004	0.009	0.020	0.009	0.001	0.011	0.004	0.001	0.003	0.015	0.010	0.037	0.032
Mg	5.991	5.811	6.026	5.865	5.903	5.853	5.080	5.045	5.259	5.220	5.298	5.451	5.376	5.393	5.453	5.233
Ca	0.009	0.015	-	-	0.003	0.068	-	-	-	-	-	-	-	-	-	0.068
Na	0.040	0.050	0.062	0.058	0.018	0.041	0.930	0.069	0.040	0.036	0.028	0.060	0.088	0.052	0.163	0.082
K	1.395	1.387	1.455	1.392	1.397	1.335	1.904	1.873	1.574	1.836	1.911	1.676	1.823	1.769	1.528	1.091
Ba	0.489	0.480	0.499	0.433	0.473	0.461	0.090	0.099	0.299	0.050	0.054	0.319	0.072	0.181	0.327	0.503
Ni	-	-	-	-	-	-	-	-	-	0.009	-	-	0.016	0.011	0.004	0.022

[a] 1-3, 4-6 T34 core-mantle zonation of groundmass crystals, 7-9 core-mantle zonation of macrocryst, 10-12, 13-15 A61-4 core-mantle zonation of macrocrysts, 16 DD 39 groundmass crystal

[b] Total Fe calculated as FeO

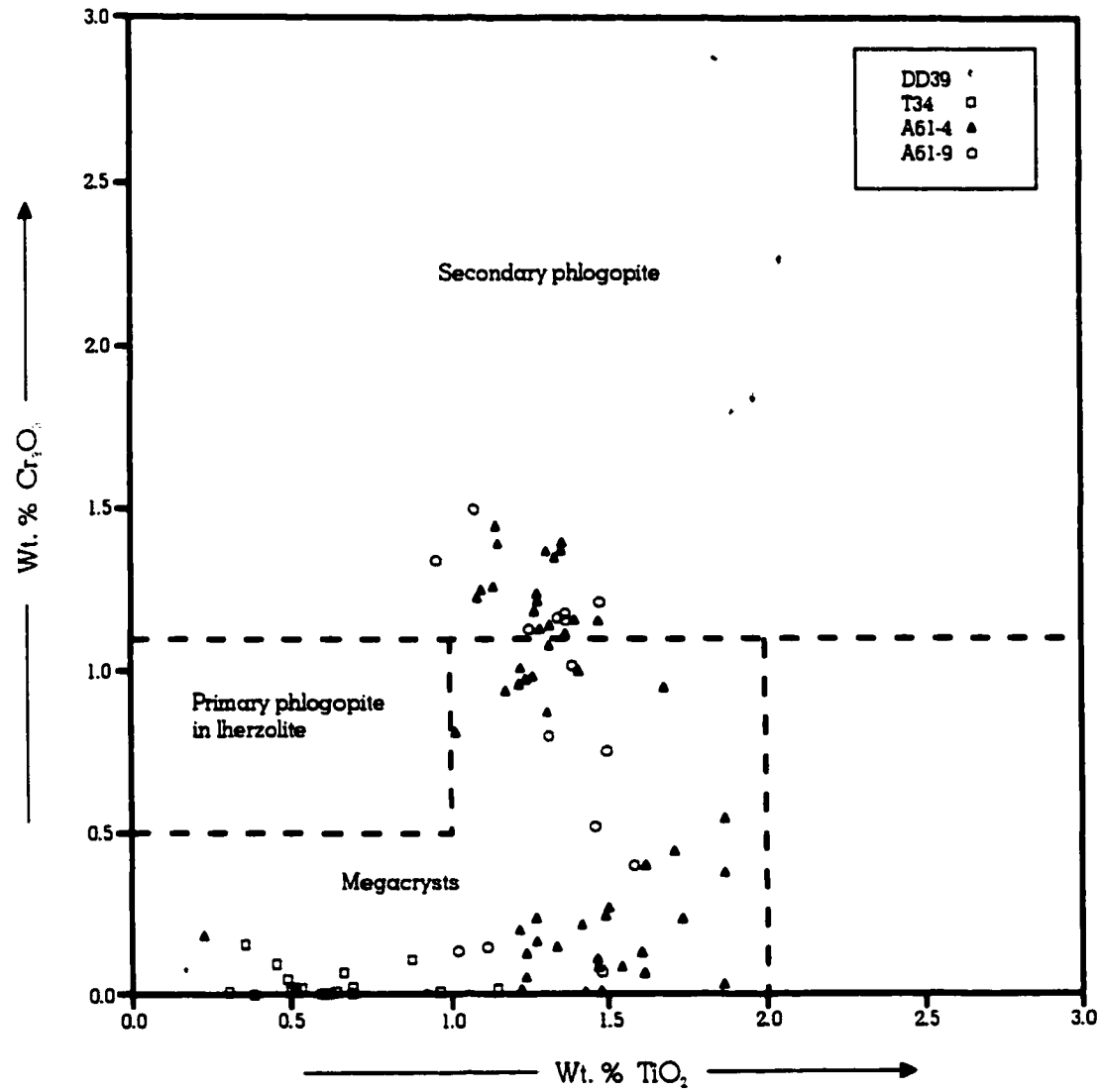

Figure 6.5. Cr_2O_3 versus TiO_2 for macrocrystal and groundmass phlogopite from the Lac de Gras kimberlites. Fields for megacrystal phlogopite, and primary and secondary phlogopite in lherzolite, from Carswell (1975) and Dawson and Smith (1975). Note that no phlogopite has compositions similar to those of primary phlogopite in lherzolite.

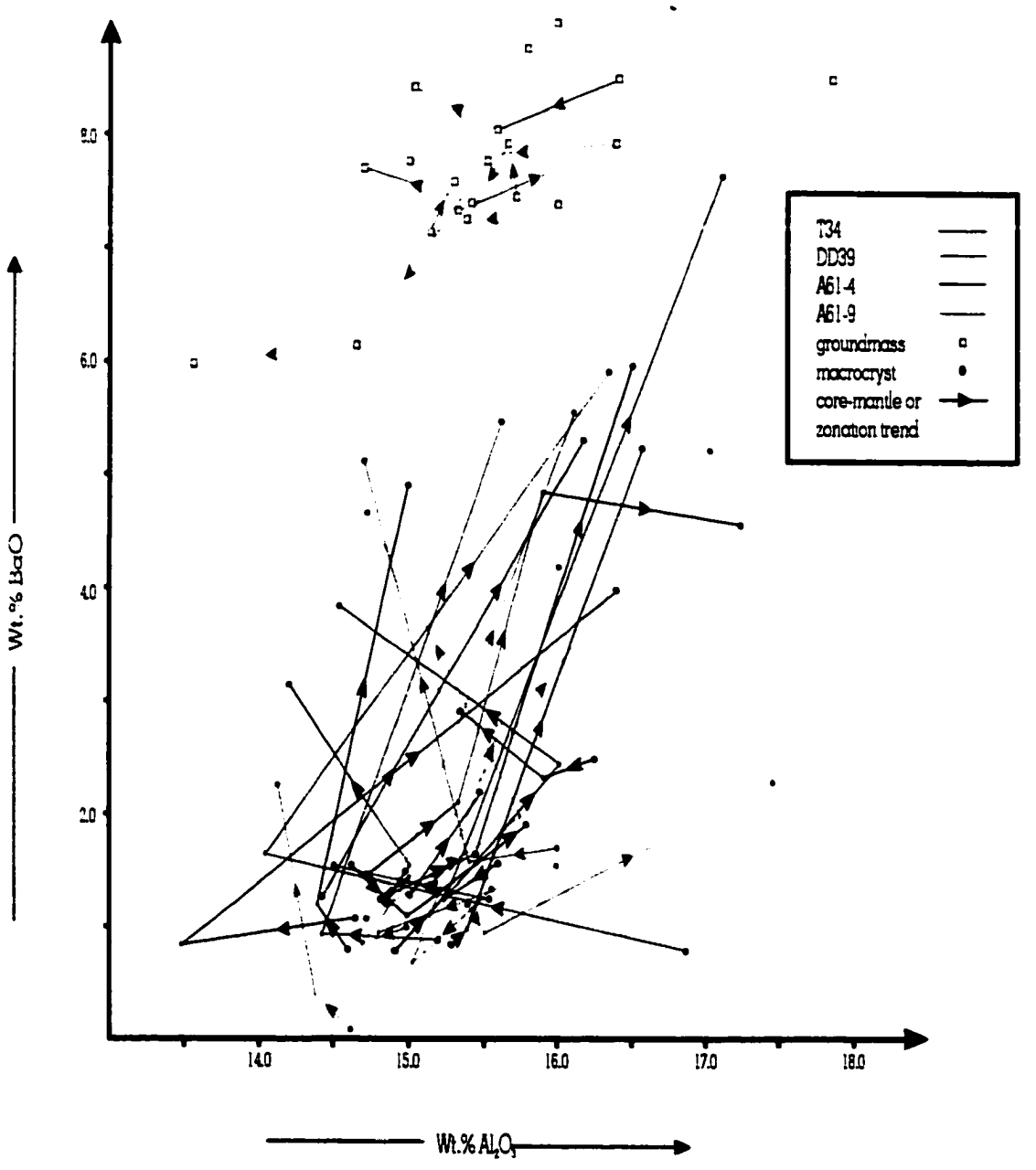

Figure 6.6. BaO versus Al_2O_3 for macrocrystal and groundmass phlogopite from the Lac de Gras kimberlite field.

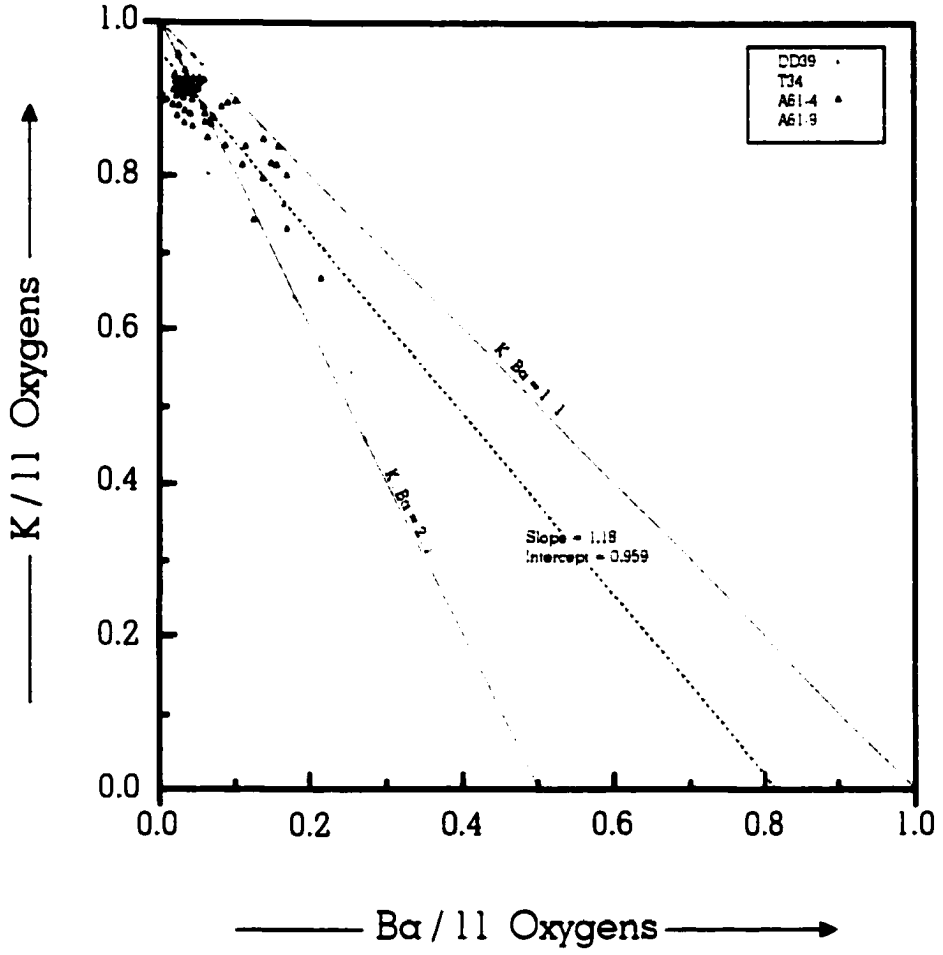

Figure 6.7. Correlations of the atomic proportion of Ba and K in Lac de Gras barian phlogopites. The least-squares line, with a slope of 1.18 and y-intercept of 0959, was fitted to all the data.

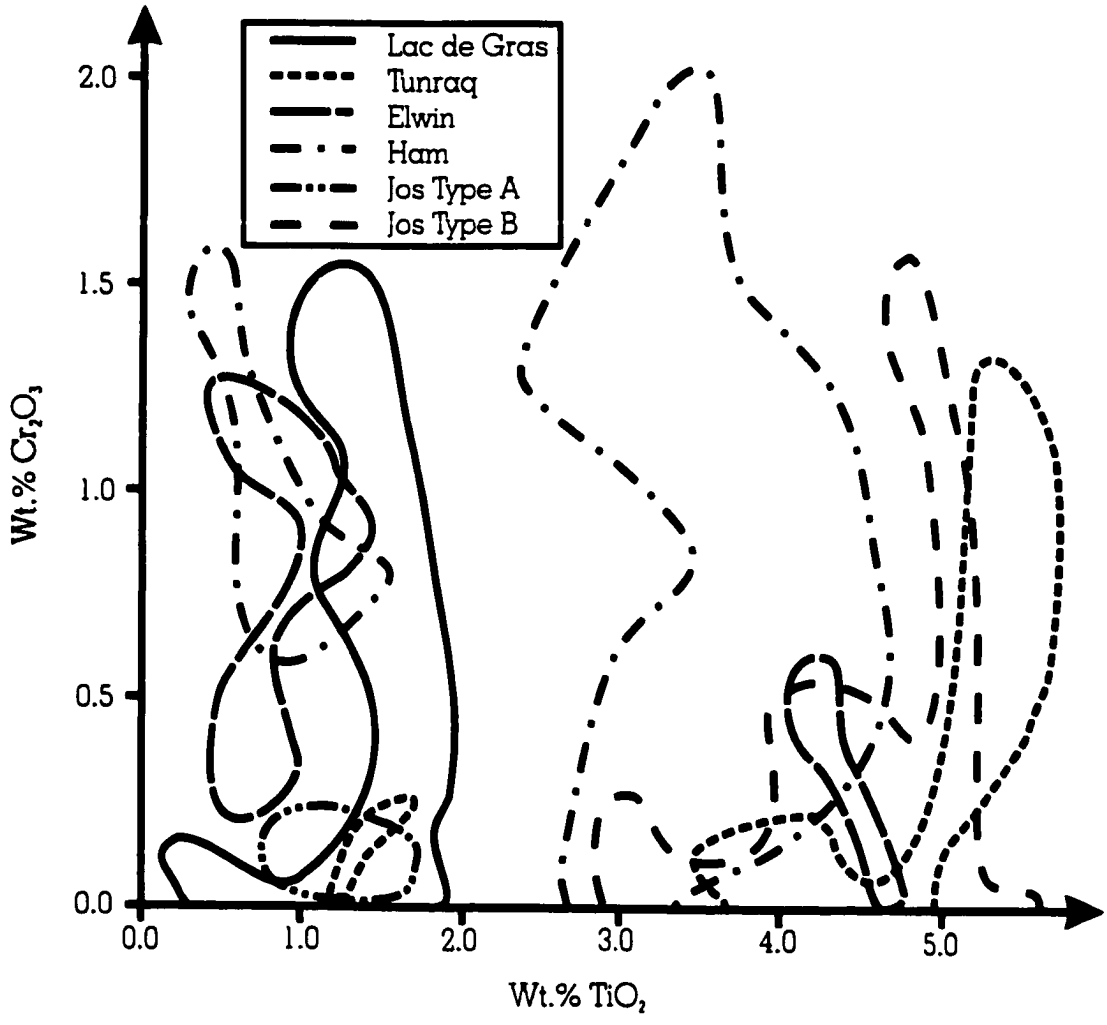

Figure 6.8. Cr_2O_3 vs. TiO_2 for phlogopites from Lac de Gras and Somerset Island kimberlites (after Mitchell 1986)

Figure 6.6 shows BaO vs Al_2O_3 content for all analyzed phlogopites. Although it is clear that BaO contents of the phlogopites generally increase from the core to the mantle of the crystals, no systematic patterns exists relating Al_2O_3 to BaO. Conversely, a distinct relationship exists between Ba and K. The diadocy of Ba and K within the micas, emphasized in Figure 6.7, exhibits the significant sympathetic variation of K with respect to Ba, that is, a fairly obvious complementary decrease in K in the interlayer sites as Ba increases. A least-squares line was fitted to all the data and its slope of 1.18 indicates little involvement of other alkali or alkaline earths in the A-site of the crystal. The slight deviation from an ideal slope of 1.0, however, may suggest potassium loss as a result of phlogopite alteration or may reflect an analytical error.

In contrast with phlogopite from Somerset Island (Figure 6.8), the Lac de Gras kimberlites show far less range in their TiO_2 content. Furthermore, TiO_2 content is, on average, much lower than other kimberlites. Conversely, Cr_2O_3 contents of the Lac de Gras kimberlites shows no significant deviation from other kimberlite intrusions.

6.1.3. Monticellite

6.1.3.1. Introduction

Prior to 1975 monticellite was considered a relatively rare and minor mineral in kimberlites. Microprobe studies have now established monticellite as a fine-grained constituent in the groundmass of many kimberlite matrices (Clement *et al.* 1975, Mitchell 1978, Skinner and Clement 1979).

Monticellite occurs principally as small (0.005-0.08 mm) subhedral-to-euhedral crystals ranging from trace quantities to a major groundmass phase (60-80 vol.%, Mitchell 1986). Monticellite occurs as colourless crystals that are typically zonation-free and lack inclusions of silicate and oxide phases. Monticellite crystallizes after spinel and perovskite and prior to late-stage primary groundmass serpentine and calcite

In this study, monticellite is present in variable quantities (up to ≈40 vol.%) in the groundmass as subhedral-to-euhedral crystals in nearly all of the kimberlites examined.

Table 6.3. Representative Compositions of Monticellite from Lac de Gras Kimberlites[a].

Wt. %	1	2	3	4	5	6	7
SiO_2	37.02	37.65	37.91	37.29	36.65	38.69	36.55
Al_2O_3	0.15	0.20	0.00	0.07	0.01	2.20	0.00
FeO[b]	7.43	5.80	7.92	6.24	5.87	6.79	6.95
MnO	0.12	0.26	0.16	0.34	0.17	0.43	0.52
MgO	20.51	22.51	20.65	23.35	22.05	23.23	24.87
CaO	35.72	33.55	34.68	33.18	34.57	28.47	32.10
	100.95	99.97	101.32	100.47	99.32	99.81	100.99
Mol % end member molecules							
Ks	16.23	13.13	17.88	13.89	13.21	16.13	15.13
Mo	82.46	82.94	81.16	79.56	85.18	69.42	73.26
Fo	1.31	3.93	0.96	6.54	1.61	14.46	11.61

Wt. %	8	9	10	11	12	13	14
SiO_2	35.11	36.78	35.21	37.89	38.66	38.42	38.21
Al_2O_3	0.66	0.01	0.00	0.00	0.00	0.04	0.00
FeO[a]	8.94	8.24	8.64	5.13	4.92	7.05	6.05
MnO	0.19	0.34	0.61	0.33	0.16	0.34	0.34
MgO	21.74	21.26	20.34	25.06	25.89	23.52	23.77
CaO	31.40	33.48	33.24	31.66	32.03	30.38	31.41
	98.04	100.11	98.04	100.07	101.66	99.75	99.78
Mol % end member molecules							
Ks	20.46	18.63	19.88	11.42	10.75	16.13	13.73
Mo	70.43	77.11	76.86	77.74	77.75	71.81	76.43
Fo	9.11	4.27	3.26	10.84	11.51	12.05	9.84

[a]1-10, T29S, 11-14 C27, 1, 3, 4, 5, 7, 11, 13 represent cores; 2, 6, 8, 9, 10, 12, 14 represent rims.
[b]Total Fe calculated as FeO; Ks = $CaFeSiO_4$, Mo = $CaMgSiO_4$, Fo = Mg_2SiO_4.

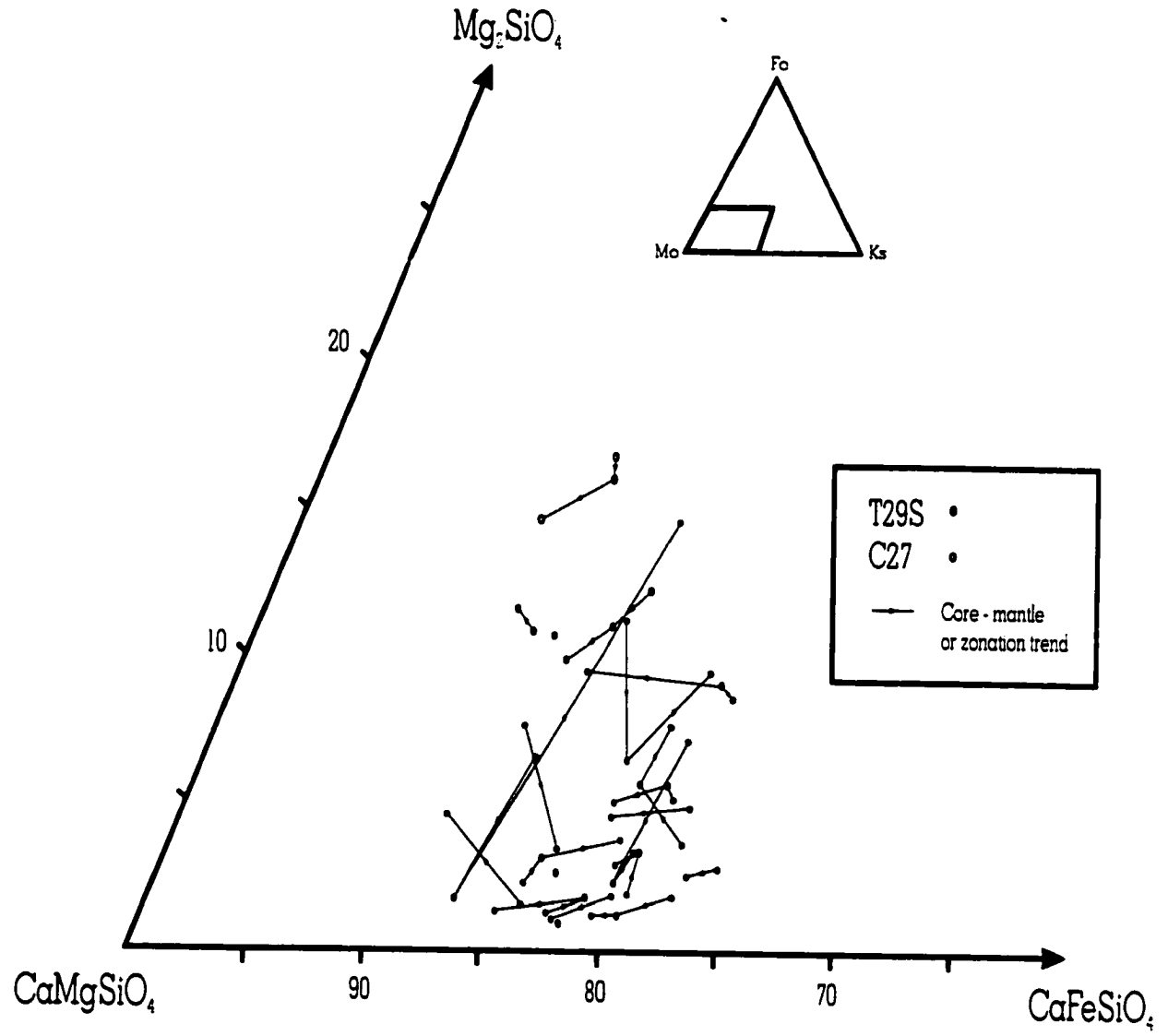

Figure 6.9. Chemical composition of monticellite from the Lac de Gras kimberlite field. Compositions are plotted on the triangular diagram forsterite (Mg_2SiO_4)-monticellite ($CaMgSiO_4$)-kirschtenite ($FeMgSiO_4$).

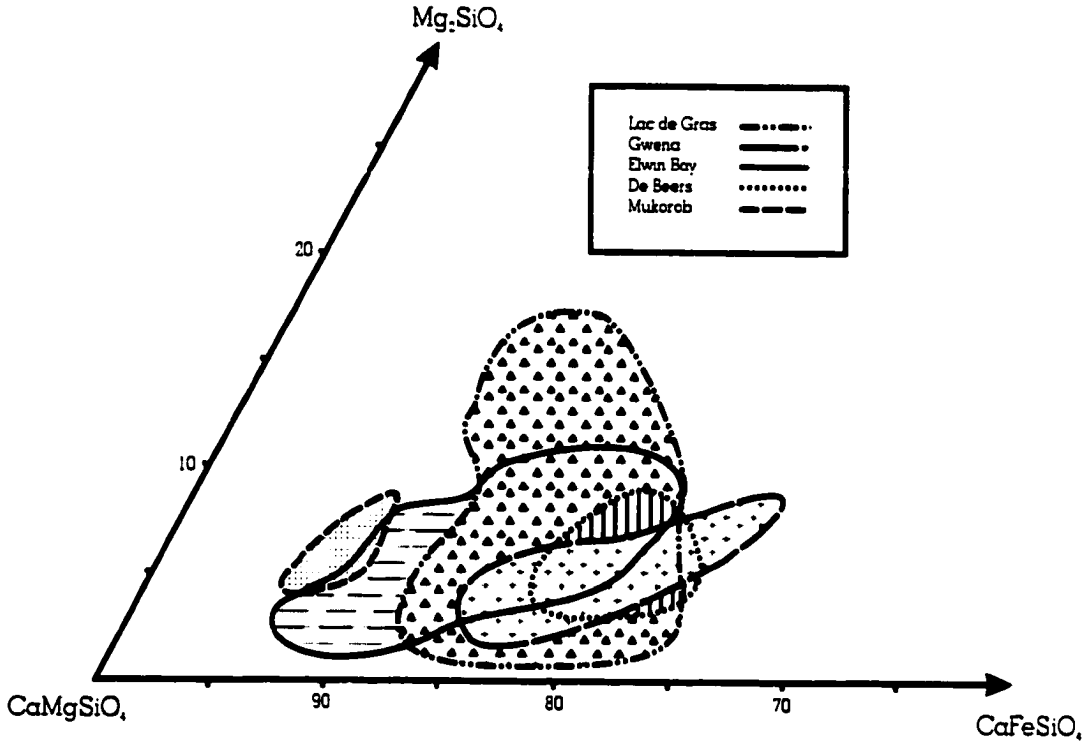

Figure 6.10. Composition of monticellite from Lac de Gras (this study), Gwena (Kampata *et al*. 1994), Elwin Bay (Mitchell 1978), De Beers (Clement *et al.* 1975) and Mukorob (Mitchell 1986).

Fresh monticellite, however, is rare; groundmass crystals are typically completely replaced by calcite and less commonly serpentine. Monticellite was also found replacing serpentinized microphenocrystal groundmass olivine. Groundmass plates of phlogopite commonly poikilitically enclose euhedral-to-subhedral monticellite.

6.1.3.2. Composition of Monticellite within the Lac de Gras Kimberlites

Monticellite within the Lac de Gras kimberlites occurs as relatively pure $CaMgSiO_4$, exhibiting moderate solid solution toward kirschtenite (10-24 mol% $CaFeSiO_4$) and forsterite (<1-12 mol% Mg_2SiO_4). The compositional variations are illustrated in Figure 6.9 and representative analyses are given in Table 6.3.

Magnesium generally increases from the core to the margins of crystals, calcite typically decreases and monticellite may be zoned from relatively iron-rich cores to iron-poor margins, or vice versa. Significant intergrain compositional variation is common and zonation-free crystals of monticellite do occur.

Comparative data for monticellite from other kimberlites are shown in Figure 6.10. Monticellite from Lac de Gras kimberlites shows a wider compositional range than monticellite from other kimberlites, particularly evident is the broad range of solid solution towards Mg_2SiO_4. Figure 6.10 also suggests that individual kimberlites are characterized by monticellite of a particular composition; however, too few data are available to confirm this observation.

6.2. SPINEL MINERALOGY OF THE FORT À LA CORNE KIMBERLITES

Representative microprobe analysis of spinels from juvenile lapilli within pyroclastic kimberlite are given in Table 6.4 and the field of compositions of the spinels is plotted in Figure 6.11 as end-member spinel molecules in a reduced-iron spinel prism as outlined by Mitchell and Clarke (1976). Three types of parageneses of spinels have been recognized, in this work, to exist in the Fort à la Corne kimberlites:

Table 6.4. Representative Compositions of Spinel from the Fort à la Corne Kimberlite Field[a].

	1	2	3	4	5	6	7	8	9	10
TiO_2	6.63	4.28	4.54	4.58	7.73	7.71	10.60	4.84	6.20	5.89
Al_2O_3	5.60	9.94	5.30	6.28	8.35	9.62	9.78	6.67	7.50	10.10
Cr_2O_3	49.62	50.16	54.77	56.46	40.89	40.00	30.71	55.66	49.03	47.43
FeO[b]	23.33	24.32	24.81	22.06	29.58	30.48	35.51	23.05	26 21	25.66
MnO	0.38	0.43	0.33	0.73	0.47	0.23	0.19	0.62	0.77	0.40
MgO	12.90	11.01	9.79	10.00	11.39	10.92	11.49	10.07	9.54	11.14
	98.46	100.14	99.54	100.11	98.41	98.96	98.28	100.91	99.25	100.62
Recalculated analyses										
$Fe^{2+}O$	18.41	20.34	21.61	21.21	22.09	23.40	25.04	21.78	23.29	21.80
$Fe^{3+}_2O_3$	5.47	4.42	3.56	0.94	8.33	7.87	11.64	1.41	3.24	4.29
	99.01	100.58	99.90	100.20	99.24	99.75	99.45	101.05	99.58	101.05

	11	12	13	14	15	16	17	18	19	20
TiO_2	15.30	5.18	21.54	21.39	18.57	13.22	22.37	21.55	18.54	19.32
Al_2O_3	12.98	9.74	8.55	7.75	15.62	13.97	11.72	10.56	9.33	9.74
Cr_2O_3	0.31	49.64	0.39	0.59	0.05	10.23	1.14	0.63	9.46	6.98
FeO[b]	53.58	23.64	50.04	51.40	46.17	43.73	41.14	42.13	41.33	41.62
MnO	0.42	0.48	0.53	0.64	0.58	0.21	0.56	0.56	0.62	0.67
MgO	12.34	10.84	13.04	13.02	16.62	13.34	21.45	22.79	16.97	21.67
	94.93	99.52	94.09	94.79	97.61	94.70	98.38	98.22	96.25	100.00
Recalculated analyses										
$Fe^{2+}O$	27.46	21.11	30.80	30.71	24.87	24.22	19.76	17.59	22.79	17.62
$Fe^{3+}_2O_3$	29.03	2.82	21.39	23.00	23.67	21.68	23.17	27.27	20.60	26.67
	97.84	99.80	96.23	97.09	99.98	96.87	100.67	100.95	98.31	102.67

[a]1-10, titanian aluminous magnesian chromite (TIAMC), 11-20, magnesian-ulvospinel-ulvospinel-magnetite (MUM)
[b]Total Fe calculated as FeO

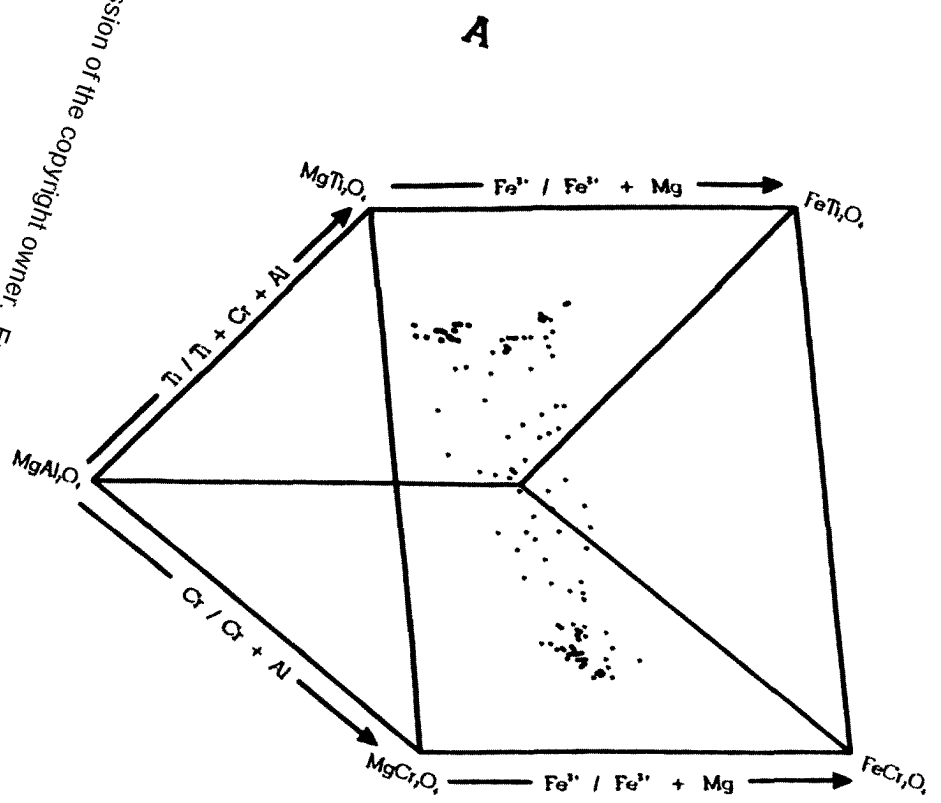

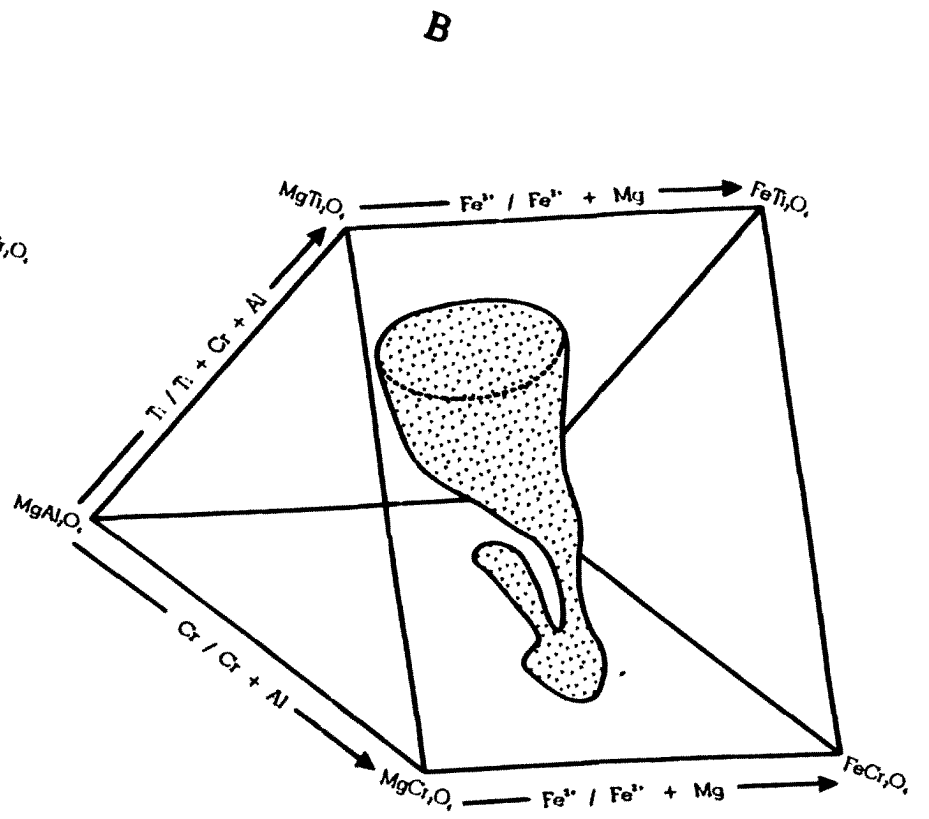

Figure 6.11. Compositions of spinels (*A*) and compositional field of spinels from the Fortà la Corne kimberlites (*B*).

1. Rare Cr-rich macrocrystal spinels;
2. TIAMC groundmass spinels;
3. Relatively pure reaction-product magnetite.

6.2.1. Homogeneous Macrocrystal Spinels

These crystals are rare (less than 5 observed in all sections) in all of the sections and typically occur as relatively large (<0.5 mm) rounded, translucent reddish-brown-to-orange grains. These crystals plot near the basal plane of the spinel prism and are typically poor in TiO_2 (<2%) and are Cr-rich. These Ti-bearing magnesian chromites are best described as aluminous magnesian chromites and are similar in composition to homogeneous titanian aluminous magnesian chromites (TIAMC) found within the groundmass of some units.

6.2.2. TIAMC Groundmass Spinels

This compositional trend is across the spinel prism from the base near the $MgCr_2O_4$-$FeCr_2O_4$ join [Cr/(Cr+Al) = 0.8-0.9, Fe/(Fe = Mg) = 0.4-0.65] toward the rear rectangular face and upward toward the Mg_2TiO_4-Fe_2TiO_4 apex. Spinel evolution is from TIMAC containing less than 5wt.% TiO_2, toward members of the magnesian ulvöspinel-ulvöspinel-magnetite, with greater than 10wt.% TiO_2, series (MUM). Fe/(Fe + Mg) ratios generally increase slightly (0.55-0.075) towards the rear plane of the spinel prism. The groundmass crystals are aluminous (6-14 wt.% Al_2O_3) and Al_2O_3 typically increases with decreasing Cr_2O_3 and increasing TiO_2 and FeO from the core to the mantle of the spinel crystal. MgO in relatively constant, but may increase or decrease slightly. As the composition of these spinels traverses the prism, Fe/(Fe + Mg) ratios remain relatively constant.

Many of the groundmass spinels within this magmatic trend show an initial enrichment in FeO, TiO_2 and Al_2O_3. These spinels show an initial decrease in the FeO, TiO_2, and Al_2O_3 and an increase in Cr_2O_3, traversing the basal plane of the spinel prism

toward the $MgCr_2O_4$-$FeCr_2O_4$ join before reversing this trend and following the basal plane of the spinel prism toward the $MgAl_2O_4$-$FeAl_2O_4$ join and up towards the Al_2TiO_4-Fe_2TiO_4 apex. This reversal is a reflection of a subsequent increase in TiO_2, FeO and Al_2O_3 with a corresponding decrease in Cr_2O_3.

In one of the kimberlites studies (H50) the groundmass spinels are homogeneous crystals that are characterized by MUM spinel series compositions. In this kimberlite TIMAC are not present. Conversely, kimberlite H32 contains homogeneous TIAMC spinels; the MUM series does not appear to have crystallized as a mantle, or has been resorbed on many groundmass crystals.

6.2.3. Reaction Product Spinels

Fort à la Corne kimberlites contain a profuse amount of small (<5μm) euhedral magnetite crystals scattered throughout the iron-poor matrix and mantling serpentinized olivines which were formed during retrograde serpentinization of the olivine under relatively oxidizing conditions. Amorphous magnetite may nearly entirely pseudomorph primary groundmass olivines and may occur as small, discontinuous veinlets cutting the kimberlite. The magnetite in both cases is very pure Ti-free magnetite.

6.2.4. Discussion

In contrast with spinel trends of the Lac de Gras kimberlites, the Fort à la Corne kimberlites contain significantly less alumina (pleonaste and titanian ferripleonaste are absent). If digestion of wall rock xenoliths is responsible for the elevated Al-contents within the Lac de Gras kimberlite and rapid cooling resulted in the preservation of Al-rich phases, because the Fort à la Corne kimberlites contain negligible amounts of wall rock fragments (all analyzed kimberlites came from juvenile lapilli within pyroclastic rocks) Al-contents would not be expected to be high. Furthermore, atoll spinels are rarely preserved at Fort à la Corne. When an outer, fretted rim is preserved, it is a

relatively pure Ti-free magnetite, whereas at Lac de Gras their outer rims contain a significant amount of MgO and TiO_2.

CHAPTER 7. SUMMARY AND DISCUSSION OF THE LAC DE GRAS KIMBERLITES

7.1. SUMMARY OF THE PETROGRAPHIC FEATURES OF THE LAC DE GRAS KIMBERLITES

The kimberlites observed within this study are composed of two broad textural types: hypabyssal kimberlite and volcaniclastic kimberlite. Hypabyssal kimberlite is commonly present as single small isolated dyke segments probably less than 100 m in length along strike. Many of these dykes exhibit a heterogeneous appearance due to the effects of flow differentiation. Contact metamorphism, when well-preserved core allows recognition, appears slight, resulting in minor baking and bleaching of the host rock. In intrusions such as T33, more spectacular effects of magmatic differentiation are observed.

These intrusions are of little economic interest, consequently delineation drilling has been limited and has not provided the necessary exposure to determine further the shape, size and depth of these dykes.

Macroscopically, the hypabyssal kimberlites appear relatively fresh gray-green to gray-black in colour. The kimberlites range from nearly aphanitic-to-macrocrystal and are composed of <5-50% fresh-to-altered olivine (up to 10 mm in size), minor pyroxene macrocrysts and subhedral-to-euhedral groundmass olivine microphenocrysts. Microxenoliths of rounded polycrystalline lherzolite may be common in individual samples. Macrocrystal mica is not typically present, but may occur rarely as a major macrocrystal phase.

Microscopic studies reveal a groundmass typically oxide-rich, composed of numerous subhedral-to-euhedral discrete and complex atoll spinels. Perovskite is usually present and may be abundant. Oxides, together with sulphides (pyrite, pyrrhotite and rare Fe-Ni-sulphides), apatite (as discrete euhedral-to-subhedral prisms or as acicular sprays of prismatic crystals) and rare accessory phase such as barite, rutile, zircon and ilmenite are set in a mesostasis composed of serpentine and calcite ± phlogopite. The constituents of the mesostasis are commonly intimately intergrown. Within a suite of samples,

commonly all are present, but within a single examples one may be absent or one may dominate. The mesostasis may exhibit a "sugary"-granular texture. This texture is generally due to the presence of small, commonly pseudomorphed (by calcite or serpentine and rarely dolomite) crystals of monticellite.

Small, amoeboid-shaped and irregular veins of oxide-free segregations filled with coarse interlocking calcite and lined with yellow-brown, botryoidal serpophite are prevalent. Euhedral calcite and dolomite rhombs may occur along their margins. Smaller segregations may be filled entirely with serpophite. The segregations may contain apatite, as stout euhedral prisms or radiating sprays of slender crystals. The margins of these segregations are generally gradational (<100 μm) with the silicate-oxide matrix and small crystals of apatite, phlogopite, calcite and rarely diopside may project from this matrix into the segregations. These segregations are clearly result from the separation of the late-crystallizing components of the magma into discrete masses (Mitchell 1986).

Hypabyssal rocks also occur in direct contact with volcaniclastic kimberlite within the vents. These rocks are similar in character to the hypabyssal dykes described above. These units of hypabyssal rock are generally thin (3 m to 15 cm in thickness). This rock may represent one of the following:

1. large autoliths of hypabyssal kimberlite, disrupted during emplacement and incorporated into the volcaniclastic host;

2. small, sub-horizontal sills which were emplaced subsequent to kimberlite emplacement and vent infill.

Lack of exposure precludes further speculation as to the nature and origin of these hypabyssal rocks.

Many of the kimberlites within this study are relatively small vents (most less than 2 ha) infilled with volcaniclastic kimberlite. A conspicuous macroscopic feature of this rock is the common presence of wood fragments and discrete xenoliths (commonly poorly consolidated) of mudstone and shale. Field and Scott Smith (1998) suggest these shale clasts must have been derived from a sedimentary cover of marine origin, which

overlay the Precambrian basement at the time of kimberlite emplacement, but which has since been eroded. Small, thin beds of laminated silt-and mudstone may represent water-lain non-kimberlite units formed during a hiatus in vent infill

Sorting is a common process during the deposition of volcaniclastic kimberlites at Lac de Gras. While a single sample may show a limited size range of olivine macrocrysts, a suite of samples from an individual vent displays a wide variety of grain sizes (from 10 mm to less than 2 mm). Volcaniclastic kimberlites are characterized by abundant xenocrysts of disseminated biotite, feldspar and minor quartz and muscovite within the groundmass. The presence of such material suggests that much of the volcaniclastic kimberlite at Lac de Gras is likely to have been deposited by resedimentation processes and so can therefore be termed resedimented volcaniclastic kimberlite. Individual beds or bedding contacts are not generally sharp, but highly gradational. Many units within the vents appear to be relatively poorly sorted suggesting gravity may have been a common transporting agent within the kimberlites at Lac de Gras.

Juvenile lapilli are common, although they may be poorly developed, in the volcaniclastic infill and may be easily mistaken for autoliths. These microphenocrystal fragments are characterized by the presents of partially fresh-to-completely altered microphenocrystal olivine, abundant groundmass spinels, common perovskite and phlogopite. The mesostasis consists of finely intergrown serpentine and calcite. Small circular-to-subcircular, calcite-filled vesicles are common. Resedimented volcaniclastic units may be rich in juvenile material.

Pyroclastic kimberlites do occur and form small parts of some vents. These units occur in contact with resedimented volcaniclastic kimberlite. Pyroclastic kimberlite contains abundant juvenile lapilli (with rare welding), common subrounded country rock fragments and mantle-free macrocrysts of olivine cemented with undoubtedly secondary, coarse, interlocking calcite. Calcite may be replaced with brown-gray serpentine. Such units may represent *in situ* lapilli tuffs that have subsequently been cemented with calcite. Rare lapilli with thin selvages are present within the kimberlites that show a superficial resemblance to the pelletal lapilli in diatreme rocks. In summary, the Lac de Gras

kimberlites appear to be mainly steep-sided vents, which are infilled with resedimented volcaniclastic kimberlite ± pyroclastic kimberlite and ± non-kimberlitic mud- and siltstone. Hypabyssal kimberlite may occur in contact with the above infill. Isolated segments of hypabyssal dykes are also common.

It is important to note that no tuffisitic kimberlite breccia, characteristic of diatreme-facies kimberlite have been identified in any of the kimberlites examined in this study. Diatreme-facies kimberlite appears to be lacking in the Lac de Gras area. Although there have been reports of diatreme-facies kimberlite occurring within the Lac de Gras region, Field and Scott Smith (1998) feel that these occurrences have been incorrectly interpreted. Hence, the presence of any diatreme-facies kimberlite has yet to be confirmed.

7.2. ROCK-TYPE CLASSIFICATION

All observed features are characteristic, but not exclusive to kimberlites. The vesicular juvenile fragments are atypical of most kimberlites, but are characteristic of kimberlites within Saskatchewan (*i.e.*, Fort à la Corne and Sturgeon Lake). The composition of spinel, monticellite and phlogopite (reviewed in Chapter 6) are typical of archetypal kimberlites, although spinels are conspicuously aluminous and phlogopites are Ba-rich. The nature of the primary mineralogy and mantle-derived xenocrysts suggests that these rocks are archetypal kimberlites as defined by Mitchell (1997) and Wooley *et al.* (1996).

7.3. MODE OF EMPLACEMENT: A COMPARISON OF THE LAC DE GRAS KIMBERLITES WITH THE SASKATCHEWAN AND SOUTHERN AFRICAN "END-MEMBER" KIMBERLITES

7.3.1. Introduction

Kimberlites differ from many volcanic rocks in that no extrusive magmatic or effusive rocks or plutonic equivalents have yet been found. Consequently kimberlites are postulated to have unique styles of eruptions (for example, Clement and Skinner 1979, 1985; Clement 1982; Clement and Reid 1989) which differ from standard volcanic processes presented in the literature (for example Fisher and Schmincke 1984; Cas and Wright 1987; McPhie *et al.* 1993). Good exposures created during extensive mining and exploration drilling over the past two decades has enabled scientists to more fully understand the complex geology of kimberlites.

Comparing the nature of kimberlite vents (refer to Chapters 4 and 5) shows that there are two contrasting end member emplacement mechanisms that are repeated in time and space. Two emplacement models illustrate these mechanisms:

1. southern African "classic" diatreme model;
2. Saskatchewan maar-like phreatomagmatic model.

The latter is driven by meteoric water in phreatomagmatic processes, whereas much debate still exists whether the former is driven by juvenile gases (fluidization model) or hydrovolcanic processes (refer to Chapter 4). Field and Scott Smith (1998) have proposed that the near surface geological setting at the time of kimberlite emplacement plays a critical role in determining the emplacement process of the kimberlite magma.

7.3.2. Juvenile Lapilli

The discussion in Chapters 4 and 5 (Orapa and Fort à la Corne kimberlites) clearly illustrates that these different kimberlite vents are characterized by different juvenile fragments. Whereas Orapa contains unique rounded "pseudo pelletal lapilli" identical to lapilli found within diatreme-facies kimberlite, of which microlitic diopside is a chief constituent, Fort à la Corne kimberlites are characterized by vesiculated amoeboid-shaped microporphyritic fragments and non-vesiculated fragments which are cored by macrocrystal or xenocrystal fragments.

Lac de Gras, in contrast, contains a variety of juvenile lapilli, many of which are superficially similar to both varieties at Fort à la Corne. Many of the juvenile lapilli within the Lac de Gras kimberlites are poorly developed and may be difficult to recognize due to extensive alteration. Most beds of volcaniclastic kimberlite contain a wide variety of juvenile lapilli; both vesiculated and non-vesiculated, aphanitic and microporphyritic, uncored and amoeboid-shaped, and rounded pelletal-lapilli like fragments. Moreover, composite structures, which likely represent recycled lapilli are common, as are fine-grained chilled margins.

The nature of the juvenile fragments further reinforces the significantly different character of volcaniclastic infill found within the Lac de Gras kimberlites when compared to the two contrasting "end-member" kimberlite models. This is undoubtedly related to different emplacement mechanisms operating within these different environments.

7.3.3. Emplacement Models

As was initially suggested by Field and Scott Smith (1998), the Lac de Gras kimberlite vents appear to be formed by two distinct processes, vent excavation and subsequent vent infilling. The presence of non-kimberlitic sediments within the vent infill (even at considerable depths) suggests that vent infilling was a long-lived process. Pyroclastic rock also contributed to vent infill.

The steep-sided, relatively shallow vents are superficially similar to the maar-like kimberlites in the Canadian Prairies. Kimberlites of the Fort à la Corne area are shallow saucer-to-champagne glass-shaped Cretaceous bodies composed of volcaniclastic kimberlite. There is no evidence of the development of any root zone or diatremes below the craters. Moreover, no hypabyssal or tuffisitic kimberlite has been encountered in any of the bodies. The vent shape and the nature of the infill at Fort à la Corne show that the southern African-style diatreme emplacement processes, which are driven by juvenile gases, have not taken place. The shape of the vents, *i.e.* flaring rapidly towards the surface with low depth to diameter ratios, are similar to maars and therefore probably represent explosion craters excavated only into the soft overlying Cretaceous sediments. The crater formation is suggested to result from maar-like phreatomagmatic processes with the resulting material deposited mainly as extra-crater deposits. Although no extra-crater deposits have been preserved in the Fort à la Corne kimberlites, the presence of a porous sandstone unit, a well-known aquifer, occurs in the area from which many of the craters flare thus providing strong circumstantial evidence for phreatomagmatic maar-like processes to have occurred.

The craters were subsequently infilled by subaerial primary pyroclastic magmatic processes ranging from Hawaiian-Strombolian, which result in the formation of true juvenile lapilli by the fragmentation of magma to a much more kimberlite-specific pyroclastic eruption style as a result from rapid degassing of magmas near surface. The latter is characterized by vesicle-free lapilli with thin selvages that are somewhat similar to the pelletal lapilli, which are the hallmark of diatreme-facies kimberlite.

The shape of the vents at Lac de Gras, with low diameter-to-depth ratios, contrast with those of kimberlites that occur at Fort à la Corne and other explosion craters which are typically much shallower. The steep-sided vents of the Lac de Gras area appear to be broadly similar in shape to southern African diatremes (cf. Clement 1982). However, the lack of tuffisitic kimberlite breccia, an integral part of diatreme infill, suggests that diatreme formation did not occur. No evidence of recycled pelletal lapilli within volcaniclastic infill was observed. Furthermore, Lac de Gras vents are much smaller than

their southern African counterparts, both in diameter and depth which suggests less powerful or shorter-lived eruptions were responsible for the excavation of these vents.

Archean basement rocks of the Lac de Gras area could have offered a difficult route to the surface for the kimberlite magma, which allowed for a moderate build up of sub-surface juvenile volatiles. However, the Lac de Gras area lacked the competent cap rocks, which in southern Africa were massive basalts. Poorly consolidated wet sediments overlaid the Archean basement at Lac de Gras and breakthrough would have been relatively easy. However, neither the overlying Cretaceous sediment nor the craters that presumably were formed within them have been preserved.

Because the kimberlite vents at Lac de Gras are predominantly filled with resedimented volcaniclastic kimberlite and minor pyroclastic lapilli tuffs, the process of vent excavation and infill must have been different from Fort à la Corne where resedimentation processes operate, but primary pyroclastic rock commonly accounts for the majority of vent infill. Furthermore, the lack of diatreme-facies tuffisitic kimberlite breccia and the smaller nature of the kimberlite vents at Lac de Gras preclude the utilization of the southern African emplacement model as a workable interpretation to their formation. Clearly, a third, intermediate model will have to be developed to account for the features observed within the Lac de Gras kimberlites.

7.4. EMPLACEMENT OF THE LAC DE GRAS KIMBERLITES

The presence of wood fragments and poorly consolidated non-kimberlitic sediments within resedimented volcaniclastic kimberlite, at depths greater than 400 m, indicates, without a doubt, that the Lac de Gras kimberlites were formed by two distinct processes: 1. vent excavation; 2. vent infill. The nature of the processes responsible for the complete evacuation of the kimberlite vents is unclear.

It has been clearly established that at the time of kimberlite emplacement significant amounts of poorly consolidated wet sediments overlay the Archean basement terrain within the Lac de Gras area. Obviously, local hydrogeological conditions were such that a significant amount of groundwater was available. Moreover, subaqueous

kimberlite eruption cannot be ruled out. As the kimberlite magma made its way to the surface [root zone development probably occurred as outlined by Clement (1979, 1982) and Clement and Reid (1989)] it likely came into contact with groundwater. Hence, phreatomagmatic processes (and perhaps downward migration of phreatomagmatic activity) contributed to the evacuation of the kimberlite vents. A flaring explosion crater or maar was likely evacuated into the soft, overlying sediments with resultant ejecta deposited as extra-crater material, perhaps as a tuff ring or cone. This material was than reworked and redeposited within the evacuated vent by debris flow and mass wasting processes, incorporating large amounts of xenolithic material. Again, whether these processes operated subaqueously in unknown.

Apparent primary pyroclastic kimberlite occurs as relatively small units within many kimberlite intrusions; however, these tuffs do not contribute significantly to the vent infill. These units are composed of abundant vesiculated and non-vesiculated juvenile lapilli, single crystals of macrocrysts and mantle-derived xenocrysts and very minor amounts of country rock xenoliths and xenocrysts. Pyroclastic kimberlite beds may also contain composite juvenile lapilli structures may suggest that minor pyroclastic activity continued through a central conduit subsequent to vent excavation and the beginnings of vent infill and disrupted previously deposited poorly consolidated beds. The pyroclastic kimberlite does not appear to have undergone resedimentation processes and the preservation of welding and molding textures as well as the lack of abrasion of fragile juvenile fragments supports this hypothesis. Conversely, these units may represent primary pyroclastic kimberlite initially deposited within the tuff cone/ring, during the initially evacuation of the vent, that subsequently fell back into the vent, with little reworking, as a large, coherent mass preserving nearly all of the primary textures within the tuff. In this case, these units are not primary pyroclastic kimberlites, but are resedimented "pseudo-pyroclastic kimberlite" that has been redeposited.

Vent infill appears to be a long-lived process. The volcaniclastic rocks that were deposited within the vent were initially unconsolidated and highly permeable. Groundwater would easily enter and fill the pore space and react with the available mineral assemblage. Therefore, the volcaniclastic material would become highly altered

and indurated. The presence of late stage intrusive hypabyssal kimberlite sills within many kimberlite vents suggests that additional batches of magma rose to near surface environments and intruded the kimberlite vents subsequent to their infill. These sills may have contributed to the alteration of the volcaniclastic infill suggesting, at least locally, some alteration may be hydrothermal.

Evidence (although scant within this study) exists that some megaxenoliths (>15 m in dimension) sit within the kimberlite vents. These likely represent large portions of wall rocks that broke off during eruption of the kimberlite and slumped back down into the vent.

7.5. FURTHER STUDIES

Obviously more detailed studies will need to be undertaken on the Lac de Gras kimberlites to further constrain the nature of the vent infill and emplacement. Such studies can only occur with the creation of better exposures during mining and advanced exploration activities.

One other enigma that remains and has never been properly addressed is the whereabouts of the extensive extra-crater material deposited during kimberlite emplacement. No secondary sources of kimberlitic-material have been discovered within the Slave Structural Province, which clearly warrants further investigation.

REFERENCES

Agee J.J., Garrison J.R., Taylor L.A. 1982. Petrogenesis of oxide minerals in kimberlite, Elliot County, Kentucky. *American Mineralogist*, **67**: 28-42.

Akella J, Rao P.S. McCallister R.H., Boyd F.R., Meyer H.O.A. 1979. Mineralogical studies of the diamondiferous kimberlite of the Wajrakharur area, Southern India. *SIKC*, **1**: 172-177.

Bates R.L., Jackson J.A. (eds.). 1984. *Dictionary of Geological Terms*. Doubleday, New York.

Berg G.W., Carlson J.A. The Leslie kimberlite pipe of Lac de Gras, Northwest Territories, Canada: Evidence for near surface hypabyssal emplacement. Extended Abstracts of the Seventh International Kimberlite Conference, Cape Town, South Africa: 81-83.

Bowring S.A., Williams I.S., Compston W. 1989. 3.96 Ga gneisses from the Slave Province, Northwest Territories, Canada. *Geology*, **17**: 971-975.

Card K.D., King J.E. 1992. The tectonic evolution of the Superior and Slave provinces of the Canadian Shield: introduction. *Canadian Journal of Earth Sciences*, **29**: 2059-2065.

Carlson J.A., Kirkley M.B., Thomas E.M., Hillier W.D. 1998. Recent major kimberlite discoveries in Canada. Extended Abstracts of the Seventh International Kimberlite Conference, Cape Town, South Africa: 127-131.

Carswell D.A. 1975. Primary and secondary phlogopites in garnet lherzolite xenoliths. *Physics and Chemistry of the Earth*, **9**: 417-430.

Cas R.A.F., Wright J.V. 1987. *Volcanic successions: Modern and Ancient*. Allen and Unwin, London. 518 pp.

Clement C.R. 1979. The origin and infilling of kimberlite pipes. *In* Extended Abstracts, Kimberlite Symposium II, Cambridge, England.

Clement C.R. 1982. A comparative geological study of some major kimberlite pipes in the northern Cape and Orange Free State. Unpublished Ph.D. thesis, University of Cape Town, South Africa.

Clement C.R., Gurney J.J., Skinner E.M.W. 1975. Monticellite: An abundant groundmass mineral in some kimberlites. Kimberlite Symposium I: Cambridge, Extended Abstracts: 71-73.

Clement C.R., Reid A.M. 1989. The origin of kimberlite pipes: an interpretation based on a synthesis of geological features displayed by southern African occurrences. *Geological Society of Australia Special Publication*, **14**: 632-646.

Clement C.R., Skinner E.M.W. 1979. A textural-genetic classification of kimberlite rocks. Kimberlite Symposium II, Cambridge, Extended Abstracts.

Clement C.R., Skinner E.M.W. 1985. A textural-genetic classification of kimberlites. *Transactions of the Geological Society of South Africa*, **88**: 403-409.

Clement C.R., Reid A.M. 1989. The origin of kimberlite pipes: an interpretation based on a synthesis of geological features displayed by southern African occurrences. *Geological Society of Australia Special Publication*, **14**: 632-646.

Cookenboo H.O. 1998. Emplacement history of the Jericho kimberlite pipe, northern Canada. Extended Abstracts of the Seventh International Kimberlite Conference, Cape Town, South Africa: 161-163.

Davis W.J., Kjarsgaard B.A. 1997. A Rb-Sr isochron age for a kimberlite from the recently discovered Lac de Gras Field, Slave Province, Northwest Canada. *Journal of Geology*, **105**: 503-509.

Dawson J.B. 1971. Advances in kimberlite geology. *Earth Science Reviews*, 7: 187-214.

Dawson J.B., Smith J.V. 1975. Chemistry and origin of phlogopite megacrysts in kimberlite. *Nature*, **253**: 336-338.

Doyle, B.J., Kivi K., Scott Smith B.H. 1998. The Tli Kwi Cho (DO27 and DO18) diamondiferous kimberlite complex, Slave Craton, Northwest Territories, Canada. Extended Abstracts of the Seventh International Kimberlite Conference, Cape Town, South Africa: 199-201.

Field M, Gibson J.G., Wilkes T.S., Gababotse J, Khujwe P. 1995. The geology of the Orapa A/K1 kimberlite, Botswana: further insight into the emplacement of kimberlite pipes. Extended Abstracts of the Sixth International Kimberlite Conference, Novosibirsk, Russia: 155-157.

Field M, Gibson J.G., Wilkes T.S., Gababotse J, Khujwe P. 1997. The geology of the Orapa A/K1 kimberlite, Botswana: further insight into the emplacement of kimberlite pipes. *In* Proceedings of the Sixth International Kimberlite Conference, *Russian Geology and Geophysics*, **38**(1). Kimberlites, Related Rocks and Mantle Xenoliths: 24-39.

Field M. Scott Smith B.H. 1998. Near Surface Emplacement of Kimberlites: Contrasting Models and Why. *Unpublished article*.

Fipke C.E., Dummett H.T., Moore R.O., Carson J.A., Ashley R.M., Gurney J.J, Kirkley M.B. 1995. History of the discovery of diamondiferous kimberlites in the Northwest Territories, Canada. Extended Abstracts of the Sixth International Kimberlite Conference, Novosibirsk, Russia: 158-160.

Fisher R.V., Schminche H-U. 1984. *Pyroclastic Rocks*. Springer Verlag. 472 pp.

Graham I., Burgess J.L., Bryan D., Ravenscroft P.J., Thomas E., Doyle B.J., Hopkins R., Armstrong K.A. 1998. The Diavik kimberlites – Lac de Gras, Northwest Territories, Canada. Extended Abstracts of the Seventh International Kimberlite Conference, Cape Town, South Africa: 259-261.

Hawthorne J.B. 1975. Model of a kimberlite pipe. ***Physics and Chemistry of the Earth***, **9**: 1-15.

Heaman L.M., Kjarsgaard B., Creaser R.A., Cookenboo H.O., Kretschmar U. 1997. Multiple episodes of kimberlite magmatism in the Slave Province, North America. *In* Cook F. and Erdmer (compilers) Slave-Northern cordillera Lithospheric Evolution (SNORCLE) transect and Cordilleran Tectonics Workshop Meeting, University of Calgary, LITHOPROBE Report No. 56: 14-17.

Kilham J., Field M., Stiefenhofer J. 1998. Orapa and Letlhakane mines. *In* Large Mines Field Excursion Guide, Seventh International Kimberlite Conference, Cape Town, South Africa: 11-21.

King J.E., Davis W.J., Relf C. 1992. Late Archean tectonomagmatic evolution of the central Slave Province, Northwest Territories. *Canadian Journal of Earth Sciences*, **29**: 2156-2170.

Kirkley M.B., Kolebaba M.R., Carlson J.A., Gonzales A.M., Dyck D.R., Dierker C. 1998. Kimberlite emplacement processes interpreted from the Lac de Gras examples. Extended Abstracts of the Seventh International Kimberlite Conference, Cape Town, South Africa: 429-431.

Kompata D.M., Nixon P.H., Salemink J. 1994. Monticellite in the Gwena kimberlite (Shaba, Zaire): evidence of late-magmatic crystallization. *Mineralogical Magazine*, **58**: 496-501.

Kopylova M.G., Russell J.K., Cookenboo H. 1998. Petrography and chemistry of the Jericho kimberlite (Slave Craton Northern Canada). Extended Abstracts of the Seventh International Kimberlite Conference, Cape Town, South Africa: 449-451.

Kretchmar, U. Drybones Bay diamondiferous kimberlite. Prepared for: Trade Winds Resources Ltd. 1997 PDAC Exploration Summary.

Leahy K. 1997. Discrimination of reworked pyroclastics from primary tephra-fall ruffs: a case study using kimberlites of Fort à la Corne, Saskatchewan, Canada. *Bulletin of Volcanology*, **59**: 65-71.

LeCheminant A.N., van Breeman O. 1994. U-Pb ages of Proterozoic dyke swarms, Lac de Gras area, NWT: Evidence for progressive break-up of an Archean supercontinent (abs.). *Geological Association of Canada, Program with Abstracts*, **19**: A62.

Leckie D.A., Kjarssguard B.A., Bloch J., McIntyre D., McNeil D., Stassiuk L., Heaman L. 1997. Emplacement and reworking of Cretaceous diamond bearing crater facies kimberlite of central Saskatchewan, Canada. *G.S.A. Bulletin*, **109**(8): 1000-1020.

Lehnert-Thiel K., Loewer R., Orr R.G., Robertshaw P. 1992. Diamond-bearing kimberlites in Saskatchewan, Canada: The Fort à la Corne case history. *Exploration and Mining Geology*, **1**(4): 391-403.

Lorenz V. 1973. On the formation of maars. *Bulletin of Volcanology*, **37**: 183-204.

Lorenz V. 1975. Formation of phreatomagmatic maar-diatreme volcanoes and its relevance to kimberlite diatremes. *Physics and Chemistry of the Earth*, **9**: 17-27.

Lorenz V. 1979. Phreatomagmatic origin of the olivine melilitite diatremes of the Swabian Al, Germany. *In Kimberlites, Diatremes and Diamonds: Their Geology, Petrology and Geochemistry* (F.R. Boyd and H.O.A. Meyer. eds.): 354-363. American Geophysical Union, Washington.

Lorenz V. 1984. Explosive volcanism of the West Eifel volcanic field, Germany. *TIKC*, **1**: 299-307.

Lorenz V. 1985. Maars and diatremes of phreatomagmatic origin, a review. *Transactions of the Geological Society of South Africa*, **88**: 459.

McKinlay F.T., Scott Smith B.H., De Gasparis S., Kong J. 1998. Geology of the recently discovered Hardy Lake kimberlites, NWT. Extended Abstracts of the Seventh International Kimberlite Conference, Cape Town, South Africa: 564-566.

McPhie J, Doyle M, Allen R. 1993. *Volcanic Textures*. Centre of Ore Deposit and Exploration Studies, University of Tasmania. 196 pp.

Mitchell R.H. 1978. Mineralogy of the Elwin Bay kimberlite Somerset Island, N.W.T., Canada. *American Mineralogist*, **63**: 47-57.

Mitchell R.H. 1986. *Kimberlites: Mineralogy, Geochemistry and Petrology.* Plenum Press, New York.

Mitchell R.H. 1995. *Kimberlites, Orangeites, and Related Rocks.* Plenum Press, New York

Mitchell R.H. 1997. *Kimberlites, Orangeites, Lamproites, Melilitites, and Minettes: A petrographic atlas.* Almaz Press Inc. 243 pp.

Mitchell R.H., Clarke D.B. 1976. Oxide and sulphide mineralogy of the Peuyuk kimberlite, Somerset Island, N.W.T., Canada. *Contributions to Mineralogy and Petrology*, **56**: 157-172.

Muan A., Hauck J., Lofall T. 1972. Equilibrium studies with a bearing on lunar rocks, *Proc. Soc. India Q. J.*, **33**: 69-87.

Nassichuk W.W., Dyck D.R. 1998. Fossils recovered from kimberlite pipes in the Lac de Gras field, Slave Province, Northwest Canada; geological implications. Extended Abstracts of the Seventh International Kimberlite Conference, Cape Town, South Africa: 612-614.

Nixon P.H., Leahy K. 1997. Diamond-bearing volcaniclastic kimberlites in Cretaceous marine sediments, Saskatchewan, Canada. *Russian Geology and Geophysics*, **38**(1): 17-23.

Padgham W.A. 1991. The Slave Province, an overview. *In* W.A. Padgham and D. Atkinson (eds.), *Mineral deposits of the Slave Province, Northwest Territories.* Geological Survey of Canada, Open File 2168: 1-40.

Padgham W.A., Fyson W.K. 1992. The Slave Province: a distinct Archean craton. *Canadian Journal of Earth Sciences*, **29**: 2072-2086.

Pasteris J.D. 1980. Opaque oxide phases of the De Beers kimberlite (Kimberley, South Africa) and their petrologic significance, Ph.D. thesis, Yale University.

Pasteris J.D. 1983. Spinel zonation in the De Beers kimberlite, South Africa: Possible role of phlogopite. *Canadian Mineralogist*, **21**: 41-58.

Pell J.A. 1996. Kimberlites in the Slave Structural Province, NWT, Canada. *The Gangue*, GAC Mineral Deposits Division Issue 51. January 1996: 1-4.

Pell J.A. 1997. Kimberlites in the Slave Craton, Northwest Territories, Canada: a preliminary review. *In* Proceedings of the Sixth International Kimberlite Conference, *Russian Geology and Geophysics*, **38**(1). Kimberlites, Related Rocks and Mantle Xenoliths: 5-16.

Roscoe S.M., Stubley M., Roach D. 1989. Archean quartz arenites and pyritic paleoplacers in the Beaulieu River supracrustal belt, Slave Structural Province, N.W.T. *In Current research, Part C.* Geological Survey of Canada, Paper 89-1C: 199-214.

Scott Smith B.H. 1995. Geology of the Sturgeon Lake 02 kimberlite block, Saskatchewan. *Exploration and Mining Geology*, **4**: 141-151.

Scott Smith B.H. 1996. Kimberlites. Chapter 10. Mineralogical Association of Canada Short Course Series. *In Undersaturated Alkaline Rocks: Mineralogy, Petrogenesis, and Economic Potential* (Mitchell R.H., ed.). Short Course Volume **24**, Winnepeg, Manitoba: 217-243.

Scott Smith B.H., Danchin R.V., Harris J.W., Stracke K.J. 1983. Kimberlites near Orroroo, South Australia: Appendix. Kimberlites III: Documents, *Annales Scientifique de l'Universite de Clermont-Ferrand II*, No. 74: 123-128.

Scott Smith B.H., Letendre J.P., Robison H.R. 1996. Geology of the Sturgeon Lake 01 kimberlite block, Saskatchewan. *Exploration and Mining Geology*, **5**: 251-261.

Scott Smith B.H., Orr R.G., Robertshaw P., Avery R.W. 1994. Geology of the Fort à la Corne kimberlites, Saskatchewan. The Sixteenth CIM district 6 Annual General Meeting, Vancouver, British Columbia.

Scott Smith B.H., Orr R.G., Robertshaw P., Avery R.W. 1995. Geology of the Fort à la Corne kimberlites, Saskatchewan. Extended Abstracts of the Sixth International Kimberlite Conference, Novosibirsk, Russia: 543-545.

Smith R.A. 1984. The lithostratigraphy of the Karoo Supergroup in Botswana. A report on the geophysical and geological results of follow-up drilling to the Aeromagnetic Survey of Botswana. *Botswana Geol. Survol. Dep. Bull.*, **26**.

Stasiuk L.D., Nassichuk W.W. 1995. Thermal history and petrology of wood and other organic inclusions in kimberlite pipes at Lac de Gras, Northwest Territories. *In Current Research* 1995-B, Geological Survey of Canada: 115-124.

Thompson P.H. 1989. Moderate overthickening of thinned sialic crust and the origin of granitic magmatism and regional metamorphism in low P - high-T terranes. *Geology*, **17**: 520-523.

Wooley A.R., Bergman S.C., Edgar A.D., Le Bas M.J., Mitchell R.H., Rock N.M.S., Scott Smith B.H. 1996. Classification of lamprophyres, lamproites, kimberlites, and the kalsilitic, melilitic, and leucitic rocks. *Canadian Mineralogist* **34**(2): 175-186.

APPENDIX A

MICROSCOPIC DIAMOND DRILL CORE LOGS FROM THE LAC DE GRAS KIMBERLITES

KCEI DIAMOND DRILL LOG

Drill Hole: 94A5-1
Northing: 7148815
Easting: 534165
Depth: 199.4 m

Dip: -90 Deg
Azimuth: 000
Core Size: NQ
Date Logged: Oct. 29 .98

0.0-22.5 m	**Water**
22.5-47.3 m	**Casing/Overburden**
47.3-78.0 m (95A5-1-1)	**Macrocrystal Kimberlite (volcaniclastic)** • much of the interval is very friable and incompetent; easily broken with hand • prevalent Fe-oxidation staining throughout interval and on open fracture surfaces • kimberlite appears to be matrix supported with abundant rounded olivine macrocrysts (up to 10 mm) • olivine population highly inequagranular and altered to a chalky white-to-pale green colour • carbonate veinlets common cutting core; may increasing in concentration producing anatomising networks • very few indicators noted; rare CD's, rare fresh olivine and garnets noted • kimberlite varies from a rubble-like competency to fairly competent core which can only be broken with a hammer • slickensides are common at high degrees to core axis • mica xenocrysts common (biotite and less common muscovite) • prevalent angular-to-subangular granodiorite xenoliths (up to 5 cm); contacts with host kimberlite tend to be sharp with little reaction • towards end of interval, larger xenoliths of granodiorite occur, up to 45cm in length along ca • mudstone xenoliths common (up to 5 cm) near end of interval
78.0-80.8 m	**Cretaceous Mudstone (inferred)** • friable, medium gray mudstone xenolith?; massive, featureless

94A5-1

80.8-81.7 m	**Granodiorite Xenolith** • highly oxidized, very broken up, highly altered granodiorite with a vuggy-like texture and secondary carbonate infilling • xenolith quite broken up, largest unbroken piece 20cm
81.7-83.1 m	**Pegmatite** • pink, pegmatite granite-quartz syenite vein • very coarse alkali feldspar of up to 4 cm in length
83.1-114.5 m	**Granodiorite Xenolith** • prevalent Fe-oxidation staining • highly altered, incompetent (may be broken with hand is some cases)
114.5-128.4 m	**Macrocrystal Kimberlite (volcaniclastic)** • kimberlite quite competent, >90% recovery • features quite similar to previous, 10% olivine macrocrysts, highly inequagranular, rounded-to-subrounded in nature • common large granodiorite xenoliths (up to 40cm); quite altered giving surface a pocked or vuggy appearance
123.0-123.15 m	• very high concentration of carbonate stringers cutting core (60-75% of core)
126.3-126.5 m (95A5-1-2)	• sudden increase in size of olivine macrocrysts and their respective concentration, no distinct contact measurable, gradual over several millimetres
128.4-132.8 m	**Granodiorite** • tonalite vein at 130.3-130.5 m (light gray, high plagioclase concentration)
132.8-137.6 m (95A5-1-3)	**Macrocrystal Kimberlite (Hypabyssal dyke?)** • high olivine content, very competent kimberlite
137.6-147.9 m	**Granodiorite with pink pegmatite intervals** • granodiorite medium-gray, medium-grained with poorly developed foliation
143.2-145.7 m	• increase in alkali feldspar concentration, more of a granitic composition

94A5-1

147.9-153.65 m	**Macrocrystal Kimberlite (hypabyssal?)** • similar to previous (132.8-137.6 m) with some obvious layering, i.e., coarse-grained, macrocrystal kimberlite versus dark-gray, fine-grained, nearly aphanitic kimberlite
147.9-151.9 m	• kimberlite very competent, composed of ≈15% (95A5-1-4) rounded, inequagranular olivine macrocrysts and micro-phenocrysts
151.9-152.9 m (95A5-1-5)	• increase in grain size of olivine, < competent and > alteration of core • > number of xenoliths and rounded cognate fragments
152.9-153.65 m	**Volcaniclastic kimberlite** • kimberlite much darker and finer grained
(95A5-1-6)	• lower contact distinct at 65-70° tca • upper contact not preserved
153.65-157.05 m	• same as 147.9-153.65 m
157.05-157.13 m	• same as 152.9-153.65 m
157.13-157.4 m	• same as 147.9-153.65 m
157.4-157.7 m	• same as 152.9-153.65 m
157.7-171.2 m	**Hypabyssal Kimberlite** • kimberlite competent, comprised of rounded macrocrysts of
(95A5-1-7)	olivine, inequagranular in nature • Fe-oxidation staining common
171.2-199.4 m	**Granodiorite**
199.4 m	**E.O.H.**

Petrographic Samples:

95A5-1-1	59.7-59.8 m
95A5-1-2	126.3-126.4 m
95A5-1-3	137.35-137.45 m
95A5-1-4	151.45-151.55 m
95A5-1-5	152.4-152.5 m
95A5-1-6	153.0 m
95A5-1-7	165.85-166.0 m

94A5-1

KCEI DIAMOND DRILL LOG

Drill Hole: 95 A2-2
Northing: 7151263
Easting: 534690
Depth: 212.0 m

Dip: -90°
Azimuth: 000
Core Size: NQ
Date Logged: Nov. 27/97

0.0-21.5 m	**Water**
21.5-27.3 m	**Overburden**
27.3-52.9 m	**Granite** • medium-to-coarse grained, pink-to-medium gray granite with common Fe-oxidation staining on fracture surfaces
51.3-52.9 m	• contact with kimberlite extremely brecciated; dissolution of feldspars within the granite occurs
52.9-62.0 m	**Intensely altered volcaniclastic kimberlite breccia** • intensely altered kimberlite with common microxenoliths of granite and common granitic fragments of up to 20 cm in length along core axis • very difficult to determine any macroscopic textural features, ≈5% loosely packed fragmental olivine macrocrysts, yellow in colour (completely serpentinized), generally 1-2mm in size. This interval is quite fine-grained, no sorting or bedding contacts observed, homogenous throughout • xenocrystal feldspars and mica common • core not very competent, most section can be broken with hand
62.0-67.6 m	**Non-kimberlitic Mudstone** • medium gray, aphanitic massive rock broken into many angular pieces • small mica crystals recognizable, however other mineralogical constituents aphanitic in nature • no reaction to HCl; small wood fragments present
67.6-69.9 m	**Intensely altered volcaniclastic kimberlite breccia** • same as previous, small wood fragments present

69.9-96.2 m	**Non-kimberlitic Mudstone** • same as previous
89.0-89.1 m, 92.33-92.4 m, 93.35-93.65 m	• these intersection may represent fragments or consolidated kimberlite incorporated into the non-kimberlitic mudstone or may be thin units of reworked volcaniclastic kimberlite • upper and lower contacts at approx. 45° tca
96.2-98.5 m	**Intensely altered volcaniclastic kimberlite breccia** • essentially the same as previous with approx. 10% loosely packed olivine pseudomorphs
98.5-99.3 m	**Non-kimberlitic Mudstone** • same as previous
99.3-99.6 m	**Intensely altered volcaniclastic kimberlite breccia** • same as previous
99.6-99.8 m	**Non-kimberlitic Mudstone** • same as previous
99.8-106.4 m	**Intensely altered volcaniclastic kimberlite breccia** • same as previous
106.4-107.3 m	**Non-kimberlitic Mudstone** • same as previous
107.3-108.5 m	**Intensely altered volcaniclastic kimberlite breccia** • same as previous
108.5-109.0 m	**Non-kimberlitic Mudstone** • same as previous, but highly brecciated and rubbley
109.0-111.2 m	**Intensely altered volcaniclastic kimberlite breccia** • dark brown in colour, friable, but more competent than previous • approx. 10-15% altered olivine macrocrysts, <2mm in dimension, common altered granitoid xenoliths and xenocrystal mica and feldspar

111.2-136.2 m	**Non-kimberlitic Mudstone** • same as previous
136.2-170.5 m	**Intensely altered volcaniclastic kimberlite breccia** • dark gray in colour with common xenoliths of granite and mica schist of up to 30 cm in length • fairly incompetent, friable with common large rubbley intervals • subtle layering throughout interval defined by varying concentration of olivine macrocrysts • common rounded-to-subrounded cognate fragments, rather small • slickensides and serpentinized shear surfaces common
168.2-170.5 m	• approx. 20% xenoliths, 3-15 cm in length and common mudstone (non-kimberlitic) clasts • sharp lower contact with granite at 70° tca
170.5-180.7 m	**Granodiorite** • medium-to-coarse-grained, light gray in colour • Fe-oxidation staining common on fracture surfaces; pyrite veneers abundant
180.7-182.4 m	**Biotite Schist** • light-to-medium gray, fine-to-medium grained rock with pyrite veneers open fracture surfaces • quartz banding at 30° tca
182.4-193.9 m	**Granodiorite** • same as previous
193.9-202.3 m	**Biotite Schist** • same as previous
202.3-212.0 m	**Granodiorite** • same as previous
212.0 m	**E.O.H.**

Petrographic Samples:

95 A2-2-1	56.2 m
95 A2-2-2	68.0 m
95 A2-2-3	80.2 m
95 A2-2-4	93.6 m
95 A2-2-5	96.4 m
95 A2-2-6	111.2 m
95 A2-2-7	120.0 m

KCEI DIAMOND DRILL LOGS

Drill Hole: 95A10-1
Northing: 7150225
Easting: 545400
Depth: 279.4 m

Dip: -90°
Azimuth: 0°
Core Size: NQ to 209.0 m; red to BQ
Date Logged: Nov. 17-18, 1997

0.0-18.5 m	**Water and Overburden**
18.5-254.0 m	**Macrocrystal Kimberlite (possible olivine crystal tuff moderately reworked?)** • dark gray-green altered macrocrystal kimberlite • inequagranular olivine macrocrysts occupy from 5-25% of the rock; appear to be intensely serpentinized with minor secondary carbonatization giving olivines a green colour • olivine concentration not homogeneous throughout the hole, no contacts or bedding defined by olivine concentration is discernible • common, quite fresh macrocrysts of biotite (may be some phlogopite) • lithic clasts are present, but occupy less than 5% of rock; clasts are predominantly granitoid, schist and minor mudstone; autolithic clasts content appears to increase downhole, they are generally subrounded-to-rounded in nature and may be up to 7 cm in diameter • kimberlite itself is not very competent, breaks easily with hand and is easily exfoliated; average unbroken length of core approx. 10 cm • incompetent, rubbley intervals appear to have a significant increase in olivine concentration • olivine concentration defining vague bedding
33.8-38.4 m	• drastic increase in olivine macrocrysts (20-25% of rock) • no contacts measurable; however likely represents bedding
120.85-122.15 m	• granitoid xenolith with pronounced foliation at 50-6° tca • xenolith has sharp contacts with host
121.3-121.5 m	• large granitic xenolith (gneissic)
188.3-188.6 m	• significant decrease in olivine concentration • kimberlite nearly aphanitic • no sharp, measurable contacts; olivine concentration discerning a vague bedding

252.3 m	• slickensides at approx. 90° tca
254.0-279.4 m	**Biotite Schist (metagreywacke)** • ubiquitous quartz veining subparalleling foliation • moderately-to-strongly foliated at ≈50° tca
279.4 m	**E.O.H.**

Petrographic Samples:

95A10-1-1	36.6 m (high proportion of olivine)
95A10-1-2	39.0 m
95A10-1-3	95.6 m (with autolithic fragments?)
95A10-1-4	159.0 m (rounded cognate fragment)
95A10-1-5	252.4 m

KCEI DIAMOND DRILL LOG

Drill Hole: 94A11-1
Northing: 7150096
Easting: 543379
Depth: 134.0 m

Dip: -90°
Azimuth: 000 -
Core Size: NQ
Date Logged: Nov. 23, 1997

0.0-16.8 m	**Casing/Overburden**
16.8-134.0 m	**Volcaniclastic Kimberlite**
16.8-23.0 m	• rubbley, dark brown, incompetent kimberlite with olivine content ranging from <5-25% (vague layering defined by olivine content) with few competent pieces of core (<10 cm in length)
23.0-23.6 m	• more competent kimberlite alternating with lighter-coloured, very competent hypabyssal rock (autoliths?) • hypabyssal rock characterized by a very high concentration of rather fresh olivine macrocrysts (<10mm in dimension)
23.6-24.2 m	**Hypabyssal Kimberlite** • light-coloured hypabyssal kimberlite with numerous olivine macrocrysts and dark, aphanitic kimberlite fragments
24.2-44.7 m	**Volcaniclastic Kimberlite** • dark coloured kimberlite with significantly less olivine (15%); olivine crystals up to 8mm in size and altered to a yellow colour (serpentinized) • olivine proportion varies greatly throughout interval defining crude bedding • poorly-consolidated kimberlitic mudstone intervals common. up to 30 cm in length
39.1-39.3 m	• lighter coloured hypabyssal kimberlite (autolithic fragment)
39.4-39.55 m	• same as previous
44.7-51.3 m	**Hypabyssal Kimberlite** • lighter-coloured, highly altered kimberlite with up to 50% large, rounded olivine (3-15mm) macrocrysts • fragments of fine-grained kimberlite common
51.3-93.1 m	• dark, competent kimberlite with 10-40% olivine pseudomorphs

	• common incompetent, rubbley intervals or core
93.1-95.0 m	• darker kimberlite with smaller (1-3mm), less common (≈20%) olivine macrocrysts • olivine macrocrysts altered to a green colour (serpentine)
95.0-133.7 m	**Hypabyssal Kimberlite** • lighter-coloured, magnetic and very heavy kimberlite (can only be broken with hammer) • kimberlite altered and olivine proportion varies throughout interval (flow differentiation) • olivine macrocrysts are partially altered and up to 3cm in dimension • lithic fragments common, but not prevalent • kimberlite appears to be micaceous and coarse calcite veins cut core • rare garnet macrocrysts with relatively thick kelphytic rims; rare CD's • rare dark, fine-grained cognate fragments • white clay and calcite common on open fracture surfaces
133.7-134.0 m	• interval quite rubbley
134.0 m	**E.O.H.**

Petrographic Samples:

94A11-2-1	18.7 m	(volcaniclastic)
94A11-2-2	23.8 m	(hypabyssal)
94A11-2-3	25.2 m	(volcaniclastic)
94A11-2-4	39.0 m	(> olv)
94A11-2-5	43.1 m	(< olv)
94A11-2-6	78.2 m	(rep. of interval with ≈30% inequ. olv set in a dark matrix)
94A11-2-7	94.0 m	
94A11-2-8	104.7 m	(hypabyssal)
94A11-2-9	113.0 m	(hypabyssal)
94A11-2-10	129.5 m	(hypabyssal)

KCEI DIAMOND DRILL LOGS

Drill Hole: 94 A61-4
Northing:7157750
Easting: 554625
Depth: 125.0 m

Dip: -50 Deg
Azimuth: 255
Core Size: NQ
Date Logged: Feb. 21.98

0.0-17.5 m	**Overburden**
17.5-22.0 m	**Granite**
22.0-51.8 m	**Metasediment**
51.8-62.0 m	**Granite**
62.0-110.0 m	**Volcaniclastic kimberlite** • very dark kimberlite, not very competent and overall, quite featureless •certain intervals appear to be a cognate clast breccia with many rounded autoliths? or lapilli? with prominent green-brown alteration • subtle differences in colour and % of clasts may define a crude bedding; no contacts appear sharp, however difficult to tell due to brecciated nature of core • from 93.1-110.0 m large intervals of metagreywacke xenoliths? exist, up to 1 m in length; xenoliths tend to be broken up(may represent wall rock)
106.7-110.0 m	• medium gray breccia; cognate and lithic clasts both represented, all highly altered
110.0-125.0 m	**Metagreywacke** • highly schistose with many examples of slickensides • highly fractured near upper contact with overlying kimberlite
125.0 m	**E.O.H.**

94A61-4

Samples:	94A61-4-1	66.4 m
	94A61-4-2	78.1 m
	94A61-4-3	81.0 m
	94A61-4-4	86.2 m
	94A61-4-5	91.2 m
	94A61-4-6	92.2 m
	94A61-4-7	98.8 m
	94A61-4-8	107.4 m
	94A61-4-9	108.1 m

Composite: VR 51006 A

KCEI DIAMOND DRILL LOG

Drill Hole: 94 C13-8
Northing: 7143125
Easting: 555260
Depth: 131.0 m

Dip: -90 Deg
Azimuth: 000
Core Size: NQ
Date Logged: Feb. 20/98

0.0-19.8 m	**Overburden** • silt, granite and metasediment
19.8-103.5 m	**Bedded Volcaniclastic Kimberlite** • beds differ with respect to olivine pseudomorph-to-matrix ratio (from <5-20% olivine) • paucity of lithic clasts or xenocrysts • bedding angles difficult to discern due to poor condition of core; core ranges from rubbley pieces to lengths of 30 cm • core can be broken with hand • olivine macrocrysts are intensely altered to a teal green colour • few autolithic fragments noted; when occur, tend to be quite rounded • rare lithic clasts up to 16 cm in length; majority are metasediment • near end of kimberlite intersection are intervals of 20-40 cm in length with a very high olivine proportion (approx. 40%-Samples 7 & 8) • olivine alignment (depositional feature) common throughout hole; defines a weak foliation
32.0-32.3 m	• slickensides at high angle to core axis (≈80-90°)
37.5-38.0 m	• bedding defined by olivine macrocrysts at 60° tca
103.5-131.0 m	**Migmatite** • pronounced foliation at 60° tca; pink-gray in colour • distinct banding concentrating mafic and felsic material
131.0 m	**E.O.H.**

94C13-8

Samples:

94C13-8-1	24.1 m
94C13-8-2	28.8 m
94C13-8-3	31.3 m
94C13-8-4	37.8 m
94C13-8-5	52.5 m
94C13-8-6	57.0 m
94C13-8-7	94.6 m
94C13-8-8	96.5 m

Composite: VR 51001 A

KCEI DIAMOND DRILL LOG

Drill Hole: 93 C27-1
Northing: 7141525
Easting: 539490
Depth: 131.7 m

Dip: -45 Deg
Azimuth: 160
Core Size: NQ
Date Logged: Feb. 20.98

0.0-8.5 m	**Overburden**
8.5-44.4 m	**Biotite Schist**
44.4-46.5 m	**Granite gneiss and pegmatite**
46.5-56.2 m	**Biotite Schist**
56.2-122.6 m	**Volcaniclastic kimberlite breccia** • common blue-clayey alteration • kimberlite dark gray-black, rather fine-grained and quite competent • common, rounded olivine macrocrysts plus microphenocrystal olivine • olivines may exhibit fresh cores • common cognate clasts, lithic clasts of biotite schist and granite and common mica xenocrysts • xenoliths tend to be rounded
56.2-63.1 m	• kimberlite darker, no blue alteration • may be finer grained, fewer olivine macrocryst, but they seem to be quite fresh
63.1-80.2 m	• blue, altered kimberlite, with relatively fresh olivine macrocrysts • common xenoliths of biotite schist and granite (i.e. breccia) • similar to above; seems coarser grained
80.2-122.6 m	• no blue alteration • no distinct contact; appears to be the same as above unit • common xenoliths of granitoid, biotite schist and biotite xenocrysts; however, may be fewer than above • dark gray-black, some fresh olivine and one

noted olivine nodule
- minor mudstone veinlets and xenoliths
- unit appears to coarsen upward
- end of interval quite brecciated

122.6-130.0 m	**Gray Granite**
123.2 m	• small veinlet of kimberlite; highly brecciated
130.0-131.7 m	**Biotite Schist**
131.7 m	**E.O.H.**

Samples:

93C27-1-1 57.4 m
93C27-1-2 73.2 m
93C27-1-3 86.5 m
93C27-1-4 107.8 m
93C27-1-5 122.5 m

KCEI DIAMOND DRILL LOG

Drill Hole: 95 C49-3
Northing:7142180
Easting: 533325
Depth: 149.0 m

Dip: -45 Deg
Azimuth: 186°
Core Size: NQ
Date Logged: March 12/98

0.0-8.0 m — **Overburden**
- broken-up, re-drilled pieces of granodiorite and metasediment

8.0-44.0 m — **Biotite Schist**
- well-foliated, porphyroblastic rock with abundant quartz veins (subparallel to foliation) and common pyrite on open fracture surfaces

44.0-86.7 m — **Volcaniclastic Kimberlite**
- massively bedded, beds 5-10 m in thickness
- bedding contacts not discernible due to broken-up core

44.0-46.6 m
- brown-gray kimberlite breccia
- numerous black, aphanitic, rounded cognate fragments
- interval highly altered; matrix an earthy-gray
- interval appears to be reworked volcaniclastics

46.6-57.6 m
- dark-gray kimberlite, quite competent-broken with hammer
- contains cognate fragments together with minor lithic clasts
- approximately 10% greenish olivine pseudomorphs (quite small) set in a black, aphanitic matrix

53.0-54.8 m
- competent kimberlite with many rounded cognate fragments
- can be described as a cognate breccia

54.8-57.0 m — **Hypabyssal Kimberlite**

54.8-57.0 m
- common dark black cognate clasts(small and rounded) plus altered granitoid xenoliths

54.8-57.0 m
- grey, competent kimberlite breccia
- many large, fresh olivine macrocrysts

57.0-76.4 m — **Volcaniclastic Kimberlite** (likely resedimented)

	• darker black, massive kimberlite with approximately 10% green, serpentinized olivine macrocrysts plus few lithic clasts (granitoid) set in a black aphanitic matrix
	• common black, rounded cognate clasts
	• one noted fresh olivine
	• interval quite broken up; few large pieces of core
76.4-86.7 m	• kimberlite coated with a white-clay alteration
	• interval appears to be a breccia with many rounded clasts; difficult to discern what features of kimberlite are
	• possibly hypabyssal
	• 10-15% rounded olivine pseudomorphs (5-7 mm); carbonatized
78.8-89.7 m	• biotite schist xenolith?
80.3-80.6 m	• biotite schist xenolith?
86.7-149.0 m	**Biotite Schist**
	• same as previous
149.0 m	**E.O.H.**

Samples:

95C49-3-1	46.5 m
95C49-3-2	48.1 m
95C49-3-3	54.3 m
95C49-3-4	55.5 m
95C49-3-5	57.2 m
95C49-3-6	85.8 m

KCEI DIAMOND DRILL LOG

Drill Hole: 95C42-3
Northing: 7147900
Easting: 533325
Depth: 326.0 m

Dip: -90°
Azimuth: 0°
Core Size: HQ to 143.0 m; red to NQ
Date Logged: Oct. 27-28, 1997

0.0-24.0 m	**Water**
24.0-44.1 m	**Overburden** • broken up blocks of granite and metasediment mixed with rubble
44.1-326.0 m	**Volcaniclastic kimberlite** (lithic breccia) • dark gray/brown-to-black in colour • kimberlite can be easily broken with hand; incompetent and quite soft • rounded-to-subrounded olivine macrocrysts comprise 10-15% of unit; highly altered (carbonatized and serpentinized) giving the olivine macrocrysts a chalky white-to-teal green colour • olivines 1-3 mm in dimension • kimberlite is quite micaceous, macrocrysts of biotite and phlogopite? common (3-7 mm in average length) • lithic xenoliths comprise approx. 5% of rock; generally subrounded in nature with relatively sharp contacts with host kimberlite, may have thin reaction rims; size of xenoliths range from less than 5 mm to 45 cm • lithic xenoliths either of granitic composition or a metasediment (metagreywacke, or less commonly chlorite schist with pronounced foliation) • macroscopically, unit appears to be massive, matrix-supported; distinct inequagranular texture of olivine macrocrysts imparts a "pseudo-porphyritic" texture to the unit • common light-to-medium gray mudstone stringers and veinlets cut core; appears to increase in abundance downhole

	• texture of kimberlite appears quite uniform (based upon macroscopic observation only) with gradual and subtle changes in grain size and degree of alteration downhole • chrome diopside macrocrysts common throughout interval with less common ilmenite; rounded-to-subrounded in nature, occasionally broken, 2-3 mm in dimension, on average
236.0-310.0 m	• olivine alterations appears to be a more teal colour vs. chalky white (greater serpentinization vs. carbonatization?) • olivine macrocrysts slightly coarser-grained • lithic xenoliths appear smaller on average (less than 5 cm, generally 1-2 cm in size) • interval not as micaceous; however mica macrocrysts still prevalent • rounded, autolithic fragments noted, mantled by a thin rind; generally approx. 1 cm in size
281.0-284.3 m	• common expansional? slickensides at approx. 20° tca • core quite broken up
281.0-281.3 m	**Metamorphosed shale** • dark gray-black, very fine-grained (appears amorphous macroscopically) with a subconcoidal fracture • has a greasy feel and sheen
315.0-326.0 m	• core very broken up; rubble-like
326.0 m	**E.O.H.**

Samples: (not all thin sectioned)

95 C42-3-1	138.8-139.9 m
95 C42-3-2	237.8-237.9 m
95 C42-3-3	281.0 m (metamorphosed shale)
95 C42-3-4	284.0 m (slickensides)
95 C42-3-5	252.0-252.1 m (mudstone)
95 C42-3-6	307.65 m
95 C42-3-7	311.55 m

KCEI DIAMOND DRILL LOG

Drill Hole: 93 DD39-1
Northing: 7148850
Easting: 505225
Depth: 107.0 m

Dip: -90°
Azimuth: 000
Core Size: NQ
Date Logged: March 19/1998

0.0-11.0 m	**Casing/Overburden**
11.0-107.0 m	**Volcaniclastic Kimberlite (crystal-rich pyroclastics?)**
11.0-13.6 m	• highly oxidized, weathered volcaniclastic kimberlite; inhomogeneous oxidation throughout interval • less oxidized sections have an earthy look • contains highly altered olivine macrocrysts (less than 10 mm) and autoliths of dark, fine-grained kimberlite • core quite incompetent, can be broken with hand
13.6-19.1 m	• medium gray, highly carbonatized kimberlite with abundant white, fibrous carbonate stringers • numerous black autolithic fragments set in a medium gray matrix • few small CD's within an olivine lherzolite nodule • fresh equivalent to previous? • olivine macrocryst are angular and seem fragmented
15.1-15.5 m	**Resedimented, Bedded Volcaniclastic Kimberlite** • dark brown-black kimberlite with approx. 10% altered olivine macrocrysts (less than 4 mm in size); distinctly different unit • open fracture surfaces oxidized • likely resedimented
17.9-18.05 m	• gray-brown kimberlite containing coarse olivine macrocrysts with UC @ 60 deg. tca (lower contact not observed) • quite altered, olivine macros a whitish-yellow in colour: few black autoliths set in a medium gray-brown matrix • similar to the first unit?? Pyroclastic??
19.1-20.9 m	• blackish kimberlite with numerous fibrous carbonate stringers; core has a fragmented look • pseudomorphed olivine macrocrysts and microphenocrysts and autoliths are all set in a black.

	aphanitic matrix • lower contact brecciated
20.9-30.8 m	• highly altered light to medium gray-green kimberlite with numerous larger, black autoliths • slickensides at high angles to core axis evident (serpentinized) • elongated constituents seem to have a common orientation approx. 90 deg tca • kimberlite changes character at end of interval with few cognate clasts and a plethora of fibrous carbonate stringers
26.3-29.0 m	• first 50 cm of interval oxidized; kimberlite an earthy brown with greenish olivine pseudomorphs • interval intensely and pervasively altered • numerous black autoliths; unit appears to be clast supported
29.0-30.0 m	• massive medium gray kimberlite with vague olivine pseudomorphs and few, small cognate clasts
30.0-30.8 m	• medium gray kimberlite with approx. 15-20% carbonatized olivine macrocrysts and few small autoliths and microphenocrystal olivine set in a grey matrix (no sample)
30.8-34.2 m	• poorly drilled, dark brown-black kimberlite with yellow olivine pseudomorphs; inhomogeneous throughout interval • up to 40% small, tightly packed olivine pseudomorphs and numerous small, cognate clasts set in a blackish matrix
34.2-35.0 m	• competent, medium-gray kimberlite with numerous greenish clasts with prevalent reaction rims; many clasts
35.0-57.2 m	• dark gray-black kimberlite with 25% olivine pseudomorphs (greeny-yellow) and numerous fibrous carbonate stringers • olivine macrocryst concentration very uneven throughout intersection (varies from 10%-greater than 40%, 1-8 mm in dimension) • common xenocrysts of metasediment of up to 50 cm in length • interval can be termed a breccia
57.2-58.7 m	• increase in olivine concentration; kimberlite lighter gray; olivines very inequagranular and numerous autoliths present; all set in a black, aphanitic matrix

93DD39-1

	• unit essentially the same as above save the increase in olivine concentration
58.7-82.0 m	• kimberlite has a bedding defined by olivine concentration • two phases of kimberlite, one is dark with a higher proportion of olivine (RVK) and other is a medium gray with less olivine (PK?)
58.7-67.5 m	• decrease in olivine percentage (approx. 10-15%) • olivine still of same character, i.e., green-yellow alteration and set in a black, aphanitic matrix
67.5-70.0 m	• increase in olivine concentration
70.0-74.1 m	• decrease in olivine concentration
74.1-82.0 m	• increase in olivine concentration
82.0-107.0 m	• the above two units are also interbedded interbedded (distinct contacts) with darker kimberlite with a higher olivine concentration that appears to be hypabyssal (DD39-1-18, DD39-1-19)
107.0 m	**E.O.H.**

Petrographic Samples:

93DD39-1-1	12.6 m
93DD39-1-2	18.0 m
93DD39-1-3	17.5 m
93DD39-1-4	20.2 m
93DD39-1-5	21.0 m
93DD39-1-6	28.5 m
93DD39-1-7	29.2 m
93DD39-1-8	33.3 m
93DD39-1-9	34.7 m
93DD39-1-10	42.0 m
93DD39-1-11	58.4 m
93DD39-1-12	63.3 m
93DD39-1-13	81.6 m
93DD39-1-14	80.0 m
93DD39-1-15	86.4 m
93DD39-1-16	86.78 m
93DD39-1-17	89.0 m
93DD39-1-18	85.8 m
93DD39-1-19	102.0 m

KCEI DIAMOND DRILL LOG

Drill Hole: 92 T29S-1
Northing: 7145405
Easting: 535595
Depth: 166.7 m

Dip: -55 Deg
Azimuth: 250 °
Core Size: NQ
Date Logged: March 12/98

0.0-4.4 m	**Overburden**
4.4-69.8 m	**Granite** (gray granite)
69.8-89.3 m	**Hypabyssal kimberlite breccia** • lithic breccia; clast generally less than 2 mm in maximum dimension, predominantly granite and metasediment • fractures often clay-coated and serpentinized • clasts rounded-to subrounded and few cognate clasts noted • kimberlite aphanitic in nature, olivine population predominantly microphenocrystal; few macrocrystal olivines-completely pseudomorphed • clasts altered to a white colour with and frequently display reaction rims
89.3-166.7 m	**Granite** • altered and oxidized at contacts for approximately 30 cm
166.7 m	**E.O.H.**

Samples:

92T29S-1-1	≈77.0 m

KCEI DIAMOND DRILL LOG

Drill Hole: 96 T237-2
Northing: 714970
Easting: 582915
Depth: 128.0 m

Dip: -45°
Azimuth: 023
Core Size: NQ
Date Logged: March 29/98

0.0-12.1 m	**Casing/Overburden**
12.1-65.7 m	**Biotite schist** • medium-to-fine grained, moderately foliated schist with c common metamorphic garnets • oxidation staining on fractures common • prevalent quartz veinlets paralleling foliation
65.65-65.7 m	• narrow (1-2 cm) kimberlite veinlets cutting schist
65.7-82.2 m	**Hypabyssal kimberlite** • greenish-gray, relatively competent rock, >90% recovery • abundant calcite-filled dilational veinlets cutting core at various angles to core axis • quite massive; local flow alignment of olivine • macrocrystal olivine comprise 5-10% of core, 0.5-3 cm in size and are generally fresh • microphenocrystal groundmass olivine abundant, fresh-to-partially altered • groundmass appears oxide-rich with common large macrocrystal oxides; micaceous • rare macrocrystal garnets • xenoliths comprise ≈5% of kimberlite; subangular-to-subrounded, partially altered (reaction rims common) schists and granites • upper and lower contacts preserved at 37° and 55° to core axis
82.2-128.0 m	**Biotite Schist** • same as uphole
128.0 m	**E.O.H.**

96T237-2

Petrographic Samples:

96T237-2-1	66.5 m
96T237-2-2	70.8 m
96T237-2-3	75.4 m
96T237-2-4	76.4 m
96T237-2-5	78.5 m
96T237-2-6	82.0 m

KCEI DIAMOND DRILL LOG

Drill Hole: 93 T36-1
Northing: 7148600
Easting: 570075
Depth: 87.5 m

Dip: -90 Deg
Azimuth: 000
Core Size: NQ
Date Logged: March 28/1998

0.0-8.6 m	**Casing and Overburden**
8.6-9.5 m	**Metagreywacke**
9.5-10.2 m	**Diabase**
10.2-87.5 m	**Hypabyssal Kimberlite Breccia** • dominant feature is fairly large granitoid xenoliths; xenoliths are bleached and clay-altered (white); they are often angular with reaction rims • kimberlite contains large (less than 10 mm) rounded olivine macrocrysts that are fresh-to-moderately altered by serpentine (macrocryst population less than 10%) • microphenocrystal olivine population consists of abundant euhedral-to-subhedral olivine pseudomorphs • abundance of large euhedral-to-subhedral opaque oxides • core very hard and competent • upper 10.2-20.1 m of kimberlite broken up • abundant calcite stringers cutting core • further downhole, metasediment intersections of up to 3 m become more predominant (to the point where metasediment equals amount of kimberlite • plethora of white-clayey alteration coatings on open fracture surfaces • features of the kimberlite quite homogeneous throughout the hole • increase of xenoliths with depth
53.8-55.4 m	• increase in olivine pseudomorph population; olivine in altered and core less competent
87.5 m	**E.O.H.**

Samples:

93T36-1-1	29.2 m
93T36-1-2	54.3 m
93T36-1-3	64.5 m
93T36-1-4	70.0 m

KCEI DIAMOND DRILL LOG

Drill Hole: 93 T35-1
Northing: 7147875
Easting: 565800
Depth: 126.0 m

Dip: -60 Deg
Azimuth: 325
Core Size: NQ
Date Logged: January 22/98

0.0-2.0 m	**Overburden/Casing**
2.0-75.3 m	**Metagreywacke**
75.3-84.5 m	**Hypabyssal Kimberlite** • much of core absent from boxes • competent, olivine macrocryst-deficient kimberlite with approx. 1% olivine macrocrysts of 1-3 mm in size • seems to be micaceous; mica macrocrysts of up to 3 mm • olivine pseudomorph population altered to predominantly calcite, and minor serpentine • fairly abundant microphenocrystal olivine, subhedral in nature, <1mm in dimension • few highly altered granitoid xenoliths of up to 5 cm in length. with thin, white alteration margins • common serpentinized, rounded clasts; likely represent a segregation-textured groundmass
84.5-126.0 m	**Metagreywacke**
126.0 m	**E.O.H.**

Petrographic Samples:

94T35-1-1	77.0 m
94T35-1-2	79.5 m

KCEI DIAMOND DRILL LOG

Drill Hole: 93 T33-2
Northing: 7146050
Easting: 567025
Depth: 124.1 m

Dip: -45 Deg
Azimuth: 130°
Core Size: NQ
Date Logged: Feb. 20.98

0.0-7.4 m	**Overburden**
7.4-74.4 m	**Biotite Schist**
74.4-100.7 m	**Hypabyssal Kimberlite breccia**
74.4-96.6 m (T34-2-2 to T34-2-5)	• medium gray kimberlite with pocked texture due to plucking of olivine macrocrysts • predominance of olivine macrocrysts, rounded with fresh relic cores and a second population of microphenocrystal olivine, imparting a pseudoporphyritic texture • interbedded with darker kimberlite (small intervals), difficult to tell nature of this rock to lack of exposure
96.6-100.7 m	• fairly dark rock composed of many rounded, cognate clasts • common large, rounded olivine pseudomorphs and many microphenocrystal olivine • could be volcaniclastic
100.7-110.9 m	**Biotite Schist**
110.9-111.9 m (T33-2-1)	**Hypabyssal kimberlite dyke** • fine grain, dark gray-black, competent • minor carbonate and common xenoliths of granite
111.9-124.1 m	**Biotite Schist**
124.1 m	**E.O.H.**

Samples:		
	93T33-2-1	111.6 m
	93T33-2-2	94.0 m (approx.)
	93T33-2-3	75.5 m
	93T33-2-4	81.6 m
	93T33-2-5	93.4 m

KCEI DIAMOND DRILL LOG

Drill Hole: 93 T7-1
Northing: 7147295
Easting: 547510
Depth: 99.7 m

Dip: -45°
Azimuth: 270
Core Size: NQ
Date Logged: Feb. 20. 98

0.0-5.2 m	**Overburden**
5.2-63.1 m	**Biotite Schist**
63.1-74.7 m	**Volcaniclastic Kimberlite breccia** • highly altered and rotten; not competent • frequent slickensides • most core lost; only small fragments remain at beginning and end of intersection • frequent large, rounded olivine pseudomorphs • probably small dike (hypabyssal) near bottom of intersection
74.7-99.1 m	**Granite**
99.1-99.7 m	**Biotite Schist**
99.7 m	**E.O.H.**

Petrographic Samples:

93 T7-1-1	≈66.2 m
93 T7-7-2	≈74.0 m

KCEI DIAMOND DRILL LOG

Drill Hole: 94 T34-1
Northing: 7147450
Easting: 566100
Depth: 92.0 m

Dip: -90°
Azimuth: 000
Core Size: NQ
Date Logged: Jan 22/98

0.0-7.0 m	**Overburden**
7.0-29.2 m	**Aphanitic Hypabyssal Kimberlite** • ≈ 60% of core missing • proportion of olivine grains differs throughout intersection; this is presumably the result of flow differentiation • kimberlite nearly aphanitic throughout entire intersection • common large metagreywacke xenoliths with white clayey alteration along margins • olivine range from fresh (yellow-green in colour) to partially and completely serpentinized/carbonatized • upper 50 cm of intersection displays Fe-oxidation staining • kimberlite quite competent • calcite veinlets/stringers common • bulk of olivine population are < 1mm, subhedral-to-euhedral (microphenocrystal groundmass constituents); macrocrystal olivine are less common, well-rounded and commonly fresh • groundmass appears to be mica-rich; few noted mica macrocrysts
29.2-75.5 m	**Metasediment**
75.5-89.9 m	**Granite**
89.9-92.0 m	**Metasediment**
92.0 m	**E.O.H.**

Samples:		
	94T34-1-1	7.6 m
	94T34-1-2	23.0 m
	94T34-1-3	27.5 m

KCEI DIAMOND DRILL LOG

Drill Hole: 92 T7E-1
Northing: 7147650
Easting: 547875
Depth: 105.2 m

Dip: -55°
Azimuth: 090
Core Size: NQ
Date Logged: March 12/98

0.0-21.3 m — **Overburden**

21.3-87.2 m — **Resedimented Volcaniclastic Kimberlite**
- dark gray with a green tinge; unit appears to be bedded
- core is fairly competent, but quite broken up

21.2-25.3 m
- very broken up: average unbroken length approximately 3-5 cm
- numerous rounded cognate clasts and a number of fine-grained, green-yellow olivine pseudomorphs (quite small <1 mm)
- kimberlite appears to be a matrix-supported, cognate breccia

25.3-26.7 m — **Volcaniclastic Kimberlite (pyroclastic?)**
- pale gray-green, clast-supported kimberlite
- olivine coarser in nature, highly carbonatized (white) and rounded
- core has a "pocked" appearance due to plucking and rotting of olivine macrocrysts

26.7-35.6 m — **Resedimented Volcaniclastic Kimberlite**
- appears very similar to previous
- kimberlite darker, more massive with few discernible features; nearly aphanitic
- few large olivine macrocrysts, rounded in habit
- top of interval slightly more altered and lighter in colour (medium gray-brown); lower in interval core becomes dark brown-black

35.6-43.9 m — **Volcaniclastic Kimberlite (pyroclastic?)**
- very similar to previous
- competent gray kimberlite (average unbroken length of core approximately 10-15 cm)
- few lithic clasts of metasediment and granitoid; approx. 5% larger olivine, rounded macrocrysts, white-gray to rusty

orange in colour
- minor pocked appearance

87.2-105.2 m	**Granite**
105.2 m	**E.O.H.**

Petrographic Samples:

92T7E-1-1	24.3 m
92T7E-1-2	25.3 m
92T7E-1-3	29.4 m
92T7E-1-4	33.9 m
92T7E-1-5	45.4 m

KCEI DIAMOND DRILL LOG

Drill Hole: 93 T14-1
Northing: 556715
Easting: 7145850
Depth: 124.7 m

Dip: -90°
Azimuth: 000
Core Size: NQ
Date Logged: March 19/1998

0.0-9.1 m	**Water**
9.1-30.0 m	**Overburden**
30.0-124.7 m	**Intensely altered volcaniclastic kimberlite (probably resedimented)** • very friable, highiy incompetent kimberlite; appears to be layered (contacts not measurable due to condition of core) • common laths of mica (probably xenocrysts of biotite and muscovite) and small crystals of feldspar • olivine population minor (5-15%), completely altered
30.5-31.4 m	• dark gray, incompetent kimberlite with minor competent kimberlitic autolithic fragments (up to 3 cm in length)
31.4-34.8 m	• brownish slightly more competent core with vague, rounded olivine pseudomorphs alternating with gray-brown kimberlitic siltstone (prob. reworked, weak reaction to HCl, features and mineralogy macroscopically indiscernible
34.8-35.6 m	• greenish-yellow, highly serpentinized, very friable kimberlite (cannot sample)
35.6-39.0 m	• same as 30.5-31.4 m
39.0-53.1 m	• silty reworked kimberlite (?) • soft, friable, no reaction to HCl
53.1-124.7 m	• dark gray-brown, friable kimberlite (similar to 30.5-31.4 m) • approximately 5-10% loosely packed olivine pseudomorphs, generally less than 1mm in dimension • olivine proportion varies slightly throughout interval, from perhaps 5%-10% • interval appears to be rather micaceous • both cognate and lithic fragments appear lower in interval (≈97.05 m); cognate clasts are rounded and more

	competent than host, however do fall apart when handled (likely autolithic). Lithic clasts are too intensely altered to determine parentage
97.05-116.8 m	• kimberlite has a yellowish hue due to intense alteration
116.8-120.9 m	• kimberlite becoming more competent • few olivine pseudomorphs discernible • to distinct upper contact exists, change in appearance of kimberlite gradual
120.9-124.7 m	• small competent intervals present • intervals of greater competency have a slightly > proportion of olivine pseudomorphs and matrix appears less altered (probably bedding, however no contacts are measurable)
124.7 m	**E.O.H.**

Petrographic Samples:

93T14-1-1	33.9 m
93T14-1-2	41.1 m (could not be thin sectioned)
93T14-1-3	48.2 m
93T14-1-4	63.1 m
93T14-1-5	??? (could not be thin sectioned)
93T14-1-6	74.1 m
93T14-1-9	97.7-100.0 m (could not be thin sectioned)
93T14-1-10	117.8 m
93T14-1-11	107.8 m
93T14-1-12	122.1 m
93T14-1-13	123.65 m (more competent kimberlite, weak rxn to HCl)

KCEI DIAMOND DRILL LOG

Drill Hole: 93 T19-2
Northing: 7147150
Easting: 582024
Depth: 124.1 m

Dip: -55 Deg
Azimuth: 000
Core Size: NQ
Date Logged: Jan. 22/1998

0.0-37.0 m	**Overburden**
37.0-97.9 m	**Biotite Schist**
97.9-102.3 m	**Non-kimberlitic siltstone** • very rubbley before and after contact • core earthy, appears to be reworked • core is soft and can be scratched with fingernail
102.3 m	• mudstone unit at approximately 102.3 m; light brown in colour, earthy, no features discernible, quite massive • does not appear to be kimberlite-derived
102.3-107.1 m	**Volcaniclastic Kimberlite**
102.3-105.8 m	• dark, rubbley kimberlite
105.8-107.0 m	• highly serpentinized, teal green coloured core; very altered
107.1-113.0 m	**Hypabyssal Kimberlite** • quite competent, possible hypabyssal kimberlite; common altered olivine macrocrysts (predominantly altered to carbonate) • abundance of calcite stringers
113.0-116.0 m	**Non-kimberlitic siltstone** • earthy brown, seemingly reworked mudstone; quite rotten
116.0-117.8 m	**Hypabyssal Kimberlite** •same as 107.0-113.0 m
117.8-124.1 m	**Metagreywacke**
124.1 m	**E.O.H.**

93T19-2

Samples:

93T19-2-1	100.0 m
93T19-2-2	104.5 m
93T19-2-3	106.5 m
93T19-2-4	111.9 m
93T19-2-5	116.0 m
93T19-2-6	117.0 m

Note: no composite sample taken

APPENDIX B

SPINEL ANALYSES (LAC DE GRAS)

	AS-1-4 SPINELS																	
	1-1	1-2	1-3	1-4	1-5	2-1	2-2	2-3	2-4	2-5	3-1	3-2	3-3	4-1	4-2	4-3	4-4	4-5	4-6
TiO_2	1 68	1 88	2 63	8 31	8 12	1 66	2 39	1 38	1 66	3 13	9 31	9 16	8 84	1 27	2 54	1 37	1 82	7 13	8 65
Al_2O_3	47 18	46 50	44 31	15 95	17 62	11 13	28 67	53 31	52 01	42 49	11 20	15 51	13 61	9 11	21 92	52 46	48 87	23 58	15 30
Cr_2O_3	0 54	0 29	0 75	0 31	0 06	50 53	24 16	1 30	0 45	0 15	1 19	0 31	-	55 24	31 19	2 24	0 31	0 14	0 20
FeO*	27 34	29 75	29 97	55 90	53 72	19 48	25 50	21 30	24 03	30 20	59 41	54 96	56 23	17 91	25 21	20 93	27 78	46 44	55 26
MnO	0 22	0 24	0 68	0 50	0 64	0 26	0 25	0 12	0 01	0 26	0 46	0 29	0 79	0 33	0 02	0 20	0 22	0 47	0 47
MgO	21 02	21 00	21 91	13 60	15 22	15 00	18 43	22 73	22 52	21 97	12 55	14 26	14 11	14 76	17 19	22 02	21 12	16 49	14 36
Total	97 98	99 66	100 25	94 57	95 38	98 06	99 40	100 14	100 68	98 20	94 12	94 49	93 58	98 62	98 07	99 22	100 12	94 25	94 24
$Fe^{2+}O$	8 35	9 00	7 71	19 62	17 43	11 64	10 39	7 13	7 82	7 56	21 38	19 55	18 44	11 42	11 14	7 68	9 26	15 25	18 67
$Fe^{3+}{}_2O_3$	21 11	23 06	24 74	40 24	40 33	8 71	16 80	15 75	18 01	25 16	42 26	39 35	42 00	7 21	15 63	14 72	20 58	34 67	40 67
Recalculated Analyses	100 09	101 97	102 73	98 60	99 42	98 93	101 08	101 72	102 49	100 72	98 35	98 43	97 79	99 34	99 64	100 70	102 18	97 72	98 31
Fe/Fe+Mg	0 3807	0 4011	0 3972	0 6602	0 6252	0 3804	0 3954	0 3070	0 5162	0 3938	0 6911	0 6456	0 6532	0 3645	0 4094	0 3100	0 3834	0 5710	0 6453
Cr/Cr+Al	0 0076	0 0020	0 0112	0 0129	0 0023	0 7528	0 3612	0 0161	0 0086	0 0024	0 6665	0 0132	0 0000	0 8027	0 4884	0 0278	0 0042	0 0043	0 0087
Ti/Ti+Cr+Al	0 0220	0 0250	0 0367	0 2471	0 2268	0 0230	0 0329	0 0160	0 0307	0 0448	0 3311	0 2711	0 2930	0 0172	0 0364	0 0159	0 0231	0 1612	0 2634
																	A61-1 SPINELS		
	5-1	5-2	5-3	6-1	6-2	6-3	7-1	7-2	7-3	8-1	8-2	8-3	8-4	9-1	9-2	9-3	1-1	1-2	1-3
TiO_2	8 03	8 85	8 53	9 23	8 44	8 38	1 53	1 63	1 09	2 51	1 28	9 22	8 84	8 12	8 14	8 61	1 10	1 80	1 19
Al_2O_3	17 29	15 12	15 74	12 66	15 95	17 25	12 57	50 64	50 66	22 76	51 05	16 22	14 71	13 87	17 73	15 31	6 41	21 73	34 06
Cr_2O_3	0 76	0 12	0 30	0 53	0 41	0 32	48 37	3 79	0 20	31 47	0 26	0 19	0 18	2 29	0 13	0 15	58 42	34 93	21 32
FeO*	53 28	56 02	54 16	57 61	54 87	53 93	20 31	20 90	20 87	25 54	22 52	54 07	55 01	55 64	53 04	54 41	18 84	24 01	21 77
MnO	0 42	0 63	0 41	0 32	0 47	0 41	0 44	0 15	0 11	-	0 05	0 58	0 53	0 48	0 50	0 58	0 30	0 36	0 27
MgO	14 63	14 10	14 65	13 05	14 42	15 30	15 74	22 12	22 11	17 43	22 03	14 54	14 02	13 11	15 06	14 19	14 68	16 85	18 69
Total	94 41	94 84	93 79	93 40	94 56	95 59	98 96	99 23	95 04	99 71	97 19	94 82	93 29	93 51	94 60	93 25	99 75	99 68	97 30
$Fe^{2+}O$	18 09	19 25	18 09	20 67	18 58	17 78	10 76	7 53	5 79	10 43	6 91	19 09	18 89	19 62	17 58	18 45	11 38	11 12	9 02
$Fe^{3+}{}_2O_3$	39 11	40 86	40 09	41 06	40 32	40 18	10 62	14 86	16 76	13 46	17 35	38 87	40 14	40 03	39 40	39 96	8 29	14 33	14 17
Recalculated Analyses	98 33	98 93	97 81	97 51	98 60	99 61	100 02	100 72	96 72	98 06	98 93	98 71	97 31	97 52	98 55	97 25	100 58	101 12	98 72
Fe/Fe+Mg	0 6825	0 6525	0 6360	0 6760	0 6427	0 6249	0 3788	0 3087	0 3085	0 3794	0 3258	0 6374	0 6497	0 6673	0 6247	0 6444	0 3776	0 4025	0 3551
Cr/Cr+Al	0 0286	0 0053	0 0126	0 0273	0 0170	0 0123	0 7208	0 0487	0 0026	0 4812	0 0034	0 0078	0 0081	0 0997	0 0049	0 0065	0 8594	0 5188	0 2957
Ti/Ti+Cr+Al	0 2235	0 2709	0 2545	0 3115	0 2492	0 2344	0 0212	0 0192	0 0135	0 0352	0 0157	0 2646	0 2755	0 2517	0 2257	0 2628	0 0152	0 0248	0 0155
	1-4	1-5	1-6	2-1	2-2	2-3	2-4	3-1	3-2	3-3	4-1	4-2	4-3	4-4	5-1	5-2	5-3	6-1	6-2
TiO_2	1 32	0 68	2 30	1 37	1 55	1 22	2 18	1 25	1 15	1 22	0 91	0 59	0 90	2 20	1 20	1 14	1 56	3 96	3 25
Al_2O_3	33 60	53 69	1 12	5 84	29 57	33 94	1 01	6 33	6 15	6 81	37 47	56 90	54 60	0 21	6 70	8 27	6 67	0 75	2 96
Cr_2O_3	22 76	1 12	0 19	56 97	24 79	22 72	1 13	58 18	58 91	49 20	16 91	0 67	0 90	0 65	57 34	48 26	53 01	-	0 06
FeO*	23 59	21 74	85 72	20 86	22 54	22 57	83 85	18 18	18 64	18 51	23 26	18 76	21 21	87 28	17 57	22 05	19 69	83 52	75 35
MnO	0 13	0 12	0 75	0 27	-	0 02	1 00	0 38	-	0 17	0 13	0 08	0 50	0 75	0 37	0 29	0 31	0 87	-
MgO	18 51	21 71	0 99	14 38	19 20	19 40	3 01	15 00	14 52	19 85	18 35	22 82	22 18	0 20	15 79	20 28	16 68	2 53	9 68
Total	99 91	99 06	91 07	99 69	97 65	99 87	92 18	99 32	99 37	95 76	97 03	99 82	100 29	91 29	98 97	100 29	97 92	91 63	91 30
$Fe^{2+}O$	10 33	7 77	30 32	12 03	8 27	9 03	27 14	10 79	11 79	2 64	9 89	6 74	7 40	31 29	9 50	3 52	8 29	29 35	18 92
$Fe^{3+}{}_2O_3$	14 74	15 52	61 66	9 82	15 86	15 04	63 02	8 21	7 61	17 64	14 86	13 35	15 35	62 22	8 97	20 59	12 67	60 20	62 71
Recalculated Analyses	101 39	100 62	97 25	100 67	99 24	101 38	98 49	100 14	100 13	97 53	98 52	101 16	101 83	97 52	99 87	102 35	99 28	97 66	97 58
Fe/Fe+Mg	0 3759	0 3213	0 9761	0 4068	0 3569	0 3548	0 9294	0 3642	0 3776	0 3059	0 3747	0 2798	0 3113	0 9952	0 3444	0 3395	0 3581	0 9398	0 7863
Cr/Cr+Al	0 3124	0 0138	0 1022	0 8674	0 3680	0 3099	0 4287	0 8604	0 8653	0 8290	0 2324	0 0078	0 0109	0 6749	0 8517	0 7965	0 8403	0 0000	0 0134
Ti/Ti+Cr+Al	0 0169	0 0079	0 5405	0 0195	0 0210	0 0156	0 4403	0 0173	0 0158	0 0192	0 0118	0 0065	0 0103	0 6848	0 0167	0 0176	0 0230	0 7711	0 4087

*Total Fe calculated as FeO

T33-1 SPINELS

	7-1	7-2	7-3	8-1	8-2	8-3	8-4	9-1	9-2	9-3	9-4	10-1	10-2	10-3	1-1	1-2	1-3	2-1	2-2
TiO_2	0 79	0 68	5 04	1 17	1 28	1 44	7 65	1 50	1 20	0 84	2 50	1 38	0 98	1 42	7 15	6 48	6 87	1 00	1 35
Al_2O_3	52 35	53 18	1 82	6 63	6 65	31 49	1 36	29 15	38 95	53 40	1 11	7 38	6 61	6 91	8 47	15 07	13 19	7 01	5 87
Cr_2O_3	1 53	1 03	0 42	57 88	56 25	23 15	0 03	24 70	15 59	1 56	0 50	56 06	58 28	58 14	0 11	0 00	0 00	56 33	57 22
FeO*	22 58	22 04	80 34	19 76	21 30	24 79	78 38	23 25	23 62	21 65	86 19	18 12	17 91	17 76	68 01	60 35	60 47	19 02	19 23
MnO	0 14	0 17	0 58	0 09	0 61	0 18	1 10	0 28	-	0 12	0 72	0 45	0 10	0 17	0 30	0 65	0 51	0 29	0 62
MgO	21 34	22 17	3 14	14 17	13 23	17 86	2 78	18 27	18 80	22 04	1 54	14 47	14 71	14 62	9 76	12 49	11 89	13 25	13 12
Total	98 73	99 27	91 34	99 70	99 32	98 91	91 30	97 15	98 16	99 61	92 56	97 86	98 59	99 02	93 80	95 04	92 93	95 90	96 06
$Fe^{2+}O$	8 11	7 02	29 69	12 45	13 35	10 74	31 90	9 13	10 19	7 54	30 09	11 33	11 07	11 71	23 46	19 69	20 12	12 65	12 81
$Fe^{3+}{}_2O_3$	16 08	16 69	56 29	8 13	8 83	15 61	51 65	15 69	14 92	15 68	62 35	7 54	7 60	6 73	49 51	45 19	44 84	7 08	7 13
Recalculated Analyses	100 34	100 94	96 98	100 51	100 20	100 47	96 47	98 72	99 65	101 18	98 80	98 62	99 35	99 69	98 76	99 57	97 42	97 61	98 12
Fe/Fe+Mg	0 3334	0 3197	0 9236	0 3973	0 4321	0 3962	0 9302	0 3756	0 3726	0 3171	0 9636	0 3718	0 3653	0 3647	0 7671	0 6955	0 7062	0 4042	0 4093
Cr/Cr+Al	0 0192	0 0128	0 1341	0 8542	0 8502	0 3303	0 0146	0 3624	0 2117	0 0192	0 2321	0 8360	0 8554	0 8495	0 0086	0 0000	0 0000	0 8435	0 8674
Ti/Ti+Cr+Al	0 0094	0 0080	0 6048	0 0162	0 0199	0 0192	0 7796	0 0205	0 0153	0 0097	0 5246	0 0192	0 0135	0 0194	0 3481	0 2153	0 2494	0 0140	0 0191

T35 SPINELS

	2-3	3-1	3-2	3-3	3-4	3-5	4-1	4-2	4-3	5-1	5-2	5-3	6-1	6-2	6-3	1-1	2-1	2-2	2-3
TiO_2	1 74	1 02	1 12	1 24	1 50	8 81	7 01	6 66	6 52	6 57	6 87	5 70	6 93	6 42	6 81	2 87	1 49	1 64	1 51
Al_2O_3	28 11	6 52	6 40	26 40	32 44	16 23	13 98	14 62	15 80	15 12	15 55	17 99	15 20	15 19	12 52	1 22	4 10	3 75	7 59
Cr_2O_3	26 98	56 45	57 02	29 35	22 45	0 00	0 12	0 15	0 00	0 00	0 00	0 01	0 01	0 05	0 00	0 79	56 97	57 01	53 91
FeO*	24 11	19 40	19 03	23 54	23 14	53 53	62 44	61 69	60 94	61 24	59 85	55 23	60 87	60 78	63 89	83 79	19 64	19 56	19 67
MnO	0 41	0 42	0 12	0 14	0 34	0 61	0 09	0 27	0 58	0 63	0 54	0 71	0 28	0 26	0 63	0 77	0 35	0 41	0 04
MgO	17 02	13 39	12 60	16 30	17 48	14 56	12 13	12 28	12 03	11 20	13 08	13 50	12 19	12 14	11 24	1 48	13 31	13 98	14 25
Total	96 63	96 18	95 17	95 73	95 85	84 93	88 76	89 01	89 35	88 19	89 02	87 44	88 55	88 42	88 28	90 92	95 86	96 35	96 97
$Fe^{2+}O$	11 34	12 35	13 61	11 53	10 83	18 32	21 35	20 69	20 87	21 66	19 59	17 18	21 07	20 51	21 57	29 91	12 11	11 33	11 96
$Fe^{3+}{}_2O_3$	14 20	7 84	6 02	13 35	13 68	39 13	45 66	45 56	44 53	43 98	44 74	42 28	44 23	44 75	47 04	59 87	8 36	9 15	8 56
Recalculated Analyses	99 79	97 98	96 89	98 31	98 72	97 66	100 34	100 23	100 33	99 17	100 37	97 38	99 91	99 32	99 80	96 92	96 74	97 27	97 83
Fe/Fe+Mg	0 4010	0 4065	0 4165	0 4057	0 3849	0 6347	0 7087	0 7037	0 7054	0 7210	0 6838	0 6591	0 7024	0 7030	0 7288	0 9640	0 4102	0 3981	0 3948
Cr/Cr+Al	0 3917	0 8531	0 8567	0 4272	0 3171	0 0000	0 0057	0 0068	0 0000	0 0000	0 0000	0 0004	0 0004	0 0022	0 0000	0 3028	0 9031	0 9107	0 8265
Ti/Ti+Cr+Al	0 0235	0 0144	0 0158	0 0169	0 0198	0 2573	0 2413	0 2240	0 2084	0 2171	0 2199	0 1681	0 2253	0 2120	0 2576	0 5113	0 0220	0 0243	0 0215

	3-1	3-2	3-3	3-4	3-5	4-1	4-2	4-3	4-4	5-1	5-2	5-3	5-4	6-1	6-2	6-3	6-4	7-1	7-2
TiO_2	1 32	1 99	1 05	1 09	2 72	1 31	0 81	1 30	1 41	1 25	1 12	1 62	1 24	1 06	1 56	1 74	1 54	1 57	2 03
Al_2O_3	6 02	7 89	34 12	33 54	0 72	6 42	6 35	5 03	31 01	7 14	6 30	6 53	30 25	6 19	5 63	17 52	31 54	5 23	6 24
Cr_2O_3	56 24	47 01	19 23	18 02	2 38	56 54	58 43	55 79	23 63	56 83	57 56	51 50	21 56	58 24	55 25	28 01	22 82	56 94	53 72
FeO*	20 11	26 13	23 87	24 87	82 91	19 36	19 45	20 95	25 02	20 16	19 69	24 14	28 24	19 38	21 74	35 87	26 50	20 48	22 72
MnO	0 41	0 35	0 00	0 59	0 43	0 83	0 38	0 54	0 00	0 07	0 50	0 34	0 52	0 00	0 00	0 00	0 00	0 37	0 57
MgO	13 40	13 78	18 54	18 97	1 33	12 76	13 59	12 62	17 36	13 21	13 25	11 92	15 50	13 76	13 78	17 81	17 63	13 03	13 04
Total	97 50	97 15	96 81	97 08	90 49	97 22	99 01	96 23	98 43	98 66	98 42	96 05	97 31	98 63	97 96	100 95	100 03	97 62	98 32
$Fe^{2+}O$	12 64	13 01	9 28	8 10	30 11	13 12	12 45	13 13	11 42	13 74	12 92	14 89	13 14	12 64	12 80	9 94	11 75	13 38	13 99
$Fe^{3+}{}_2O_3$	8 30	14 58	16 21	18 64	58 67	6 93	7 78	8 69	15 11	7 14	7 52	10 28	16 78	7 49	9 93	28 81	16 40	7 89	9 70
Recalculated analyses	98 33	98 61	98 43	98 95	96 37	97 90	99 79	97 10	99 94	99 37	99 17	97 08	98 99	99 38	98 96	103 84	101 67	98 41	99 29
Fe/Fe+Mg	0 4150	0 4727	0 3783	0 3826	0 9672	0 4176	0 4035	0 4397	0 4052	0 4191	0 4126	0 4891	0 46	0 3997	0 4272	0 4877	0 4154	0 4262	0 4516
Cr/Cr+Al	0 8624	0 7999	0 2744	0 2639	0 6892	0 8552	0 8606	0 8815	0 3383	0 8423	0 8597	0 8410	0 3235	0 8632	0 8681	0 5175	0 3268	0 8796	0 8524
Ti/Ti+Cr+Al	0 0189	0 0312	0 0149	0 0150	0 4283	0 0182	0 0112	0 0192	0 0188	0 0173	0 0157	0 0245	0 0174	0 0147	0 0228	0 0297	0 0205	0 0225	0 0297

* Total Fe calculated as FeO

T34 SPINELS

	7-3	7-4	1-1	1-2	1-3	2-1	2-2	2-3	3-1	3-2	3-3	4-1	4-2	4-3	4-4	5-1	5-2	5-3	5-4
TiO_2	1 99	1 61	1 11	1 05	1 72	0 86	1 12	1 54	3 92	4 01	3 46	1 12	1 35	1 19	1 69	1 02	1 46	1 15	2 13
Al_2O_3	18 14	31 62	5 66	8 62	18 86	6 49	5 39	15 53	5 76	6 76	6 12	6 43	6 44	31 37	4 36	5 22	27 43	33 24	0 91
Cr_2O_3	38 97	21 95	56 94	54 98	29 23	56 57	58 15	41 32	0 08	0 13	0 00	56 60	56 15	23 38	1 37	57 08	27 84	21 87	0 60
FeO*	25 87	26 26	18 70	18 97	22 64	16 86	17 96	23 48	67 84	65 88	66 52	18 35	19 48	22 57	64 89	18 46	23 76	21 95	82 45
MnO	0 33	0 56	0 20	0 13	0 15	0 48	0 48	0 61	0 79	0 86	1 12	0 50	0 14	0 12	0 26	0 31	0 00	0 13	0 25
MgO	15 61	17 16	15 09	15 91	24 54	15 48	14 31	17 15	13 61	14 75	14 35	15 08	14 77	20 12	19 67	14 96	19 13	20 96	4 19
Total	100 91	99 16	97 70	99 66	97 14	96 74	97 41	99 63	92 00	92 39	91 57	98 08	98 33	98 75	92 24	97 05	99 62	99 30	90 53
$Fe^{2+}O$	13 04	11 69	10 10	9 97	1 57	8 81	10 86	9 20	13 34	11 84	11 39	10 06	11 19	7 07	2 59	9 83	8 61	6 22	25 51
$Fe^{3+}{}_2O_3$	14 25	16 19	9 55	10 00	26 91	8 94	7 89	15 87	60 56	60 06	61 26	9 21	9 21	17 22	69 23	9 59	16 84	17 48	63 28
Recalculated analyses	102 34	100 78	98 66	100 66	99 84	97 64	98 20	101 22	98 07	98 32	97 71	99 00	99 25	100 47	99 17	98 01	101 34	101 05	96 87
Fe/Fe+Mg	0 4393	0 4197	0 3694	0 3604	0 3037	0 3398	0 3723	0 3929	0 7020	0 6786	0 6866	0 3651	0 3840	0 3465	0 5830	0 3684	0 3699	0 3311	0 9029
Cr/Cr+Al	0 5904	0 3177	0 8709	0 8106	0 5097	0 8540	0 8786	0 6809	0 0093	0 0129	0 0000	0 8552	0 8540	0 3333	0 1741	0 8800	0 4051	0 3062	0 3067
Ti/Ti+Cr+Al	0 0279	0 0217	0 0159	0 0145	0 0277	0 0122	0 0158	0 0222	0 3008	0 2747	0 2651	0 0158	0 0211	0 0159	0 1696	0 0147	0 0198	0 0151	0 5087

All SPINELS (HK)

	6-1	6-2	6-3	6-4	6-5	7-1	7-2	7-3	7-4	7-5	1-1	1-2	1-3	2-1	2-2	2-3	2-4	3-1	3-2
TiO_2	1 16	1 27	0 81	2 97	6 15	1 12	1 31	1 11	0 91	2 39	1 94	2 96	6 23	1 52	3 41	4 85	5 71	1 59	1 75
Al_2O_3	5 63	34 97	44 52	0 69	0 21	5 84	8 17	36 56	37 49	3 89	8 95	7 55	11 45	7 85	8 26	10 78	12 10	9 62	9 45
Cr_2O_3	57 95	19 10	9 12	0 89	1 11	57 53	53 82	19 18	19 56	0 49	53 41	48 33	30 88	54 12	46 11	37 84	30 12	51 84	52 87
FeO*	18 45	23 02	22 88	85 11	84 39	18 01	18 44	20 80	19 91	72 94	19 68	24 86	34 97	21 12	26 41	30 25	34 56	19 89	19 89
MnO	0 43	0 35	0 02	0 25	1 29	0 63	0 31	0 23	0 06	0 95	0 49	0 46	0 65	0 72	0 23	0 57	0 48	0 78	0 79
MgO	14 79	20 56	22 67	0 91	1 36	15 23	16 79	21 52	20 89	12 02	12 63	12 55	12 75	12 87	12 78	13 00	13 64	13 30	13 12
Total	98 41	99 27	100 02	90 82	94 51	98 36	98 84	99 40	98 82	92 68	97 10	96 71	96 93	98 20	97 20	97 29	96 61	97 02	97 87
$Fe^{2+}O$	10 58	6 98	5 45	31 28	33 46	9 70	8 48	5 77	6 65	14 24	14 59	15 39	18 65	13 83	15 96	17 06	17 01	13 07	13 71
$Fe^{3+}{}_2O_3$	8 74	17 82	19 38	59 82	56 59	9 24	11 07	16 71	14 74	65 32	5 66	10 52	18 14	8 10	11 61	14 66	19 50	7 58	6 87
Recalculated analyses	99 29	101 05	101 96	96 81	100 18	99 29	99 77	101 07	100 30	99 21	97 67	97 76	98 75	99 10	98 36	98 76	98 56	97 81	98 56
Fe/Fe+Mg	0 3709	0 3461	0 3230	0 9779	0 9670	0 3585	0 3417	0 3136	0 3106	0 7415	0 4241	0 4835	0 5645	0 4368	0 4941	0 5238	0 5450	0 4141	0 4174
Cr/Cr+Al	0 8735	0 2682	0 1208	0 4639	0 7800	0 9078	0 8155	0 2603	0 2593	0 0779	0 8001	0 8111	0 6480	0 8222	0 7892	0 7019	0 6255	0 7834	0 7896
Ti/Ti+Cr+Al	0 0164	0 0167	0 0101	0 5955	0 8043	0 0174	0 0185	0 0141	0 0113	0 2655	0 0269	0 0451	0 1100	0 0215	0 0526	0 0907	0 1191	0 0223	0 0243
	3-3	3-4	4-1	4-2	4-3	4-4	5-1	5-2	5-3	6-1	6-2	7-1	7-2	7-3	7-4	7-5	8-1	8-2	8-3
TiO_2	1 52	1 59	1 91	2 08	1 84	1 49	2 05	1 87	1 56	1 68	1 75	3 80	3 99	6 87	8 60	3 25	13 40	13 39	11 87
Al_2O_3	9 34	8 78	9 62	10 12	10 53	10 81	8 19	9 03	10 47	11 12	9 89	8 76	7 95	13 01	12 99	0 89	9 49	8 78	9 31
Cr_2O_3	52 16	53 14	51 40	51 12	50 90	50 28	52 49	52 42	50 16	51 57	52 90	43 16	44 33	22 98	13 98	0 52	1 50	1 06	0 34
FeO*	19 84	20 13	20 14	19 41	19 91	19 17	20 58	19 96	19 40	19 35	19 45	27 45	26 23	38 26	44 26	81 12	54 30	55 01	57 32
MnO	0 48	0 49	0 43	0 52	0 20	0 38	0 30	0 45	0 68	0 20	0 56	0 40	0 72	0 74	0 46	1 54	0 51	0 69	0 63
MgO	12 97	12 87	13 26	13 01	13 20	13 98	12 58	13 04	13 11	13 79	13 12	13 25	12 90	14 08	14 17	4 75	14 76	13 91	14 53
Total	96 31	97 00	96 76	96 26	96 58	96 11	96 19	96 77	95 38	97 71	97 67	96 82	96 12	95 94	94 46	92 07	93 96	92 84	94 00
$Fe^{2+}O$	13 65	13 87	13 86	14 02	14 01	12 23	14 56	13 86	13 03	13 42	13 93	15 41	15 42	17 12	18 43	24 84	21 22	21 86	20 13
$Fe^{3+}{}_2O_3$	6 88	6 96	7 18	5 99	6 55	7 71	6 69	6 78	7 08	6 59	6 13	13 38	12 01	23 50	28 71	62 55	36 76	36 84	41 33
Recalculated analyses	96 90	97 70	97 48	96 86	97 24	96 88	96 86	97 45	96 09	98 37	98 28	98 16	97 32	98 29	97 34	98 34	97 64	96 53	98 14
Fe/Fe+Mg	0 4215	0 4251	0 4179	0 4136	0 4162	0 3933	0 4361	0 4198	0 4116	0 3988	0 4120	0 4947	0 4901	0 5622	0 5962	0 8898	0 6349	0 6515	0 6509
Cr/Cr+Al	0 7893	0 8024	0 7819	0 7721	0 7643	0 7573	0 8113	0 7957	0 7627	0 7568	0 7812	0 7677	0 7891	0 5423	0 4193	0 2816	0 0959	0 0749	0 0239
Ti/Ti+Cr+Al	0 0214	0 0223	0 0269	0 0290	0 0256	0 0209	0 0293	0 0263	0 0221	0 0229	0 0240	0 0604	0 0633	0 1336	0 1970	0 6260	0 4489	0 4737	0 4426

*Total Fe calculated as FeO

	9-1	9-2	9-3	10-4	10-2	10-3	10-4	11-1	11-2	11-3	11-4	12-1	12-2	12-3	13-1	13-2	13-3	13-4	14-1
TiO_2	1 82	8 19	2 39	1 97	1 83	2 03	10 91	1 95	2 12	2 15	11 03	11 91	12 46	12 91	1 97	1 55	1 73	3 16	2 03
Al_2O_3	7 72	13 04	6 78	10 27	10 17	7 05	13 40	7 34	10 72	10 45	13 01	11 81	10 54	9 81	9 61	9 73	9 74	7 30	9 88
Cr_2O_3	54 80	19 98	53 45	50 21	50 78	52 87	7 60	53 89	52 11	52 16	0 33	1 88	0 96	0 36	53 93	55 31	53 64	51 16	53 15
FeO*	20 32	40 12	21 53	18 27	18 16	20 78	50 43	21 15	19 09	19 01	54 46	53 26	54 35	55 42	19 38	19 37	19 30	24 12	19 72
MnO	0 60	0 46	0 62	0 11	0 52	0 25	0 02	0 30	0 35	0 95	0 66	0 32	0 68	0 72	0 78	0 00	0 59	0 21	0 35
MgO	12 10	12 74	11 25	18 19	16 26	13 82	13 96	12 22	11 87	12 02	11 87	12 24	11 80	11 45	12 25	12 26	11 61	10 94	12 69
Total	97 36	94 53	96 02	99 02	97 72	96 80	96 32	96 85	96 26	96 74	91 36	91 42	90 79	90 67	97 92	98 22	96 61	96 89	97 82
$Fe^{2+}O$	15 07	20 17	16 29	7 39	9 36	12 75	21 98	15 10	16 02	15 34	23 05	23 42	23 83	24 59	15 25	15 75	15 79	18 24	15 08
$Fe^{3+}{}_2O_3$	5 83	22 17	5 83	12 10	9 78	8 93	31 61	6 73	3 41	4 08	34 91	33 16	33 91	34 27	4 59	4 02	3 90	6 53	5 15
Recalculated analyses	97 94	96 75	96 60	100 14	98 70	97 69	99 49	97 52	96 60	97 15	94 86	94 74	94 19	94 10	98 38	98 62	97 00	97 54	98 34
Fe/Fe+Mg	0 4425	0 5981	0 4749	0 3219	0 3455	0 4154	0 6307	0 4500	0 4319	0 4278	0 6844	0 6729	0 6852	0 6958	0 4278	0 4275	0 4490	0 5103	0 4235
Cr/Cr+Al	0 8265	0 5069	0 8410	0 7660	0 7701	0 8342	0 2756	0 8312	0 7653	0 7700	0 0167	0 0965	0 0576	0 0240	0 7901	0 7922	0 7870	0 8246	0 7830
Ti/Ti+Cr+Al	0 0254	0 1650	0 0345	0 0278	0 0257	0 0296	0 2734	0 0278	0 0288	0 0293	0 3472	0 3676	0 4155	0 4504	0 0267	0 0207	0 0236	0 0462	0 0277

A61-9 SPINELS (PK)

	14-2	14-2	15-1	1-1	1-2	1-3	1-4	2-1	2-2	2-3	3-1	3-2	3-3	3-4	4-1	4-2	4-3	5-1	5-2
TiO_2	1 81	1 52	13 89	1 19	1 40	1 47	1 83	10 46	10 43	9 45	1 67	2 95	10 16	10 09	10 82	11 46	10 61	9 15	7 81
Al_2O_3	10 18	11 03	8 08	8 25	5 49	5 38	5 07	3 48	3 42	3 84	7 36	4 56	5 33	4 68	2 39	2 45	2 40	4 97	3 56
Cr_2O_3	51 79	53 73	0 98	55 62	59 74	58 97	56 30	0 05	0 07	0 05	58 05	48 58	0 43	0 09	0 00	0 06	0 27	0 06	0 35
FeO*	19 17	18 31	60 04	18 45	17 64	18 72	21 31	70 33	70 42	70 24	18 30	30 11	69 44	69 63	72 31	71 52	71 17	70 24	73 58
MnO	0 94	0 14	0 11	0 34	0 29	0 45	0 36	0 57	0 34	0 71	0 23	0 54	0 33	0 38	0 64	0 68	0 61	0 58	0 54
MgO	12 22	11 81	11 14	12 69	12 05	12 13	11 95	8 27	8 56	8 78	13 09	10 49	8 55	8 49	8 43	8 27	8 55	8 61	6 98
Total	96 11	96 54	94 24	12 69	96 61	97 12	96 82	93 16	93 24	93 07	98 70	97 23	94 24	93 36	94 59	94 44	93 61	93 61	92 82
$Fe^{2+}O$	14 51	15 91	27 46	13 67	14 45	14 40	14 98	27 43	27 21	25 65	14 15	18 20	27 59	27 28	27 75	28 47	27 09	26 12	27 02
$Fe^{3+}{}_2O_3$	5 18	2 66	36 20	5 30	3 45	4 80	7 03	47 68	48 02	49 55	4 62	13 24	46 51	47 07	49 52	47 85	48 99	49 03	51 75
Recalculated analyses	96 63	96 81	97 87	97 06	96 97	97 60	97 52	97 94	98 05	98 03	99 16	98 56	98 90	98 25	99 55	99 23	98 52	98 52	98 00
Fe/Fe+Mg	0 4258	0 4229	0 7181	0 4072	0 4090	0 4218	0 4574	0 8008	0 7954	0 7909	0 3979	0 5757	0 7933	0 7949	0 8022	0 8034	0 7973	0 7941	0 8328
Cr/Cr+Al	0 7734	0 7657	0 0752	0 8189	0 8795	0 8803	0 8816	0 0095	0 0135	0 0087	0 8410	0 8773	0 0513	0 0123	0 0000	0 0162	0 0702	0 0083	0 0619
Ti/Ti+Cr+Al	0 0251	0 0202	0 5036	0 0164	0 0192	0 0204	0 0265	0 6551	0 6575	0 6089	0 0225	0 0482	0 5357	0 5663	0 7428	0 7460	0 7240	0 5382	0 5677

T7 SPINELS (HK)

	1-1	1-2	1-3	1-4	1-5	1-6	2-1	2-2	2-3	2-4	2-5	3-1	3-2	3-3	4-1	4-2	4-3	5-1	5-2
TiO_2	1 70	2 03	1 99	4 47	4 26	10 09	1 79	1 80	1 55	1 65	1 87	10 12	10 14	9 78	4 45	4 71	4 67	10 23	10 13
Al_2O_3	6 20	5 24	5 33	7 30	20 07	12 85	6 99	6 51	5 97	4 83	5 23	15 28	12 96	13 19	11 80	8 03	10 36	14 18	14 46
Cr_2O_3	57 53	56 88	56 56	42 84	26 37	0 23	57 21	57 18	57 14	59 29	57 84	0 11	0 00	0 08	36 29	39 57	38 84	0 11	0 03
FeO*	20 22	20 29	22 63	31 19	32 43	57 91	19 84	19 89	19 57	20 91	19 11	55 39	58 11	57 23	30 34	32 32	31 35	56 92	56 59
MnO	0 74	0 68	0 43	0 25	0 44	0 42	0 29	0 28	0 59	0 39	0 58	0 45	0 33	0 51	0 61	0 36	0 26	0 31	0 46
MgO	12 49	12 59	12 26	12 29	15 58	12 66	12 78	12 67	12 87	12 08	12 91	13 51	12 75	12 64	14 96	13 80	13 66	12 98	13 11
Total	98 88	97 71	99 20	98 34	99 15	94 16	98 90	98 33	97 69	99 15	97 54	94 86	94 29	93 43	98 45	98 79	99 14	94 73	94 78
$Fe^{2+}O$	14 48	14 17	15 40	17 92	14 85	22 19	14 71	14 62	13 50	15 29	13 57	21 46	22 25	21 66	14 24	16 02	16 75	22 31	21 93
$Fe^{3+}{}_2O_3$	6 38	6 81	8 03	14 75	19 54	39 70	5 76	5 85	6 74	6 25	6 16	37 71	39 86	39 52	17 89	18 11	16 22	38 47	38 52
Recalculated analyses	99 52	98 39	100 00	99 82	101 11	98 14	99 53	98 92	98 37	99 78	98 16	98 64	98 28	97 39	100 24	100 60	100 76	98 58	98 64
Fe/Fe+Mg	0 4315	0 4324	0 4659	0 5454	0 4959	0 6838	0 4238	0 4260	0 4182	0 4500	0 4116	0 6596	0 6830	0 6815	0 4894	0 5254	0 5203	0 6746	0 6711
Cr/Cr+Al	0 8616	0 8793	0 8768	0 7974	0 4685	0 0119	0 8459	0 8549	0 8652	0 8917	0 8812	0 0048	0 0000	0 0041	0 6735	0 7678	0 7155	0 0052	0 0014
Ti/Ti+Cr+Al	0 0236	0 0290	0 0285	0 0733	0 0672	0 3311	0 0246	0 0250	0 0218	0 0231	0 0264	0 2960	0 3330	0 3203	0 0728	0 0800	0 0756	0 3141	0 3086

* Total Fe calculated as FeO

C49 SPINELS (HK)

	5-3	6-1	6-2	6-3	6-4	7-1	7-2	7-3	8-1	8-2	8-3	8-4	1-1	1-2	1-3	1-4	2-1	2-2	2-3
TiO_2	9 01	1 75	1 90	3 69	2 79	10 53	9 87	5 51	1 55	1 63	1 80	1 42	1 67	1 45	1 42	3 42	1 65	1 60	2 59
Al_2O_3	15 17	6 40	6 01	8 37	27 86	14 29	15 65	3 01	6 34	6 11	5 73	7 23	9 03	9 64	9 89	5 40	9 09	9 01	19 52
Cr_2O_3	0 00	55 91	56 75	44 03	24 57	0 04	0 17	0 28	57 32	58 16	55 52	49 80	51 82	51 12	50 13	1 76	53 42	52 75	32 14
FeO*	56 08	20 64	20 57	27 45	25 40	54 29	54 80	71 84	19 80	19 33	20 36	18 78	17 39	18 01	19 13	61 65	19 07	19 18	25 30
MnO	0 60	0 30	0 22	0 71	0 02	0 29	0 37	1 64	0 24	0 27	0 29	0 43	0 43	0 42	0 46	0 79	0 24	0 51	0 34
MgO	13 98	14 20	13 62	14 84	19 63	13 61	15 53	9 02	13 88	13 63	15 28	19 29	17 23	16 97	16 89	22 97	17 41	17 29	20 12
Total	94 84	99 20	99 07	99 09	100 27	93 05	96 39	91 30	99 13	99 13	98 98	96 95	97 57	97 61	97 92	95 99	100 88	100 34	100 01
$Fe^{2+}O$	19 61	12 53	13 51	13 27	9 31	21 08	18 81	20 23	12 85	13 22	10 78	3 84	7 61	7 94	8 15	0 08	8 59	8 16	6 71
$Fe^{3+}{}_2O_3$	40 53	9 01	7 84	15 76	17 88	36 90	40 00	57 35	7 73	6 79	10 64	16 60	10 87	11 20	12 21	68 60	11 64	12 24	20 66
Recalculated analyses	98 90	100 10	99 86	100 67	102 06	96 75	100 40	97 04	99 90	99 81	100 05	98 61	98 66	98 73	99 14	102 86	102 05	101 47	102 08
Fe/Fe+Mg	0 6547	0 4072	0 4165	0 4605	0 3795	0 6534	0 6252	0 7901	0 4027	0 4013	0 3864	0 3151	0 3230	0 3341	0 3487	0 5592	0 3411	0 3440	0 3728
Cr/Cr+Al	0 0000	0 8542	0 8637	0 7792	0 3717	0 0019	0 0072	0 0587	0 8585	0 8646	0 8667	0 8221	0 7938	0 7806	0 7727	0 1794	0 7977	0 7971	0 5248
Ti/Ti+Cr+Al	0 2748	0 0248	0 0268	0 0585	0 0386	0 3194	0 2855	0 5237	0 0216	0 0225	0 0260	0 0218	0 0238	0 0206	0 0204	0 2490	0 0229	0 0211	0 0387
	2-4	3-1	3-2	3-3	3-4	4-1	4-2	4-3	5-1	5-2	5-3	6-1	6-2	6-3	7-1	7-2	7-3	8-1	8-2
TiO_2	6 55	1 41	2 05	1 72	1 47	1 54	1 65	1 80	1 51	1 43	2 05	1 62	2 20	2 04	2 43	2 28	1 94	1 76	1 28
Al_2O_3	2 88	8 56	22 69	8 75	8 78	27 56	28 05	27 10	8 12	9 17	21 43	10 10	26 73	29 26	21 07	15 49	27 85	8 95	10 02
Cr_2O_3	0 76	50 34	34 07	51 71	52 13	29 35	27 14	27 97	54 42	54 07	34 28	53 12	29 06	25 47	32 12	40 85	26 01	53 87	51 97
FeO*	67 94	18 08	20 75	18 14	17 91	23 03	22 81	23 54	18 51	18 69	22 47	18 35	23 54	22 33	24 92	22 59	22 41	18 82	18 60
MnO	0 60	0 23	0 31	0 51	0 33	0 00	0 00	0 23	0 36	0 42	0 06	0 35	0 33	0 35	0 18	0 00	0 09	0 27	0 26
MgO	16 53	18 98	19 78	17 01	16 52	18 03	18 84	17 12	14 56	14 34	18 77	14 45	17 74	19 25	17 02	15 72	17 86	14 60	14 09
Total	95 26	78 62	99 65	97 84	97 14	99 51	98 49	97 76	97 48	98 12	99 06	97 99	99 60	98 70	97 74	96 93	96 16	98 27	96 22
$Fe^{2+}O$	12 05	4 90	7 06	7 96	8 44	9 34	8 93	11 06	11 40	11 97	8 48	12 14	10 90	8 56	10 90	11 74	9 80	12 04	11 90
$Fe^{3+}{}_2O_3$	62 11	14 65	15 21	11 31	10 53	15 21	15 42	13 87	7 90	7 47	15 55	6 90	14 04	15 30	15 58	12 06	14 01	7 54	7 44
Recalculated analyses	101 48	99 07	101 17	98 97	98 19	101 84	100 03	99 15	98 27	98 87	100 62	98 68	101 01	100 23	99 30	98 14	97 56	99 03	96 97
Fe/Fe+Mg	0 6602	0 3105	0 3315	0 3351	0 3388	0 3662	0 3640	0 3939	0 3753	0 3812	0 3614	0 3751	0 3854	0 3541	0 4090	0 4045	0 3723	0 3786	0 3842
Cr/Cr+Al	0 1504	0 7978	0 5018	0 7986	0 7993	0 4167	0 3936	0 4091	0 8180	0 7982	0 5176	0 7792	0 4217	0 3687	0 5056	0 6389	0 3852	0 8015	0 7768
Ti/Ti+Cr+Al	0 5521	0 0208	0 0279	0 0246	0 0210	0 0204	0 0223	0 0244	0 0211	0 0197	0 0286	0 0221	0 0295	0 0273	0 0351	0 0328	0 0266	0 0243	0 0179

T29S SPINELS (HK)

	8-3	8-4	9-1	9-2	9-3	9-4	10-1	10-2	10-3	10-4	1-1	1-2	1-3	1-4	1-5	2-1	2-2	2-3	2-4
TiO_2	1 89	2 15	1 40	1 71	2 03	11 38	1 70	1 41	2 19	2 21	0 76	0 62	1 42	7 06	7 70	0 70	0 23	10 97	7 02
Al_2O_3	23 82	22 83	9 46	10 15	28 94	1 05	9 68	10 55	24 12	32 59	56 19	54 21	47 91	17 53	14 07	0 30	0 28	8 60	17 96
Cr_2O_3	29 56	30 10	52 70	51 45	26 87	1 01	53 16	52 48	31 52	21 96	0 59	0 00	0 06	0 03	0 05	0 33	0 34	0 28	0 00
FeO*	25 13	25 04	19 78	20 12	21 93	65 52	19 00	19 60	24 24	24 38	20 41	22 69	27 92	57 00	59 71	87 36	87 95	65 77	56 21
MnO	0 28	0 13	0 27	0 48	0 32	0 66	0 13	0 49	0 27	0 34	0 12	0 10	0 19	0 19	0 49	0 02	0 15	0 19	0 25
MgO	15 86	15 75	13 82	13 81	17 48	13 38	14 02	14 14	16 99	18 54	22 73	22 06	20 59	14 77	12 10	2 55	2 75	8 13	14 53
Total	96 54	96 00	97 43	97 72	97 57	93 00	97 69	98 67	99 33	100 02	100 80	99 68	98 09	96 58	94 12	91 26	91 70	85 81	95 97
$Fe^{2+}O$	12 12	12 34	12 72	13 01	10 83	19 96	12 93	12 59	11 60	10 75	7 22	7 50	8 95	18 04	17 89	27 16	26 46	29 42	18 16
$Fe^{3+}{}_2O_3$	14 46	14 12	7 84	7 90	12 34	50 65	6 75	7 79	14 04	15 14	14 66	16 88	21 08	43 30	46 48	66 90	68 33	40 40	42 28
Recalculated analyses	97 99	97 41	98 22	98 51	98 81	98 07	98 37	99 45	100 74	101 54	102 27	101 37	100 20	100 92	101 45	97 96	98 54	97 99	100 21
Fe/Fe+Mg	0 4282	0 4290	0 4035	0 4078	0 3723	0 6983	0 3905	0 3958	0 4028	0 3833	0 2980	0 3271	0 3906	0 6458	0 6565	0 9418	0 9380	0 7927	0 6465
Cr/Cr+Al	0 4543	0 4693	0 7889	0 7728	0 3838	0 3922	0 7865	0 7694	0 4671	0 3113	0 0070	0 0000	0 0008	0 0011	0 0024	0 4246	0 4489	0 0214	0 0000
Ti/Ti+Cr+Al	0 0269	0 0309	0 0195	0 0238	0 0268	0 0078	0 0234	0 0193	0 0299	0 0289	0 0085	0 0072	0 0185	0 2042	0 2584	0 4614	0 2241	0 4434	0 1996

* Total Fe calculated as FeO

	3-1	3-2	3-3	4-1	4-2	4-3	5-1	5-2	5-3	6-1	6-2	6-3	6-4	6-5	6-6	7-1	7-2	7-3	7-4
TiO_2	4 51	3 98	3 91	5 57	4 03	2 49	7 55	7 86	7 67	0 84	0 88	0 98	7 84	7 49	7 84	0 59	0 88	2 35	7 18
Al_2O_3	0 53	0 11	0 45	0 00	0 21	0 25	19 70	17 77	17 00	54 73	54 39	52 54	15 03	17 24	17 05	54 48	51 79	47 76	16 88
Cr_2O_3	0 87	0 19	0 10	0 11	0 07	0 12	0 00	0 00	0 05	0 65	0 59	0 06	0 00	0 09	0 00	0 58	0 27	0 00	0 00
FeO*	82 87	84 27	85 01	83 26	84 37	87 03	55 37	56 15	56 88	21 31	20 61	22 17	56 26	56 96	57 72	20 03	22 44	26 79	52 43
MnO	0 56	0 59	0 81	0 90	0 77	1 18	0 38	0 38	0 80	0 16	0 21	0 13	0 25	0 34	0 53	0 09	0 04	0 03	0 40
MgO	4 50	3 45	2 79	1 35	1 68	2 03	15 90	14 26	14 44	21 76	21 36	21 31	12 97	14 10	13 58	21 09	21 05	19 88	17 60
Total	93 84	92 59	93 07	91 19	91 13	93 10	98 90	96 42	96 84	99 45	98 04	97 19	92 35	96 22	96 72	96 86	96 47	96 81	94 49
$Fe^{2+}O$	27 83	28 48	29 40	32 25	30 56	28 94	17 62	19 29	18 47	8 07	7 97	7 87	19 64	19 12	20 16	7 51	7 92	10 55	12 84
$Fe^{3+}{}_2O_3$	61 17	62 01	61 79	56 68	59 80	64 56	41 95	40 96	42 69	14 71	14 05	15 89	40 70	42 06	41 74	13 92	16 14	18 05	44 00
Recalculated analyses	99 97	98 80	99 26	96 87	97 12	99 57	103 10	100 52	101 12	100 92	99 45	98 78	96 43	100 43	100 90	98 25	98 09	98 62	98 90
Fe/Fe+Mg	0 8970	0 9203	0 9351	0 9668	0 9596	0 9530	0 6221	0 6505	0 6506	0 3164	0 3132	0 3296	0 6722	0 6563	0 6677	0 3098	0 3351	0 3891	0 5847
Cr/Cr+Al	0 5241	0 5368	0 1297	1 0000	0 1827	0 2436	0 0000	0 0000	0 0020	0 0079	0 0072	0 0008	0 0000	0 0035	0 0000	0 0071	0 0035	0 0000	0 0000
Ti/Ti+Cr+Al	0 7210	0 9145	0 8283	0 9797	0 9091	0 8278	0 1965	0 2201	0 2232	0 0096	0 0101	0 0118	0 2497	0 2164	0 2268	0 0068	0 0107	0 0304	0 2135
	8-1	8-2	8-3	9-1	9-2	9-3	9-4	9-5	10-1	10-2	10-3	10-4	10-5	10-6	11-1	11-2	11-3	11-4	12-1
TiO_2	8 30	7 88	7 25	0 80	0 75	1 22	1 43	2 09	1 48	1 75	1 74	0 88	1 60	7 04	0 90	1 44	4 88	8 32	2 14
Al_2O_3	14 83	15 43	14 64	55 13	55 33	46 57	5 50	8 65	5 21	4 90	33 32	53 86	46 14	19 16	52 97	47 21	29 38	15 64	5 13
Cr_2O_3	0 00	0 00	0 06	0 78	0 17	8 62	57 43	47 78	58 61	56 92	21 30	0 41	0 20	0 27	0 55	0 01	0 08	0 00	52 66
FeO*	59 02	57 14	60 13	20 35	21 92	21 90	22 84	27 91	19 52	20 46	23 51	22 02	28 92	54 12	21 82	26 69	43 15	57 46	23 44
MnO	0 53	0 38	0 41	0 18	0 13	0 14	0 34	0 44	0 36	0 17	0 11	0 18	0 14	0 39	0 08	0 11	0 27	0 33	0 47
MgO	12 04	12 96	11 79	21 88	21 82	19 72	12 72	13 13	13 03	13 32	18 67	21 45	19 63	14 35	21 00	19 76	17 81	13 55	12 77
Total	94 72	93 79	94 28	99 12	100 12	98 17	100 26	100 00	98 21	97 52	98 65	98 80	96 63	95 33	97 32	95 22	95 57	95 30	96 61
$Fe^{2+}O$	21 93	20 09	21 35	7 78	8 17	9 84	14 67	15 03	13 47	13 22	10 04	8 23	9 89	18 26	8 41	9 26	12 72	20 16	13 89
$Fe^{3+}{}_2O_3$	41 22	41 17	43 10	13 97	15 28	13 40	9 08	14 31	6 72	8 05	14 97	15 33	21 15	39 86	14 90	19 37	33 81	41 46	10 61
Recalculated analyses	98 85	97 91	98 60	100 52	101 65	99 51	101 17	101 43	98 88	98 33	100 15	100 34	98 75	99 32	98 81	97 16	98 96	99 45	97 67
Fe/Fe+Mg	0 6985	0 6757	0 7068	0 3054	0 3220	0 3442	0 4591	0 5012	0 4146	0 4206	0 3731	0 3267	0 4105	0 6406	0 3294	0 3897	0 5338	0 6672	0 4646
Cr/Cr+Al	0 0000	0 0000	0 0027	0 0094	0 0021	0 1105	0 8751	0 7875	0 8830	0 8863	0 3001	0 0051	0 0029	0 0094	0 0069	0 0001	0 0018	0 0000	0 8732
Ti/Ti+Cr+Al	0 2631	0 2458	0 2396	0 0091	0 0086	0 0147	0 0203	0 0317	0 0208	0 0253	0 0228	0 0103	0 0216	0 1885	0 0107	0 0191	0 0957	0 2534	0 0326
										DD39-13 (PK)									
	12-2	12-3	12-4	12-5	12-6	13-1	13-2	13-3	13-4	1-1	1-2	1-3	1-4	1-5	1-6	2-1	2-2	2-3	2-4
TiO_2	0 80	1 07	3 30	7 65	7 57	0 79	0 85	7 82	5 04	0 76	0 90	1 99	2 16	4 32	13 01	4 35	2 47	2 40	15 11
Al_2O_3	43 21	52 96	40 68	17 39	14 06	53 79	52 02	15 33	0 81	5 69	5 68	14 29	10 15	11 47	16 13	10 50	11 56	13 33	16 15
Cr_2O_3	14 82	0 73	0 11	0 00	0 20	0 53	0 36	0 00	0 00	59 98	60 39	49 01	49 57	41 14	4 11	41 92	48 27	46 89	2 62
FeO*	20 45	23 37	35 00	57 63	59 37	20 85	21 79	58 13	83 54	19 03	19 53	19 28	20 57	27 39	46 10	25 40	19 87	19 87	45 23
MnO	0 09	0 28	0 16	0 30	0 47	0 00	0 00	0 36	0 66	0 75	0 20	0 37	0 32	0 46	0 48	0 21	0 40	0 30	0 41
MgO	19 13	20 47	17 68	13 49	14 16	21 27	21 40	13 34	3 11	13 12	12 89	15 46	14 33	16 87	16 89	14 71	14 45	14 27	19 27
Total	98 50	98 88	96 93	96 46	95 83	97 23	96 42	94 98	93 16	99 33	99 59	100 40	97 10	101 65	96 72	97 09	97 02	97 06	98 79
$Fe^{2+}O$	9 96	9 11	13 66	20 32	18 40	8 06	7 42	19 86	30 13	12 73	13 84	12 35	12 59	12 31	19 45	14 21	12 79	13 38	18 44
$Fe^{3+}{}_2O_3$	11 66	15 84	23 71	41 46	45 53	14 21	15 97	42 53	59 36	7 00	6 33	7 70	8 86	16 76	29 62	12 44	7 87	7 21	29 77
Recalculated analyses	99 67	100 47	99 31	100 61	100 39	98 65	98 02	99 24	99 11	100 03	100 22	101 17	97 99	103 33	99 69	98 34	97 81	97 78	101 77
Fe/Fe+Mg	0 3357	0 3505	0 4834	0 6688	0 6646	0 3166	0 3249	0 6732	0 9270	0 4067	0 4173	0 3709	0 4042	0 4342	0 5633	0 4494	0 3939	0 3969	0 5259
Cr/Cr+Al	0 1870	0 0092	0 0018	0 0000	0 0095	0 0066	0 0046	0 0000	0 0000	0 8761	0 8770	0 7742	0 7661	0 7064	0 4160	0 7281	0 7369	0 7024	0 0981
Ti/Ti+Cr+Al	0 0095	0 0126	0 0491	0 2192	0 2539	0 0092	0 0103	0 2456	0 7988	0 0104	0 0123	0 0305	0 0308	0 0659	0 3053	0 0670	0 0346	0 0331	0 3500

* Total Fe calculated as FeO

																	DD39-19 SPINELS (HK)		
	3-1	3-2	3-3	3-4	4-1	4-2	4-3	4-4	5-1	5-2	5-3	5-4	5-5	6-1	6-2	6-3	1-1	1-2	1-3
TiO_2	2 24	2 17	1 79	6 07	2 16	2 06	2 19	4 56	2 07	1 97	1 79	2 17	6 88	1 80	2 17	2 08	2 24	4 22	6 30
Al_2O_3	10 63	13 58	6 63	16 50	11 63	13 04	7 25	13 61	11 86	12 09	10 90	6 28	14 96	12 94	14 33	13 71	6 50	10 11	16 47
Cr_2O_3	50 73	48 68	53 91	26 12	49 23	47 65	50 75	33 41	50 41	51 09	52 90	53 19	25 26	48 81	47 48	46 94	53 49	43 44	27 03
FeO*	20 01	19 62	20 25	30 10	19 75	19 34	21 49	27 90	19 63	19 80	19 39	21 79	31 64	19 42	19 27	18 93	21 38	26 88	33 08
MnO	0 27	0 06	0 41	0 35	0 35	0 38	0 48	0 38	0 24	0 07	0 29	0 51	0 56	0 34	0 10	0 30	0 52	0 51	0 61
MgO	14 36	15 30	13 10	16 03	14 92	14 47	13 32	14 63	15 02	14 50	14 16	13 08	15 39	15 26	15 52	15 23	13 19	14 81	16 21
Total	98 24	99 41	96 09	95 17	98 04	96 94	95 48	94 49	99 23	99 52	99 43	97 02	94 69	98 57	98 87	97 19	97 32	99 97	99 70
$Fe^{2+}O$	13 09	12 64	13 16	14 01	12 19	12 61	13 04	14 05	12 48	13 47	13 38	13 69	15 12	11 73	12 21	11 74	13 70	14 52	15 17
$Fe^{3+}{}_2O_3$	7 69	7 75	7 88	17 88	8 40	7 48	9 39	15 39	7 95	7 04	6 68	9 00	18 36	8 54	7 84	7 99	8 53	13 74	19 91
Recalculated analyses	99 01	100 19	96 88	96 96	98 88	97 69	96 42	96 03	100 03	100 22	100 10	97 92	96 53	99 43	99 66	97 99	98 17	101 35	101 69
Fe/Fe+Mg	0 3971	0 3774	0 4222	0 4702	0 3849	0 3872	0 4326	0 4741	0 3819	0 3923	0 3929	0 4405	0 4928	0 3756	0 3698	0 3701	0 4338	0 4618	0 4910
Cr/Cr+Al	0 7620	0 7063	0 8451	0 5150	0 7396	0 7103	0 8244	0 6222	0 7404	0 7392	0 7650	0 8503	0 5311	0 7167	0 6897	0 6967	0 8466	0 7424	0 5240
Ti/Ti+Cr+Al	0 0310	0 0291	0 0260	0 1022	0 0299	0 0284	0 0327	0 0747	0 0281	0 0264	0 0240	0 0319	0 1209	0 0245	0 0291	0 0285	0 0326	0 0624	0 1041
																		DD39-18 (HK)	
	2-1	2-2	2-3	2-4	2-5	3-1	3-2	3-3	3-4	4-1	4-2	4-3	4-4	5-1	5-2	5-3	5-4	1-1	1-2
TiO_2	2 21	2 14	2 11	4 03	13 09	2 15	1 98	2 13	1 87	3 82	3 94	6 45	11 29	2 61	2 30	2 82	13 53	3 11	1 65
Al_2O_3	11 34	12 04	9 70	11 28	15 33	12 39	12 39	11 82	10 62	5 59	5 73	14 66	18 55	14 76	14 39	9 68	16 83	10 45	7 61
Cr_2O_3	50 71	49 53	51 59	41 76	2 77	48 87	49 33	48 68	50 09	48 92	49 75	29 12	6 54	44 31	45 25	47 52	2 55	46 16	54 58
FeO*	20 26	19 83	19 88	26 45	45 95	19 44	19 88	19 48	19 99	26 37	26 45	31 97	41 81	19 35	19 82	22 11	46 79	22 01	18 98
MnO	0 00	0 00	0 78	0 40	0 46	0 16	0 00	0 53	0 43	0 52	0 07	0 23	0 28	0 43	0 42	0 11	0 60	0 44	0 50
MgO	14 77	14 64	14 78	14 37	17 51	14 72	14 56	14 20	13 76	12 79	12 36	15 20	17 44	14 45	15 04	13 23	18 95	13 54	12 68
Total	99 29	98 18	98 84	98 29	95 11	97 73	98 14	96 84	96 76	98 01	98 30	97 63	95 91	95 91	97 22	95 47	99 25	95 71	96 00
$Fe^{2+}O$	13 16	13 05	11 88	14 77	17 97	12 68	13 07	12 71	13 04	15 87	17 18	16 24	17 34	13 02	12 23	14 48	17 61	14 14	13 68
$Fe^{3+}{}_2O_3$	7 89	7 54	8 89	12 99	31 09	7 51	7 57	7 52	7 72	11 67	10 30	17 48	27 19	7 04	8 43	8 48	32 43	8 75	5 89
Recalculated analyses	100 08	98 93	99 73	99 59	98 22	98 48	98 90	97 59	97 53	99 18	99 33	99 38	98 63	96 61	98 06	96 32	102 50	96 59	96 59
Fe/Fe+Mg	0 3933	0 3903	0 3887	0 4652	0 5536	0 3843	0 3922	0 3934	0 4071	0 4935	0 5029	0 4985	0 5312	0 3876	0 3838	0 4413	0 5385	0 4345	0 4144
Cr/Cr+Al	0 7500	0 7340	0 7811	0 7129	0 1081	0 7257	0 7276	0 7342	0 7599	0 8545	0 8535	0 5713	0 1913	0 6682	0 6784	0 7671	0 0923	0 7477	0 8279
Ti/Ti+Cr+Al	0 0302	0 0293	0 0295	0 0614	0 3270	0 0295	0 0270	0 0297	0 0263	0 0597	0 0604	0 1074	0 2390	0 0361	0 0318	0 0415	0 3177	0 0457	0 0233
	1-3	2-1	2-2	2-3	2-4	3-1	3-2	3-3	4-1	4-2	4-3	4-4	5-1	5-2	5-3	5-4	5-5	*	
TiO_2	1 95	1 97	1 50	4 11	5 12	1 87	2 82	3 66	2 35	2 19	1 99	1 96	2 00	2 10	2 29	2 30	2 55		
Al_2O_3	8 07	9 61	13 15	11 86	11 41	12 84	8 47	10 02	10 20	10 40	7 83	10 96	7 19	8 13	7 29	6 66	6 93		
Cr_2O_3	53 82	49 05	47 70	42 62	39 67	49 14	52 58	46 76	51 21	51 76	55 80	50 68	55 83	54 79	54 95	55 14	54 24		
FeO*	18 99	20 10	19 28	23 85	27 65	19 74	22 19	24 52	19 78	19 48	19 68	19 49	20 47	19 97	20 10	20 71	20 42		
MnO	0 58	0 41	0 89	0 19	0 51	0 39	0 29	0 47	0 19	0 16	0 65	0 11	0 00	0 35	0 10	0 47	0 36		
MgO	12 52	13 72	15 01	16 72	13 32	14 28	14 46	13 86	13 44	14 22	14 26	13 84	13 09	13 28	13 64	13 17	13 47		
Total	95 93	94 86	97 53	99 35	97 68	98 26	100 81	99 29	97 17	98 21	100 21	97 04	98 58	98 62	98 37	98 45	97 97		
$Fe^{2+}O$	14 15	12 46	11 00	11 89	17 05	13 11	13 95	15 22	14 24	13 31	12 83	13 45	14 64	14 25	13 91	14 20	13 97		
$Fe^{3+}{}_2O_3$	5 38	8 49	9 20	13 29	11 78	7 37	9 16	10 33	6 15	6 85	7 62	6 71	6 48	6 36	6 88	7 23	7 17		
Recalculated analyses	96 47	95 71	98 45	100 68	98 86	99 00	101 73	100 33	97 79	98 90	100 97	97 71	99 23	99 26	99 06	99 17	98 69		
Fe/Fe+Mg	0 4179	0 4091	0 3778	0 4027	0 4952	0 3952	0 4204	0 4554	0 4102	0 3930	0 3948	0 3996	0 4250	0 4155	0 4106	0 4264	0 4174		
Cr/Cr+Al	0 8173	0 7740	0 7087	0 7068	0 6999	0 7197	0 8064	0 7579	0 7711	0 7695	0 8270	0 7562	0 8389	0 8189	0 8349	0 8474	0 8400		
Ti/Ti+Cr+Al	0 0274	0 0287	0 0208	0 0609	0 0791	0 0254	0 0395	0 0534	0 0326	0 0300	0 0273	0 0271	0 0278	0 0290	0 0320	0 0325	0 0362		

* Total Fe calculated as FeO

APPENDIX C

PHLOGOPITE ANALYSES (LAC DE GRAS)

	T34 PHLOGOPITE (GROUNDMASS)														A61-9 PHLOGOPITE		
	1-1	1-2	1-3	2-1	2-2	2-3	3-1	3-2	3-3	4-1	4-2	4-3	5-1	5-2	5-3	6-1	6-2	1-1	1-2	1-3
SiO_2	33 91	34 04	33 53	34 45	35 08	36 21	34 36	32 91	33 92	33 20	32 72	34 14	34 47	33 63	32 75	35 14	33 74	37 87	36 54	34 49
TiO_2	0 50	0 45	0 31	0 71	0 96	0 61	0 51	0 38	0 69	0 66	0 35	0 49	0 69	0 64	0 53	1 14	0 87	1 35	1 33	1 48
Al_2O_3	16 41	15 58	15 18	15 53	14 67	13 57	15 32	16 37	14 96	15 72	15 66	15 40	15 99	15 16	15 29	15 43	14 71	15 03	14 70	17 08
Cr_2O_3	0 00	0 10	0 00	0 01	0 00	0 00	0 02	0 00	0 02	0 07	0 16	0 05	0 00	0 00	0 02	0 02	0 11	1 16	1 02	0 07
FeO*	3 51	3 23	3 30	3 22	3 50	4 23	3 56	3 38	3 91	3 62	3 10	3 36	3 07	3 19	3 05	0 35	3 27	4 48	4 48	3 72
MnO	0 06	0 00	0 15	0 00	0 10	0 06	0 03	0 07	0 16	0 25	0 08	0 06	0 10	0 00	0 00	0 03	0 05	0 17	0 16	0 00
MgO	27 33	25 81	26 72	26 72	26 54	26 70	26 17	26 09	25 98	26 59	25 73	26 00	27 57	26 11	25 90	26 83	25 85	23 53	22 92	23 19
CaO	0 06	0 09	0 00	0 11	0 39	0 59	0 00	0 02	0 42	0 01	0 00	0 00	0 00	0 00	0 00	0 14	0 00	0 00	0 00	0 00
Na_2O	0 14	0 17	0 21	0 19	0 06	0 34	0 20	0 06	0 14	0 16	0 07	0 00	0 17	0 12	0 22	0 00	0 13	0 22	0 23	0 00
K_2O	7 42	7 18	7 52	7 64	7 31	6 76	7 24	7 20	6 91	7 30	7 40	7 44	7 47	7 52	7 32	7 87	7 69	10 51	9 96	8 46
BaO	8 48	8 11	8 41	7 80	6 14	5 95	7 35	7 95	7 76	7 51	7 93	7 24	7 40	7 15	7 58	7 39	7 70	1 00	0 85	6 24
NiO	n/d	n/d	n/d	n/d	n/d	n/d	n/d	n/d	n/d	n/d	n/d	n/d	n/d	n/d	n/d	n/d	n/d	n/d	n/d	n/d
Total	97 82	94 76	95 33	96 38	94 75	95 02	94 76	94 43	94 87	95 09	93 20	94 18	96 93	93 52	92 66	94 34	94 12	95 32	92 19	94 73
Structural Formula based on 22 oxygens																				
Si	4 988	5 143	5 074	5 114	5 226	5 371	5 167	4 996	5 128	5 006	5 042	5 162	5 061	5 126	5 061	5 235	5 144	5 481	5 459	5 161
Ti	0 055	0 051	0 035	0 079	0 108	0 068	0 058	0 043	0 078	0 075	0 041	0 056	0 076	0 073	0 062	0 128	0 100	0 147	0 149	0 167
Al	2 846	2 775	2 708	2 718	2 577	2 373	2 716	2 930	2 666	2 794	2 845	2 745	2 768	2 724	2 785	2 710	2 644	2 565	2 589	3 013
Cr	-	0 012	-	0 001	-	-	0 002	-	0 002	0 008	0 019	0 006	-	-	0 002	0 002	0 013	0 133	0 120	0 008
Fe	0 432	0 408	0 418	0 400	0 436	0 525	0 448	0 429	0 494	0 456	0 400	0 425	0 377	0 407	0 394	0 004	0 417	0 542	0 560	0 466
Mn	0 007	-	0 019	-	0 013	0 008	0 004	0 009	0 020	0 032	0 010	0 008	0 012	-	-	0 004	0 006	0 021	0 020	-
Mg	5 991	5 811	6 026	5 911	5 893	5 902	5 865	5 903	5 853	5 975	5 909	5 858	6 033	5 931	5 965	5 956	5 874	5 075	5 104	5 172
Ca	0 009	0 015	-	0 017	0 062	0 094	-	0 003	0 068	0 002	-	-	-	-	-	0 022	-	-	-	-
Na	0 040	0 050	0 062	0 055	0 017	0 098	0 058	0 018	0 041	0 047	0 021	-	0 048	0 035	0 066	-	0 038	0 062	0 067	-
K	1 395	1 387	1 455	1 450	1 392	1 282	1 392	1 397	1 335	1 407	1 458	1 438	1 402	1 465	1 446	1 499	1 499	1 944	1 902	1 618
Ba	0 489	0 480	0 499	0 454	0 358	0 346	0 433	0 473	0 461	0 444	0 479	0 429	0 426	0 427	0 459	0 431	0 460	0 057	0 050	0 366
Ni	-	-	-	-	-	-	-	-	-	-	-	-	-	-	-	-	-	-	-	-

	A61-4 PHLOGOPITE (MACROCRYSTS)																			
	2-1	2-2	2-3	3-1	3-2	3-3	4-1	4-2	4-3	5-1	5-2	5-3	1-1	1-2	1-3	2-1	2-2	2-3	3-1	3-2
SiO_2	36 39	36 94	34 36	37 33	35 67	36 92	36 95	37 06	37 25	37 20	36 66	35 14	36 41	37 18	35 45	37 56	38 15	36 40	37 39	36 24
TiO_2	1 37	1 48	1 58	1 32	1 50	1 02	1 25	1 08	1 46	0 96	1 37	1 12	1 37	1 87	1 27	1 10	1 34	1 22	1 18	1 31
Al_2O_3	15 54	15 07	16 09	15 41	15 98	14 71	15 37	15 51	17 44	15 97	14 80	16 18	14 71	15 77	14 75	15 60	15 25	17 12	14 88	15 02
Cr_2O_3	1 18	1 21	0 05	0 79	0 76	0 14	1 13	1 50	0 52	1 34	1 15	0 15	1 02	0 38	0 17	1 25	1 33	0 20	0 94	0 87
FeO*	4 21	4 47	4 58	4 88	5 44	4 68	3 90	4 73	5 33	4 40	4 57	4 03	4 45	5 59	4 58	4 22	3 94	3 67	4 00	4 68
MnO	0 13	0 10	0 04	0 07	0 01	0 09	0 00	0 00	0 01	0 04	0 05	0 06	0 06	0 11	0 07	0 02	0 03	0 11	0 00	0 01
MgO	23 04	22 93	22 65	23 46	22 87	23 82	23 01	23 31	23 43	23 70	22 75	23 60	23 11	23 42	23 46	23 68	23 83	24 77	23 59	22 85
CaO	0 00	0 00	0 00	0 00	0 00	0 00	0 00	0 00	0 00	0 03	0 13	0 01	0 00	0 19	0 00	0 00	0 12	0 00	0 00	0 00
Na_2O	0 30	0 12	0 04	0 33	0 24	0 14	0 29	0 17	0 43	0 21	0 31	0 19	0 25	0 23	0 25	0 18	0 21	0 31	0 48	0 19
K_2O	10 00	10 07	8 99	10 25	9 90	8 31	10 18	9 94	9 87	10 25	9 90	8 94	9 48	9 66	8 85	9 91	10 08	7 32	9 96	9 67
BaO	1 33	0 67	4 44	1 58	1 70	5 15	1 18	0 96	2 32	1 56	0 95	5 53	1 07	1 99	4 69	1 62	1 28	7 65	1 21	1 54
NiO	n/d	n/d	n/d	n/d	n/d	n/d	n/d	n/d	n/d	n/d	n/d	n/d	n/d	n/d	n/d	n/d	n/d	n/d	n/d	n/d
Total	93 49	93 06	92 82	95 42	94 07	94 98	93 26	94 26	98 06	95 63	92 54	95 07	91 94	96 20	93 73	95 14	95 44	98 89	93 63	92 38
Structural Formula based on 22 oxygens																				
Si	5 377	5 454	5 222	5 423	5 280	5 469	5 452	5 416	5 281	5 382	5 460	5 239	5 447	5 369	5 346	5 443	5 491	5 223	5 492	5 424
Ti	0 152	0 164	0 181	0 144	0 167	0 114	0 139	0 119	0 156	0 104	0 153	0 126	0 154	0 203	0 144	0 120	0 145	0 132	0 130	0 147
Al	2 707	2 623	2 883	2 639	2 789	2 569	2 674	2 672	2 915	2 724	2 599	2 844	2 595	2 685	2 622	2 665	2 588	2 896	2 576	2 650
Cr	0 138	0 141	0 006	0 091	0 089	0 016	0 132	0 173	0 058	0 153	0 135	0 018	0 121	0 043	0 020	0 143	0 151	0 023	0 109	0 103
Fe	0 520	0 552	0 582	0 593	0 673	0 580	0 481	0 578	0 632	0 532	0 569	0 503	0 557	0 675	0 578	0 511	0 474	0 440	0 491	0 586
Mn	0 016	0 013	0 005	0 009	0 001	0 011	-	-	0 001	0 005	0 006	0 008	0 008	0 013	0 009	0 002	0 004	0 013	-	0 001
Mg	5 074	5 046	5 130	5 080	5 045	5 259	5 060	5 077	4 951	5 110	5 050	5 244	5 153	5 040	5 272	5 114	5 112	5 297	5 164	5 097
Ca	-	-	-	-	-	-	-	-	-	-	0 005	0 021	0 002	-	0 031	-	-	0 018	-	-
Na	0 086	0 034	0 012	0 930	0 069	0 040	0 083	0 048	0 118	0 059	0 089	0 055	0 073	0 064	0 073	0 051	0 059	0 086	0 137	0 055
K	1 889	1 901	1 746	1 904	1 873	1 574	1 920	1 857	1 789	1 895	1 885	1 704	1 813	1 783	1 706	1 836	1 855	1 343	1 870	1 850
Ba	0 077	0 039	0 264	0 090	0 099	0 299	0 068	0 055	0 129	0 088	0 055	0 323	0 063	0 113	0 277	0 092	0 072	0 430	0 070	0 090
Ni	-	-	-	-	-	-	-	-	-	-	-	-	-	-	-	-	-	-	-	-

*Total Fe calculated as FeO

				G/M															
	4-1	5-1	5-2	5-3	5-4	6-1	6-2	6-3	6-4	7-1	7-2	8-1	8-2	8-3	9-1	9-2	9-3	10-1	10-2	10-3
SiO_2	36 80	37 33	37 86	34 11	36 10	36 90	36 33	36 91	37 34	38 59	37 01	36 51	37 65	35 66	38 25	36 90	35 20	37 95	38 53	37 28
TiO_2	1 48	1 36	1 23	1 62	1 61	1 71	1 42	1 60	1 46	1 41	1 27	1 01	1 22	1 22	1 37	1 32	1 49	1 24	1 09	1 68
Al_2O_3	14 26	14 58	14 39	14 97	14 65	14 83	15 32	15 91	17 25	15 52	14 49	16 88	14 10	16 36	14 63	15 00	15 80	15 05	14 80	15 45
Cr_2O_3	1 16	0 98	1 01	0 05	0 92	0 44	0 00	0 13	0 11	1 00	1 19	0 81	0 96	0 01	0 55	1 08	0 15	0 97	1 23	0 95
FeO*	4 47	4 60	4 48	4 40	4 93	5 30	5 56	4 57	4 30	4 18	4 33	6 94	4 57	3 70	4 28	4 11	5 89	4 23	4 54	4 67
MnO	0 04	0 00	0 00	0 15	0 08	0 01	0 08	0 08	0 12	0 07	0 00	0 01	0 06	0 09	0 00	0 02	0 00	0 08	0 00	0 01
MgO	23 03	23 87	23 42	22 89	22 81	23 04	22 93	24 41	25 40	24 85	23 68	22 13	23 40	24 67	24 14	23 07	22 90	23 87	23 99	24 35
CaO	0 00	0 00	0 00	0 00	0 00	0 00	0 00	0 00	0 01	0 00	0 00	0 00	0 00	0 00	0 00	0 00	0 00	0 00	0 00	0 00
Na_2O	0 08	0 30	0 23	0 30	0 26	0 40	0 21	0 21	0 16	0 16	0 05	0 47	0 09	0 55	0 23	0 17	0 52	0 04	0 22	0 11
K_2O	9 87	9 45	9 41	8 30	9 63	9 63	9 29	8 65	8 27	10 24	9 69	9 94	9 74	8 55	9 97	9 55	9 65	9 46	10 02	9 73
BaO	1 01	0 80	1 21	4 93	1 42	1 47	2 09	4 86	4 54	1 28	1 53	0 80	1 62	5 96	1 56	1 08	1 88	1 42	1 26	1 67
NiO	n/d	n/d	n/d	n/d	n/d	n/d	n/d	n/d	n/d	n/d	n/d	n/d	n/d	n/d	0 00	0 05	0 00	0 03	0 13	0 02
Total	92 20	93 27	93 24	91 72	92 41	93 73	93 23	97 33	98 96	97 30	93 24	95 50	93 41	96 77	94 98	92 15	93 48	94 34	95 81	95 92
Structural Formula based on 22 oxygens																				
Si	5 496	5 485	5 569	5 261	5 411	5 448	5 410	5 327	5 256	5 452	5 475	5 310	5 563	5 217	5 542	5 479	5 260	5 515	5 537	5 370
Ti	0 166	0 150	0 136	0 188	0 181	0 190	0 159	0 174	0 155	0 150	0 141	0 110	0 136	0 134	0 149	0 147	0 167	0 136	0 118	0 182
Al	2 511	2 526	2 495	2 722	2 589	2 581	2 690	2 707	2 863	2 585	2 527	2 884	2 456	2 822	2 499	2 626	2 784	2 579	2 507	2 624
Cr	0 137	0 114	0 117	0 006	0 109	0 051	-	0 015	0 012	0 112	0 139	0 093	0 112	0 001	0 063	0 127	0 018	0 111	0 140	0 108
Fe	0 558	0 565	0 551	0 568	0 618	0 654	0 692	0 552	0 506	0 494	0 536	0 844	0 565	0 453	0 519	0 510	0 736	0 514	0 546	0 563
Mn	0 005	-	-	0 020	0 010	0 001	0 010	0 010	0 014	0 008	-	0 001	0 008	0 011	-	0 003	-	0 010	-	0 001
Mg	5 126	5 227	5 134	5 262	5 096	5 069	5 089	5 251	5 328	5 232	5 221	4 797	5 157	5 379	5 212	5 105	5 100	5 170	5 138	5 227
Ca	-	-	-	-	-	-	-	-	0 002	-	-	-	-	-	-	-	-	-	-	-
Na	0 023	0 085	0 066	0 090	0 076	0 114	0 061	0 059	0 044	0 044	0 014	0 137	0 026	0 156	0 065	0 049	0 151	0 011	0 061	0 031
K	1 884	1 775	1 769	1 636	1 845	1 817	1 768	1 596	1 488	1 849	1 832	1 848	1 839	1 599	1 846	1 813	1 843	1 757	1 840	1 791
Ba	0 059	0 046	0 070	0 298	0 083	0 085	0 122	0 275	0 250	0 071	0 089	0 046	0 094	0 342	0 089	0 063	0 110	0 081	0 071	0 094
Ni	-	-	-	-	-	-	-	-	-	-	-	-	-	-	-	0 006	-	0 004	0 015	0 002

	10-4	11-1	11-2	11-3	11-4	12-1	12-2	12-3	13-1	13-2	13-3	14-1	14-2	14-3	15-1	15-2	15-3	16-1	16-2	16-3
SiO_2	37 71	37 07	37 70	35 88	34 67	38 10	37 81	35 21	36 88	35 97	35 06	38 21	38 22	35 10	37 47	37 63	39 95	37 76	38 40	37 51
TiO_2	1 24	1 29	1 39	1 85	1 34	1 36	1 28	1 34	1 47	1 50	1 47	1 35	1 14	1 27	1 31	1 28	0 61	1 16	1 73	1 42
Al_2O_3	16 52	15 39	14 90	16 09	14 54	15 27	15 38	16 58	16 22	15 93	15 35	15 21	14 43	15 59	15 83	15 35	10 02	14 65	13 48	16 40
Cr_2O_3	0 13	1 13	1 16	0 02	0 15	1 39	1 21	0 05	0 09	0 26	0 01	1 39	1 26	0 22	1 37	1 22	0 07	1 40	0 24	0 22
FeO*	3 89	4 17	4 44	5 71	4 60	4 02	4 21	4 36	5 99	5 26	5 54	4 36	4 51	4 63	3 99	4 22	5 52	4 62	4 40	4 45
MnO	0 02	0 04	0 05	0 08	0 15	0 00	0 00	0 05	0 00	0 04	0 00	0 03	0 01	0 02	0 08	0 07	0 10	0 00	0 20	0 00
MgO	24 56	24 73	24 55	23 72	23 95	24 92	25 03	24 34	23 92	23 90	23 21	24 56	24 70	24 72	24 76	24 36	24 98	24 29	24 31	25 11
CaO	0 00	0 00	0 00	0 01	0 81	0 00	0 00	0 07	0 00	0 00	0 04	0 00	0 00	0 00	0 00	0 00	0 71	0 00	0 00	0 00
Na_2O	0 25	0 34	0 42	0 31	0 31	0 29	0 39	0 25	0 29	0 18	0 27	0 13	0 10	0 21	0 39	0 31	0 19	0 19	0 15	0 23
K_2O	7 99	9 89	9 81	9 36	8 65	9 82	9 75	8 65	9 43	9 27	9 25	10 07	10 39	8 86	9 44	9 96	8 82	9 80	9 92	9 00
BaO	6 03	1 59	0 79	2 46	3 85	0 82	0 99	5 25	2 48	2 30	2 80	0 90	0 96	5 51	1 58	1 62	3 13	1 08	0 86	3 98
NiO	0 03	0 08	0 14	0 07	0 05	0 00	0 00	0 05	0 11	0 10	0 04	0 08	0 00	0 00	0 04	0 05	0 12	0 13	0 14	0 02
Total	98 37	95 72	95 35	95 56	93 07	95 99	96 05	96 20	96 88	94 71	93 04	96 29	95 72	96 13	96 26	96 07	94 22	95 08	93 83	98 34
Structural Formula based on 22 oxygens																				
Si	5 378	5 353	5 433	5 244	5 255	5 433	5 401	5 174	5 310	5 282	5 281	5 450	5 500	5 193	5 356	5 410	5 920	5 470	5 612	5 320
Ti	0 133	0 140	0 151	0 203	0 153	0 146	0 138	0 148	0 159	0 166	0 167	0 145	0 123	0 141	0 141	0 138	0 068	0 126	0 190	0 151
Al	2 778	2 620	2 531	2 772	2 598	2 567	2 590	2 872	2 753	2 758	2 726	2 557	2 448	2 719	2 668	2 602	1 751	2 502	2 322	2 794
Cr	0 015	0 129	0 132	0 002	0 018	0 157	0 137	0 006	0 010	0 030	0 001	0 157	0 143	0 026	0 155	0 139	0 008	0 160	0 028	0 025
Fe	0 464	0 504	0 535	0 698	0 583	0 479	0 503	0 536	0 721	0 646	0 698	0 520	0 543	0 573	0 477	0 507	0 684	0 560	0 538	0 528
Mn	0 002	0 005	0 006	0 010	0 019	-	-	0 006	-	0 005	-	0 004	0 001	0 003	0 010	0 009	0 013	-	0 025	-
Mg	5 220	5 322	5 273	5 167	5 410	5 296	5 329	5 330	5 133	5 231	5 210	5 220	5 298	5 451	5 275	5 220	5 517	5 244	5 295	5 308
Ca	-	-	-	0 002	0 132	-	-	0 011	-	-	0 006	-	-	-	-	-	0 113	-	-	-
Na	0 063	0 095	0 117	0 088	0 091	0 080	0 108	0 071	0 081	0 051	0 079	0 036	0 028	0 060	0 108	0 086	0 055	0 053	0 042	0 063
K	1 457	1 826	1 807	1 749	1 676	1 790	1 780	1 625	1 736	1 740	1 781	1 836	1 911	1 676	1 725	1 831	1 671	1 815	1 853	1 632
Ba	0 337	0 090	0 045	0 141	0 229	0 046	0 055	0 302	0 140	0 132	0 165	0 050	0 054	0 319	0 089	0 091	0 182	0 061	0 049	0 221
Ni	0 003	0 009	0 016	0 008	0 006	-	-	0 006	0 013	0 012	0 005	0 009	-	-	0 005	0 006	0 014	0 015	0 016	0 002

*Total Fe calculated as FeO

DD39 PHLOGOPITE (GROUNDMASS)

	17-1	17-2	18-1	18-2	18-3	1-1	1-2	1-3	2-1	3-1	4-1
SiO_2	37 42	36 30	37 51	35 49	34 95	37 79	37 95	35 92	32 50	33 82	34 26
TiO_2	1 15	1 54	1 32	1 22	1 86	1 90	2 05	1 97	0 70	0 17	0 92
Al_2O_3	14 96	15 47	14 43	15 18	16 15	14 62	14 38	14 11	17 85	15 79	16 04
Cr_2O_3	1 45	0 09	1 14	0 19	0 03	1 80	2 24	1 72	0 00	0 08	0 00
FeO*	3 05	4 30	3 14	4 25	2 83	3 53	3 64	4 05	6 18	4 72	4 70
MnO	0 10	0 03	0 12	0 08	0 30	0 00	0 00	0 06	0 25	0 02	0 22
MgO	25 30	23 66	24 68	24 16	24 80	26 42	26 64	26 30	23 20	26 48	24 96
CaO	0 00	0 00	0 00	0 00	0 00	0 00	0 01	0 17	0 42	0 00	0 44
Na_2O	0 58	0 40	0 31	0 18	0 57	0 20	0 00	0 09	28	0 42	0 37
K_2O	9 42	8 96	9 76	9 24	8 10	9 99	9 84	8 63	5 64	6 14	4 80
BaO	1 31	2 19	1 25	3 09	5 65	0 14	0 39	2 27	8 49	8 77	9 40
NiO	0 05	0 22	0 14	0 09	0 37	0 00	0 00	0 00	0 18	0 00	0 11
Total	94 79	93 16	93 80	93 17	95 61	96 39	97 14	95 29	95 41	96 41	96 22
Structural Formula based on 22 oxygens											
Si	5 408	5 381	5 482	5 316	5 156	5 350	5 34	5 230	4 918	5 058	5 118
Ti	0 125	0 172	0 145	0 137	0 206	0 202	0 217	0 216	0 080	0 019	0 103
Al	2 549	2 704	2 486	2 681	2 809	2 440	2 387	2 422	3 185	2 784	2 825
Cr	0 166	0 011	0 132	0 023	0 003	0 201	0 249	0 198	-	0 009	-
Fe	0 369	0 533	0 384	0 532	0 349	0 418	0 429	0 493	0 782	0 590	0 587
Mn	0 012	0 004	0 015	0 010	0 037	-	-	0 007	0 032	0 003	0 028
Mg	5 449	5 227	5 376	5 393	5 453	5 575	5 589	5 707	5 233	5 902	5 558
Ca	-	-	-	-	-	-	0 002	0 027	0 068	-	0 070
Na	0 162	0 115	0 088	0 052	0 163	0 055	-	0 025	0 082	0 122	0 107
K	1 740	1 698	1 823	1 769	1 528	1 808	1 771	1 606	1 091	1 174	0 917
Ba	0 074	0 127	0 072	0 181	0 327	0 008	0 022	0 130	0 503	0 514	0 550
Ni	0 006	0 026	0 016	0 011	0 004	-	-	-	0 022	-	0 013

*Total Fe calculated as FeO

APPENDIX D

MONTICELLITE ANALYSES (LAC DE GRAS)

T29S MONTICELLITE

	1-1	1-2	2-1	3-1	3-2	4-1	4-2	5-1	5-2	5-3	6-1	6-2	6-3	7-1	7-2	7-3	8-1	8-2	8-3
SiO_2	37.02	37.65	37.91	36.60	36.86	37.10	36.11	37.29	36.65	38.69	36.19	36.89	36.92	35.61	36.48	35.91	35.87	36.13	35.64
Al_2O_3	0.15	0.20	0.00	0.00	0.17	0.00	0.81	0.07	0.01	2.20	0.00	0.00	0.32	0.00	0.09	0.00	0.00	0.00	0.17
FeO*	7.43	5.80	7.92	8.61	7.51	8.90	8.56	6.24	5.87	6.79	8.31	8.22	6.88	10.01	9.99	8.43	9.76	8.70	8.08
MnO	0.12	0.26	0.16	0.23	0.00	0.24	0.67	0.34	0.17	0.43	0.43	0.29	0.11	0.57	0.45	0.44	0.62	0.12	0.33
MgO	20.51	22.51	20.65	20.10	19.80	19.80	19.96	23.35	22.05	23.23	19.26	20.41	21.24	19.26	19.60	19.96	18.91	19.52	19.16
CaO	35.72	33.55	34.68	33.90	33.28	33.70	32.56	33.18	34.57	28.47	34.34	34.21	34.53	33.28	33.47	33.10	33.39	33.62	32.76
Total	100.95	99.97	101.32	99.44	97.62	99.74	98.67	100.47	99.32	99.81	98.53	100.02	100.00	98.73	100.08	97.84	98.55	98.09	96.14
Mol % end member molecules																			
Ks	16.23	13.13	17.88	19.72	17.69	20.50	20.07	13.89	13.21	16.13	18.95	18.71	15.56	23.16	22.90	19.63	22.78	20.23	19.32
Mo	82.46	82.94	81.16	78.51	81.49	77.71	76.49	79.56	85.18	69.42	80.12	79.79	83.25	74.25	74.15	77.89	75.80	78.66	79.75
Fo	1.31	3.93	0.96	1.77	0.82	1.79	3.45	6.54	1.61	14.46	0.92	1.50	1.19	2.58	2.96	2.48	1.42	1.11	0.94

	9-1	9-2	10-1	10-2	11-1	12-1	12-2	12-3	13-1	13-2	13-3	14-1	14-2	14-3	15-1	15-2	16-1	16-2	16-3
SiO_2	36.40	35.21	37.94	36.13	36.72	35.37	36.48	37.40	36.55	35.55	35.11	37.08	36.41	35.71	35.64	36.78	36.77	36.09	35.21
Al_2O_3	0.00	0.00	0.00	0.01	0.02	0.00	0.14	0.61	0.00	0.00	0.66	0.00	0.00	0.00	0.00	0.01	0.00	0.00	0.00
FeO*	9.94	9.57	5.86	7.30	7.28	9.68	9.70	6.54	6.95	8.38	8.94	6.75	7.04	8.37	9.42	8.24	9.12	8.50	8.64
MnO	0.55	0.53	0.31	0.42	0.35	0.56	0.34	0.17	0.52	0.32	0.19	0.39	0.22	0.48	0.55	0.34	0.68	0.44	0.61
MgO	18.73	18.70	23.46	21.31	21.20	21.80	22.39	23.93	24.87	22.68	21.74	20.95	21.40	20.54	20.01	21.26	21.47	20.04	20.34
CaO	32.37	32.41	32.47	33.46	33.51	32.37	32.94	32.62	32.10	33.97	31.40	33.26	33.56	32.99	32.52	33.48	32.56	33.41	33.24
Total	97.99	96.42	100.04	98.63	99.08	99.78	101.99	101.27	100.99	100.90	98.04	98.43	98.63	98.09	98.14	100.11	100.60	98.48	98.04
Mol % end member molecules																			
Ks	23.59	22.82	13.21	16.67	16.65	21.64	21.26	14.46	15.13	18.26	20.46	15.67	16.07	19.31	21.85	18.63	20.55	19.66	19.88
Mo	73.59	74.92	79.36	79.97	80.30	69.89	70.05	76.80	73.26	75.39	70.43	82.00	80.83	76.95	73.58	77.11	72.45	78.09	76.86
Fo	2.81	2.26	7.43	3.37	3.05	8.47	8.69	8.74	11.61	6.35	9.11	2.33	3.11	3.74	4.57	4.27	6.99	2.25	3.26

C27 MONTICELLITE

	16-4	17-1	17-2	17-3	1-1	2-1	2-2	3-1	3-2	3-3	4-1	4-2	4-3
SiO_2	35.67	36.60	37.19	35.92	37.64	37.89	38.66	37.61	37.14	37.65	38.42	38.55	38.21
Al_2O_3	0.00	0.00	0.13	0.00	0.08	0.00	0.00	0.00	0.09	0.00	0.04	0.16	0.00
FeO*	8.45	9.58	8.66	8.52	5.77	5.13	4.92	7.09	7.00	6.40	7.05	6.65	6.05
MnO	0.31	0.50	0.51	0.36	0.37	0.33	0.16	0.41	0.44	0.45	0.34	0.38	0.34
MgO	20.37	19.95	21.14	22.26	24.70	25.06	25.89	23.07	23.53	23.24	23.52	23.33	23.77
CaO	33.38	33.22	33.06	32.75	31.88	31.66	32.03	29.82	30.21	31.02	30.38	30.66	31.41
Total	98.18	99.85	100.69	99.81	100.44	100.07	101.66	98.00	98.41	98.76	99.75	99.73	99.78
Mol % end member molecules													
Ks	19.43	21.98	19.65	19.01	12.81	11.42	10.75	16.50	16.07	14.70	16.13	15.29	13.73
Mo	77.67	74.45	75.23	73.44	76.70	77.74	77.75	71.30	71.64	75.45	71.81	73.86	76.43
Fo	2.90	3.57	5.12	7.54	10.50	10.84	11.51	12.20	12.30	9.85	12.05	10.85	9.84

*Total Fe calculated as FeO; Ks = $CaFeSiO_4$, Mo = $CaMgSiO_4$, Fo = Mg_2SiO_4

APPENDIX E

SPINEL ANALYSES (FORT À LA CORNE)

	H50 SPINELS																	
	1-1	1-2	1-3	1-4	2-1	2-2	2-3	2-4	3-1	3-2	3-3	3-4	4-1	4-2	4-3	5-1	5-2	5-3	5-4
TiO_2	25 15	22 51	22 37	24 55	21 84	22 79	23 76	24 22	21 55	24 04	28 02	25 91	23 77	22 95	23 46	20 54	22 83	24 03	24 55
Al_2O_3	11 21	11 79	11 72	11 02	12 29	11 67	12 27	11 75	10 56	10 96	10 83	10 52	11 70	11 23	11 38	14 89	12 32	11 88	10 68
Cr_2O_3	1 41	1 05	1 14	1 31	1 24	0 90	1 15	1 39	0 63	0 61	1 66	2 48	1 11	1 15	1 53	1 54	1 37	1 33	1 00
FeO*	36 35	40 61	41 14	38 71	40 72	37 98	37 57	34 58	42 13	41 60	37 02	34 23	38 47	38 21	35 34	37 59	38 28	33 78	30 16
MnO	0 49	0 54	0 56	0 53	0 73	0 68	0 70	0 52	0 56	0 40	0 40	0 60	0 79	0 21	0 43	0 19	0 21	0 56	0 57
MgO	24 56	21 97	21 45	23 00	21 91	22 69	23 40	24 59	22 79	20 75	23 26	24 85	24 23	23 00	23 34	22 56	23 28	24 79	27 13
Total	99 17	98 47	98 38	99 12	98 73	96 71	98 85	97 05	98 22	98 36	101 19	98 59	100 07	96 75	95 48	97 31	98 29	96 37	94 09
$Fe^{2+}O$	18 47	19 93	19 76	20 25	19 40	18 34	18 87	16 96	17 59	23 11	23 64	18 27	17 85	18 43	17 72	17 71	18 55	16 24	12 21
$Fe^{3+}{}_2O_3$	19 87	22 98	23 17	20 52	23 69	21 83	20 78	19 58	27 27	20 55	14 86	17 73	22 91	21 99	19 58	22 09	21 92	19 49	19 95
Recalculated Analyses	101 16	100 77	100 67	101 18	101 10	98 90	100 93	99 01	100 95	100 42	102 68	100 37	102 37	98 95	97 44	99 52	100 49	98 32	96 09
Fe/Fe+Mg	0 4116	0 4663	0 4663	0 4431	0 4676	0 4417	0 4315	0 3993	0 4663	0 4865	0 4293	0 3943	0 4287	0 4399	0 4171	0 4406	0 4373	0 3992	0 3445
Cr/Cr+Al	0 0778	0 0564	0 0613	0 0739	0 0634	0 0492	0 0592	0 0735	0 0385	0 0360	0 0932	0 1366	0 0598	0 0643	0 0827	0 0649	0 0694	0 0699	0 0591
Ti/Ti+Cr+Al	0 5690	0 5348	0 5334	0 5683	0 5150	0 5423	0 5376	0 5492	0 5559	0 5743	0 5995	0 5757	0 5493	0 5496	0 5468	0 4515	0 5239	0 5455	0 5798
	V89 SPINELS																		
	6-1	6-2	6-3	7-1	1-1	1-2	2-1	2-2	2-3	2-4	2-5	2-6	3-1	3-2	3-3	3-4	3-5	3-6	4-1
TiO_2	21 64	22 44	22 49	15 85	0 00	0 00	7 98	10 29	17 11	18 54	19 32	17 02	6 52	6 58	6 75	9 50	15 18	16 47	8 15
Al_2O_3	11 69	9 95	10 80	11 94	0 00	0 09	6 78	7 58	9 30	9 33	9 74	9 98	5 92	5 87	5 84	8 74	10 46	10 73	7 08
Cr_2O_3	1 26	1 23	1 18	10 47	0 00	0 00	41 03	33 51	12 94	9 46	6 98	6 73	48 82	49 31	48 42	30 50	16 32	15 32	40 51
FeO*	39 24	38 37	32 81	36 05	93 68	93 69	27 79	32 17	39 09	41 33	41 62	37 49	23 70	23 67	23 66	31 87	39 07	38 05	28 10
MnO	0 60	0 31	0 50	0 65	0 10	0 25	0 74	0 27	0 30	0 62	0 67	0 18	0 11	0 00	0 00	0 50	0 36	0 59	0 34
MgO	21 50	22 58	26 23	24 97	0 58	0 95	13 34	14 41	16 57	16 97	21 67	28 75	13 04	12 84	12 68	14 97	17 49	18 44	13 54
Total	95 93	94 88	94 01	99 93	94 36	94 98	97 66	98 23	95 31	96 25	100 00	100 15	98 11	98 27	97 35	96 08	98 88	99 60	97 72
$Fe^{2+}O$	18 97	17 72	11 64	9 83	30 47	29 97	18 60	19 88	22 10	22 79	17 62	5 44	18 32	18 82	18 92	17 61	20 26	19 99	18 91
$Fe^{3+}{}_2O_3$	22 53	22 94	22 83	29 14	70 25	70 81	10 22	13 66	18 88	20 60	26 67	35 62	5 98	5 39	5 27	15 85	20 90	20 07	10 21
Recalculated Analyses	98 19	97 18	95 67	102 85	101 40	102 07	98 68	99 60	97 20	98 31	102 67	103 72	98 71	98 81	97 88	97 67	100 97	101 01	98 74
Fe/Fe+Mg	0 4631	0 4454	0 3670	0 4056	0 9938	0 9790	0 4961	0 5134	0 5272	0 5351	0 4758	0 3813	0 4621	0 4656	0 4686	0 5016	0 5136	0 4938	0 4952
Cr/Cr+Al	0 0674	0 0766	0 0683	0 3704	1 0000	0 0000	0 8024	0 7478	0 4828	0 4048	0 3247	0 3115	0 8469	0 8493	0 8476	0 7007	0 5114	0 4892	0 7933
Ti/Ti+Cr+Al	0 5241	0 5706	0 5532	0 3478	1 0000	0 0000	0 1292	0 1798	0 3778	0 4301	0 4608	0 4283	0 0971	0 0773	0 1010	0 1719	0 3115	0 3334	0 1318
																		H32	
	4-2	4-3	4-4	5-1	5-2	5-3	5-4	5-5	5-6	5-7	5-8	6-1	6-2	6-3	7-1	7-2	7-3	*1-1	1-2
TiO_2	7 55	7 85	19 02	6 82	6 63	6 88	7 22	11 00	13 73	17 38	15 10	15 16	12 81	15 81	12 34	9 29	9 52	0 08	0 94
Al_2O_3	5 96	5 68	10 12	5 85	5 60	5 60	6 37	13 13	13 38	10 71	11 55	8 41	10 17	12 92	10 66	9 23	9 26	0 00	0 21
Cr_2O_3	41 01	42 75	11 54	47 24	49 62	47 87	44 02	24 55	17 10	9 96	12 96	20 59	24 46	14 32	24 11	30 70	28 12	0 03	0 09
FeO*	27 51	26 26	42 54	24 22	23 33	25 03	26 35	33 07	37 84	38 03	38 09	38 32	35 11	36 11	33 78	32 58	31 65	91 58	91 21
MnO	0 44	0 75	0 36	0 55	0 38	0 47	0 24	1 15	0 05	0 70	0 00	0 27	0 60	0 68	0 73	0 31	0 19	0 10	0 03
MgO	13 06	13 32	14 31	12 86	12 90	13 09	12 95	15 21	16 11	16 03	17 86	16 05	16 11	19 54	16 41	14 68	18 10	0 66	0 70
Total	95 53	96 61	97 89	97 54	98 46	98 94	97 15	98 11	98 21	92 81	95 56	98 80	99 26	99 38	98 03	96 79	96 84	92 45	93 18
$Fe^{2+}O$	18 13	17 97	28 31	18 24	18 41	18 44	18 76	19 27	21 58	22 17	19 09	22 14	20 00	17 90	18 67	18 36	13 54	29 78	30 80
$Fe^{3+}{}_2O_3$	10 42	9 21	16 01	6 65	5 47	7 32	8 44	15 33	18 07	17 63	21 11	17 98	16 79	20 23	16 79	15 80	20 12	68 68	67 13
Recalculated Analyses	96 57	97 53	99 49	98 21	99 01	99 67	98 00	99 65	100 02	94 58	97 67	100 60	100 94	101 41	99 71	98 37	98 86	99 33	99 90
Fe/Fe+Mg	0 4989	0 4824	0 5842	0 4710	0 4609	0 4747	0 4903	0 5068	0 5261	0 5286	0 5020	0 5302	0 5074	0 4662	0 4932	0 5120	0 4525	0 9928	0 9840
Cr/Cr+Al	0 8219	0 8347	0 4334	0 8442	0 8560	0 8515	0 8226	0 5564	0 4616	0 3842	0 4295	0 6216	0 6174	0 4265	0 6027	0 6905	0 6707	1 0000	0 2233
Ti/Ti+Cr+Al	0 1258	0 1272	0 4046	0 1039	0 0981	0 1043	0 1137	0 1917	0 2606	0 3894	0 3225	0 3033	0 2352	0 3093	0 2269	0 1658	0 1776	0 7172	0 6893

*Total Fe calculated as FeO

	1-3	2-1	2-2	2-3	3-1	3-2	3-3	4-1	4-2	4-3	5-1	5-2	5-3	5-4	5-5	6-1	6-2	6-3	6-4
TiO_2	0 54	0 06	0 29	0 13	4 70	4 28	4 19	4 54	4 97	11 73	5 37	5 12	4 58	7 07	13 22	15 39	8 76	5 65	5 28
Al_2O_3	0 04	0 00	0 00	0 05	9 94	9 94	6 43	5 30	6 15	8 59	11 21	11 46	6 28	6 47	13 97	8 31	7 42	7 40	9 77
Cr_2O_3	0 06	0 10	0 25	0 13	49 54	50 16	53 15	54 77	50 42	26 08	49 84	49 95	56 46	45 52	10 23	18 64	34 55	54 23	51 46
FeO*	90 47	91 56	90 18	89 89	23 51	24 32	24 44	24 81	27 50	37 98	22 87	22 56	22 06	28 65	43 73	42 42	31 14	22 69	23 86
MnO	0 00	0 11	0 31	0 25	0 28	0 43	0 28	0 33	0 27	0 52	0 00	0 44	0 73	0 49	0 21	0 57	0 38	0 58	0 40
MgO	0 25	1 32	1 10	1 03	10 60	11 01	10 01	9 79	9 95	11 87	10 24	10 73	10 00	10 02	13 34	11 96	12 39	10 21	10 45
Total	91 36	93 15	92 13	91 48	98 57	100 14	98 50	99 54	99 26	96 77	99 53	100 26	100 11	98 22	94 70	97 29	94 64	100 76	101 22
$Fe^{2+}O$	30 54	28 98	28 97	28 79	20 97	20 34	20 86	21 61	21 90	24 53	22 87	21 74	21 21	23 18	24 22	27 78	20 28	22 38	22 40
$Fe^{3+}{}_2O_3$	66 60	69 54	68 02	67 90	2 82	4 42	3 98	3 56	6 22	14 95	0 00	0 91	0 94	6 08	21 68	16 27	12 07	0 34	1 62
Recalculated Analyses	98 03	100 12	98 94	98 28	98 85	100 58	98 90	99 90	99 88	98 27	99 53	100 35	100 20	98 83	96 87	98 92	95 85	100 79	101 38
Fe/Fe+Mg	0 9942	0 9704	0 9748	0 9763	0 5118	0 5108	0 5358	0 5450	0 5664	0 6020	0 5153	0 4984	0 5105	0 5747	0 6078	0 6264	0 5430	0 5123	0 5190
Cr/Cr+Al	0 5016	1 0000	1 0000	0 6356	0 7698	0 7720	0 8472	0 8739	0 8461	0 6707	0 7489	0 7452	0 8578	0 8252	0 3294	0 6008	0 7575	0 8310	0 7794
Ti/Ti+Cr+Al	0 8111	0 3633	0 5246	0 3768	0 0649	0 0590	0 0597	0 0645	0 0735	0 2229	0 0713	0 0677	0 0621	0 1087	0 2882	0 3205	0 1545	0 0761	0 0707
			HI4 SPINELS																
	6-5	7-3	1-1	1-2	1-3	1-4	1-5	1-6	1-7	2-1	2-2	2-3	2-4	2-5	2-6	3-1	3-2	3-3	3-4
TiO_2	14 68	1 53	13 84	5 32	7 42	11 49	13 54	15 88	18 23	21 25	23 57	23 22	22 56	21 81	24 02	23 82	22 60	19 28	7 73
Al_2O_3	7 66	0 00	8 83	7 32	8 39	9 41	9 19	8 28	7 34	8 41	7 61	7 95	8 31	8 65	6 96	7 39	8 07	8 89	8 35
Cr_2O_3	20 94	0 00	18 83	43 57	37 16	25 52	17 90	11 57	8 41	1 47	1 10	0 53	0 59	0 32	0 08	1 05	2 91	10 00	40 89
FeO*	39 65	90 36	37 71	25 23	27 90	33 83	39 98	40 90	42 50	47 25	48 74	48 79	48 56	49 95	49 56	49 03	47 59	45 70	29 58
MnO	0 76	0 25	0 20	0 33	1 01	0 47	0 59	0 83	0 88	0 51	0 53	0 67	0 67	0 71	0 61	0 54	0 85	0 61	0 47
MgO	11 45	0 11	15 95	13 00	13 16	14 47	13 61	16 14	15 38	15 20	13 74	13 62	13 11	12 63	12 20	13 38	13 34	13 19	11 39
Total	95 14	92 25	95 36	94 77	95 04	95 19	94 81	93 60	92 74	94 09	95 29	94 78	93 80	94 07	93 43	95 21	95 36	97 67	98 41
$Fe^{2+}O$	26 90	31 65	20 16	16 29	17 53	20 01	22 95	20 47	23 26	27 24	31 75	31 37	31 30	31 48	33 71	32 45	31 25	29 60	22 09
$Fe^{3+}{}_2O_3$	14 17	65 24	19 50	9 94	11 52	15 36	18 92	22 70	21 38	22 24	18 88	19 36	19 18	20 52	17 61	18 43	18 16	17 90	8 33
Recalculated Analyses	96 56	98 78	97 31	95 77	96 19	96 73	96 71	95 87	94 88	96 32	97 18	96 72	95 72	96 13	95 19	97 06	97 18	99 46	99 24
Fe/Fe+Mg	0 6207	0 9974	0 5277	0 4784	0 5005	0 5250	0 5813	0 5450	0 5664	0 5950	0 6264	0 6287	0 6365	0 6515	0 6575	0 6340	0 6277	0 6209	0 5511
Cr/Cr+Al	0 6471	1 0000	0 5886	0 7997	0 7482	0 6453	0 5665	0 4838	0 4346	0 1050	0 0884	0 0428	0 0455	0 0242	0 0077	0 0870	0 1948	0 4301	0 7666
Ti/Ti+Cr+Al	0 3014	1 0000	0 2915	0 0946	0 1244	0 2165	0 2895	0 3871	0 4726	0 5907	0 6431	0 6408	0 6231	0 6109	0 6860	0 6525	0 5900	0 4409	0 1211
	3-5	3-6	3-7	3-8	4-1	4-2	4-4	4-5	5-1	5-2	5-3	5-5	5-6	6-1	6-2	6-3	6-4	6-6	6-7
TiO_2	5 04	7 71	10 60	9 67	21 54	21 39	18 23	13 02	21 13	20 95	19 73	18 57	18 63	5 24	5 28	4 84	7 09	22 58	23 72
Al_2O_3	7 23	9 62	9 78	9 46	8 55	7 75	11 53	10 90	10 90	11 03	12 47	15 62	15 09	12 48	12 32	6 67	9 97	8 19	7 87
Cr_2O_3	53 28	40 00	30 71	32 65	0 39	0 59	0 15	0 00	0 24	0 13	0 29	0 05	0 02	48 36	48 33	55 66	44 79	3 77	0 64
FeO*	24 86	30 48	35 51	32 67	50 04	51 40	50 38	57 03	47 83	46 88	46 62	46 17	46 35	21 67	23 06	23 05	27 28	47 27	48 00
MnO	0 54	0 23	0 19	0 62	0 53	0 64	0 47	0 67	0 23	0 53	0 47	0 58	0 65	0 42	0 43	0 62	0 04	0 57	0 74
MgO	9 93	10 92	11 49	11 04	13 04	13 02	12 59	9 57	14 49	14 47	14 38	16 62	15 68	11 00	11 08	10 07	10 75	13 15	12 90
Total	100 88	98 96	98 28	96 11	94 09	94 79	93 35	91 19	94 82	93 99	93 96	97 61	96 42	99 17	100 50	100 91	99 92	95 53	93 87
$Fe^{2+}O$	22 35	23 40	25 04	23 68	30 80	30 71	28 84	27 92	29 11	28 42	27 75	24 87	25 82	21 26	21 58	21 78	23 59	31 86	32 51
$Fe^{3+}{}_2O_3$	2 79	7 87	11 64	9 99	21 39	23 00	23 94	32 35	20 81	20 51	20 98	23 67	22 82	0 46	1 64	1 41	4 10	17 13	17 21
Recalculated Analyses	101 16	99 75	99 45	97 11	96 23	97 09	95 75	94 43	96 90	96 04	96 06	99 98	98 71	99 22	100 66	101 05	100 33	97 25	95 59
Fe/Fe+Mg	0 5420	0 5688	0 5936	0 5831	0 6446	0 6511	0 6541	0 7380	0 6094	0 6050	0 6051	0 5677	0 5828	0 4822	0 4959	0 5197	0 5453	0 6295	0 6375
Cr/Cr+Al	0 8318	0 7361	0 6781	0 6984	0 0297	0 0486	0 0087	0 0000	0 0146	0 0078	0 0154	0 0021	0 0009	0 7222	0 7246	0 8484	0 7509	0 2359	0 0517
Ti/Ti+Cr+Al	0 0696	0 1189	0 1821	0 1644	0 0693	0 0262	0 5000	0 4325	0 5493	0 5459	0 4985	0 4308	0 4404	0 0693	0 0700	0 0656	0 1016	0 5734	0 6458

*Total Fe calculated as FeO

	7-1	7-2	7-3	7-4	7-5	7-6	7-7	8-1	8-2	8-3	8-4	8-5	8-6	9-1	9-2	9-3	9-4	9-5	9-6
TiO_2	14 21	6 20	13 91	5 89	9 71	16 22	15 30	22 74	20 18	18 27	20 09	22 75	19 79	5 18	5 01	15 94	23 46	20 89	17 56
Al_2O_3	10 77	7 50	11 16	10 10	9 72	13 71	12 98	7 99	8 70	9 93	9 19	8 39	12 04	9 74	6 67	10 82	8 25	10 78	8 06
Cr_2O_3	19 84	49 03	21 89	47 43	34 65	0 40	0 31	1 48	7 45	9 77	7 60	1 84	0 17	49 64	55 42	16 17	0 42	0 34	0 01
FeO*	40 31	26 21	37 84	25 66	32 68	50 08	53 58	48 73	46 51	44 62	46 67	48 68	48 39	23 64	23 37	40 52	48 58	48 97	53 44
MnO	0 70	0 77	0 52	0 40	0 57	0 74	0 42	0 74	0 66	0 55	0 58	0 68	0 63	0 48	0 61	0 29	0 88	0 54	0 56
MgO	13 20	9 54	12 17	11 14	11 10	13 00	12 34	12 87	12 80	13 03	12 61	13 24	13 19	10 84	9 94	12 80	13 45	13 62	12 04
Total	99 03	99 25	97 49	100 62	98 43	94 15	94 93	94 55	96 30	96 17	96 74	95 58	94 21	99 52	101 02	96 54	95 04	95 14	91 67
$Fe^{3+}O$	25 63	23 29	26 62	21 80	24 45	26 76	27 46	31 94	30 48	28 67	30 98	31 84	29 47	21 11	22 17	27 40	31 76	30 00	27 98
$Fe^{3+}_2O_3$	16 31	3 24	12 47	4 29	9 15	15 91	29 03	18 66	17 81	17 72	17 43	18 72	21 02	2 82	1 33	14 59	18 70	21 08	28 30
Recalculated Analyses	100 66	99 58	98 74	101 05	99 35	96 75	97 84	96 42	98 08	97 95	98 49	97 45	96 32	99 80	101 15	98 00	96 91	97 25	94 50
Fe/Fe+Mg	0 5907	0 5650	0 5951	0 5212	0 5819	0 6457	0 6724	0 6415	0 6320	0 6181	0 6363	0 6348	0 6342	0 5076	0 5264	0 5994	0 6306	0 6296	0 6772
Cr/Cr+Al	0 5527	0 8148	0 5682	0 7591	0 7051	0 0192	0 0158	0 1105	0 3649	0 3976	0 3568	0 0094	0 0094	0 7737	0 8479	0 5006	0 0330	0 0207	0 0008
Ti/Ti+Cr+Al	0 2735	0 0892	0 2556	0 0823	0 1582	0 4250	0 4254	0 6176	0 4845	0 4142	0 4729	0 5095	0 5095	0 0713	0 0679	0 3194	0 6370	0 5477	0 5814

	9-7
TiO_2	20 60
Al_2O_3	10 81
Cr_2O_3	0 32
FeO*	47 91
MnO	0 61
MgO	12 96
Total	93 21
$Fe^{3+}O$	30 04
$Fe^{3+}_2O_3$	19 86
Recalculated Analyses	95 20
Fe/Fe+Mg	0 6360
Cr/Cr+Al	0 0195
Ti/Ti+Cr+Al	0 5438

*Total Fe calculated as FeO